# Novel Diagnostic and Prognostic Biomarkers in Prostate Cancer

**Luke Thomas Quigley**

This thesis is submitted in total fulfilment of a Master of Science Degree

School of Cancer Medicine

College of Science, Health and Engineering

La Trobe University, Victoria, Australia

**October 2020**

## TABLE OF CONTENTS

## ABSTRACT

Prostate cancer remains one of the most prevalent cancers detected in males; yet current detection methods still lack adequate specificity and sensitivity. While major improvements in screening have led to a reduction in advanced disease and mortality, patient overdiagnosis and overtreatment have in turn, become problematic. The development and nature of most prostate tumours tend to be slow-growing and indolent, yet such high prevalence of the disease still results in a range of heterogenous clinical outcomes varying on a patient-by-patient basis. Many clinical, pathologic, molecular and genetic factors have been explored for prognostic utility, yet few are routinely used. These factors emphasise the growing need for the discovery of novel diagnostic and prognostic biomarkers capable of effectively distinguishing healthy and benign patients from those with prostate cancer, and effectively delineating indolent from aggressive disease.

In this study, we screened a cohort (n=110) of retrospective serum samples from prostate cancer patients using a customised cancer array (CT100+) containing 123 cancer antigens, generating discrete autoantibody profiles for each patient. Downstream analyses were conducted to assess the efficacy of discovered cancer-associated autoantibodies as diagnostic and prognostic biomarkers using clinicopathological data, where available. Findings inferred that combinations of unique autoantibodies could be used to detect prostate cancer with high sensitivity and specificity and aid in the prediction of disease outcome (i.e., relapse and survival). We also conducted multiplex immunohistochemistry on prostatectomy tissue samples from a subset of these patients (n=64) in order to investigate correlations between the production, presence and quantity of antibody-secreting cells and autoantibody profiles. Finally, our array-based diagnostic findings were validated using an additional external cohort (n=99) of prostate cancer patients.

In conclusion, the incorporation of circulating autoantibodies with current prostate cancer screening procedures has the potential to substantially improve diagnostics and prognostics, thereby reducing overdiagnoses and enabling informed therapeutic interventions.

STATEMENT OF AUTHORSHIP

Except where reference is made in the text of the thesis, this thesis contains no material published elsewhere or extracted in whole or in part from a thesis accepted for the award of any other degree or diploma. No other person's work has been used without due acknowledgement in the main text of the thesis. This thesis has not been submitted for the award of any degree or diploma in any other tertiary institution.

Luke Quigley 19 October 2020

**This work was supported by an Australian Government Research Training Program Scholarship.**

ACKNOWLEDGMENTS

Throughout the writing of this dissertation, I received a great deal of support and assistance.

First and foremost, immense gratitude goes out to my supervisor, mentor and friend, Dr. Jessica Da Gama Duarte. Thank you for your unending support and guidance. Your insightful feedback and deep understanding of the field pushed me to sharpen my mind and shape me into the researcher I am today.

I would also like to thank Dr. Andreas Behren for his active supervision throughout the course of the project. The plethora of knowledge and exceptional advice that was always readily available and willingly provided enabled this body of research to be carried out at high standards.

Moreover, appreciation is extended to Leire Moya from the Australian Prostate Bioresource and Gavin Higgins from the Victorian Cancer Biobank for organising the utilised serum and tissue specimens, and of course to the patients that kindly donated them. This project would not have been possible without these invaluable samples.

Additionally, I would like to thank all current members of the Tumour Immunology Lab at the Olivia-Newton John Cancer Research Institute (i.e. Candani Tutuka, Simone Ostrouska, Cyril Deceneux, Ensieh Poursani, Josh Adalin and Elnaz Tavancheh) for their wonderful collaboration over the course of this study, as well as my tutors and lecturers from La Trobe University (i.e. Prof. Paul Fisher, Assoc. Prof. Christine Hawkins, Assoc. Prof. Karla Helbig, Dr. Steve Petrovski, Dr. Lisa Francione, and Carolyn Bell) whom I had the luxury of gaining a plethora of knowledge from during my undergraduate degree.

Lastly, I would like to thank my close friends (i.e., Daniel Hunt, Brad Reardon, David Wisniewski and Kate Kelly) for their support, as well as my immediate family for their wise counsel.

ABBREVIATIONS

| | |
|---|---|
| APCB | Australian Prostate Cancer Bioresource |
| ASC | Antibody-Secreting Cell |
| AUC | Area Under Curve |
| BCA | B Cell Aggregate |
| BCCP | Biotin Carboxyl Carrier Protein |
| Breg | Regulatory B Cell |
| BSA | Bovine Serum Albumin |
| CD | Cluster of Differentiation |
| CT | Cancer-Testis |
| CV | Coefficient of Variation |
| DAPI | 4',6-Diamidino-2-Phenylindole |
| dH2O | Deionised Water |
| ELISA | Enzyme-Linked Immunosorbent Assay |
| ER | Epitope Retrieval |
| FFPE | Formalin-Fixed Paraffin-Embedded |
| H&E | Haematoxylin and Eosin |
| H202 | Hydrogen Peroxide |
| HD | Healthy Donor |
| HEPES | 4-(2-Hydroxyethyl)-1-Piperazineethanesulfonic Acid |
| HLA | Human Leukocyte Antigen |
| ICL | Insect Cell Lysate |
| IgG | Immunoglobulin G |
| IT | Intratumoural |
| KCL | Potassium Chloride |
| MHC | Major Histocompatibility Complex |
| mIHC | Multispectral Immunohistochemistry |
| MSI | Multispectral Image |
| PBS | Phosphate-buffered Saline |
| PBST | Phosphate-buffered Saline, 0.1% Tween-20 |
| PCa | Prostate Cancer |
| PMT | Photomultiplier Tube |

| | |
|---|---|
| PSA | Prostate-Specific Antigens |
| PT | Peritumoural |
| RFU | Relative Fluorescent Unit |
| ROC | Receiver Operating Characteristic |
| RPM | Revolutions Per Minute |
| RT | Room Temperature |
| SD | Standard Deviation |
| STRING | Search Tool for the Retrieval of Interacting Genes/Proteins |
| TLS | Tertiary Lymphoid Structure |
| TME | Tumour Microenvironment |
| Treg | Regulatory T Cell |

# CHAPTER 1

# INTRODUCTION

## *1.1 Prostate Cancer Epidemiology*

Prostate cancer is the second-most frequently diagnosed cancer and fifth-leading cause of cancer-related deaths among males worldwide. GLOBOCAN estimates recently reported 1,276,106 new cases and 358,999 fatalities during 2018 Bray et al (2018). Incidence and mortality rates vary widely between countries and ethnic populations. Countries of high incidence include Australia, New Zealand, Northern and Western Europe, and Northern America, whereas in countries constituting Asia, incidence is significantly lower. Such variability could be explained by differences in genetic susceptibility, exposure to unknown risk factors, or differences in health care systems (e.g. cancer registration protocols) Grönberg (2003). Globally, incidence of prostate cancer is predicted to steadily increase as the average life expectancy rises and screening tools become more prevalent Pishgar et al (2018).

Thus far, few well-established risk factors exist pertaining to prostate cancer. These include advanced age, genetic susceptibility, ethnicity and familial history Menegoz et al (1994). Prostate cancer has the highest established age-incidence curve among all cancer types, with both incidence and mortality increasing at an almost exponential rate after the age of 50 Pienta (1993). Autopsy studies show that most men older than 85 years of age have undiagnosed histological prostate cancer Sakr et al (1993). Concerning race, men of African American descent have a higher disposition towards developing prostate cancer and a far higher mortality rate in contrast to Hispanic and Caucasian men, though demographic factors do play a role (e.g., access to health care, poor lifestyle choices). Moreover, the risk of prostate cancer development for men with first-degree relatives that have the disease is nearly double Cuzick et al (2014). Genetic susceptibility can result from rare, high penetrant

mutations, genetic variants, or a combination of the two, though known prostate cancer-associated genes explain only 35% of familial risk.

prostate cancer is generally indolent in nature (besides from some rare, aggressive phenotypes) and upon early intervention is highly curable. In developed countries, approximately 90% of prostate cancer cases are identified prior to malignant transformation. In addition, the 5-year survival rate for localised and regional prostate cancer is almost 100%. Moreover, the 10-year survival rate for local, regional, and distant prostate cancer combined is around 98%.

Although prostate cancer screening has led to a reduction in advanced disease and mortality, its implementation has resulted in a consequential increase in patient overdiagnoses, and hence overtreatment Esserman et al (2014); Loeb et al (2014).

Due to the poor prognostic outlook associated with late-stage prostate cancer, early detection and intervention is critical in reducing morbidity and mortality. Current treatment options depend on the extent of disease and include active surveillance (low-risk cancer: small, slow growing, unlikely to spread), watchful waiting (monitoring of Prostate-Specific Antigen (PSA) levels), surgery (radical prostatectomy), radiotherapy and/or androgen deprivation therapy (combination hormone therapy). From the current literature, areas requiring urgent attention include validated diagnostic biomarkers to complement PSA for more sensitive screening and prognostic biomarkers Attard et al (2016). In this study, we will be specifically addressing the discovery of novel diagnostic and prognostic biomarkers using circulating tumour antigen-specific autoantibodies.

### *1.2 Current Detection Methods for Prostate Cancer*

Current prostate cancer screening approaches include a blood-based test that measures circulating levels of PSA, with above-normal levels being indicative of disease Filella & Foj

(2015). However, major controversy still exists pertaining to its overall diagnostic accuracy and reliability Rao et al (2008). Namely, elevated PSA levels are not necessarily indicative of prostate cancer, as these may also be caused by benign prostatic hyperplasia, age, prostatitis and urinary tract infections Filella & Foj (2015). This often leads to overdiagnoses, overtreatment and unnecessary patient discomfort Ilic et al (2013). In addition to benign conditions, overdiagnosis also occurs with indolent prostate cancers that are incapable of causing harm within a patient's lifetime. Despite the primarily indolent nature of prostate cancer, more than 90% of detected tumours are treated with radiation or surgery Esserman et al. (2014). Unnecessary medical interventions (e.g. radical prostatectomy, androgen deprivation therapy) of indolent disease poses risks and may lead to the development of life-long morbidities (e.g. sexual, urinary, gastrointestinal) Loeb et al. (2014). Moreover, overdiagnosis and overtreatment of prostate cancer presents an enormous burden on healthcare expenditure Krahn et al (2010).

PSA levels lack reliability when distinguishing aggressive phenotypes from those that are indolent. Furthermore, little evidence suggests that routine PSA screening reduces overall patient mortality rates Ilic et al. (2013), despite remaining the best first line method for prostate cancer diagnosis Artibani (2012). This emphasises the need for more robust and accurate diagnostic and prognostic biomarkers, thereby allowing effective patient management strategies to be implemented Cuzick et al. (2014).

To overcome the limitations of PSA screens, these are usually combined with a digital rectal exam, particularly if PSA levels are highly elevated, rising consistently over time, or accompanied by physical symptoms Cuzick et al. (2014). Prostate cancer diagnosis can be confirmed using transrectal or transperineal ultrasound-guided tissue biopsies, that albeit effective, may result in post-surgical infections Guo et al (2015). Incorrect tumour sampling can also occur, leading to false negative results. Recently, magnetic resonance imaging

(MRI) has shown potential in surpassing the issues with systematic ultrasound-guided biopsies Marks et al (2013).

Once resected, disease severity is generally classified using the Gleason Score system based on histopathologic tumour features Sadi (2017). Due to tumour heterogeneity, two scores are stipulated per tumour for each of their predominant heterogenic aspects Sadi (2017). Final Gleason Score grades therefore range from 2(1+1) to 10(5+5), with higher scores representing significant differentiation of the tumour and hence a greater chance of developing metastases and poor patient prognosis Sadi (2017). Genomic tests are currently being investigated that could aid determination of patient prognosis and improve predictions regarding likelihood of therapeutic response Boström et al (2015).

## *1.3 Prostate Cancer*

### *1.3.1 Brief Overview of the Hallmarks of Cancer*

Oncogenesis is a complex multi-step process that is defined by the transition of normal human cells into cancer cells. Past research suggests that there are six essential alterations in cell physiology that simultaneously bring about cellular malignancy (Hanahan & Weinberg, 2000). These core hallmarks of cancer are a result of genome instability and mutation. Such alterations consist:

1. Self-sufficiency in growth signals
2. Insensitivity to growth-inhibitory signals
3. Evasion of programmed cell death
4. Limitless reproductive potential
5. Sustained angiogenesis
6. Tissue invasion and metastasis

Acquisition of the ability to generate mitogenic growth signals intracellularly, allows tumour cells to autonomously bind distinct classes of signalling molecules (i.e., diffusible

growth factors, extracellular matrix components, cell-to-cell adhesion molecules), and thus remain in an active proliferative state regardless of their tissue microenvironment. In addition, acquisition of the ability to evade antiproliferative signals (i.e., soluble growth inhibitors, immobilised extracellular matrix and cell surface inhibitors) allows tumour cells to remain in this autonomously induced active proliferative state. To continue to expand in population size, cellular attrition rates are also minimised by tumour cells. They achieve this by evading mechanisms of programmed-cell death. This system is employed in latent forms of nearly all cell types throughout the body, and broadly speaking, is facilitated by sensors (responsible for monitoring the intracellular and extracellular environments for abnormalities) and effectors (responsible for inducing cell death). Perturbances in these normal homeostatic mechanisms (e.g., mutations in the P53 tumour suppressor gene, a DNA damage sensor) result in resistance capabilities to apoptosis, and hence proliferation of tumour cells. While acquisition of growth signal autonomy, insensitivity to antigrowth signals, and resistance to apoptosis all lead to uncontrolled cell growth and proliferation, disruption of an intrinsic cell program limiting the number of times a cell can replicate, is also required to ensure expansive growth of a tumour growth. This immortality phenotype results from genetic mutations that essentially act to effectively maintain the cells chromosomal telomeres (e.g., upregulating expression of telomerase) and avoid their progressive shortening which would ultimately lead to cell death.

Another trait adapted by tumour cells is their ability to induce angiogenesis. They are able to do so by upregulating factors that exemplify angiogenesis-initiating signals (e.g., VEGF, FGF1/2), and/or downregulating endogenous factors that inhibit angiogenesis (e.g., thrombospondin-1, ß-interferon). This process leads to the growth of new blood vessels, and it is these blood vessels that provide the oxygen and nutrients critical for cell function and survival. Lack of angiogenic capabilities would ultimately restrict the expansion of aberrant proliferative lesions. Eventually, in most types of human cancer, primary tumours

will spawn cells capable of branching out and invading adjacent tissues, and therefrom travel to distant sites where they may potentially found new colonies. These distant settlements are better known as metastases. The genetic and biochemical determinants that govern the invasive and metastatic properties of cancer cells are extremely intricate and yet to be fully understood. That said, changes in the physical coupling of cells to their microenvironment (cell-cell adhesion molecules (CAMs) such as E-cadherin, and integrins), as well as regulation of extracellular proteases, are undoubtably necessary in the attainment of this capability (Hanahan & Weinberg, 2000; Hanahan & Weinberg, 2011).

Though an immense body of knowledge has been unveiled by focusing on cancer from a simplified perspective, a new focus has emerged whereby tumours are now being regarded as complex tissues in which mutant cancer cells have conscripted normal host cells and altered the surrounding microenvironment in order to coordinate success of their neoplastic development. It is this perspective that is now one of the main underlying factors when considering most cancer research (Hanahan & Weinberg, 2000; Hanahan & Weinberg, 2011).

### *1.3.2 The Tumour Microenvironment and Prostate Cancer*

Prostate cancer tissue is comprised of tumour cells, host cells and the components derived from each Roca et al (2017). Host components comprise of soluble factors (e.g., cytokines), the stromal matrix and cells. The host cells and their derivatives present within the tumour are termed the tumour microenvironment (TME). The cellular component of the TME consists of host cells initially present within the primary or metastatic lesion, and those that are recruited in response to either host or tumour-derived factors Roca et al. (2017). Host cells, with the inclusion of stromal cells, vasculature and immune cells, can essentially all contribute to the TME. Furthermore, the TME acts as a platform for tumour growth and evolution, ultimately influencing tumour progression. Thus, the interactions that exist between tumour cells and the TME orchestrate evolution of both the tumour and the TME

Roca et al. (2017). Not only can these interactions influence tumour development, but also those that are facilitated directly by the immune system.

A vital function of the immune system is to detect and eliminate pre-cancerous cells prior to their malignant transformation Da Gama Duarte et al (2018b). Such processes facilitating the surveillance and elimination of pre-cancerous cells are mediated by highly specialised immune effectors cells, molecules and signalling pathways, which vary depending on tissue type Swann & Smyth (2007). Failure of immunosurveillance mechanisms or incomplete elimination of persistent pre-cancerous cells can result in chronic inflammation, whereby the residual pre-cancerous cells act as chronic inflammatory stimuli. Pre-cancerous cells that avoid elimination bring about a bi-directional relationship between tumour progression and anti-tumour responses Dunn et al (2004). During this time, it is believed that pre-cancerous cells either exhibit dormancy or undergo evolutionary changes that modulate the molecular structure and/or function of their stress-induced, tumour-associated antigens Swann & Smyth (2007). While in this state, the immune system exerts selective pressures by eliminating susceptible tumour cells where possible. This process inadvertently selects for tumour cell variants capable of avoiding, resisting or suppressing anti-tumour immune responses. The immune system is then rendered incapable of containing the tumour at which point the tumour is free to grow progressively Dunn et al (2002). This fundamental process is known as immunoediting and has been thoroughly reviewed in recent literature Da Gama Duarte et al. (2018b).

### *1.3.3 Unique and Shared Antigens*

There are two key types of tumour antigens that are expressed by tumour cells: *unique* antigens and *shared* antigens. Unique antigens are specific to tumour cells, absent from normal host cells and generally arise from mutations in ubiquitously expressed genes, forming neoantigens. Shared antigens are tumour-associated antigens that are expressed by normal host cells as well as tumour cells, albeit slightly modified or at higher frequencies

and in ectopic locations. Shared antigens can be further sub-divided into three categories: 1) *Tumour-specific antigens* that exhibit restricted normal expression, but are aberrantly expressed in tumours, 2) *Differentiation antigens* that are expressed on non-malignant cells prior to the occurrence of malignancy, and 3) *Overexpressed antigens* that are expressed by normal cells but overexpressed by tumour cells Vigneron (2015).

Cancer-Testis (CT) antigens are a family of >90 shared tumour-specific antigens that are typically expressed in germ cells of the adult testis, ovaries and placental trophoblast cells, but are also aberrantly expressed by somatic tissue in a variety of cancers Simpson et al (2005). This aberrant expression occurs during tumourigenesis due to complex mechanisms involved in gene regulation. Such antigens are naturally produced in the immune-privileged site of the testis, and thus expression elsewhere (i.e., somatic tissue) triggers a spontaneous immune response. CT antigens are known to be expressed in a range of cancer types, but no single CT antigen can be directly linked with a particular type of cancer Scanlan et al (2002). That said, it remains feasible that correlations between multiple CT antigens and/or other unique or shared antigens could be indicative of a specific cancer types, or hold value in detecting disease onset or progression Scanlan et al. (2002). Their strong immunogenicity has promoted much research based around their exploitation for anticancer vaccines, and their potential use as diagnostic biomarkers continues to be unveiled Whitehurst (2014).

The immune system monitors and regulates the homeostasis of human tissue by mounting immune responses against foreign pathogens, substances, and host abnormalities (e.g. cancer), while concomitantly maintaining tolerance towards self-antigens De Visser et al (2006). Development of cancer cells is acquired by two distinct *enabling characteristics*: genomic instability, and hence mutability that endows cancer cells with genetic alterations driving tumourigenesis, as well as an innate immune cell-mediated induction of local inflammation and corresponding pro-tumoural consequences Hanahan & Weinberg (2011). Failure of the immune system to effectively detect and eliminate such cells prior to their

malignant transformation via immunosurveillance, can result in immunoediting and hence, tumour formation (Swann & Smyth, 2007).

### *1.3.4 Anti- and Pro-Tumoural Responses*

During manifestation of cancerous cells in cancerous tissue, both arms of the immune system (innate and adaptive) collectively orchestrate an inflammatory response that, once chronic, results in the upregulation of several immune pro-tumour effector mechanisms Disis (2010). This dynamic relationship between both sets of anti- and pro-tumoural mediators is complex and paradoxical in effect; essentially involving a constant tug-of-war between the tumour and hosts immune system, whereby the prevailing side is that which is dominated by an imbalance of either an anti-tumoural (i.e. tumour recognition, engagement and destruction) or pro-tumoural (i.e. tumour survival, proliferation and dissemination) response by immune cell subtypes, their derivatives and interactions, an immune-mediated chronic inflammatory environment, and the genomic instability and mutability gained by cancer cells, capable of generating genetic alterations which may drive tumour progression and enable immune evasion mechanisms Hanahan & Weinberg (2011).

Such pro-tumoural properties contribute to the development of the hallmarks of cancer and are primarily acquired through a combination of genetic instability, generally in combination with chronic inflammatory-mediated disturbances of the innate and adaptive (e.g. regulatory B and T cell-mediated suppression of immune response) arms of the immune system De Visser et al. (2006); Hanahan & Weinberg (2011). Such chronic perturbations of tissue homeostasis can disrupt the dynamic and interactive relationship that is coordinated by both the innate and adaptive arms of the immune system De Visser et al. (2006).

## *1.4 Immune Landscape of Prostate Cancer*

### *1.4.1 B Cells and Autoantibodies as Diagnostic Biomarkers for Prostate Cancer*

Though the vast majority of past research regarding immune response to cancer has been T cell focused, recent evidence has surfaced highlighting the importance of B cells and antibodies in pro- and anti-tumoural immune responses within the TME and circulation Da Gama Duarte et al. (2018b). Moreover, B cells and antibodies have proven useful as diagnostic and prognostic markers for a variety of cancer types Da Gama Duarte et al (2018a). Antibodies in particular are attractive cancer biomarkers due to their molecular stability in serum, ease of extraction, presence in early stages of disease and extensive half-life in serum Zaenker et al (2016). Furthermore, the presence of B cell subsets in the TME may also provide potential prognostic value Fujii et al (2013); Woo et al (2014).

B cells are fundamental in the humoral immune component of the adaptive immune system, known widely for their ability to produce antibodies Gorosito Serrán et al (2015). They may also act as antigen-presenting cells, secrete cytokines, and facilitate interaction by surface co-stimulatory/inhibitory molecules. Thus, these immune cells may act as drivers of both innate and adaptive immunity Gorosito Serrán et al. (2015). Furthermore, a subtype known as regulatory B cells (Bregs) are a heterogeneous population of B cells that function to directly/indirectly supress chronic inflammatory responses caused by cancer, and thus contribute to tumour progression Gorosito Serrán et al. (2015).

B cell implications in both pro- and anti-tumour responses influenced by dynamic sub-population balance has been recently outlined He et al (2014), though little understanding has been achieved pertaining to exactly how and why this occurs. This is largely due to current research focused on mapping B cell infiltrates using pan-B cell markers in contrast to markers capable of identifying terminally differentiated antibody-secreting B cells (e.g. plasmablasts or plasma cells) Da Gama Duarte et al. (2018a). As a result of inadequate B cell phenotyping, correlation of a B cell infiltrate with clinical features or patient outcomes are

yet to yield consistent findings Flammiger et al (2012); Fujii et al. (2013); Woo et al. (2014). As such, the complete characterization of B cell subsets in the TME of prostate cancers remains to be investigated and may be of prognostic value Da Gama Duarte et al. (2018a).

Antibodies are large, heavy plasma glycoproteins produced by antibody-secreting B cells (ASCs), specifically plasmablast (short-lived, proliferative) and plasma cell (short- or long-lived, non-proliferative) subsets, in response to an immune stimulus. B cell activation and maturation is facilitated by B cell receptor interaction with an antigen supplied by an antigen-presenting cell, which is internalised and displayed via major histocompatibility complex class 2 (MHC-II), followed by interactions with pre-activated cognate $CD4^+$ helper T cells Cyster (1999); Garside et al (1998).

Activation of the humoural immune system results in the secretion of these highly variable and specific proteins that mediate functions such as neutralisation, agglutination, fixation with activation of complement, and activation of effector cells targeted towards foreign biological material Gundem et al (2015). This adaptive immune response occurs through binding between produced antibodies and their cognate antigens. Autoantibodies, while fundamentally similar to antibodies, are produced via stimulation of autologous cell antigens. They are generally involved in autoimmune diseases, though their production has also been established in response to tumourigenesis Zaenker et al. (2016). Furthermore, both antibodies (from unique antigens) and autoantibodies (from shared antigens) appear to play an important role in anti-tumoural immune responses.

As cancer involves the genetic mutation and proliferation of autologous cells and molecules, the exact causative mechanisms that influence autoantibody production in response to tumourigenesis remain somewhat elusive, though major theories have been established in recent literature. Such mechanisms include tolerance defects and inflammation, altered antigen structure, cellular death mechanisms and, alterations to TAA expression Zaenker & Ziman (2013) (see **Figure 1**).

*Tolerance defects and inflammation* resulting in autoantibody production include defects in clonal selection, down regulation of regulatory T cells (Tregs) and abnormal expression of intracellular antigens in the inflammatory TME Carl et al (2005). Tregs modulate the immune system by supressing effector T cells via both receptor-mediated interaction and release of soluble factors (i.e. cytokines and chemokines), and are key mediators of self-tolerance Kim et al (2010). Downregulation of Tregs has been correlated with high titres of autoantibodies in the TME leading to delayed tumour growth Kim et al. (2010). In contrast, upregulation of Tregs is seen to decrease autoantibody titres in the TME and hence promote tumour progression Zaenker et al. (2016). Additionally, *cell death mechanisms* (i.e. apoptosis, necrosis, and autophagy) resulting in aberrant release of autologous intracellular tumour content containing shared antigens into the blood, can effectively elicit the production of cognate autoantibodies Peter et al (2010); Tan & Zhang (2008). Furthermore, *alterations to shared antigen expression*, such as expression in aberrant locations (e.g. CT expression in somatic tissue) or overexpression (e.g. PSA overexpression in prostate tissue) play a role in facilitating an auto-immune response, and can lead to autoantibody production Watanabe et al (2000). Lastly, *altered unique antigen structures* resulting from neoepitope exposure from mutations that alter antigen conformation, and/or post-translational modifications (e.g. glycosylation, methylation etc.) have been shown to elicit immunological responses in cancer patients, including antibody production Liu et al (2012).

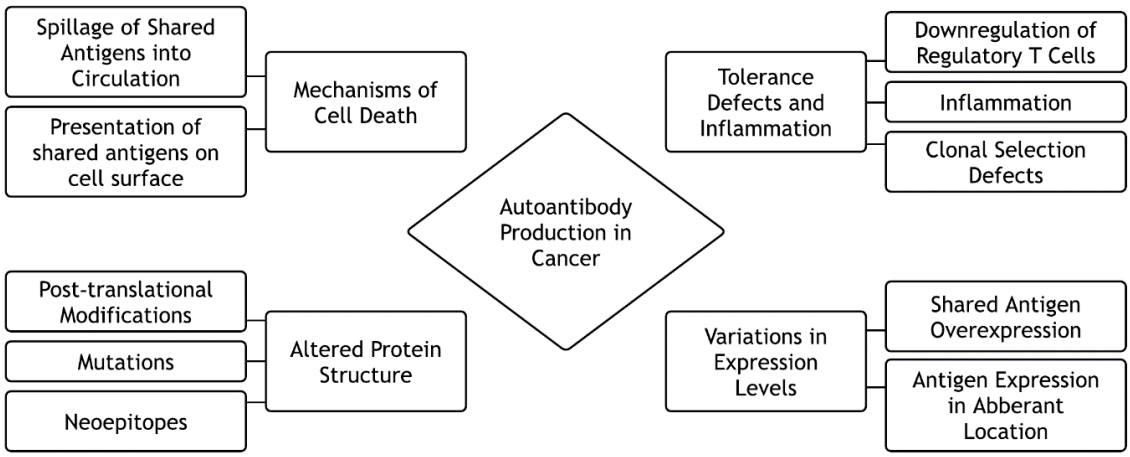


***Figure 1. Proposed causes of autoantibody production in cancer.*** *The four main causes of autoantibody production in cancer; mechanisms of cell death, tolerance defects and inflammation, altered protein structure, and variation in expression levels. Image adapted from* Zaenker et al. (2016).

Circulating autoantibodies can be measured using various techniques, predominantly among them being enzyme-linked immunosorbent assay (ELISA) and protein microarrays. ELISA techniques tend to lack sensitivity and multiplexing capacity, albeit simple to prepare Da Gama Duarte et al. (2018a). The high-throughput, multiplexing capacity of protein microarrays in conjunction with their ability to achieve high-specificity and minimal non-specific binding when optimised, makes them more versatile as screening tools for cancer biomarkers Da Gama Duarte et al. (2018a).

### *1.4.2 Tertiary Lymphoid Structures in Prostate Cancer*

Tertiary lymphoid structures (TLSs) are ectopic, specialised lymphoid aggregates that develop at sites of chronic inflammation Dieu-Nosjean et al (2014). In the context of cancer, their presence in the vicinity of many solid tumours for certain cancer types has been correlated with favourable patient outcomes Dieu-Nosjean et al (2016). As the name suggests, TLSs are lymph node-like structures that, when fully-formed and functional, exhibit all characteristics observed in an effective, adaptive immune response (e.g. antibody secretion and T cell-mediated cytotoxicity) Dieu-Nosjean et al. (2014). A functional TLS consists of a

marginal T cell zone containing mature dendritic cells (DC) adjacent to a B cell zone containing a germinal centre defined by a follicular dendritic cell (FDC) network, and localised high endothelial venules (HEVs) enabling extravasation of immune cells to the site of solid tumours Dieu-Nosjean et al. (2014). Presence of all features enable the proliferation, activation and maturation of B cells, leading to the development of antibody-secreting cells that are capable of tumour antigen-triggered cognate autoantibody production. Tertiary lymphoid structures are yet to be clearly detailed in a prostate cancer setting.

As the main function of these tertiary lymphoid structures is to provide a localised factory for antigen sampling, B cell activation, proliferation and ultimately differentiation of B cells into antibody-secreting cells (i.e., plasmablasts, plasma cells), one would assume that they play an anti-tumoural role in the TME of most cancers. The truth is, in the context of prostate cancer, the exact type of effect (i.e., anti- or pro-tumoural) and magnitude of impact that these structures exert is largely unknown. The presence of B cells themselves have been considered to be fairly reliable as predictors of patient survival and favourable outcomes, but many reports have surfaced regarding both anti- and pro-tumoural roles that they may play in the TME Shalapour et al (2014).

Moreover, it is believed that B cell localisation in either immature or mature TLSs play varying roles in either promoting or suppressing the immune system's ability to kill tumour cells (see **Figure 2**). It has been hypothesised that B cells situated within poorly structured, immature TLSs (**a**) secrete inhibitory factors that dampen the response of other local immune cell, or molecules present of the surface of B cells that hinder the targeting and destruction of tumour cells. This is thought to be a result of relatively limited B cell interaction with T cells, and instead more interaction with the tumour itself. This has been indirectly shown in multiple recent studies Cabrita et al (2020); Helmink et al (2020); Petitprez et al (2020). Alternatively, these studies also show that B cells situated within well-

structured, mature TLSs (**b**) can release antibodies and present antigens to T cells in the tumour, activating them. B cell abundance within mature TLSs has been correlated with increased T cell activity, tumour targeting and destruction, and tumour response to immunotherapy Cabrita et al. (2020); Helmink et al. (2020); Petitprez et al. (2020).

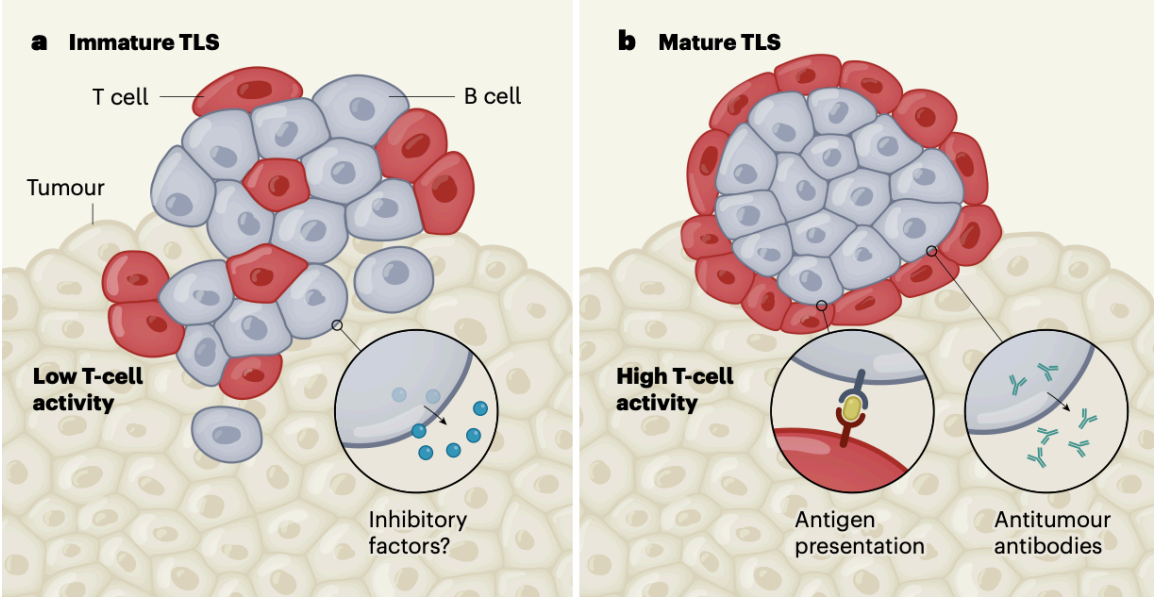


***Figure 2. Varying B cell roles in tertiary lymphoid structures present within the tumour microenvironment*** Bruno (2020)***.*** *(**a**) Immature TLS with B cells secreting inhibitory factors that suppress the immune systems activity, likely resulting from increased interaction with the tumour. (**b**) Mature TLS with B cells producing / secreting antibodies and engaging in presentation of tumour antigens to T cells.*

### *1.5 Cancer-Specific Protein Microarray*

Recent research has resulted in the development of a readily customisable cancer-specific protein microarray platform in conjunction with robust bioinformatics tools, capable of quantifying patient serum autoantibody profiles to 100 CT antigens in the pg/mL range Beeton-Kempen et al (2014). The study conducted by Beeton-Kempen *et al.* investigated the potential of using a CT antigen microarray to quantify shared tumour antigen-specific autoantibody profiles from melanoma patient sera. Through exploitation of the strong

affinity between shared tumour-specific antigens and their cognate autoantibodies, linearity of response and minimal non-specific binding was achieved. In addition, healthy individuals yielded no detectable autoantibodies, thus highlighting the specificity of this tool to cancer. The high specificity and sensitivity of this array may facilitate the discovery of novel cancer biomarkers, thereby potentially enabling pre-symptomatic cancer detection.

The custom array used in this project consists of an expanded version of the above CT antigen array and contains 123 tumour-specific and associated antigens of interest. Quantification of patient autoantibody profiles to CT antigens could theoretically distinguish between cancer types and provide insight into disease progression Beeton-Kempen et al. (2014). Preliminary data using this array on a cohort of 20 prostate cancer patients from a South African cohort showed that it can be used to identify potential diagnostic biomarkers with high sensitivity, while distinguishing prostate cancer from benign prostate hyperplasia and healthy individuals Adeola et al (2016). Promising tumour antigens identified included GAGE1, ROPN1, SPANXA1 and PRKCZ. Others have also investigated candidate shared tumour-specific antigens for prostate cancer via the detection of cognate autoantibodies in an ELISA or protein microarray–based assay format, and identified additional promising CT antigens (NY-ESO-1, SSX2, SSX4 and XAGE1B), all which are included in the custom array used in this study O'Rourke et al (2012); Wang et al (2005); Xie et al (2011). As such, this array will provide a suitable means to validate the above findings using a large adequately powered prostate cancer patient Australian cohort.

### *1.6 Aims and Hypotheses*

Aims:

1) Screen retrospective serum samples from 54 low-grade and 56 high-grade prostate cancer patients for the presence of autoantibodies against cognate tumour-specific antigens using a customised tumour antigen microarray (Discovery Cohort);
2) Validate array-based findings using a separate cohort of 50 low-grade and 49 high-grade prostate cancer patients (Validation Cohort);
3) Investigate prostatectomy specimens from 64 matched discovery cohort patients for the presence of antibody-secreting cells and tertiary-lymphoid structures using novel fluorescence multispectral immunohistochemistry panels.
4) Compare these findings with available clinical characteristics (i.e., PSA levels, Gleason scores, PSA biochemical recurrence, and overall survival, where applicable).

Hypotheses:

- Circulating tumour autoantibodies can be used in combination with conventional PSA testing to increase sensitivity and specificity of prostate cancer detection.
- Circulating tumour autoantibodies can be used to distinguish patients with indolent diseases from those with aggressive forms of prostate cancer.
- Detectable circulating tumour autoantibodies reflect the presence of antibody-secreting cells in the tumour microenvironment.
- Tertiary Lymphoid Structures are present in prostate cancer tumours and responsible for the local production of antibody-secreting cells in the tumour microenvironment.

# CHAPTER 2

# MATERIALS AND METHODS

## *2.1 Sample Size and Statistical Justification*

*A priori* size-power calculations determined that a minimum sample size of 54 patients was recommended per patient group (i.e. G*Power 3.1.9.7 program, T-test, difference between two dependent means [matched pairs]) with a given probability of error ($\alpha$=0.05), power (1-$\beta$=0.95) and effect size (dz=0.5) (Faul et al., 2007). Hence, 54 low-grade and 54 high-grade patients in each patient cohort would ensure that the study resulted in findings with 95% statistical power. Furthermore, novel biomarker regulations require the use of separate discovery and validation cohorts to ensure clinical applicability of findings.

The prostate cancer patient samples used in this study were obtained via the Australian Prostate Cancer BioResource (APCB) and the Victorian Cancer Biobank (VCB). Full ethical approval for this study was granted by La Trobe University, Melbourne, Australia (HEC19147).

From APCB, our discovery cohort included serum samples (n=110) from 54 low-grade and 56 high-grade prostate cancer patients determined via Gleason score. In conjunction, complete clinical information, including PSA levels, Gleason scores, BPH status, PSA biochemical recurrence and overall survival was also provided. A single haematoxylin and eosin (H&E) stained slide and 7 unstained sequential Formalin-Fixed Paraffin-Embedded (FFPE) prostatectomy tissue sections were obtained from 64 of the above patients. Serum samples and PSA levels from 14 age- and gender-matched healthy individuals were also obtained.

From VCB, our validation cohort included serum samples (n=99) from 50 low-grade and 49 high-grade prostate cancer patients also determined via Gleason score. This is slightly

below the recommended cohort sample size, but still ensures a statistical power of 93% (*post hoc* analysis). PSA values, Gleason scores, and benign conditions of the prostate were provided for each patient. Serum samples were obtained from 6 age- and gender-matched healthy individuals. FFPE prostate tissue sections were obtained from 5 bladder cancer patients presenting with clinically normal prostates. In addition, serum samples were obtained from 13 individuals with benign conditions of the prostate. FFPE prostate biopsy tissue sections were obtained from 16 individuals with benign prostate hyperplasia, 3 of which included matched serum.

### *2.2 CT100$^+$ Protein Microarray Fabrication*

CT100+ protein microarrays were prepared by Dr. Jessica Duarte, as described previously (Beeton-Kempen et al., 2014). Briefly, crude insect lysates of 123 tumour antigens (see **Table 1**) were diluted in printing buffer at a 1:1 ratio (1x PBS, 20% sucrose) and 40µL of the diluted crude protein extract for each BCCP-myc tagged protein was transferred to individual wells of a 384-well plate. Residual cell debris was pelleted via plate centrifugation at 1000 x *g* for 2 minutes at 4ºC and kept at 4ºC until, and during each microarray print run. Thawed streptavidin-coated microarray slides were printed with four identical CT100$^+$ arrays using a QArray2 robotic arrayer (Genetix®) equipped with 8 x 300µm flat-tipped solid pins. Arrays were printed in eight grids of 8 x 8 spots with ample spot-to-spot spacing of 562µm, allowing for all 123 tumour antigens, negative (BCCP-myc, ICL, buffer) and positive (biotinylated Cy3- BSA at 5, 10 and 15ng/µL, human IgG at 10ng/µL and anti-human IgG at 100ng/µL) controls to be printed in triplicate within each array field, as per the array layout **(Figure 3**).

***Table 1. List of the 123 tumour antigens included on the CT100$^{+}$ array.***

| ID | Name | ID | Name | ID | Name | ID | Name | ID | Name |
|---|---|---|---|---|---|---|---|---|---|
| **001** | BAGE2 | **026** | LEMD1 | **051** | SGY-1 | **076** | CDK7 | **101** | 5T4/TPBG |
| **002** | BAGE3 | **027** | LIP1 | **052** | SILV | **077** | FES | **102** | XAGE1B |
| **003** | BAGE4 | **028** | MAGEA1 | **053** | SPAG9 | **078** | FGFR2 | **103** | SOX2 |
| **004** | BAGE5 | **029** | MAGEA10 | **054** | SPANXA1 | **079** | MAPK1 | **104** | ACVR2A |
| **005** | CCDC33 | **030** | MAGEA11 | **055** | SPANXB1 | **080** | MAPK3 | **105** | ACVR2B |
| **006** | CEP290 | **031** | MAGEA2 | **056** | SPANXC | **081** | PRKCZ | **106** | ITGB1 |
| **007** | COL6A1 | **032** | MAGEA3 | **057** | SPANXD | **082** | RAF | **107** | MAP9 |
| **008** | COX6B2 | **033** | MAGEA4v2 | **058** | SPO11 | **083** | SRC | **108** | PIM1 |
| **009** | CSAG2 | **034** | MAGEA4v3 | **059** | SSX1 | **084** | CALM1 | **109** | TKTL1 |
| **010** | CT47.11 | **035** | MAGEA4v4 | **060** | SSX2A | **085** | CDC25A | **110** | SPATS1 |
| **011** | CT62 | **036** | MAGEA5 | **061** | SSX4 | **086** | CREB1 | **111** | DPPA2 |
| **012** | CTAG2 | **037** | MAGEB1 | **062** | SYCE1 | **087** | CTNNB1 | **112** | SOX1 |
| **013** | CXorf48.1 | **038** | MAGEB5 | **063** | SYCP1 | **088** | TP53 | **113** | ROPN1A |
| **014** | DDX53 | **039** | MAGEB6 | **064** | THEG | **089** | ZBTB7B | **114** | CEACAM |
| **015** | DSCR8 | **040** | MART-1 | **065** | TPTE | **090** | PRKCH | **115** | POU5F1 |
| **016** | FTHL17 | **041** | MICA | **066** | TSGA10 | **091** | PCTK1 | **116** | NANOG |
| **017** | GAGE1 | **042** | NLRP4 | **067** | TSSK6 | **092** | PQBP1 | **117** | BORIS B0 |
| **018** | GAGE2A | **043** | NXF2 | **068** | TYR | **093** | UBE2V1 | **118** | DPPA4 |
| **019** | GAGE4 | **044** | NY-CO-45 | **069** | XAGE-2 | **094** | IRF4 | **119** | DPPA3 |
| **020** | GAGE5 | **045** | NY-ESO-1 | **070** | XAGE3av1 | **095** | MAPK8_tv2 | **120** | GDF3 |
| **021** | GAGE6 | **046** | OIP5 | **071** | XAGE3av2 | **096** | MSN | **121** | LAGE-1b |
| **022** | GAGE7 | **047** | p53 | **072** | ZNF165 | **097** | TPM1 | **122** | CAMEL |
| **023** | GRWD1 | **048** | PBK | **073** | AKT1 | **098** | CYP450 | **123** | NY-ESO-1 |
| **024** | HORMAD1 | **049** | RELT | **074** | CDK2 | **099** | CYP450 red | | |
| **025** | LDHC | **050** | ROPN1 | **075** | CDK4 | **100** | EGFR | | |

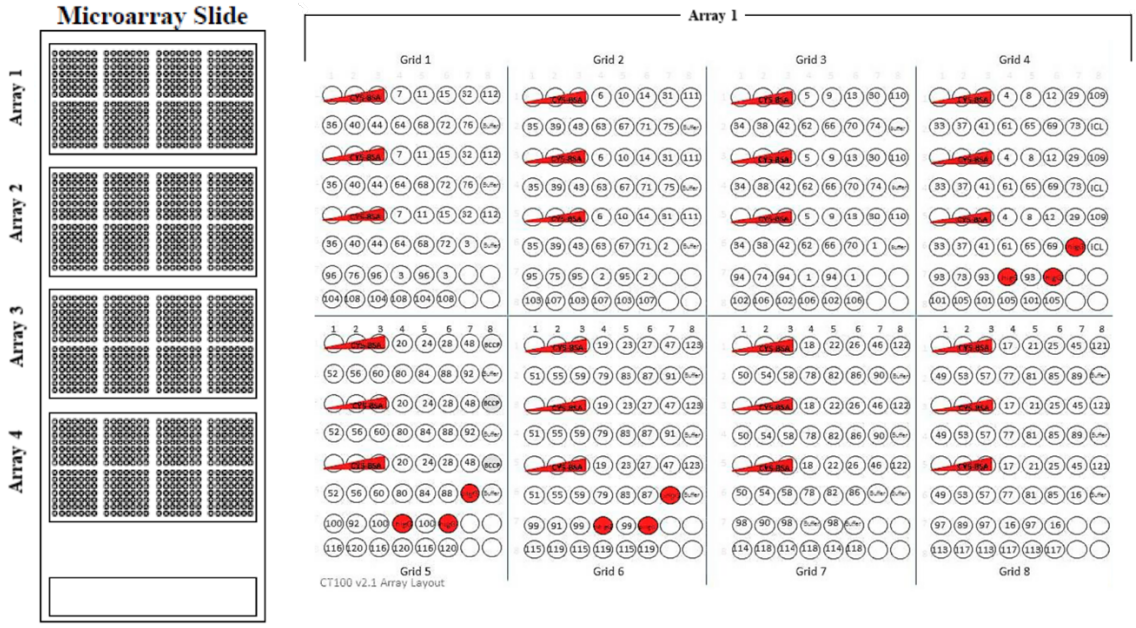


***Figure 3. CT100+ protein microarray layout.*** *The printing layout of four replicate arrays on each glass slide is depicted on the left. Each of the four arrays are direct replicates and the layout is depicted on right with BSA controls shown as circles with increasing red volume (5, 10 and 15ng/µL) and hIgG (grid 4 & 5) / αhIgG (grid 6) controls shown as complete red circles. All other circles in the array are triplicates of immobilised antigens and their respective numbers can be referred to the antigen list described above (**Table 1**).*

## *2.3 CT100+ Protein Microarray Assay*

### *2.3.1 Determination of Optimal Patient Serum Concentration*

Prior to assaying patient samples, an optimal patient serum concentration was determined. In order to obtain the most optimal signal-to-noise ratio, a single patient sample with a known positive autoantibody profile was assayed on CT100+ arrays at four dilutions (1:800, 1:400, 1:200, 1:100 serum dilutions in PBST). The optimal sample dilution was selected based on detectable autoantibody levels well above background noise.

### *2.3.2 CT100+ Protein Microarray Quality Control Assays*

In order to ensure that each microarray print run met a pre-determined set of quality standards, quality control assays were performed per print run prior to assaying prostate cancer patient samples.

#### *2.3.2.1 Validation of Immobilised BCCP-tagged Proteins to Array Surface*

A c-Myc assay was conducted per individual print run to confirm that all antigens were successfully immobilised on the array surface. A single array was incubated with 300µL of 13µg/ml monoclonal Cy3-anti-c-Myc goat antibody (Sigma, 1.3mg/mL, #C6594; 1:100 dilution in PBST) for 1 hour at RT on an orbital shaker (20-40 rpm). The arrays were scanned at Cy3 to enable the detection of all c-Myc-tagged tumour antigens and Cy3-biotin-BSA control spots, and hence confirm their presence. The resultant data was extracted and processed using Microsoft Excel.

#### *2.3.2.2 Validation of CT100$^+$ Microarray Specificity for Cancer*

In order to validate the specificity of the CT100$^+$ array for cancer, two control groups (i.e., healthy and cancer) were assayed per print run. The healthy donor (HD) group consisted of 14 age- and gender-matched donors, ensuring all utilised antigens were in fact cancer-specific. The cancer patient control consisted of a prostate cancer patient (ONJCRI#50035) with known signals for NY-ESO-1 and CTAG2.

Both assays were conducted as patient serum assays and were anticipated to show either cancer antibody signals or no cancer antibody signals for the cancer and HD control groups, respectively. The resultant data was extracted and processed using Microsoft Excel.

### *2.3.3 Patient Serum Assays*

CT100$^+$ printed microarray slides were thawed for 1 hour at RT, blocked (50mM KCl, 20% glycerol, 0.1% Triton X-100, 25mM HEPES pH 7.5, 50µM biotin in $dH_2O$) for 1 hour on ice, washed thrice in PBST for 5 minutes each at RT on an orbital shaker (20-40 rpm), and

dried via centrifugation at 287 x *g* for 5 minutes at RT. Customised 4-plex gaskets (Grace Bio-Labs, Oregon, USA) were assembled over the slides and clips were applied to hold them in place. Patient serum dilutions of 1:100 were prepared in PBST and 400µL added to each array chamber, wrapped in foil and incubated at RT for 1 hour on an orbital shaker (20-40 rpm). Following sample incubation, each array chamber was washed thrice in 300µL PBST for 5 minutes each at RT on an orbital shaker (20-40 rpm). Array chambers were then subjected to 300µL of 20µg/ml polyclonal Cy5-anti-human IgG detection antibody (Invitrogen, Alex fluor™ 647/Cy5, 2mg/mL, #A21445; 1:100 dilution in PBST), wrapped in foil and incubated at RT for 1 hour on an orbital shaker (20-40 rpm). Following detection antibody incubation, the gaskets were disassembled, and the slides were washed thrice in PBST and once in $dH_2O$ for 5 minutes each at RT on an orbital shaker (20-40 rpm). Slides were then dried via centrifugation at 287 x *g* for 5 minutes at RT and stored in an appropriate dark slide container until scanning. A flowchart of this assay pipeline is indicated in **Figure 4**.

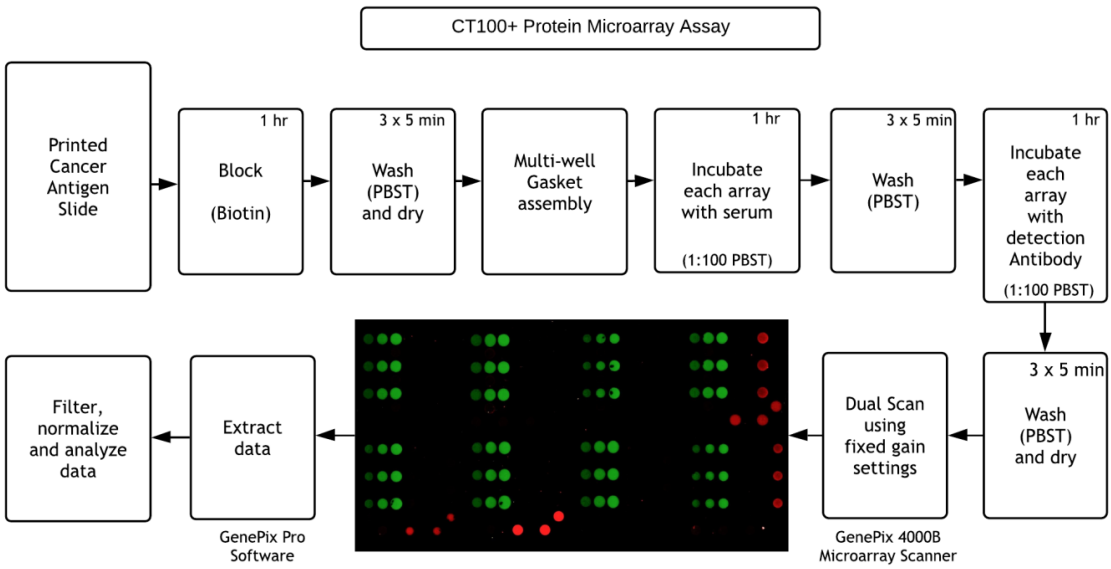


***Figure 4. Flowchart of CT100⁺ protein microarray assay.*** *Printed slides are blocked, assembled with a multi-well gasket, incubated with patient serum samples, and cognate antibodies detected using a fluorescently labelled anti-human IgG antibody. Slides are imaged using a fluorescent scanner and the resulting data is then extracted, processed and analysed.*

### *2.4 CT100+ Protein Microarray Scanning and Data Analysis*

The scanning of all slides was performed at Monash University using an on-site GenePix® 4000B microarray scanner.

#### *2.4.1 GenePix Pro Settings Files and Photomultiplier Tube Gain Optimisation*

In order for consistent array analysis to be performed between slides and batches, two file types were prepared and generated when using the GenePix Pro Software (i.e. .gps and .gal) and then routinely applied to all subsequent CT100+ protein microarray slides prior to scanning. The GenePix Settings (.gps) file contains designated acquisition settings (i.e., Photomultiplier tube (PMT) gain and scan area), analysis settings (i.e., identification and locations of blocks) and display settings (i.e., brightness and contrast settings). The PMT gain settings were defined by averaging the optimal values observed across three individual patient samples (1:100 dilution) with positive autoantibody profiles.

The GenePix Array List (.gal) file describes the number, position and size of each grid, the layout of spots within them, and the names, identities and annotations corresponding to each spot. These virtual parameters were set in accordance with the physical parameters used during the printing process (i.e., the physical distribution of the pins in the pinhead correlate with the virtual distribution of the spots within each grid, as well as their individual identities).

#### *2.4.2 Patient Array Scanning and Data Extraction*

All patient slides were dual (Cy3 and Cy5) scanned using a GenePix® 4000B microarray scanner. PMT gain settings were kept constant at 520 and 500 for the Cy5 and Cy3 lasers respectively, and a scan power of 100%. Prior to scanning, the GenePix Settings file was opened and integrated using GenePix Pro Version 4.0.0.54 to ensure that the settings were applied and remained constant amongst samples. Following scanning, the GenePix Array List file was opened and integrated, allowing automatic, and when required (e.g., as a result

of artefacts or spot merging), manual alignment of the grid and spot overlay to scanned images. Once effectively aligned, the resultant data from each array was extracted as text files. In addition, Tagged Image Format (TIF) and Joint Photographic Expert Group (JPEG) files of each slide were extracted at Cy3 and Cy5 wavelengths individually, as well as simultaneously for analysis.

### *2.4.3 Patient Array Data Processing and Analysis*

Extracted array data was imported to Microsoft Excel where the median relative fluorescent units (RFU) (raw florescent intensity minus the average local background) of all tumour antigens and control spots (including replicates) at both Cy3 and Cy5 wavelengths (i.e., F532 – B532, F635 – F635) was separated out from the original raw data file. For each set of three replicates, the average and standard deviation (SD) was calculated, and a coefficient of variation (CV) threshold was set at ≤20%. For triplicates with a CV value >20%, a replicate outlier was removed from analysis. The resultant averages of all triplicates or duplicates were then used for further analyses.

Noise thresholds were calculated for all patient and control arrays by adding the average background (i.e., B532 or B635) of all spots to 2x the average SD (i.e., B532 SD or B635 SD) of all spots. All autoantibody signals below this threshold were excluded from subsequent analyses.

Data analysis included detectable autoantibody and antigen specificity prevalence across patient cohorts, univariate and multivariate receiver-operating-characteristic curves (ROC) exploring the discriminative ability of candidate antigen signatures, protein-protein functional interaction networks (STRING), and correlation to clinical features (age, PSA levels, disease grade) and patient outcomes (PSA relapse and overall survival. Results were further compared to matched mRNA expression from an independent prostate cancer cohort accessible via the TCGA (CBIO), and protein expression in prostate cancer tissues accessible via the Human Protein Atlas.

### *2.5 Multispectral IHC Staining of Patient Prostatectomy Tissue*

In order to investigate the presence of B cells and antibody-secreting cells (ASCs) in prostate tumours, a 5-plex ASC panel containing anti-CD19, CD38, CD45 and CD138, with DAPI counterstaining, was performed on 64 formalin-fixed paraffin-embedded (FFPE) prostatectomy tissue specimens.

In addition, the presence of TLSs containing organized B and T cell zones with surrounding high endothelial venules were investigated using a 7-plex TLS panel containing anti-CD4, CD8, CD19, CD21, DC-LAMP and PNAd, with DAPI counterstaining, was performed on 64 FFPE prostatectomy tissue specimens.

All fluorescent mIHC staining (incl. optimisations and controls) was conducted using a BOND RX® Automated Research Stainer (Leica Biosystems, Newcastle, UK).

#### *2.5.1 Spectral Library Development*

For precise and comparable means of obtaining quantitative fluorescent data from multiplexed tissue samples, batch-specific spectral characteristics were determined for each fluorophore. Once defined, these spectral characteristics are used to accurately unmix images containing multiple fluorophores. This unmixing process allows crosstalk to be removed among markers that fluoresce at overlapping wavelengths, thus allowing markers to be distinctly examined, either individually or in combination.

To build these libraries for the ASC panel, Opal™ fluorophores (Opal 540, 570, 620 and 650) contained within each Opal™ IHC 50 slide kit (Cat# NEL821001KT, Perkin Elmer), were used to detect Human Leukocyte Antigen (HLA) 1 on HeLa cell lines. To build these libraries for the TLS panel, Opal™ fluorophores (Opal 520, 540, 570, 620, 650 and 690) contained within each Opal™ IHC 50 slide kit (Cat# NEL821001KT, Perkin Elmer), were used to detect Human Leukocyte Antigen (HLA) 1 on HeLa cell lines. The abundant expression of HLA on HeLa cell lines enabled inForm® to effectively extract each unique

spectral characteristic corresponding to each Opal fluorophore, used for subsequent unmixing of patient specimens.

### *2.5.2 Primary Antibody Optimisation*

Optimisation of individual primary antibodies was performed to determine the most effective concentration (i.e., highest signal-to-background ratio) for staining of prostate cancer tissue prior to integration into multiplexed assays. Antibodies were tested at three distinct concentrations across two heat-induced epitope retrieval (ER) pH conditions (pH 6.0 and 9.0) using marker-specific positive control FFPE healthy tissue. Starting concentrations were as recommended by each supplier and half-log (3.16-fold) serial dilutions were performed twice from that point onwards. Negative control tissues were included for comparison and confirmation of accurate staining, as well as tissue-specific autofluorescence controls.

### *2.5.3 Multiplex Optimisation*

Following primary antibody optimisation, the most effective multiplex stain order was determined using a range of both 5-plex (ASC panel), and 7-plex (TLS panel) stain order variants. Each variant involved different combinations of primary antibodies and Opal Fluorophores, as well as different orders to find that which clearly labelled each antibody and exhibited the highest resolution of signal-to-noise ratio. In conjunction, primary antibodies from each multiplex panel were applied, in a monoplex manner, to positive control tissue at their optimal concentrations to ensure successful staining alongside their involvement in multiplex panels. The multiplex protocol deemed most optimal, as per its ability to retain all signals following staining while maintaining a relatively high signal-to-noise ratio, was used for all patient mIHC assays.

### *2.5.4 Multiplex Staining of Patient Prostate Cancer Tissue*

The optimal mIHC protocols for each panel (ASC & TLS) were performed on all 64 patient tissue specimens using the Bond RX Automated Stainer. Slides were placed on slide trays,

labelled with printed barcodes corresponding to the protocol performed on each slide and cover-tiled accordingly. Slide trays were then placed into the Bond RX autostainer following addition of all required reagents (antibodies, buffers, dewax, etc.) and the automated staining process initiated. Positive control specimens were included per batch of patient slides, undergoing the same protocols to ensure all antibodies and fluorophores worked effectively.

Each specimen was first deparaffinised using Bond® Dewax Solution (Cat# AR9222, Leica Biosystems), followed by a 3% H2O2 (Cat# HA154-500M, Chem-Supply) treatment for peroxidase blocking purposes. Specimens then underwent sequential target staining through repetition of the following series of events: heat-induced epitope retrieval using Bond® Epitope Retrieval Solution (Leica Biosystems), blocking buffer (Product# ARD1001EA, PerkinElmer), primary antibody incubation, secondary antibody incubation (Opal® Polymer HRP, Product# ARH1001EA) and Opal fluorophore (PerkinElmer) incubation. After successful addition of all markers, slides were counterstained with Spectral DAPI (Product# FP1490, PerkinElmer). All wash phases were done using Bond® Wash Solution (Cat# AR9590) and deionised water. A flowchart of this assay pipeline is indicated in **Figure 5**. Following staining, all slides were coverslipped using VECTASHIELD® Hardset™ Antifade Mounting Solution (Cat# H-1400, Vector Laboratories), and left overnight in the dark.

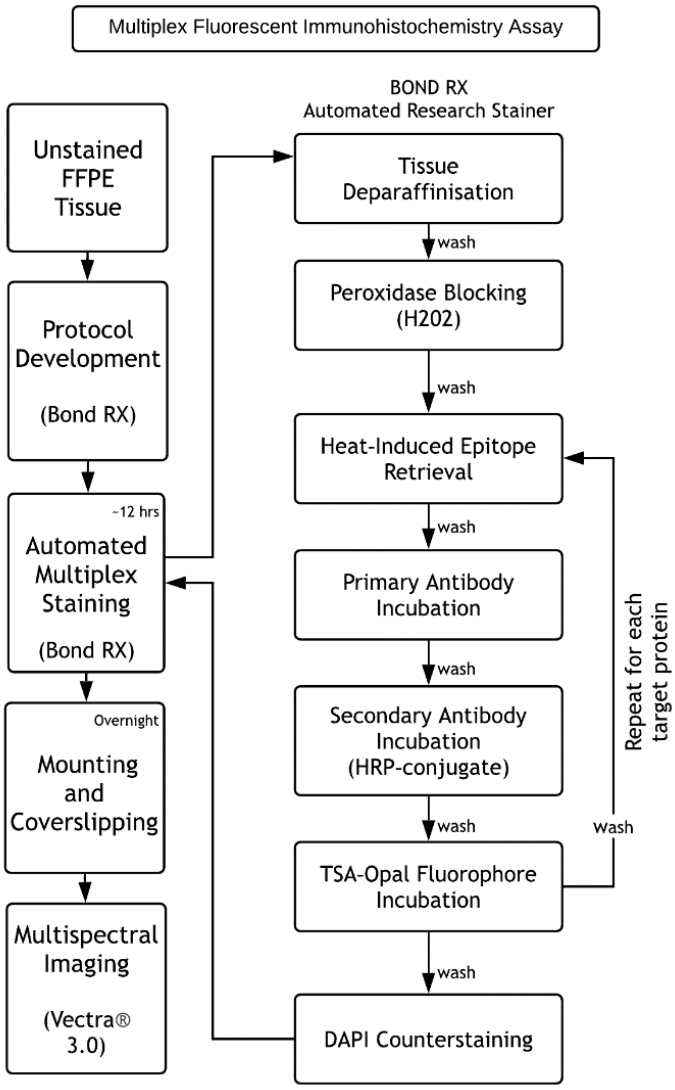


***Figure 5. Flowchart of multiplex fluorescent immunohistochemistry assay.*** *Unstained FFPE tissue is loaded into the Bond RX. A protocol is developed and then initiated. Each tissue section is deparaffinised, and endogenous peroxidases are quenched. Sequential rounds of staining follow, involving epitope retrieval(s), primary / secondary antibody incubation(s), and detection via desired fluorophore(s). Each section is counterstained with DAPI, mounted with appropriate solution, coverslipped and then imaged using the Vectra 3.0® Automated Multispectral Imaging System*

### *2.5.5 Vectra 3.0® Multispectral Imaging*

Following immunofluorescence staining, each sample was microscopically imaged using a Vectra 3.0® Automated Multispectral Imaging System (PerkinElmer, Massachusetts, US.). Exposure time settings were defined per specimen across five major channels (DAPI, FITC,

Cy3, Texas Red and Cy5) for optimal Whole Slide Scanning (10x) and Multispectral Imaging (20x). Once optimal exposure times had been set, slides were loaded into a slide cassette and processed for automated whole slide scanning. Following whole-slide scanning, regions of interest were selected using Phenochart™ whole slide viewer and captured using Vectra automated multispectral image (MSI) capture.

To accurately delineate areas of tumour tissue, a trained pathologist Dr. Louise Jackett (Austin Hospital Pathology) annotated sequential H&E slides for all prostate cancer and benign specimens used in the study (cut directly from the same tissue block).

### *2.5.6 InForm® Data Processing and Analysis*

All acquired high-resolution MSIs (20x mag.) generated from the Vectra® 3.0 fluorescence microscope were spectrally unmixed using the inForm® Cell Analysis software (PerkinElmer, Massachusetts, U.S.), using a pre-generated spectral library.

For the ASC panel, the software was trained to recognise various tissue segments including prostate glands (epithelial and basal cells), stroma and fibrous muscle by visually defining the respective areas with a drawing tool on, at minimum, 5 individual MSIs containing each tissue variety, prior to initiation of automated segmentation. As CD38 also stained prostate epithelium, CD138 stained basal cells, and DAPI counterstained cell nuclei, tissue segmentation training was effective. Following tissue segmentation, prostate epithelial and basal cells, all lymphocytes, B cells and ASCs were phenotyped using a similar training method. This method involved programming the software to identify cells based on individual or combined expression of their respective markers (CD38+ exclusively – prostate epithelium, CD138+ exclusively – basal cells, CD45+ exclusively – lymphocytes, CD19+CD45+ – B Cells, CD45+CD38+CD138- – plasmablasts, CD45+CD38+CD138+ – plasma cells). Cell phenotyping was achieved by specifying at minimum, 50 cells of each type manually before automatic phenotyping could be performed. Abundance of ASC counts were defined as follows: absent (0), scarce (1 to 20), abundant (20+). Abundance of

B cell aggregate (BCA) counts were defined as follows: absent (0), scarce (1 to 4), abundant (4+). Distance to tumour tissue was defined as intratumoural (IT) if within tumour regions and peritumoural (PT) if outside of tumour regions.

For the TLS panel, identified aggregates were classified as TLSs if these contained organised T and B cell zones with CD4+ and CD8+ cells, and CD19+ cells respectively, and high endothelial venules (HEVs) as PNAd+. These were further classified in accordance with their abundance (TLS0: none, TLS1-4: 1 to 4, and TLS5+: more than 5) and distance to tumour tissue, proximal if within or up to 500um from tumour tissue and distal if more than 500um. TLSs were deemed mature if these were releasing ASCs, or immature if not. Finally, CD8+ T cell abundance was defined as absent (0), poor (1 to 20), or rich (20+).

# CHAPTER 3

# RESULTS

## *3.1 Patient Cohort Characteristics*

This Section includes a summary of the clinical characteristics of all patient cohorts investigated in this study (i.e., cancer, healthy and benign).

### *3.1.1 Prostate Cancer Cohorts*

All prostate cancer patient samples were categorised into two groups based on Gleason score. Low-grade samples were classified as having a Gleason score of 6-7 and high-grade samples of 8-10. Gleason scores were determined at diagnosis via analysis of radical prostatectomy or biopsy tissue. The grading classification used here was based on the sample allocation attributed by the APCB and the VCB and may not reflect the current clinical grading. However, this was maintained for the purposes of this study. Patient PSA levels were measured at time of patient consent and enrolment prior to surgical intervention. As autoantibody half-lives are between 30 to 90 days in circulation, it is anticipated that their presence would remain in samples up to at least 30 days following radical prostatectomy. However, after surgical resection of the cancerous prostate and associated tumour antigens, autoantibody production would cease and eventually be cleared from circulation. As such, all blood samples used in this study for antibody profiling were taken before or within a 30-day timeframe following radical prostatectomy, where performed.

#### *3.1.1.1 Discovery Cohort*

The patient characteristics at baseline of the discovery cohort accessed via the APCB are summarised in **Table 2** below.

***Table 2. Discovery patient characteristics at baseline.*** *This table summarises the clinical characteristics of all patients in the discovery cohort.*

| Characteristic | Low-Grade Patients (n=54) | High-Grade Patients (n=56) | Total Patients (n=110) |
|---|---|---|---|
| Age* — yr | | | |
| Mean | 62.5 | 64.0 | 63.2 |
| Range | 50.1–74.2 | 47.8–78.1 | 47.8–78.1 |
| Age Category — no. (%) | | | |
| <60 yr | 23 (42.6) | 15 (26.8) | 38 (34.6) |
| ≥60 to <70 yr | 25 (46.3) | 32 (57.1) | 57 (51.8) |
| ≥70 yr | 6 (11.1) | 9 (16.1) | 15 (13.6) |
| PSA Level† — ng/mL | | | |
| Mean | 6.6 | 11.6 | 9.1 |
| Range | 0.9–17.9 | 2.0–98.0 | 0.9–98.0 |
| PSA Category — no. (%) | | | |
| <4 ng/mL | 10 (18.5) | 6 (10.7) | 16 (14.6) |
| ≥4 to ≤12 ng/mL | 40 (74.1) | 39 (69.7) | 79 (71.8) |
| >12 ng/mL | 4 (7.4) | 11 (19.6) | 15 (13.6) |
| Gleason Score Source — no. (%) | | | |
| Radical Prostatectomy | 54 (100.0) | 40 (71.4) | 94 (85.5) |
| Core Biopsy | 0 (0.0) | 16 (28.6) | 16 (14.5) |
| Gleason Score | | | |
| Range | 6–7 | 8–10 | 6–10 |
| Prior Treatment — no. (%) | | | |
| Yes | 0 (0.0) | 3 (5.4) | 3 (2.7) |
| No | 54 (100.0) | 53 (94.6) | 107 (97.3) |
| Radical Prostatectomy — no. (%) | | | |
| Yes | 54 (100.0) | 48 (85.7) | 102 (92.7) |
| No | 0 (0.0) | 8 (14.3) | 8 (7.3) |
| Biochemical Recurrence‡ — no. (%) | | | |
| Yes | 5 (9.3) | 11 (19.6) | 16 (14.6) |
| No | 45 (83.3) | 37 (66.1) | 82 (74.5) |
| Not Applicable | 4 (7.4) | 8 (14.3) | 12 (10.9) |
| Ethnicity — no. (%) | | | |
| European | 53 (98.1) | 38 (67.9) | 91 (82.7) |
| Other | 1 (1.9) | 0 (0.0) | 1 (0.9) |
| Unknown | 0 (0.0) | 18 (32.1) | 18 (16.4) |
| Disease Specific Survival — no. (%) (as of 9/3/2020) | | | |
| Alive | 54 (100.0) | 48 (85.7) | 102 (92.7) |
| Dead | 0 (0.0) | 8 (14.3) | 8 (7.3) |

** Patient ages were recorded at diagnosis of disease. † PSA levels were those provided at informed patient consent. ‡ Biochemical recurrence was determined as a detected PSA level of at least 0.4ng/mL followed by another subsequent increase, after radical prostatectomy where applicable (with surgery) and available (with follow-up)* Stephenson et al (2006). *Patients classified as 'Dead' included only individuals with prostate cancer-related deaths. The follow-up time for disease-specific survival was 6.8years. Any patients with disease-specific death after 6.8 years were classified as alive. Abbreviations: PSA, prostate-specific antigen.*

This patient cohort contained a relatively comprehensive coverage and distribution of age of those typically seen to develop prostate cancer, with all patients displaying a mean of 63.2 years, ranging from 47.8 to 78.1 years. The cohort ethnicity was largely of European descent (82.7%). PSA levels were higher in high-grade patients, exhibiting a mean of 11.6ng/mL, and an overall range of 2.0 to 98.0ng/mL, in contrast to that of low-grade patients which displayed a mean of 6.6ng/mL and range of 0.9ng/mL to 17.9ng/mL. Gleason scores and hence diagnoses, were mainly determined via radical prostatectomy (85.5%), with the remaining samples determined by core biopsy (14.5%). Biochemical recurrence rates were higher amongst high-grade patients (19.6%) than low-grade patients (9.3%), with a mean PSA follow-up time of 45.3 months. Similarly, disease-specific survival at 6.8 years of follow-up was lower in high-grade patients (92.7%), with no deaths reported in low-grade patients.

#### *3.1.1.2 Validation Cohort*

The patient characteristics at baseline of the validation cohort accessed via the VCB are summarised in **Table 3** below.

***Table 3. Validation patient characteristics at baseline.*** *This table summarises the clinical characteristics of all patients in the validation cohort.*

| Characteristic | Low-Grade Patients (n=50) | High-Grade Patients (n=49) | Total Patients (N=99) |
|---|---|---|---|
| Age* — yr | | | |
| Mean | 61.9 | 62.4 | 62.2 |
| Range | 51.0–85.0 | 46.0–81.0 | 46.0–85.0 |
| Age Category — no. (%) | | | |
| <60 yr | 22 (44.0) | 17 (34.7) | 39 (39.4) |
| ≥60 to <70 yr | 24 (48.0) | 26 (53.1) | 50 (50.5) |
| ≥70 yr | 4 (8.0) | 6 (12.2) | 10 (10.1) |
| PSA Level† — ng/mL | | | |
| Mean | 5.7 | 15.8 | 10.7 |
| Range | 2.3–12.0 | 2.6–63.5 | 2.3–63.5 |
| PSA Range — no. (%) | | | |
| <4 ng/mL | 10 (20.0) | 3 (6.1) | 13 (13.1) |
| ≥4 to ≤12 ng/mL | 40 (80.0) | 25 (51.0) | 65 (65.7) |
| >12 ng/mL | 0 (0.0) | 21 (42.9) | 21 (21.2) |
| Gleason Score Source — no. (%) | | | |
| Radical Prostatectomy | 47 (94.0) | 44 (89.8) | 91 (91.9) |
| Core Biopsy | 3 (6.0) | 5 (10.2) | 8 (8.1) |
| Gleason Score | | | |
| Range | 6–7 | 8–10 | 6–10 |
| Radical Prostatectomy — no. (%) | | | |
| Yes | 47 (94.0) | 44 (89.8) | 91 (91.9) |
| No | 3 (6.0) | 5 (10.2) | 8 (8.1) |
| Benign Conditions — no. (%) | | | |
| Present | 32 (64.0) | 26 (53.1) | 58 (58.6) |
| Absent | 18 (36.0) | 23 (46.9) | 41 (41.4) |

** Patient ages were recorded at diagnosis of disease. † PSA samples were those provided at informed patient consent. Abbreviations: PSA, prostate-specific antigen.*

This patient cohort displayed a comparable mean age of 62.2 years, ranging from 46.0 to 85.0 years. PSA levels were higher in high-grade patients, displaying a mean of 15.8ng/mL, and an overall range of 2.63ng/mL to 63.5ng/mL, in contrast to that of low-grade patients which displayed a mean of 5.7ng/mL and range of 2.3ng/mL to 12.0ng/mL. Gleason scores and diagnoses were mainly determined via radical prostatectomy (91.9%), with the remaining samples determined by core biopsy (8.1%). Benign conditions were present in 58.6% of patients and absent in 41.4%, with greater numbers observed among low-grade individuals.

### *3.1.2 Healthy and Benign Cohorts*

#### *3.1.2.1 Healthy Cohort*

The clinical characteristics of all healthy donors accessed via the APCB are summarised in **Table 4** below.

***Table 4. Healthy donor characteristics.*** *This table summarises the characteristics of all healthy donors used in this study.*

| Characteristic | Healthy Donor Patients (n=14) |
|---|---|
| Age — yr | |
| Mean | 72.2 |
| Range | 65.3–79.3 |
| PSA Level† — ng/mL | |
| Mean | 2.1 |
| Range | 0.1–5.6 |
| PSA Category — no. (%) | |
| <4 ng/mL | 11 (78.6) |
| ≥4 to ≤12 ng/mL | 3 (21.4) |
| >12 ng/mL | 0 (0.0) |

*† PSA levels used for calculations were those provided at informed patient consent.*
*Abbreviations: PSA, prostate-specific antigen.*

The healthy donor cohort displayed a mean age of 72.2 years, ranging from 65.3 to 79.3 years. The mean PSA level was 2.1ng/mL, ranging from 0.1 to 5.6ng/mL, with most individuals below the threshold of concern (4.0ng/mL).

#### *3.1.2.2 Benign Cohort*

The clinical characteristics of all benign donors accessed via the VCB are summarised in **Table 5** below. Benign conditions of the prostate included benign prostate hyperplasia, prostatic intraepithelial neoplasia, nodular hyperplasia, basal cell hyperplasia, squamous metaplasia, acinar hyperplasia, and parenchyma hyperplasia.

***Table 5. Benign donor characteristics.*** *This table summarises the characteristics of all benign donors used in this study.*

| Characteristic | Benign Disease Patients (N=13) |
|---|---|
| Age* — yr | |
| Mean | 71.2 |
| Range | 48.0–85.0 |
| PSA Level† — ng/mL | |
| Mean | 2.4–7.6 |
| Range | 5.0 |
| PSA Category — no. (%) | |
| <4 ng/mL | 1 |
| ≥4 to ≤12 ng/mL | 1 |
| Unknown | 11 |

** Patient ages used for calculations were at diagnosis of benign disease. † PSA samples used for calculations were those provided at informed patient consent. Abbreviations: PSA, prostate-specific antigen.*

The benign donor cohort displayed an average age of 71.2 years, ranging from 48.0 to 85.0 years. The majority of these patients did not have available PSA level measurements, and hence resulted in a limitation on potential analyses.

### *3.2 CT100+ Protein Microarray Data*

This Section includes the complete set of results obtained whilst performing quality controls, optimisations and autoantibody profiling of healthy, benign, discovery and validation cohort patient samples on the CT100+ protein microarray. All arrays were dual scanned using fixed gain setting of 520(λ635) and 500(λ532) at 100% scan power.

#### *3.2.1 Determination of Optimal Patient Serum Concentration*

To determine the optimal serum dilution capable of resolving clear antibody signals concurrently with low background noise, serum dilution optimisation assays were performed. Serial dilutions of a known prostate cancer patient samples at 1:800, 1:400, 1:200 and 1:100 were used to determine the optimal ratio of serum to PBST. The resulting

autoantibody profiles are graphed in **Figure 6** below. It was apparent that a dilution of 1:100, was able to resolve NY-ESO-1 and CTAG2 signals most optimally (best signal / noise ratio; e.g. signal / net intensity of NY-ESO-1 [23034 RFU] to noise / array background [354 RFU) ratio: 64.5), compared to the other dilutions tested. This was within the linear range (1:50 to 1:1250 serum dilutions) previously determined Beeton-Kempen et al. (2014). Henceforth, a 1:100 dilution of patient serum to PBST was conducted for patient, healthy and benign assays.

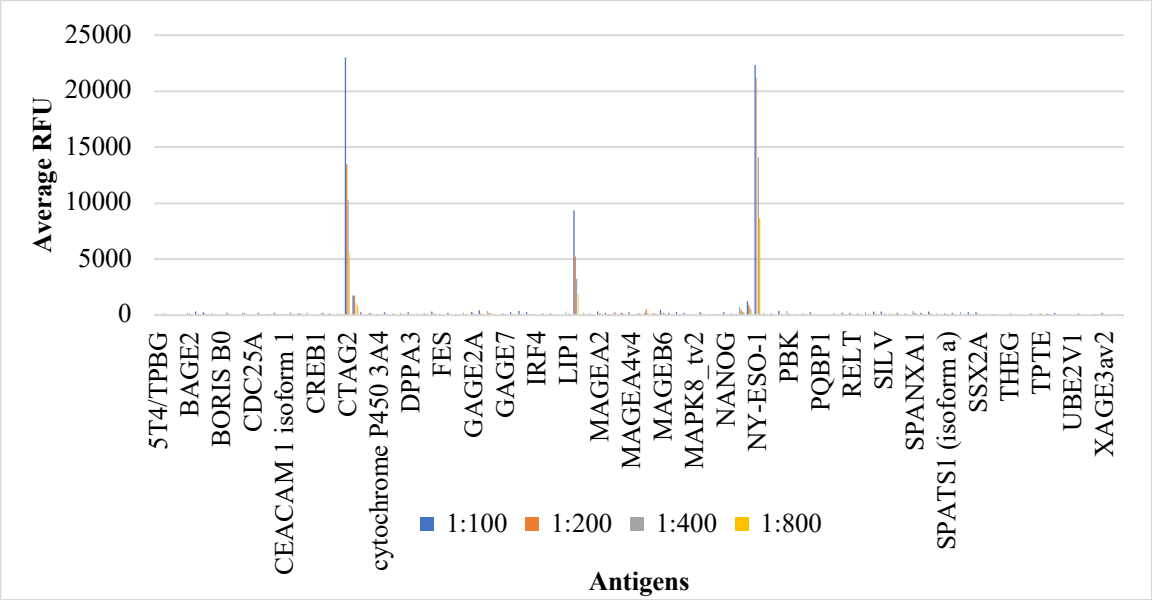


***Figure 6. Serum dilution optimisation assay.*** *This graph depicts the average RFU for a known prostate cancer patient at four dilutions (1:100, 1:200, 1:400 and 1:800).*

### *3.2.2 CT100+ Protein Microarray Quality Control Assays*

Serum samples were assayed across 3 separate CT100+ print runs for the discovery cohort and 3 separate CT100+ print runs for the validation cohort, and hence warranted quality control assays to be performed for each batch to ensure robust array specificity, quality, antigen immobilisation and reproducibility.

#### *3.2.2.1 Validation of Immobilised BCCP-Myc-tagged Proteins to Array Surface*

As all antigens contain a c-Myc tag, anti-c-Myc assays were performed per print run to confirm antigen immobilisation on the array surface. The resulting c-Myc assays for all

batches used are graphed in **Figure 7** below, as well as a representative scanned array image.

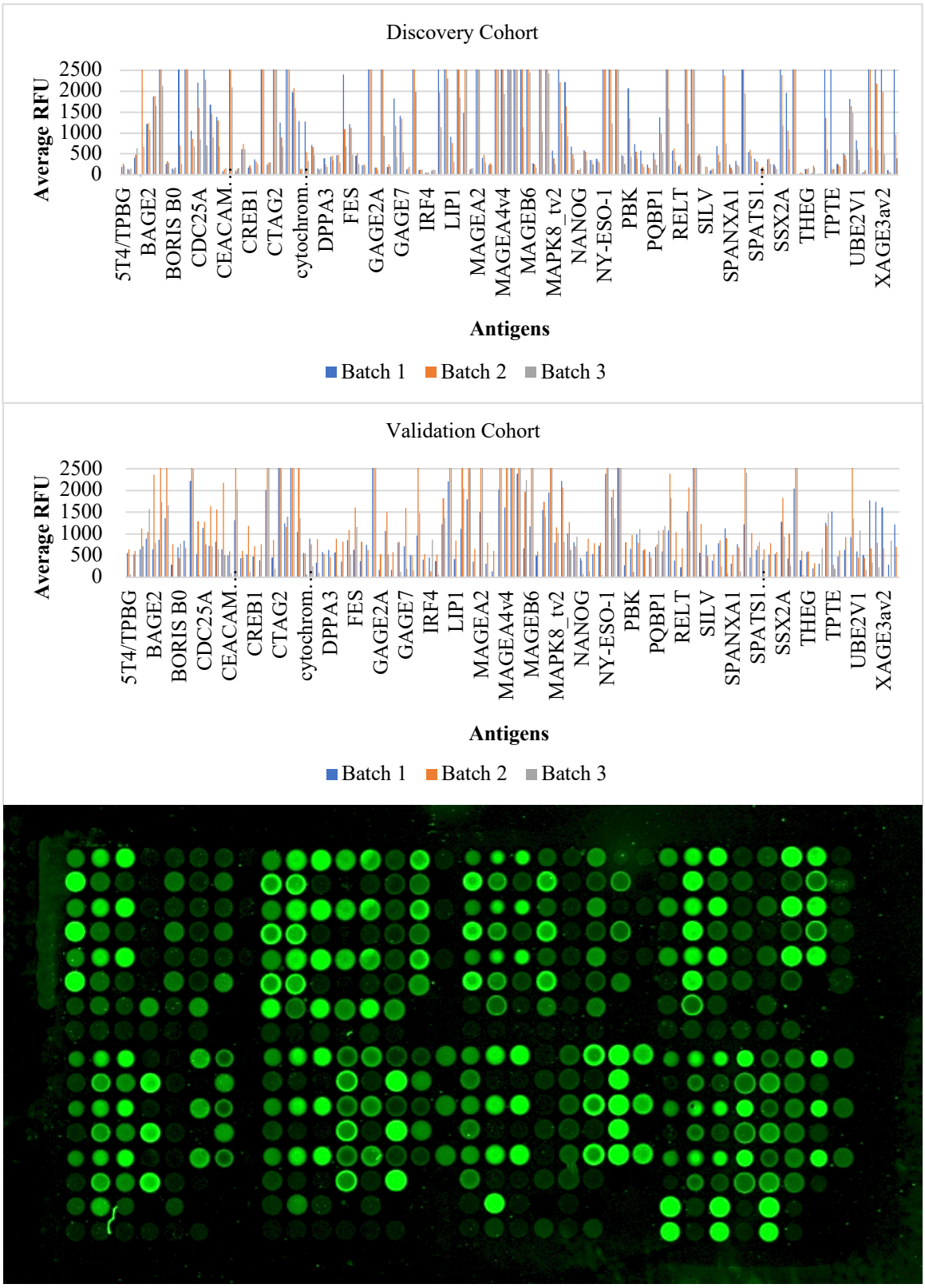


***Figure 7. Graphical and visual representations of CT100+ anti-c-myc assays. (Above)*** *The bar charts depict the average RFU values for antigens that were successfully printed and immobilised*

*across all batches for each patient cohort. The average RFU scale was adjusted to a max of 2500 for comparative purposes and hence does not provide complete coverage of all values. Antigens exceeding 2500RFU ranged from 2500 to 20665 for the discovery cohort, and from 2500 to 10707 for the validation cohort. (**Below**) The image is a visual representation of a selected anti-c-myc assay conducted on a CT100+ array from batch 1, discovery cohort. Positive controls and antigens are depicted in green.*

Although the c-myc signals show significant differences in antigen densities, it is unlikely that these will be reflected in the resulting bound cognate antibody intensities because we (Figure 6) and others (Beeton-Kempen et al., 2014) have shown that decreasing serum dilutions down to 1:100 results in increased antibody signals, without reaching saturation. Hence, normalisation of subsequent serological data is not required.

For the batches used in the discovery cohort, all but two antigens, ATK1 and SILV, showed successful immobilisation on the arrays across all 3 batches. A cut-off of <15 average RFU was used to define those that were not printed. In addition, instances involving inconsistent printing of antigens across all batches were removed, including GAGE2A, IRF4, MAGEA11, MAPK8_tv2, PCTK1, PQBP1, PRKCH, SYCP1, TP53, TPM1, UBE2V1 and ZBTB7B. All unprinted (2) and inconsistent (12) antigens mentioned above were removed from all subsequent analyses.

For the batches used in the validation cohort, all but two antigens, TP53 and ZBTB7B, showed successful immobilisation on the array across all 3 batches. IRF4, MAPK8_tv2, MSN, PCTK1, PQBP1, PRKCH, SPATS1, SYCP1, TPTE, UBE2V1 and XAGE1B showed inconsistent printing. All unprinted (2) and inconsistent (11) antigens mentioned above were removed from subsequent analyses.

#### *3.2.2.2 Validation of CT100$^{+}$ Microarray Specificity for Cancer*

In order to reconfirm CT100+ array specificity for cancer, a selected cancer patient and healthy individuals were tested. The first set of assays for each cohort involved testing of

serum from a single prostate cancer patient with a known, strong positive autoantibody profile across all batches. Here, a selected cancer patient (ONJ 072) with known, strong autoantibody titres against NY-ESO-1 and CTAG2 consistently reproduced significant titres across 4 different batches (see **Figure 8**).

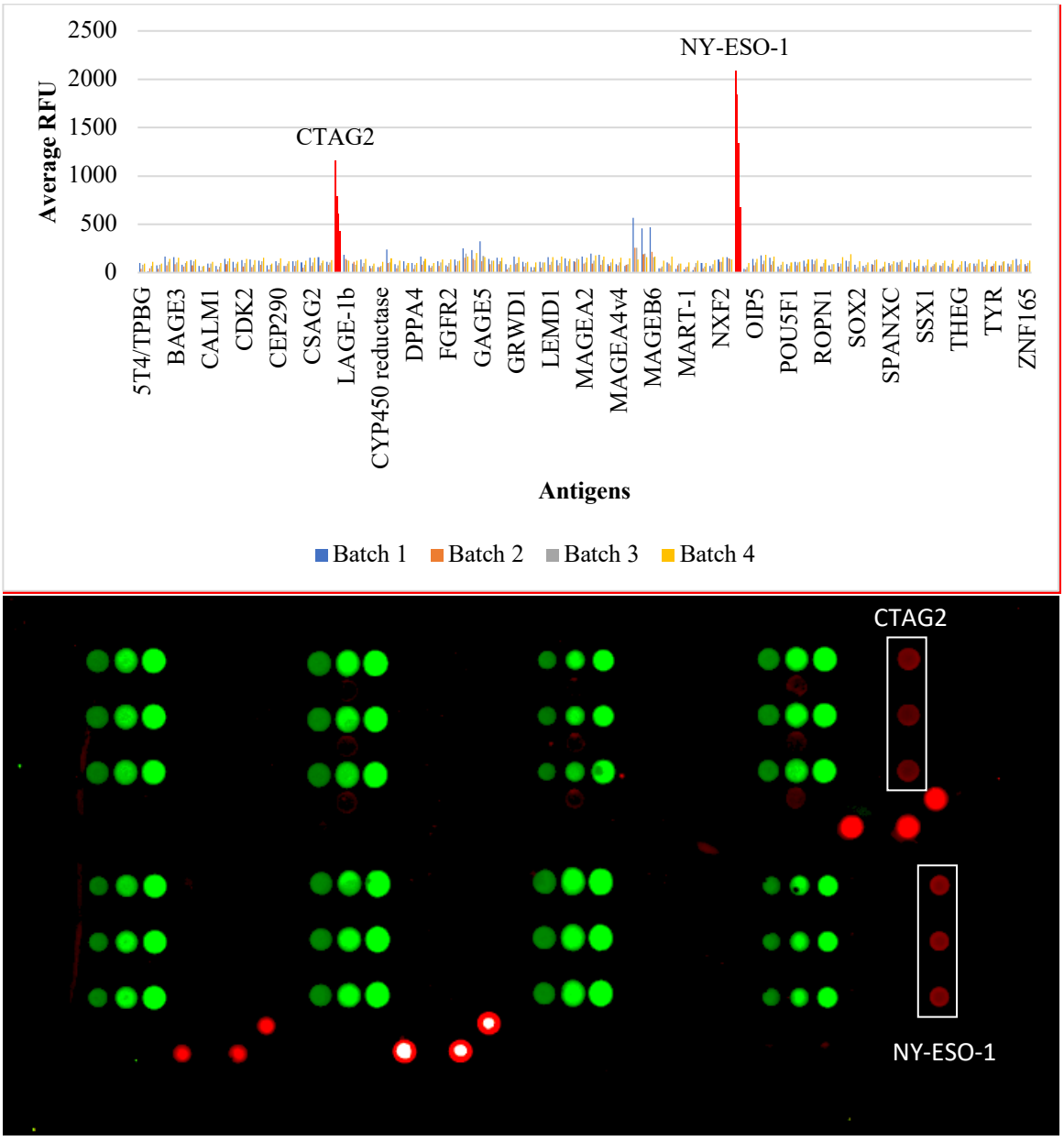


***Figure 8. Graphical and visual representations of CT100+ positive control assays. (Above)*** *The graphs depict the presence of consistently high autoantibody titres against CTAG2 and NY-ESO-1 across all batches in both patient cohorts.* ***(Below)*** *The image is a visual representation of a selected positive control assay performed on a CT100+ array from batch 1 (discovery cohort) with triplicate spots of CTAG2 and NY-ESO-1 antigen.*

The second set of assays involved individual incubation of serum from 14 age and gender-matched healthy donor (HD) samples. The resulting individual autoantibody levels were averaged across HD samples for each antigen, to generate a pooled HD profile (see **Figure 9** below). The resulting autoantibodies were negligible across all antigens, as expected. The average RFU and SD were calculated for the pooled data and combined (Average RFU of all healthy patients +1SD of all healthy patients = 307RFU cut-off) to determine a threshold (≥307 RFU) capable of detecting true autoantibody signals among cancer patients.

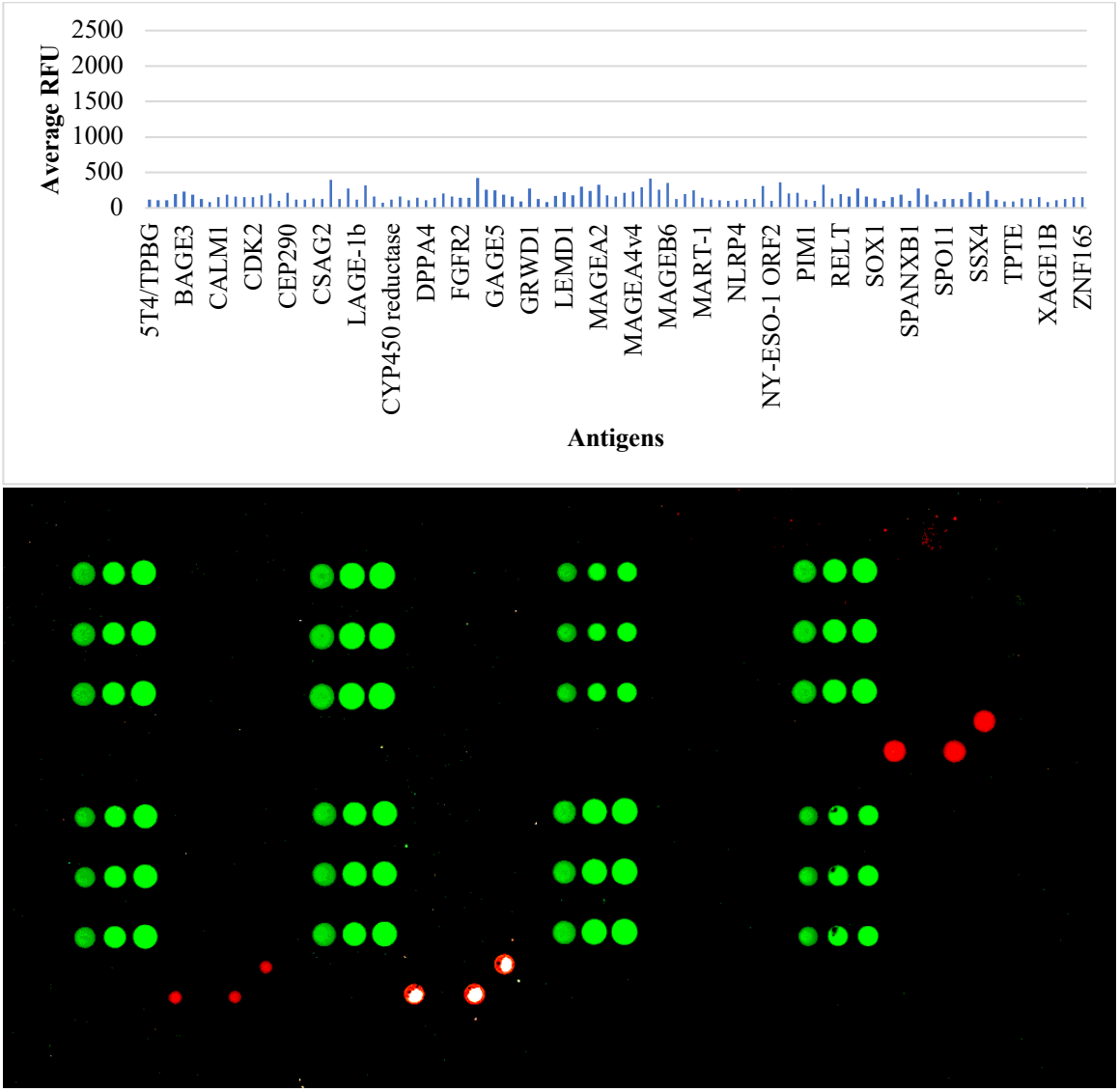


***Figure 9. Graphical and visual representations of CT100+ negative control assays. (Above)*** *The graph depicts the average RFU for each antigen resulting from a pool of 14 individual HD patients.* ***(Below)*** *The image is a visual representation of a healthy donor patient assay performed on a CT100+ array.*

### *3.2.2.3 Verification of Control Spots on CT100+ Array Surface*

Each batch of CT100+ arrays included a range of printed positive and negative controls to ensure that a high level of quality was achieved. These controls for a representative batch are shown in **Figure 10**. As expected, all negative controls displayed expected intensities; the 'BCCP-myc', 'buffer' and 'insect cell lysate' each displayed naught or negligible fluorescent intensities, confirming absence of non-specific binding. Positive controls also displayed expected intensities. All 5, 10 and 15ng/µL Cy3-biotin-BSA controls exhibited increasing intensities that neatly correlated with the increases in BSA concentration. The biotin-human IgG (hIgG) controls displayed stable intensities across all arrays confirming the addition of detection antibody for all assays. The anti-human IgG (ahIgG) displayed stable intensities across all arrays providing assurance that serum was always added and that autoantibodies were able to bind to cognate antigens present on the array. These controls yielded similar and consistent readouts across all array batches used in this study.

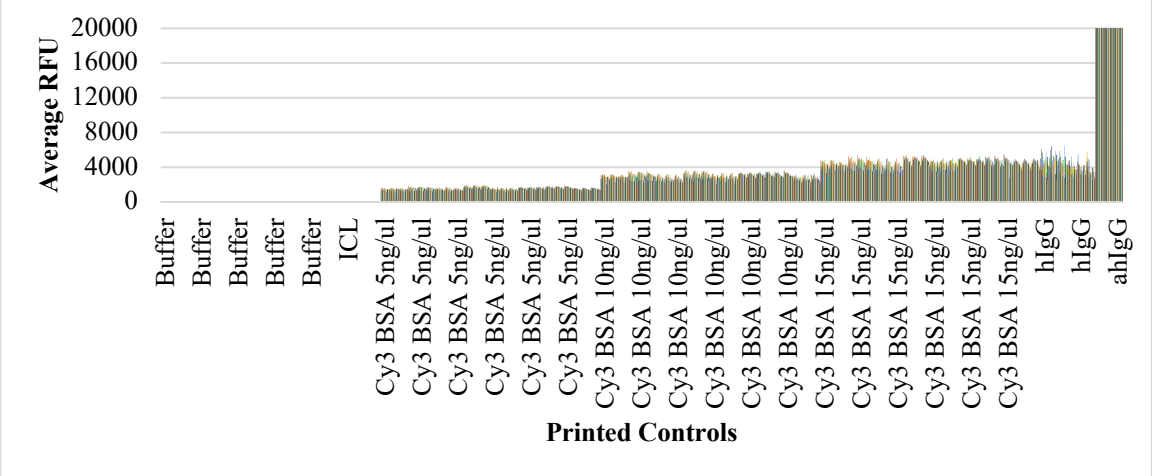


***Figure 10. Positive and negative controls for a selected batch of CT100+ arrays.*** *The graph provides a full set of average RFU measurements for negative (buffer, ICL and BCCP-myc) and positive (Cy3-biotin-BSA at 5, 10 and 15ng/µl, biotin-hIgG at 10ng/µl and biotin-αhIgG at 100ng ng/µl) printing controls on all arrays for batch 1.*

### *3.2.3 CT100+ Patient Sera Data Analyses*

The following Sections detail the array data analyses pertaining to the healthy, benign, discovery and validation patient cohorts. Following optimisation and screening for prominent antigens, three types of analyses were performed, where possible:

1. Univariate antigen ROC curves and associated violin plots
2. CombiROC multivariate antigen ROC curves
3. mRNA expression hierarchical clustering and associated heat maps using TCGA prostate cancer data (PanCancer cohort) for all significant antigens

The goal of performing these analyses was to obtain antigen combinations most capable of stratifying patients into pre-defined groups based on their autoantibody profiles. The best univariate antigens by count or capability of distinguishing between two groups of interest (e.g., healthy vs. cancer, relapse vs. non-relapse patients, low-grade vs. high grade patients) using relevant array data were defined. These antigens were then combined to generate multivariate antigen ROC curves (signatures) that surpass the ability of single markers at distinguishing between groups of interest. To strengthen our findings, we analysed mRNA expression data from an independent cohort accessible via the TCGA (PanCancer PRAD cohort – 460 patients) using CBIO (a user-friendly interface that allows non-bioinformaticians to access, analyse and extract data from TCGA) to create heat maps which delineate the presence and prominence of these antigens in prostate cancer patients Cerami et al (2012); Gao et al (2013).

In this study, we attempt to combine associated patient and healthy PSA levels with quantified array findings (autoantibody titres), to significantly improve diagnostic and prognostic potential of biomarker signatures when stratifying patients. Hence, it is necessary to first provide an overview of the diagnostic capability of PSA among the discovery and validation patient cohorts (see **Figure 11** below). At a cut-off of 4ng/mL, an identical sensitivity and specificity of 84.6% and 78.6% respectively, was observed for both

patient cohorts. It is important to note that the observed diagnostic sensitivity and specificity for PSA seen among our cohorts was inflated in contrast to that commonly recorded at a clinical level. This is a direct result of sample collection, where cancer patients were selected upon confirmation of cancer presence (i.e., via biopsy or resection), hence displaying heightened PSA levels, in addition to the vast number of healthy donors displaying normal PSA levels (<4ng/mL).

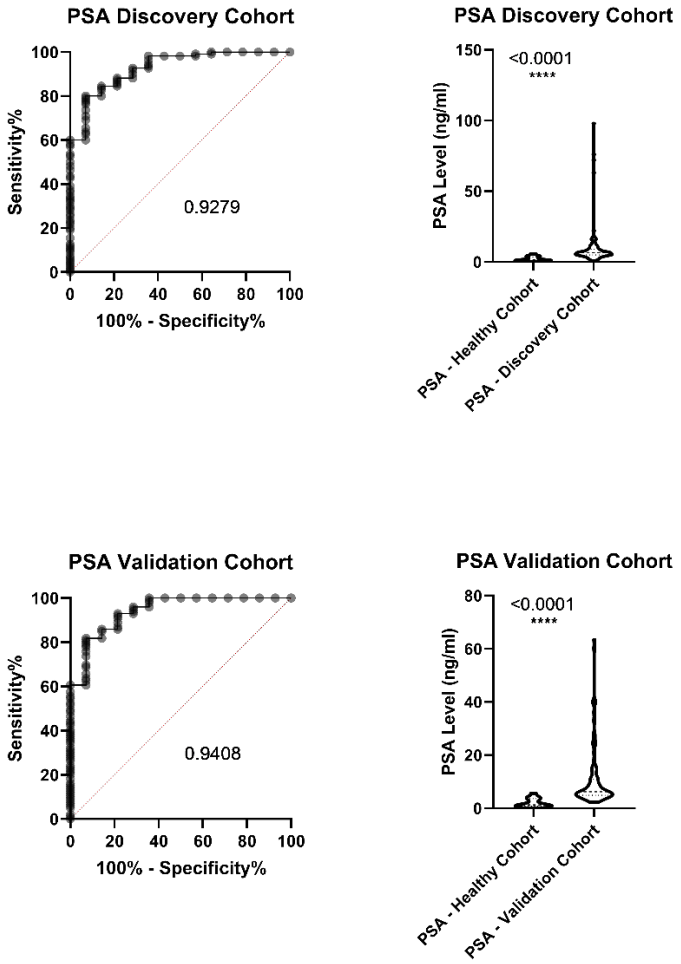


***Figure 11. PSA level ROC curves and violin plots for discovery and validation prostate cancer cohorts.*** *ROC curves (on left) outline the capabilities of PSA antigen levels to discriminate discovery and validation patients with healthy individuals, as indicated by their associated AUC values. Corresponding AUC values of 0.9279 (discovery cohort) and 0.9408 (validation cohort) were observed. Violin plots showing PSA data distribution (on right) using the Mann-Whitney U test. Values ≤0.05 were considered significant.*

### *3.2.3.1 Healthy and Benign Cohorts*

Based on the established concept / understanding that benign conditions (e.g., high-grade PIN) commonly act as precursors to prostate cancer, we generated univariate and multivariate ROC curves comparing our healthy (n=14) and (n=13) benign cohorts to determine if there were any key markers capable of distinguishing these (see **Figures 12 and 13**). Remarkably, four antigens consisting COL6A1 (AUC 0.7198; p-value 0.0543), COX6B2 (AUC 0.7033; p-value 0.0743), MART-1 (AUC 0.7143; p-value 0.0592), and MICA (AUC 0.7143; p-value 0.0609) showed strong discriminative capabilities for distinguishing benign patients from healthy individuals.

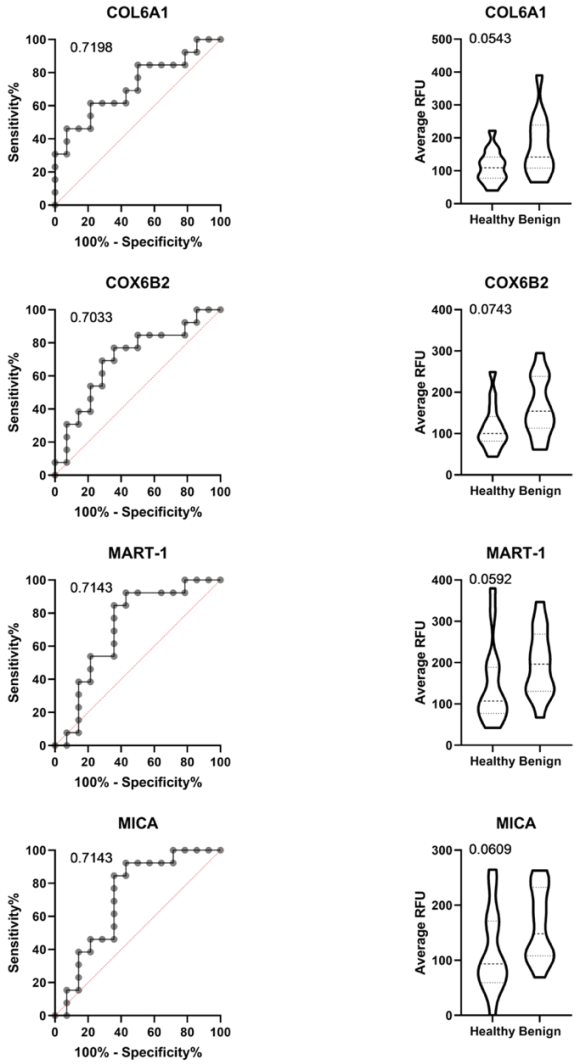


***Figure 12. Top univariate antigen ROC curves and violin plots capable of distinguishing healthy from benign individuals.*** *ROC curves for the top univariate antigens observed when comparing*

*healthy and benign cohort array data (on left) with AUC values of 0.7198 (COL6A1), 0.7033 (COX6B2), 0.7143 (MART-1), and 0.7143 (MICA). Corresponding antigen violin plots are shown (on right), with included Mann-Whitney U test (CI of 95%) p-values of 0.0543 (COL6A1), 0.0743 (COX6B2), 0.0592 (MART-1), and 0.0609 (MICA).*

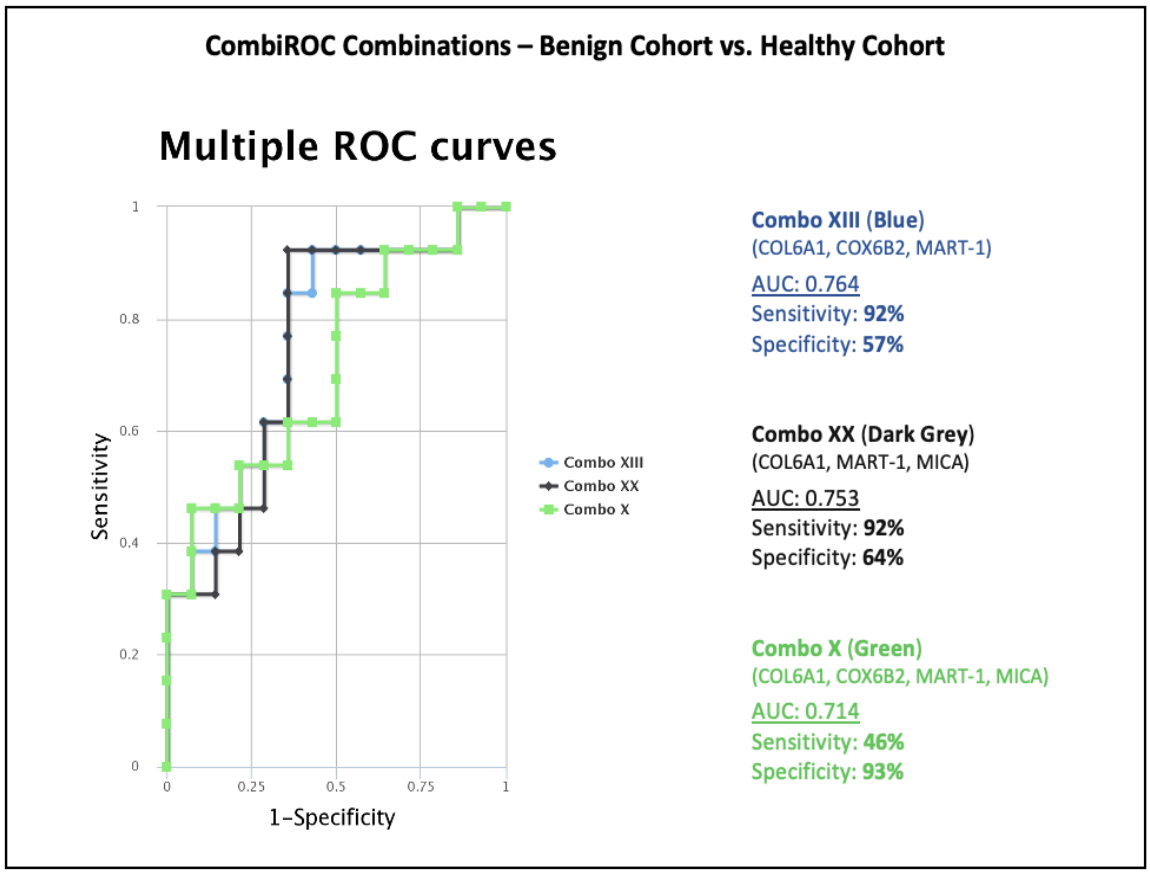


***Figure 13. Top multivariate antigen ROC curves discriminating benign from healthy individuals.*** *Top AUC combination – Combo XIII (blue) consisting of COL6A1, COX6B2, and MART-1 generating an AUC of 0.764, sensitivity of 92%, and specificity of 57%. Highest sensitivity combination – Combo XX (dark grey) consisting of COL6A1, MART-1, and MICA generating an AUC of 0.753, sensitivity of 92%, and specificity of 64%. Highest specificity combination – Combo X (green) consisting of COL6A1, COX6B2, MART-1 and MICA generating an AUC of 0.714, sensitivity of 46%, and specificity of 93%.*

### *3.2.3.2 Discovery Cohort*

#### *3.2.3.2.1 Prevalence of Autoantibodies in Prostate Cancer (Discovery Cohort)*

The following Section details the prevalence of autoantibodies in all discovery cohort prostate cancer patients (n=110).

The prevalence of autoantibodies towards specific tumour antigens was determined by quantifying autoantibody signals above the determined threshold for all 110 patients in the APCB cohort. Throughout the entire cohort, autoantibody signals were detected in 86 of 110 patients (78%). It was apparent that antigen specificities varied among the patient cohort. Patients either exhibited high autoantibody titres towards multiple or few tumour antigens or lacked detectable autoantibodies entirely (**Figure 14**).

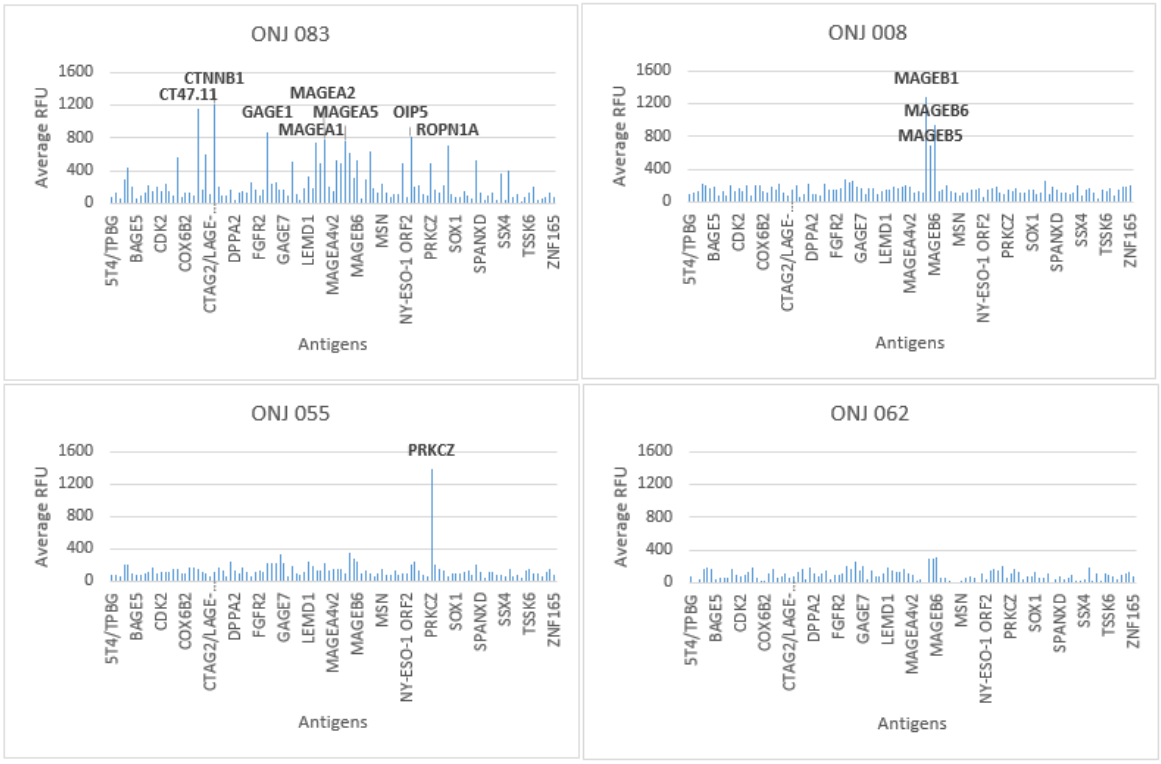


***Figure 14. Representative autoantibody profiles of prostate cancer patients.*** *These graphs portray an overview of the types of autoantibody profiles that were generated while sampling prostate cancer patients using the CT100+ array.*

Prevalent autoantibodies were detected against 16 leading antigens, included in **Figure 15**. These included MAGEB1 (n=70/110; 64%), MAGEB6 (n=62/110; 56%), MAGEB5 (n=57/110; 52%), GAGE4 (n=31/110; 28%), GAGE1 (n=30/110; 27%), CTNNB1 (n=28/110; 25%), GAGE5 (n=27/110; 25%), OIP5 (n=26/110; 24%), SPANXC (n=25/110; 23%), CT47.11 (n=23/110; 21%), LEMD1 (n=23/110; 21%), MAPK3 (n=23/110; 21%), GRWD1 (n=22/110; 20%), MAGEA2 (n=22/110; 20%), MAGEA4v4 (n=22/110; 20%),

and MAGEA1 (n=21/110; 19%), in order of prevalence. The number of patients exhibiting autoantibody titres towards the top 16 antigens varied from 22 to 70, with the top antigen MAGEB1, detected above the pre-determined threshold (≥307 RFU) in 70 of 110 patients (64% of the cohort).

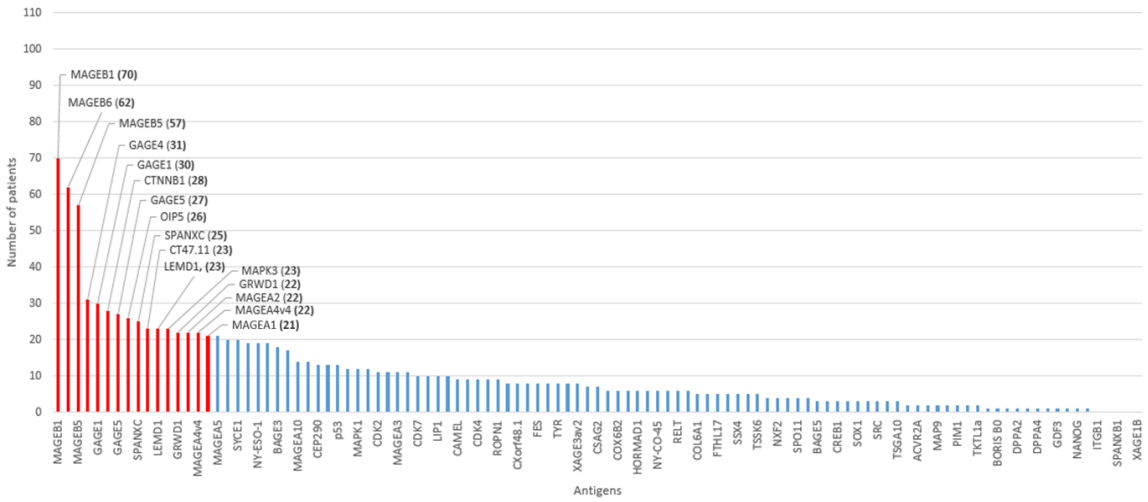


***Figure 15. Top antigens detected among the discovery patient cohort.*** *A graphical breakdown of all antigens detected among the patient cohort determined by prevalence, with the top 16 highlighted in red. Antigens (in red) from left to right: MAGEB1, MAGEB6, MAGEB5, GAGE4, GAGE1, CTNNB1, GAGE5, OIP5, SPANXC, CT47.11, LEMD1, MAPK3, GRWD1, MAGEA2, MAGEA4v4 and MAGEA1.*

In regard to the prevalence of autoantibody titres against these top 16 antigen specificities for the entire cohort, a stacked graph was generated showing the combined RFU per antigen (**Figure 16**). Some patients exhibited high autoantibody titres towards all top antigens (e.g., ONJ 075), whereas others displayed titres towards only few or one antigen.

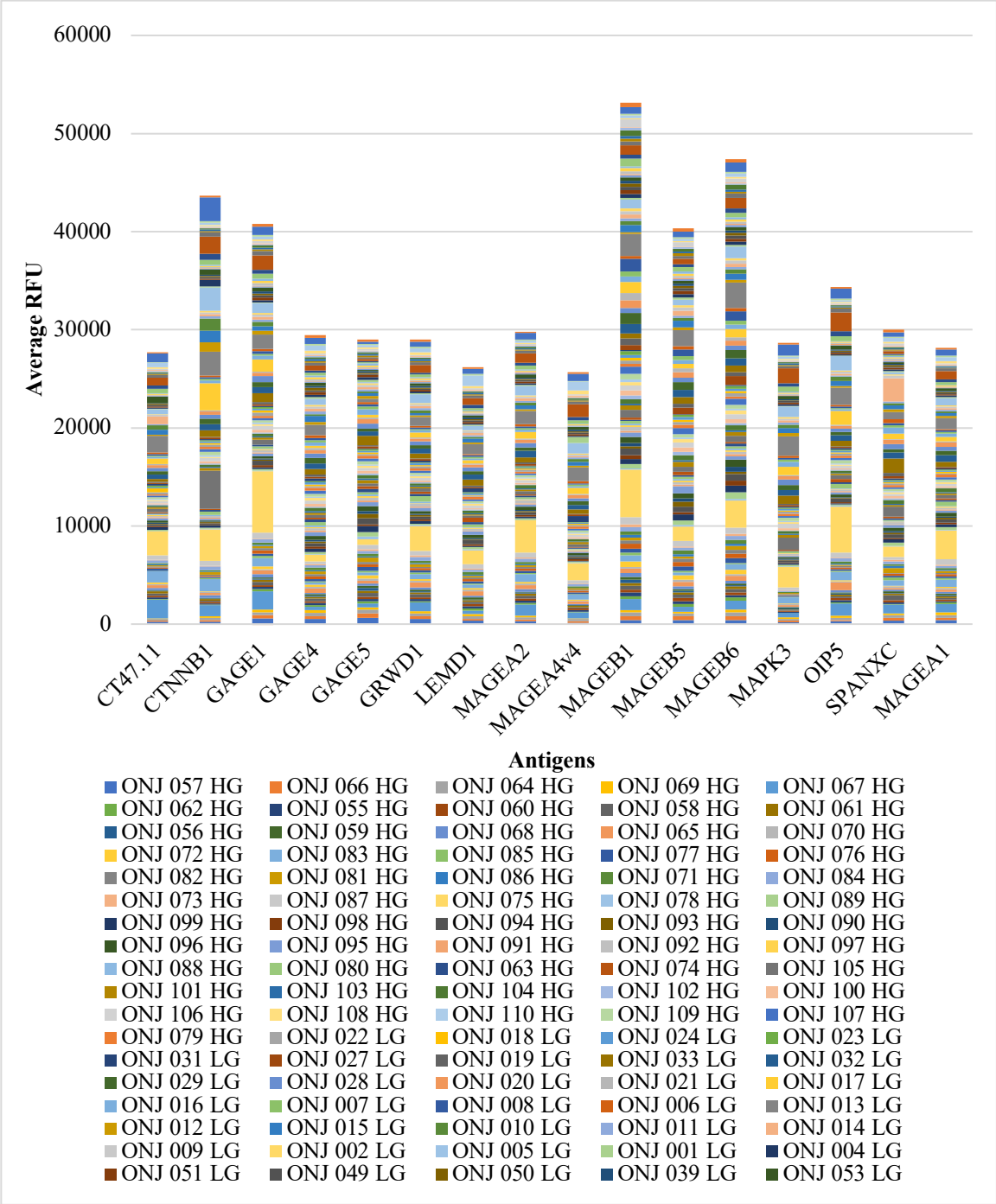


***Figure 16. Average RFU values for the top 16 antigens among the entire patient cohort.*** *This graph illustrates the distribution of average RFU values between prostate cancer patients for the top 16 most prevalent antigen specificities. Each bar is the stacked average RFU value for a particular antigen, with each colour corresponding to an individual patient. Patient IDs are denoted as 'ONJ 001' to 'ONJ 110' under the graph. Abbreviations: LG, low-grade; HG, high-grade.*

As a means of further understanding why these particular antigen specificities would be seen so prevalently among the prostate cancer patient cohort, a STRING (Search Tool for the Retrieval of Interacting Genes/Proteins, https://string-db.org/) analysis was conducted. This tool is capable of identifying functional enrichments that exist within a given network of defined proteins using access to publication and protein databases, such as KEGG, UniProt, PFAM, INTERPRO, and SMART. The resulting network derived from our top antigens shown below (**Figure 17**) had a PPI enrichment p-value of $<1.0e^{-16}$, indicating that the identified top proteins were not co-occurring randomly and hence, are at least in part biologically connected as a group. The STRING analysis revealed a high association between 8 of our identified proteins (i.e. top antigens detected using the CT100+ array) and those identified in the Adeola *et al.* study via the reference publication analysis with a false discovery rate of $2.13e^{-11}$ (red nodes in **Figure 17**) Adeola et al. (2016). This was the preliminary study using the CT100+ array on a South African Prostate cancer cohort. In addition, 7 of our identified proteins were present in another study investigating inducible expression of CT antigens in human prostate cancer Heninger et al (2016), with a false discovery rate of $2.88e^{-10}$ (blue nodes in **Figure 17**). Note that GAGE4 was unable to be included in the STRING analysis due it its absence from the STRING protein database.

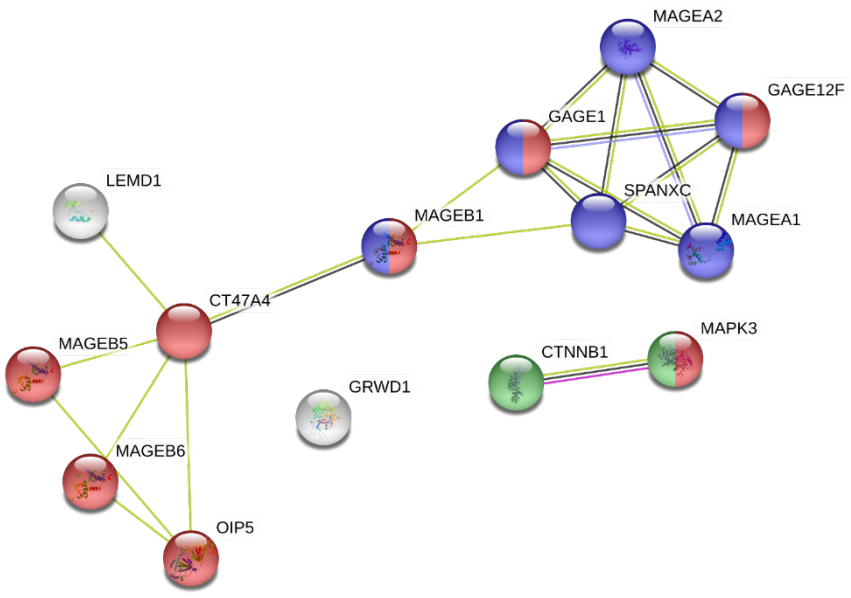

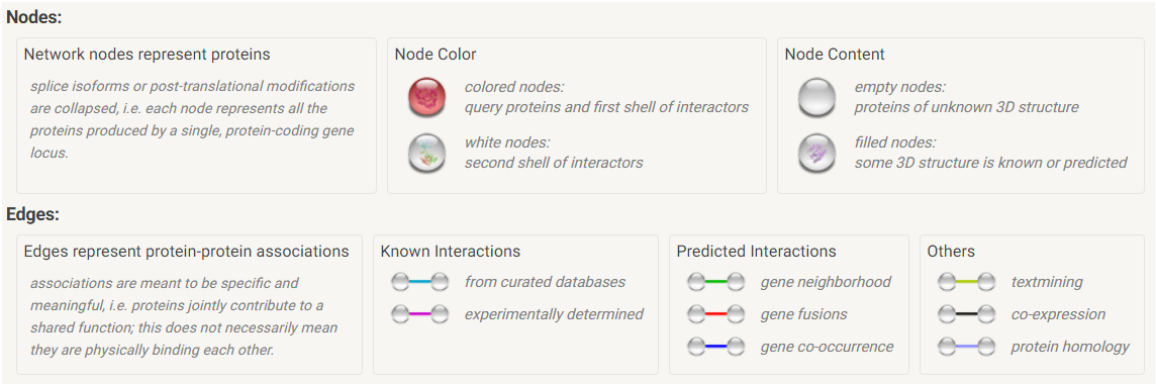


***Figure 17. STRING network of the top antigens detected among the discovery patient cohort.*** *Coloured nodes are indicative of proteins found to be significant among prostate cancer patients in alternate prostate cancer studies conducted by Adeola et al. (red nodes) and Heninger et al. (cyan nodes). Protein aliases include GAGE5 = GAGE12F. Legend corresponding to the network features is displayed below the netork.*

Confirmation of mRNA transcripts for these proteins in known prostate cancer patients was conducted using data from an external patient cohort (The Cancer Genome Atlas (TCGA) PanCancer Atlas – Prostate Adenocarcinoma Cohort; accessed via CBIO) consisting 494 patients, 493 with mRNA data Cerami et al. (2012); Gao et al. (2013). Of the patients with accessible mRNA data, 33 were removed due to lack of one or more data points. CT47.11, GAGE5, BAGE5, and MAGEB5 were removed entirely from analyses due to lack of data for these antigens. Ultimately, 460 patients remained, and their data was used to generate all heat maps in this study. All mRNA data was quantified using RSEM quantification software to obtain absolute values, then converted to z-score for heat map construction Li & Dewey (2011). Prevalence of mRNA expression among patients is shown as a percentage of the cohort (i.e., n=n/460x100).

As seen in **Figure 18** below, mRNA expression was observed in prostate cancer patients for antigens MAGEB1 (2%), MAGEB6 (1%), GAGE4 (2%), GAGE1 (1%), LEMD1 (53%), MAPK3 (100%), GRWD1 (100%), MAGEA2 (15%), MAGEA4 (6%), CTNNB1 (100%), MAGEA1 (20%), SPANXC (1%), and OIP5 (100%). mRNA findings for

MAGEB1, MAGEB6, GAGE4, GAGE1, MAGEA4 and SPANXC were inconsistent with the prevalence of antigens obtained when probing autoantibodies in prostate cancer patients with the CT100+ array.

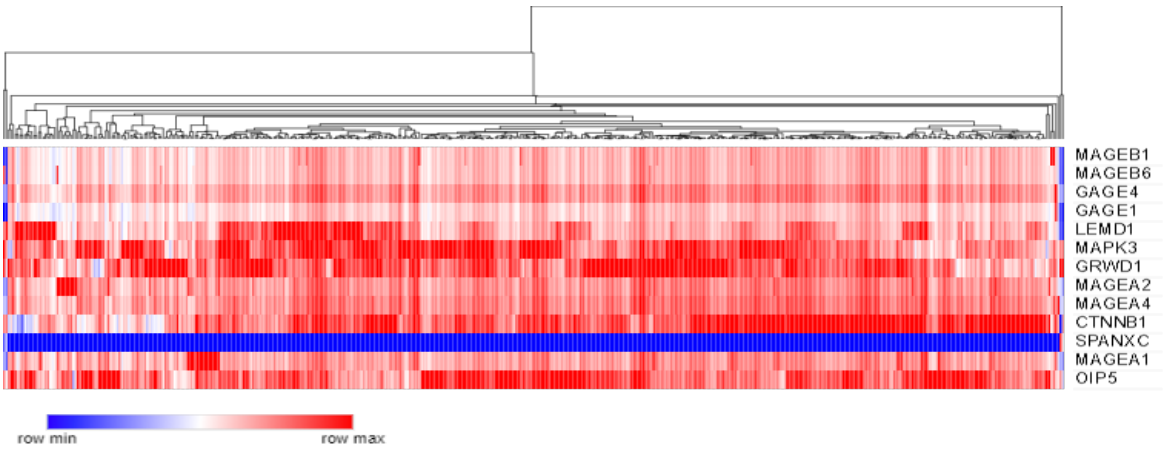


***Figure 18. mRNA expression heat map of available antigens from CBIO for the most prominent antigens in the discovery cohort.*** *The heat map represents the hierarchical clustering by Pearson correlation of MAGEB1, MAGEB6, GAGE4, GAGE1, LEMD1, MAPK3, GRWD1, MAGEA2, MAGEA4, CTNNB1, SPANXC, MAGEA1 and OIP5 mRNA expression in 460 prostate adenocarcinoma cancer patients (PanCancer Atlas– TCGA Database). mRNA expression is displayed as z-scores (RNA Seq V2 RSEM).*

#### *3.2.3.2.2 Diagnostic Efficacy of Autoantibodies in Prostate Cancer (Discovery Cohort)*

The following Section details the results pertaining to the assessment of cancer-associated autoantibodies as diagnostic biomarkers, generated using the discovery cohort.

Following rigorous trialling with numerous antigens, data from 4 of the 16 most prevalent antigens (CTNNB1, MAGEA1, OIP5 and SPANXC, univariate ROC curves seen in **Figure 19** below), and 3 of the best antigen univariate ROC curves (CAMEL, LAGE1b/CTAG2 and ROPN1A, univariate ROC curve seen in **Figure 20** below) were selected. The prominent univariate antigens (MAGEA1, SPANXC, OIP5, and CTNNB1) were selected as having a presence of at least 19% among the 110 patients from the discovery cohort (MAGEA1 19.1%, SPANXC 22.7%, OIP5 23.6% and CTNNB1 25.5%). Best univariate

antigens (CAMEL, LAGE1b and ROPN1A) were selected as having ROC curves with corresponding AUC values >0.7000. This combination of markers was best in terms of cohort coverage, while concomitantly maintaining high sensitivity and specificity for distinguishing cancer patients from healthy individuals.

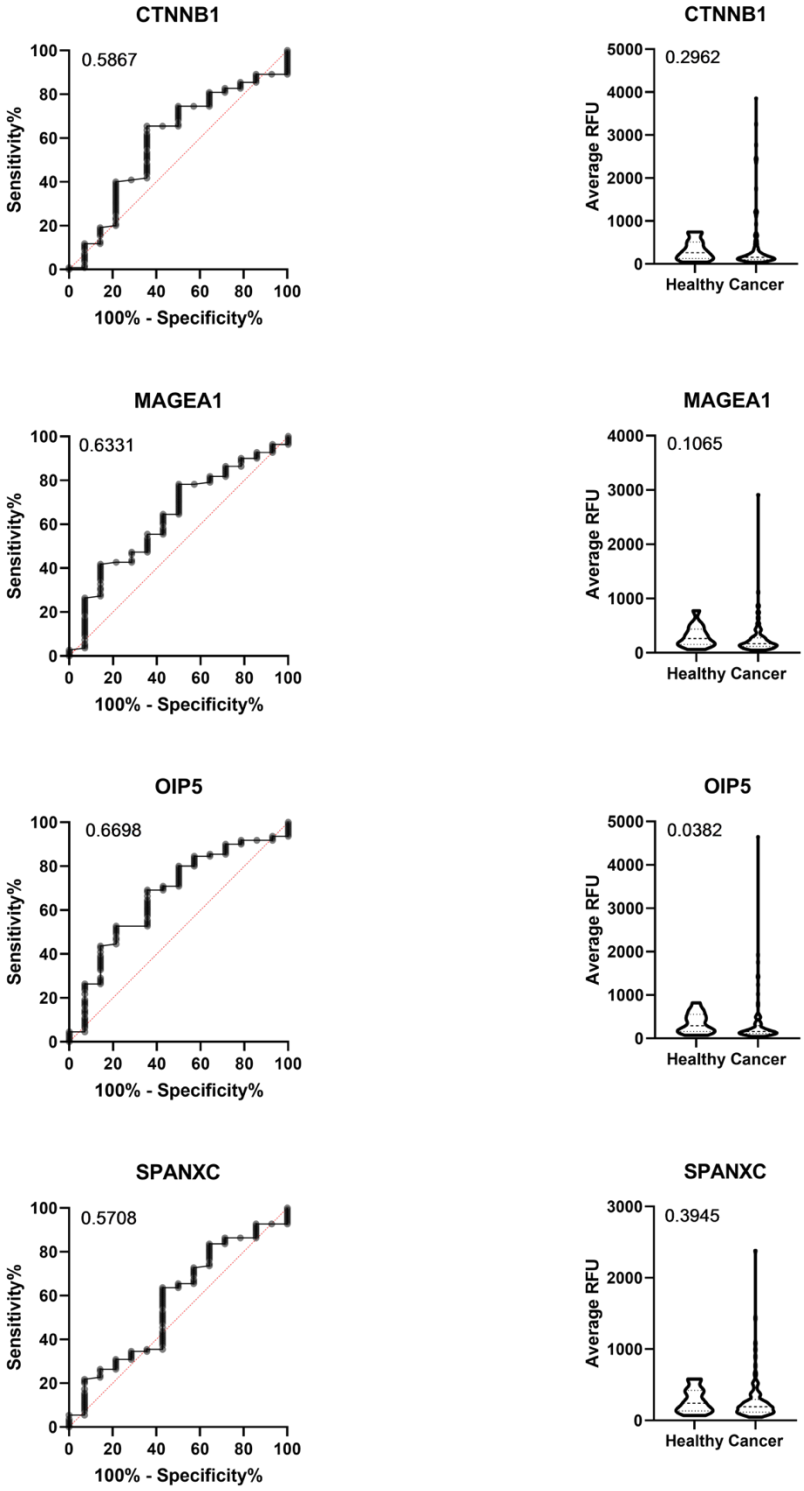

***Figure 19. Top univariate ROC Curves for 4 prevalent antigens found in the discovery cohort.*** *ROC curves for the top 4 most prevalent antigens determined by counts above threshold (≥307 RFU), generated by comparing prostate cancer patients (discovery cohort) and healthy individuals (healthy cohort) array data (on left), with AUC values of 0.5867 (CTNNB1), 0.6331 (MAGEA1), 0.6698 (OIP5), and 0.5708 (SPANXC). Corresponding antigen violin plots are shown (on right), with included Mann-Whitney U test (CI of 95%) p-values of 0.2962 (CTNNB1), 0.1065 (MAGEA1), 0.0382 (OIP5), and 0.3945 (SPANXC).*

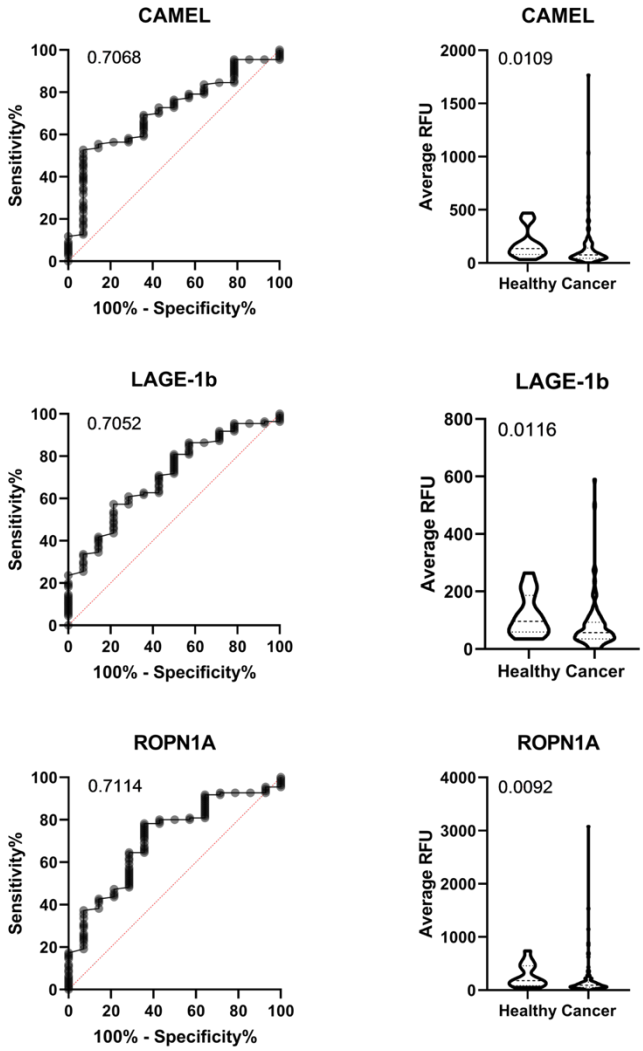


***Figure 20. Top univariate antigen ROC curves capable of distinguishing prostate cancer patients (discovery cohort) from healthy individuals (healthy cohort).*** *ROC curves for the top univariate antigens observed when comparing discovery cohort prostate cancer patients from healthy individuals using array data (on left) with AUC values of 0.7068 (CAMEL), 0.7052 (LAGE-1b), and 0.7114 (ROPN1A). Corresponding antigen violin plots are shown (on right), with included*

*Mann-Whitney U test (CI of 95%) p-values of 0.0109 (CAMEL), 0.0116 (LAGE-1b), and 0.0092 (ROPN1A).*

In order to test the diagnostic potential of these univariate antigens, CombiROC analyses were then conducted Mazzara et al (2017). This web application allows users to input multimarker panels and define the stringency of their test by adjusting sensitivity and specificity thresholds in order to determine the combination of markers capable of best distinguishing between two groups of interest. RFU values for each of these antigens from all patients was uploaded to the web application, and when appropriate, corresponding PSA values were added as well. The lowest threshold for sensitivity and specificity was selected in order to ensure that all possible combinations and their resulting AUCs, sensitivities, and specificities could be assessed. This was the case for all further CombiROC analyses.

Of the marker combinations resulting from the CombiROC analysis (using the previously defined univariate antigens), Combo LXXI had the highest AUC (0.847), with a 90% sensitivity a 64% specificity. The combination with the highest sensitivity was Combo XCVI, with an AUC of 0.847, a 92% sensitivity and a 64% specificity, while the highest specificity was Combo C, with an AUC of 0.802, a 56% sensitivity and a 100% specificity. These 3 combinations were plotted as multivariate ROC curves below in **Figure 21**.

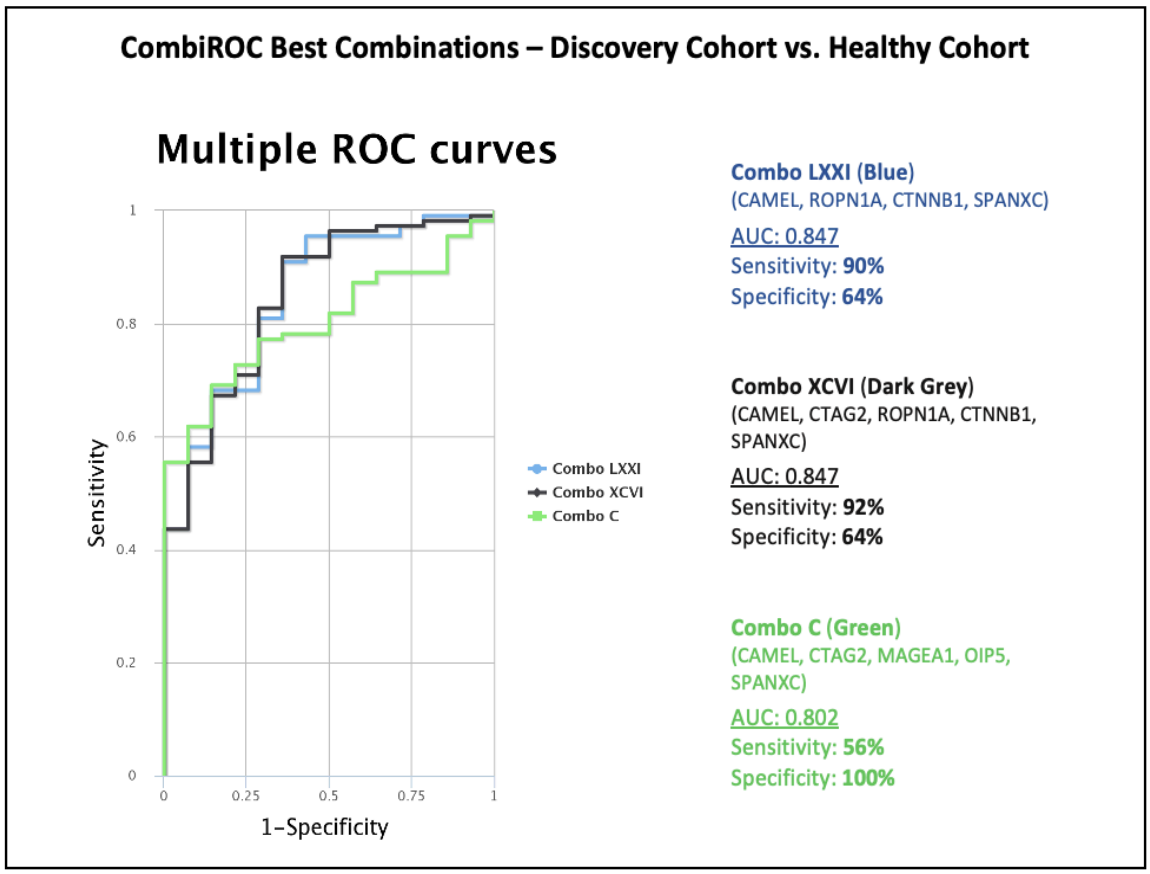


***Figure 21. Top multivariate antigen ROC curves discriminating prostate cancer patients (discovery cohort) from healthy individuals (healthy cohort).*** *Top AUC combination – Combo LXXI (blue) consisting of CAMEL, ROPN1A, CTNNB1, and SPANXC generating an AUC of 0.847, sensitivity of 90%, and specificity of 64%. Highest sensitivity combination – Combo XCVI (dark grey) consisting of CAMEL, CTAG2, ROPN1A, CTNNB1, and SPANXC generating an AUC of 0.847, sensitivity of 92%, and specificity of 64%. Highest specificity combination – Combo C (green) consisting of CAMEL, CTAG2, MAGEA1 and SPANXC generating an AUC of 0.802, sensitivity of 56%, and specificity of 100%.*

A realistic application of a novel diagnostic test would be to complement current screening methods, such as PSA levels testing. The inclusion of PSA levels would also render any resultant diagnostic signatures specific to prostate cancer. To test whether the addition of patient PSA levels (univariate AUC 0.9279) bolstered the 3 best marker combinations a second CombiROC analysis was performed. We found that the incorporation of PSA levels substantially improved diagnostic potential. Combo CLXXXIII (above Combo LXXI

+PSA) generated an AUC of 0.959, with an 89% sensitivity a 93% specificity; Combo CCXIX (above Combo XCVI +PSA) generated an AUC of 0.960, an 89% sensitivity and a 93% specificity; Combo CCXXIV (above Combo C +PSA) generated an AUC of 0.942, a 90% sensitivity and an 86% specificity. These 3 combinations were plotted below in **Figure 22**.

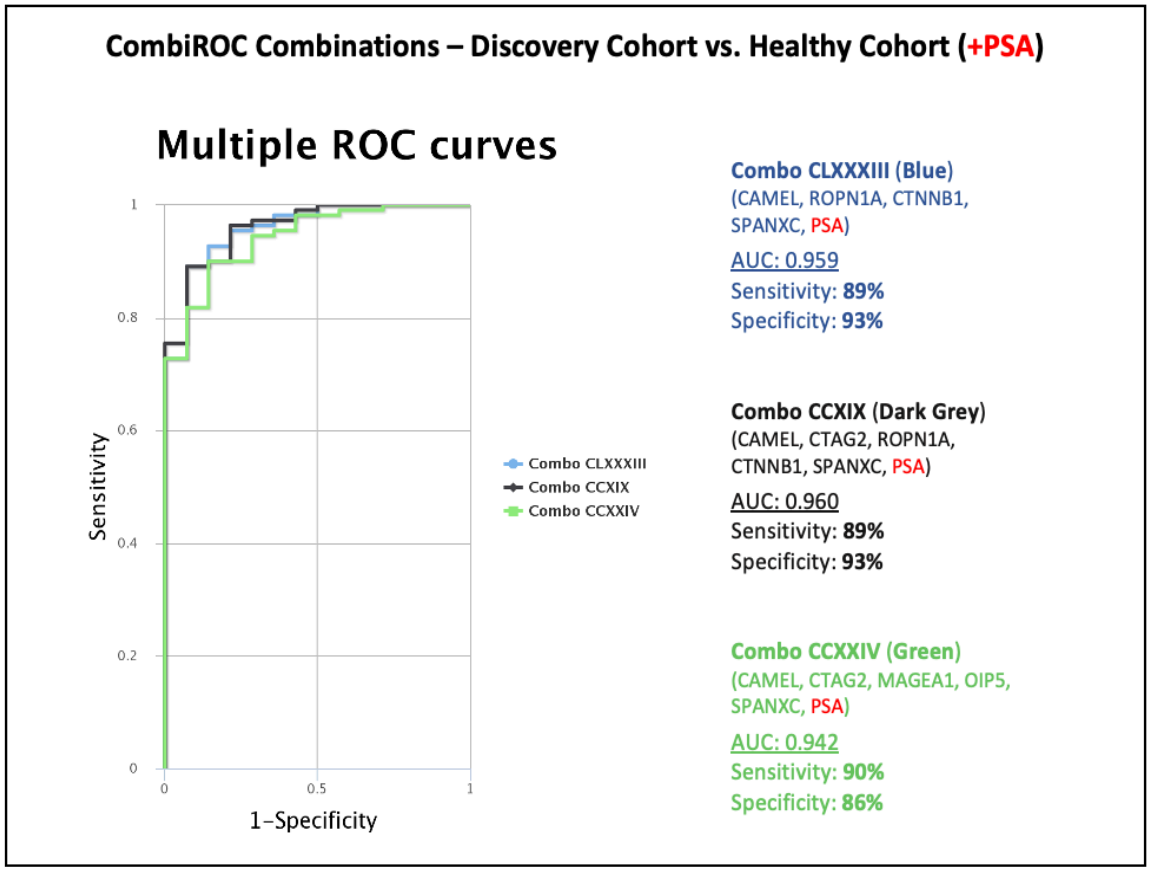


***Figure 22. Top multivariate antigen/PSA ROC curves discriminating prostate cancer patients (discovery cohort) from healthy individuals (healthy cohort).*** *Top AUC combination – Combo CCXIX (dark grey) consisting of CAMEL, ROPN1A, CTNNB1, SPANXC, and PSA generating an AUC of 0.960, sensitivity of 89%, and specificity of 93%. Highest sensitivity combination – Combo CCXXIV (green) consisting of CAMEL, CTAG2, MAGEA1, OIP5, SPANXC, and PSA generating an AUC of 0.942, sensitivity of 90%, and specificity of 86%. Highest specificity combination – Combo CLXXXIII (blue) consisting of CAMEL, ROPN1A, CTNNB1, SPANXC and PSA generating an AUC of 0.959, sensitivity of 89%, and specificity of 93%.*

Following multivariate ROC analysis to distinguish discovery cohort prostate cancer patients from healthy individuals, mRNA expression of genes associated with the resultant

antigens involved was assessed using the PanCancer Atlas cohort. Of these genes displayed in **Figure 23** below, ROPN1 (99%), CTNNB1 (100%), OIP5 (100%), and KLK3 (PSA; 100%) displayed mRNA expression in relatively high quantities in the majority of the cohort, whereas CTAG2 (17%), MAGEA1 (20%), and SPANXC (1%) displayed relatively low / negligible expression.

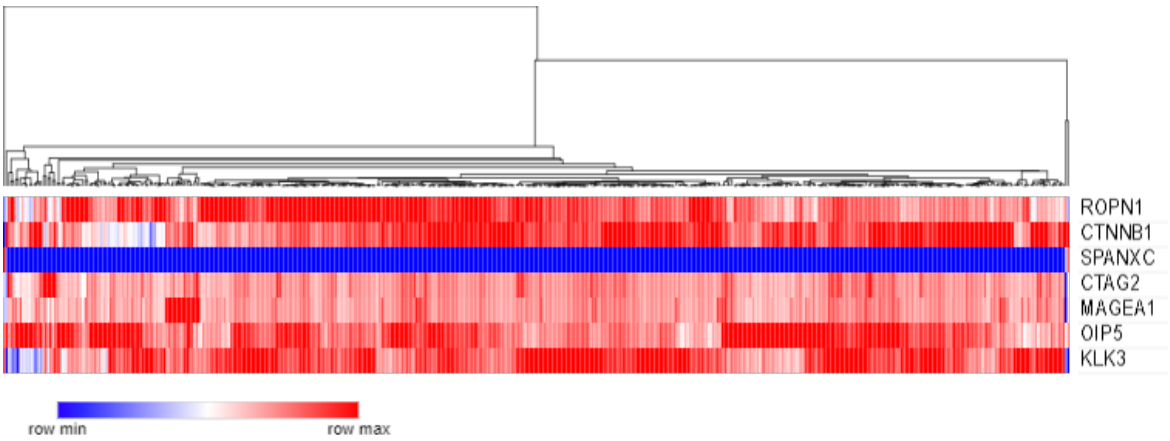


***Figure 23. mRNA expression heat map of available antigens from CBIO included in the top multivariate combinations that discriminate prostate cancer patients (discovery cohort) from healthy individuals (healthy cohort).*** *The heat map represents the hierarchical clustering by Pearson correlation of ROPN1, CTNNB1, SPANXC, STAG2, MAGEA1, and OIP5, and KLK3 (PSA) mRNA expression in 460 prostate adenocarcinoma cancer patients (PanCancer Atlas–TCGA Database). mRNA expression is displayed as z-scores (RNA Seq V2 RSEM).*

Following acquisition of benign samples during the validation phase of this study, we were able to assess whether there were any potential univariate antigens capable of not only distinguishing cancer from healthy individuals, but distinguishing cancer from healthy AND benign individuals; eliminating individuals with benign conditions from being detected. Each univariate ROC curve was generated using the fluorescence values of all antigens for all patients among the healthy, benign and discovery cohorts.

Top univariate antigens (i.e., ACVR2B, CAMEL, CT47.11v, NY-ESO-1, ROPN1A, CALM1, CEP290, MART-1 and PRKCZ) were chosen if their corresponding ROC curve

AUC values were >0.6500. ROC curves with AUC values and associated violin plots with Mann-Whitney U test results can be seen in **Figure 24** below.

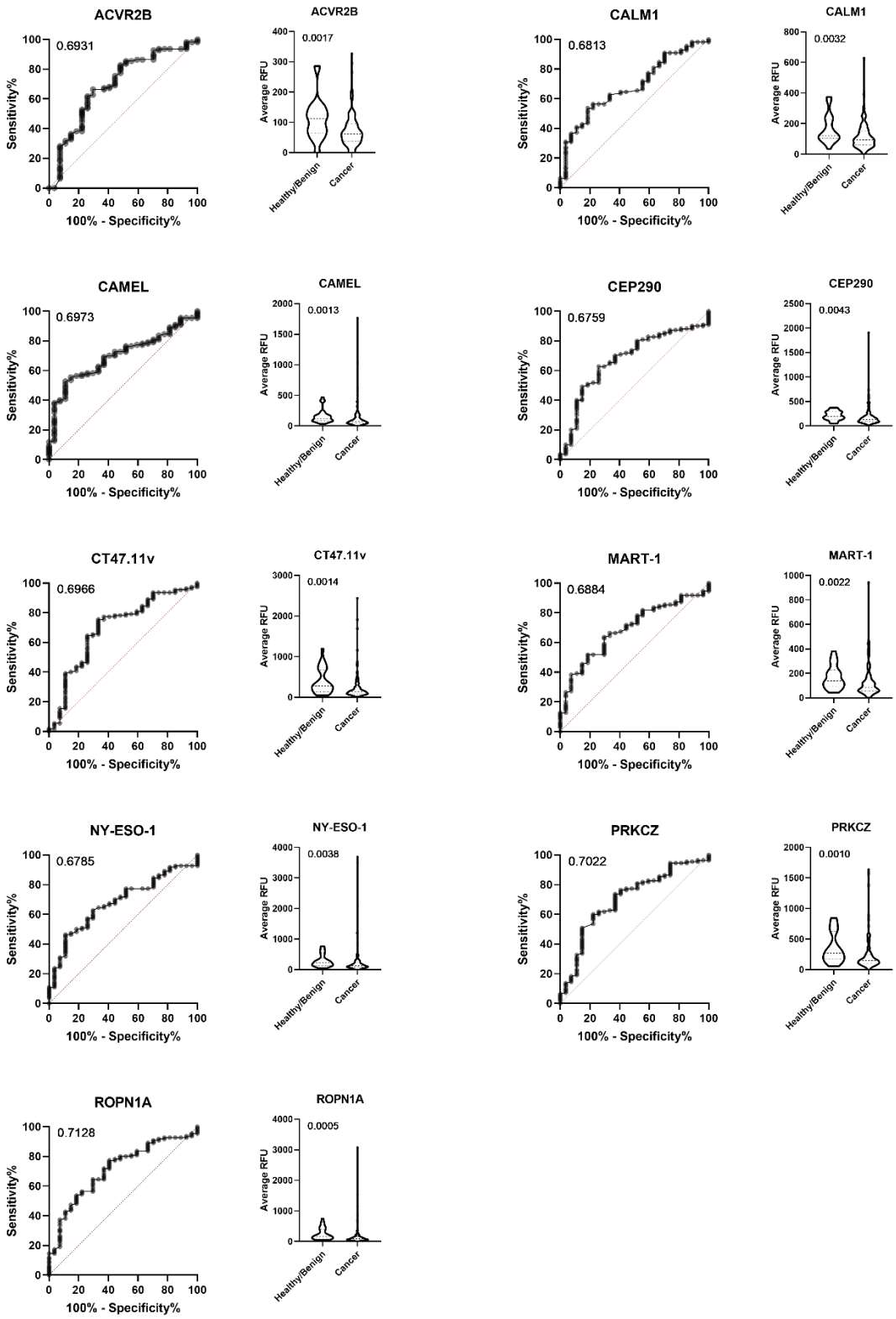


***Figure 24. Top univariate antigen ROC curves capable of distinguishing prostate cancer patients (discovery cohort) from healthy and benign individuals (healthy and benign cohorts).*** *ROC*

*curves for the top univariate antigens observed when comparing prostate cancer patients from healthy individuals using array data (on left) with AUC values of 0.6931 (ACVR2B), 0.6973 (CAMEL), 0.6966 (CT47.11v), 0.6785 (NY-ESO-1), 0.7128 (ROPN1A), 0.6813 (CALM1), 0.6759 (CEP290), 0.6884 (MART-1), and 0.7022 (PRKCZ). Corresponding antigen violin plots are shown (on right), with included Mann-Whitney U test (CI of 95%) p-values of 0.0017 (ACVR2B), 0.0013 (CAMEL), 0.0014 (CT47.11v), 0.0038 (NY-ESO-1), 0.0005 (ROPN1A), 0.0032 (CALM1), 0.0043 (CEP290), 0.0022 (MART-1), and 0.0010 (PRKCZ).*

Top univariate antigens able to distinguish prostate cancer patients from healthy and benign individuals were plotted as multivariate antigen ROC curves (**Figure 25**). Of the 511 potential combinations created using these univariate antigens, Combo CDLVIII generated the highest AUC of 0.769, with a sensitivity and specificity of 78% and 73%, respectively. Combo CCLXXXII (AUC 0.742) and Combo CCCXL (AUC 0.754) were also plotted as they displayed the highest sensitivity and specificity, following that of the combination with the top AUC (Combo CDLVIII).

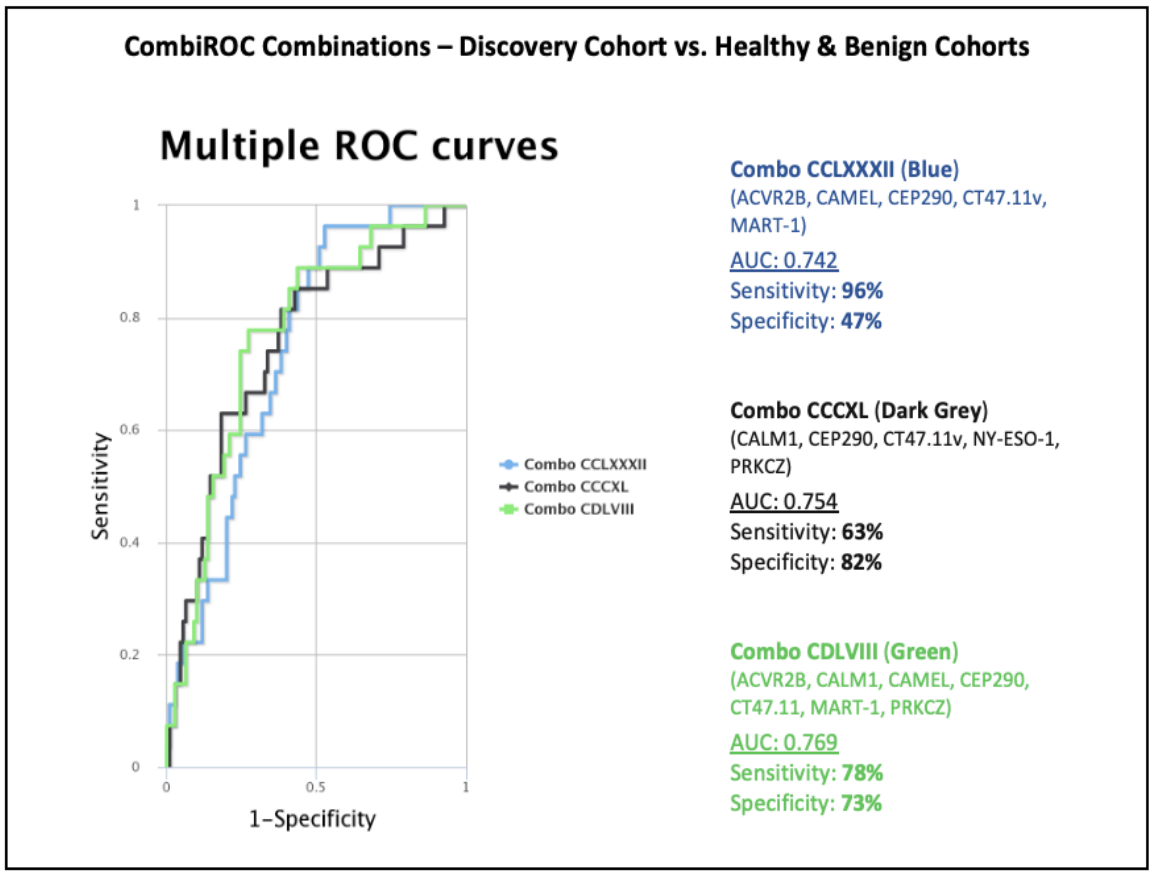


***Figure 25. Top multivariate antigen ROC curves discriminating prostate cancer patients (discovery cohort) from healthy and benign individuals (healthy and benign cohorts).*** *Top AUC combination – Combo CDLVIII (green) consisting of ACVR2B, CALM1, CAMEL, CEP290, CT47.11, MART-1 and PRKCZ generating an AUC of 0.769, sensitivity of 78%, and specificity of 73%. Highest sensitivity combination – Combo CCLXXXII (blue) consisting of ACVR2B, CAMEL, CEP290, CT47.11 and MART-1 generating an AUC of 0.742, sensitivity of 96%, and specificity of 47%. Highest specificity combination – Combo CCCXL (dark grey) consisting of CALM1, CEP290, CT47.11, NY-ESO-1 and PRKCZ generating an AUC of 0.754, sensitivity of 63%, and specificity of 82%.*

Following multivariate ROC analysis to distinguish discovery cohort prostate cancer patients from healthy and benign individuals, mRNA expression of genes associated with the resultant antigens involved was assessed using the PanCancer Atlas cohort. Of these genes displayed in the heat map below (see **Figure 26**), CALM1 (100%), CEP290 (100%), MLANA (MART-1; 82%), PRKCZ (100%), ACVR2B (100%) and KLK3 (PSA; 100%) displayed relatively higher levels of mRNA transcripts in the majority of the cohort, with

conversely lower transcript levels seen in fewer patients for CTAG2 (CAMEL; 17%) and CTAG1B (30%). Moreover, mRNA of all genes was expressed in levels that sufficiently correlated with antigen prevalence found using the CT100+ arrays.

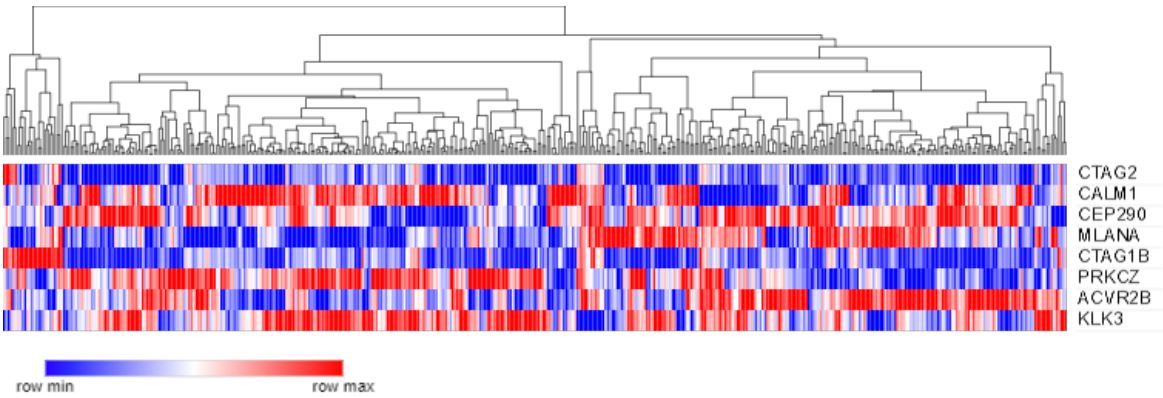


***Figure 26. mRNA expression heat map of available antigens from CBIO included in the top multivariate combinations that discriminate prostate cancer patients (discovery cohort) from healthy and benign individuals (healthy and benign cohorts).*** *The heat map represents the hierarchical clustering by Pearson correlation of CTAG2, CALM1, CEP290, MLANA (MART-1), CTAG1B, PRKCZ, ACVR2B, and KLK3 (PSA) mRNA expression in 460 prostate adenocarcinoma cancer patients (PanCancer Atlas– TCGA Database). mRNA expression is displayed as z-scores (RNA Seq V2 RSEM).*

#### *3.2.3.2.3 Prognostic Efficacy of Autoantibodies in Prostate Cancer (Discovery Cohort)*

The following Section details the results pertaining to the assessment of cancer-associated autoantibodies as prognostic biomarkers, generated using the discovery cohort.

To assess the ability of autoantibody profiles at distinguishing relapse and non-relapse prostate cancer patients, univariate ROC curves were generated using average antigen fluorescence values from both groups in the discovery cohort and plotted accordingly. Top univariate antigens (i.e., BAGE5, CAMEL, MART-1 and RAF) were selected based on their corresponding ROC curve AUC scores displayed values above >0.6000. ROC curves with AUC values and associated violin plots with Mann-Whitney U test results can be seen in **Figure 27** below.

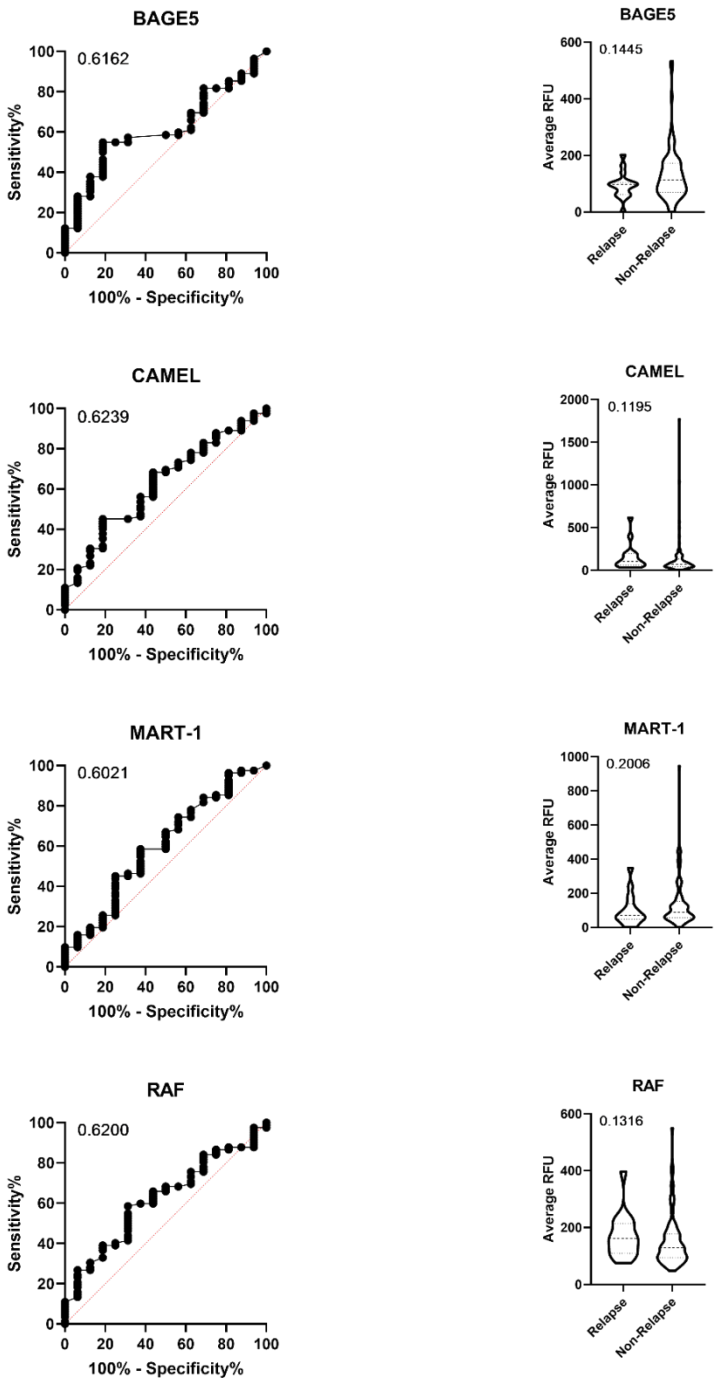


***Figure 27. Top univariate antigen ROC curves capable of distinguishing relapse and non-relapse prostate cancer patients (discovery cohort).*** *ROC curves for the top univariate antigens observed when comparing relapse and non-relapse cancer patients within the discovery cohort using array data (on left) with AUC values of 0.6162 (BAGE5), 0.6239 (CAMEL), 0.6021 (MART-1), and 0.6200 (RAF). Corresponding antigen violin plots are shown (on right), with included Mann-Whitney U test (CI of 95%) p-values of 0.1445 (BAGE5), 0.1195 (CAMEL), and RAF (0.1316).*

Top univariate antigens able to distinguish relapse and non-relapse prostate cancer patients were plotted as multivariate antigen ROC curves without PSA (**Figure 28**) and with PSA (**Figures 29**). Without PSA included, of the 14 possible combinations, Combo XI generated the highest AUC of 0.682, with a sensitivity and specificity of 50% and 82%, respectively. Combo VI (AUC 0.644) and Combo X (AUC 0.675) were also plotted as they displayed the highest sensitivity and specificity, following that of the combination with the top AUC (Combo XI). With PSA, of the 31 possible combinations, Combo XXV generated the highest AUC of 0.707, with a sensitivity and specificity of 94% and 48%, respectively. Combo XXVI (AUC 0.704) and Combo XX (AUC 0.675) were also plotted as they displayed the highest sensitivity and specificity, following that of the combination with the top AUC (Combo XXV).

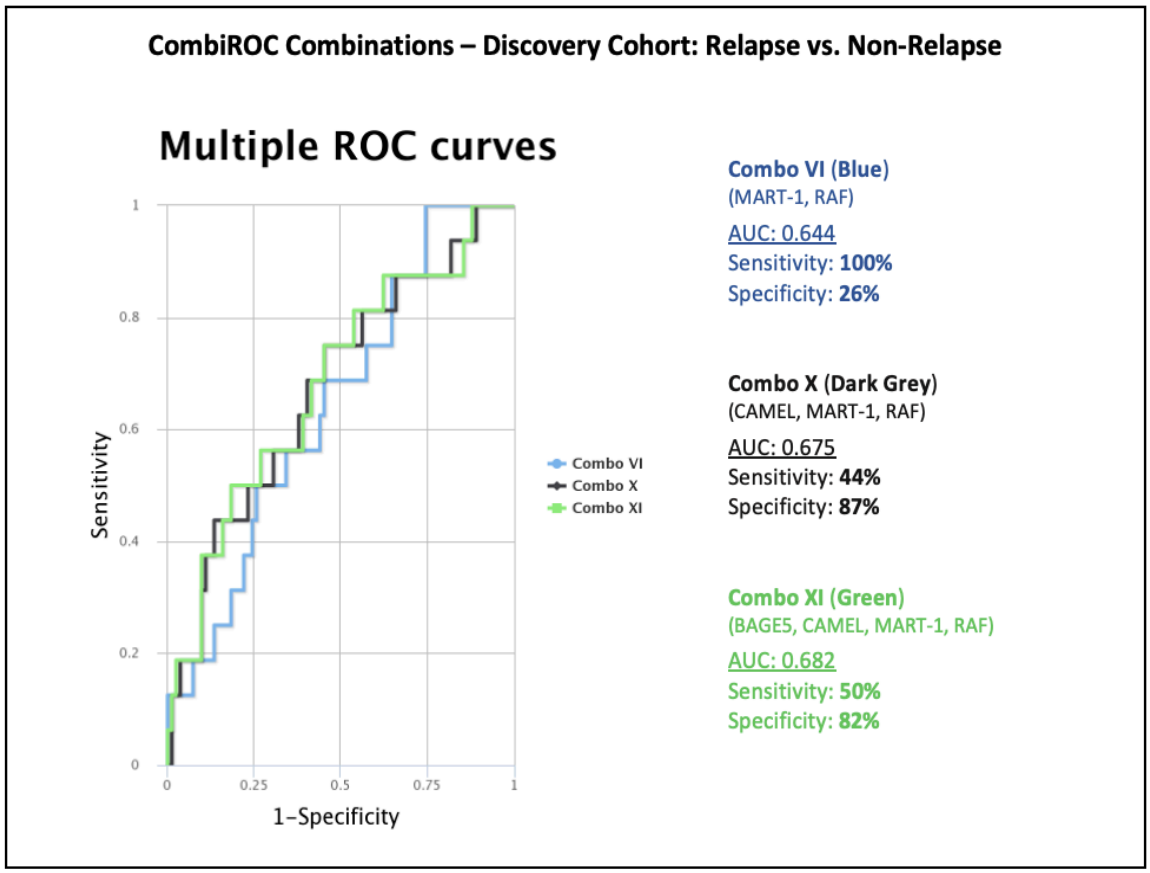


***Figure 28. Top multivariate antigen ROC curves discriminating relapse and non-relapse prostate cancer patients (discovery cohort).*** *Top AUC combination – Combo XI (green) consisting of BAGE5, CAMEL, MART-1 and RAF generating an AUC of 0.682, sensitivity of 50%, and specificity*

*of 82%. Highest sensitivity combination – Combo VI (blue) consisting of MART-1 and RAF generating an AUC of 0.644, sensitivity of 100%, and specificity of 26%. Highest specificity combination – Combo X (green) consisting of CAMEL, MART-1 and RAF generating an AUC of 0.675, sensitivity of 44%, and specificity of 87%.*

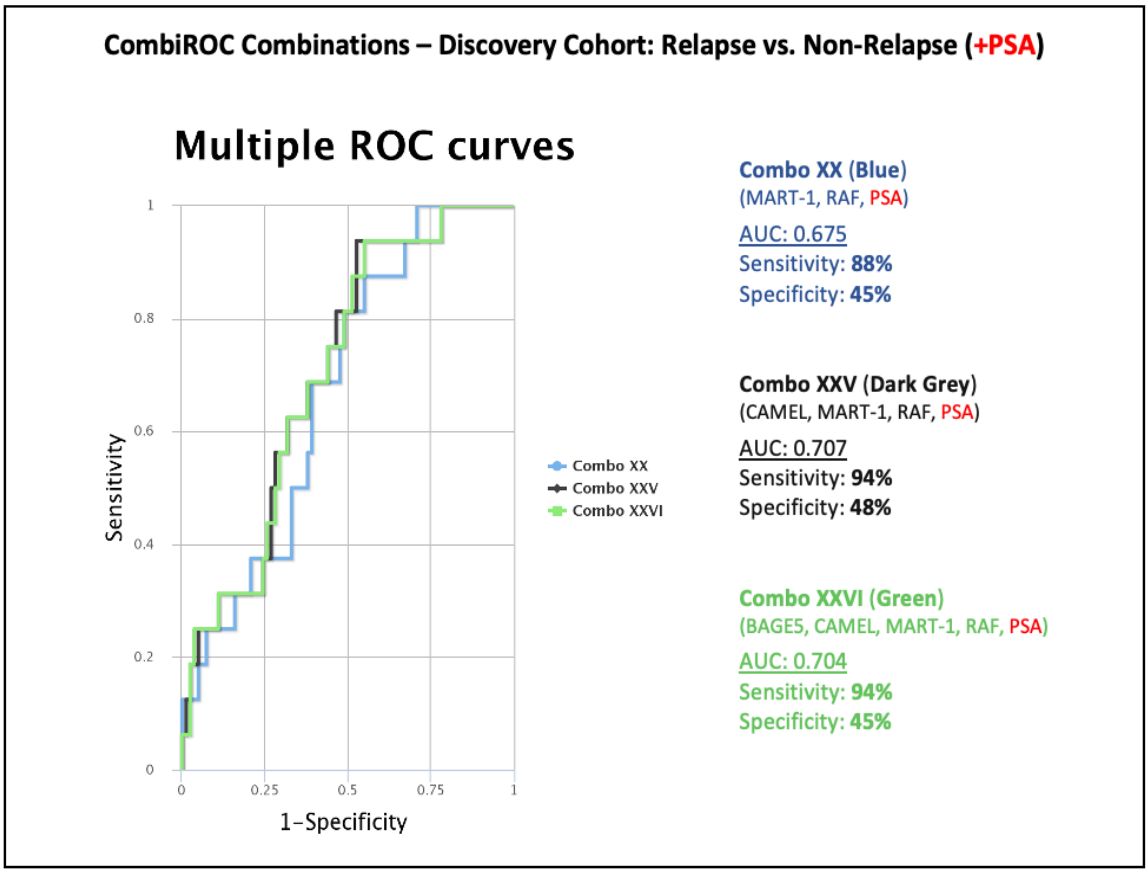


***Figure 29. Top multivariate antigen/PSA ROC curves discriminating relapse and non-relapse prostate cancer patients (discovery cohort).*** *Top AUC combination – Combo XXV (dark grey) consisting of CAMEL, MART-1, RAF and PSA generating an AUC of 0.707, sensitivity of 94%, and specificity of 48%. Highest sensitivity combination – Combo XXVI (green) consisting of BAGE5, CAMEL, MART-1, RAF and PSA generating an AUC of 0.704, sensitivity of 94%, and specificity of 45%. Highest specificity combination – Combo XX (blue) consisting of MART-1, RAF and PSA generating an AUC of 0.675, sensitivity of 88%, and specificity of 45%.*

Following multivariate ROC analysis to distinguish relapse and non-relapse prostate cancer patients (discovery cohort), mRNA expression of genes associated with the antigens involved was assessed using the PanCancer Atlas cohort. Of these genes displayed in the heat map below (see **Figure 30**), MLANA (MART-1; 82%), RAF1 (RAF; 100%) and

KLK3 (PSA; 100%) displayed relatively high levels of mRNA transcripts in the majority of prostate adenocarcinoma patients, with conversely low levels expressed for CTAG2 (CAMEL; 17%) in negligible patient numbers. Moreover, mRNA of all genes was expressed in levels that sufficiently correlate with antigen prevalence found using the CT100+ arrays.

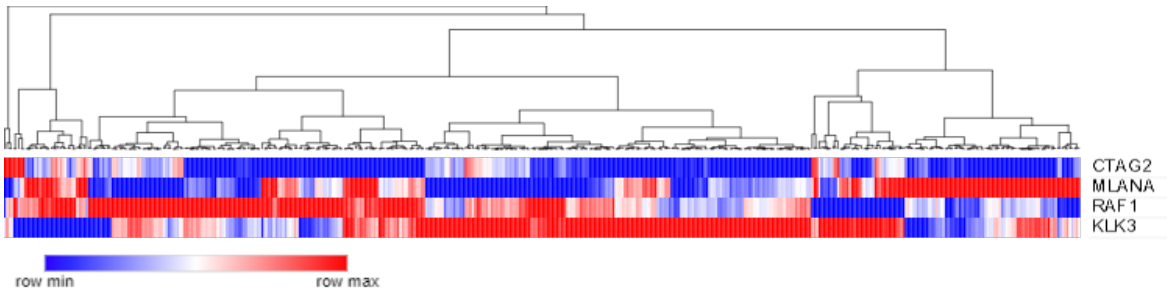


***Figure 30. mRNA expression heat map of available antigens from CBIO included in the top multivariate combinations that discriminate relapse and non-relapse prostate cancer patients (discovery cohort).*** *The heat map represents the hierarchical clustering by Pearson correlation of CTAG2 (CAMEL), MLANA (MART-1), RAF1 (RAF) and KLK3 (PSA) mRNA expression in 460 prostate adenocarcinoma cancer patients (PanCancer Atlas– TCGA Database). mRNA expression is displayed as z-scores (RNA Seq V2 RSEM).*

To assess the ability of autoantibody profiles at distinguishing survivability of prostate cancer patients, univariate ROC curves were generated using average antigen fluorescence values from two distinct patient groups (deceased and alive, discovery cohort). Top univariate antigens (i.e., ACVR2B, BAGE5, COX6B2, MAP9, XAGE-2) were selected based on their corresponding ROC curve AUC scores displayed values above >0.6500. ROC curves with AUC values and associated violin plots with Mann-Whitney U test results can be seen in **Figure 31** below.

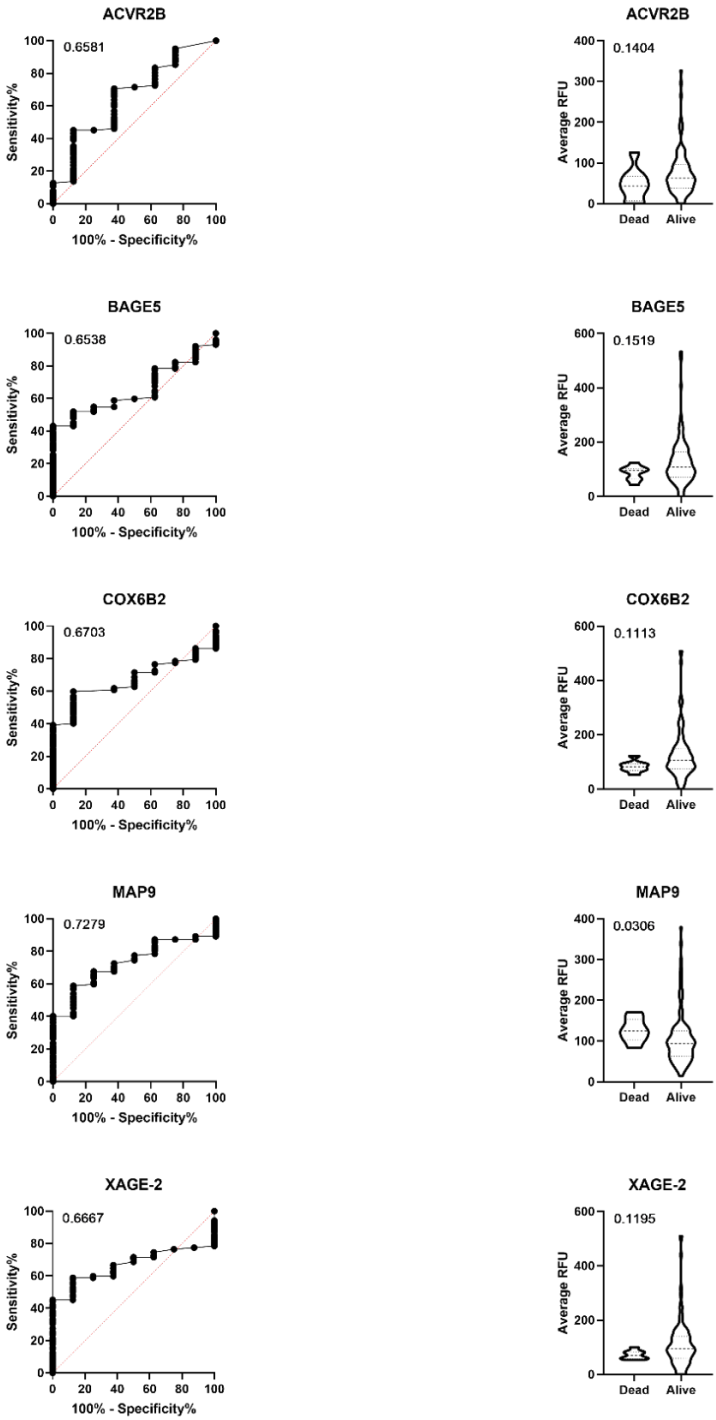


***Figure 31. Top univariate antigen ROC curves capable of distinguishing survivability in prostate cancer patients (discovery cohort).*** *ROC curves for the top univariate antigens observed when comparing alive and dead grade prostate cancer patients within the discovery cohort using array data (on left) with AUC values of 0.6581 (ACVR2B), 0.6538 (BAGE2), 0.6703 (COX6B2), 0.7279 (MAP9), and 0.6667 (XAGE-2). Corresponding antigen violin plots are shown (on right), with included Mann-Whitney U test (CI of 95%) p-values of 0.1404 (ACVR2B), 0.1519 (BAGE2), 0.1113 (COX6B2), 0.0306 (MAP9), and 0.1195 (XAGE-2).*

Top univariate antigens able to distinguish alive and deceased prostate cancer patients were plotted as multivariate antigen ROC curves without PSA (**Figure 32**) and with PSA (**Figure 33**). Without PSA included, of the 31 possible combinations, Combo XII generated the highest AUC of 0.848, with a sensitivity and specificity of 86% and 76%, respectively. Combo XXIII (AUC 0.835) and Combo IV (AUC 0.588) were also plotted as they displayed the highest sensitivity and specificity, following that of the combination with the top AUC (Combo 0.848). With PSA, of the 126 possible combinations, Combo LIV generated the highest AUC of 0.863, with a sensitivity and specificity of 88% and 83%, respectively. Combo XL (AUC 0.827) and Combo XXV (AUC 0.777) were also plotted as they displayed the highest sensitivity and specificity, following that of the combination with the top AUC (Combo LIV).

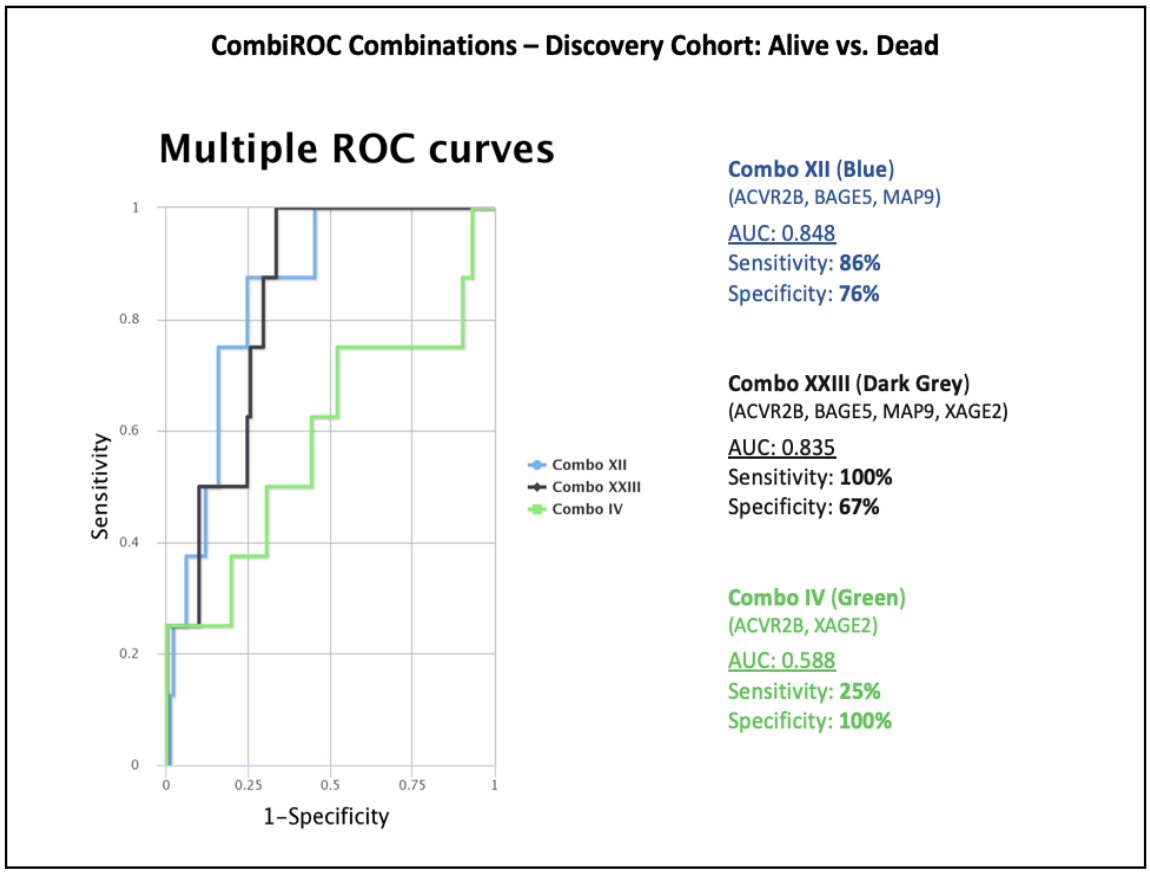


***Figure 32. Top multivariate antigen ROC curves discriminating survivability in prostate cancer patients (discovery cohort).*** *Top AUC combination – Combo XII (blue) consisting of ACVR2B, BAGE5, and MAP9 generating an AUC of 0.848, sensitivity of 86%, and specificity of 76%. Highest*

*sensitivity combination – Combo XXIII (dark grey) consisting of ACVR2B, BAGE5, MAP9 and XAGE2 generating an AUC of 0.835, sensitivity of 100%, and specificity of 67%. Highest specificity combination – Combo IV (green) consisting of ACVR2B and XAGE2 generating an AUC of 0.588, sensitivity of 25%, and specificity of 100%.*

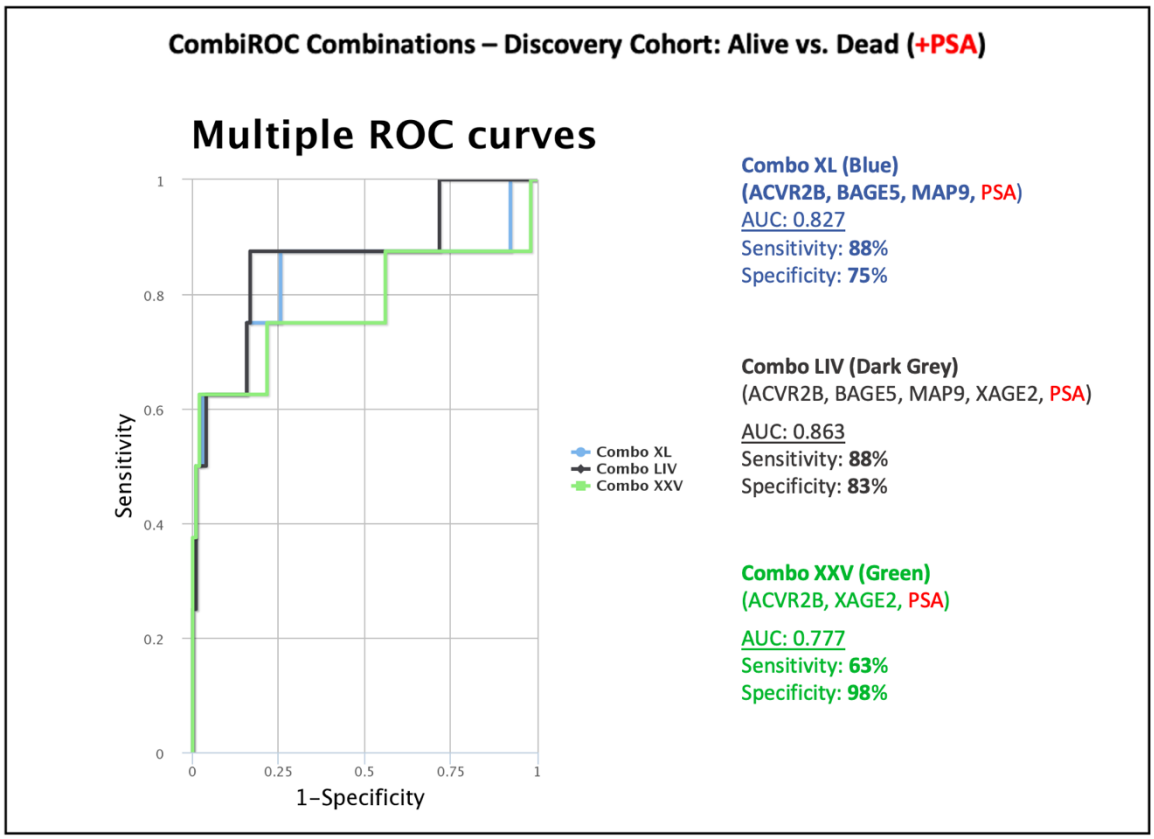


***Figure 33. Top multivariate antigen/PSA ROC curves discriminating survivability in prostate cancer patients (discovery cohort).*** *Top AUC combination – Combo LIV (dark grey) consisting of ACVR2B, BAGE5, MAP9, XAGE2 and PSA generating an AUC of 0.863, sensitivity of 88%, and specificity of 83%. Highest sensitivity combination – Combo XL (blue) consisting of ACVR2B, BAGE5, MAP9 and PSA generating an AUC of 0.827, sensitivity of 88%, and specificity of 75%. Highest specificity combination – Combo XXV (green) consisting of ACVR2B, XAGE2 and PSA generating an AUC of 0.777, sensitivity of 63%, and specificity of 98%.*

Following multivariate ROC analysis to distinguish alive and deceased prostate cancer patients (discovery cohort), mRNA expression of genes associated with the antigens involved was assessed using the PanCancer Atlas cohort. Of these genes displayed in the heat map below (see **Figure 34**), ACVR2B (100%), MAP9 (100%) and KLK3 (PSA;

100%) displayed relatively high levels of mRNA transcripts in prostate adenocarcinoma patients, with conversely low transcript levels seen for XAGE2 (XAGE-2; 1%).

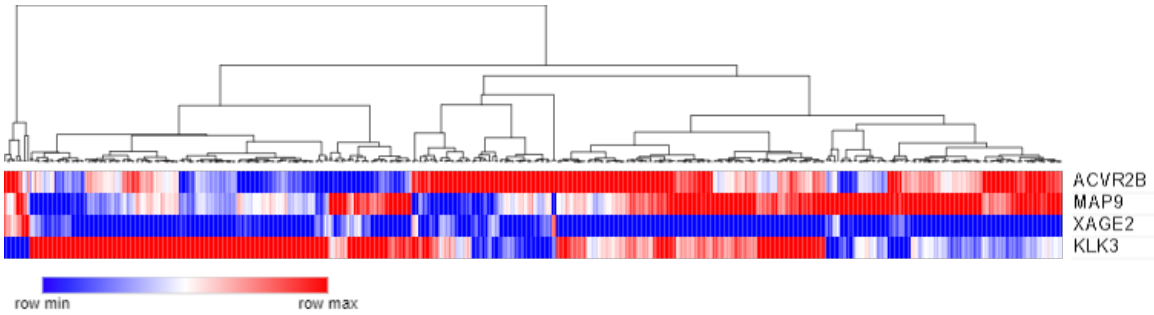


***Figure 34. mRNA expression heat map of available antigens from CBIO included in the top multivariate combinations that discriminate survivability in prostate cancer patients (discovery cohort).*** *The heat map represents the hierarchical clustering by Pearson correlation of ACVR2B, MAP9, XAGE2 and KLK3 (PSA) mRNA expression in 460 prostate adenocarcinoma cancer patients (PanCancer Atlas– TCGA Database). mRNA expression is displayed as z-scores (RNA Seq V2 RSEM).*

#### *3.2.3.2.4 Disease Stratification of Autoantibodies in Prostate Cancer (Discovery Cohort)*

The following Section details the results pertaining to the assessment of cancer-associated autoantibodies as prognostic biomarkers, generated using the discovery cohort.

To assess the ability of autoantibody profiles at distinguishing low- and high-grade prostate cancer patients, univariate ROC curves were generated using average antigen fluorescence values from both groups in the discovery cohort and plotted accordingly. Top univariate antigens (i.e., GAGE5, MICA and SSX4) were selected based on their corresponding ROC curve AUC scores displayed values above >0.7000. ROC curves with AUC values and associated violin plots with Mann-Whitney U test results can be seen in **Figure 35** below.

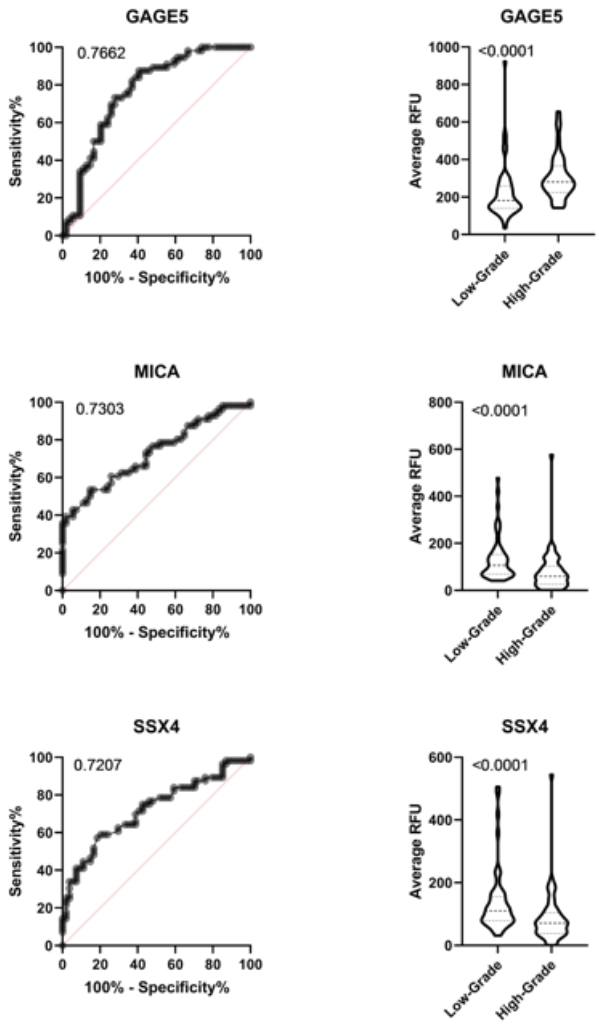


***Figure 35. Top univariate antigen ROC curves capable of distinguishing low- and high-grade prostate cancer patients (discovery cohort).*** *ROC curves for the top univariate antigens observed when comparing high- and low-grade prostate cancer patients within the discovery cohort using array data (on left) with AUC values of 0.7662 (GAGE5), 0.7303 (MICA), and 0.7207 (SSX4). Corresponding antigen violin plots are shown (on right), with included Mann-Whitney U test (CI of 95%) p-values of >0.0001 (GAGE5), >0.0001 (MICA), and >0.0001 (SSX4).*

Top univariate antigens able to distinguish low- from high-grade prostate cancer patients were plotted as multivariate antigen ROC curves without PSA (**Figure 36**) and with PSA (**Figure 37**). Without PSA included, of the 7 possible combinations, Combo IV generated the highest AUC of 0.937, with a sensitivity and specificity of 93% and 80%, respectively. Combo I (AUC 0.930) and Combo II (AUC 0.928) were also plotted as they displayed the

highest sensitivity and specificity, following that of the combination with the top AUC (Combo IV). With PSA, of the 14 possible combinations, Combo XI generated the highest AUC of 0.953, with a sensitivity and specificity of 93% and 89%, respectively. Combo IX (AUC 0.949) and Combo VIII (AUC 0.945) were also plotted as they displayed the highest sensitivity and specificity, following that of the combination with the top AUC (Combo IX).

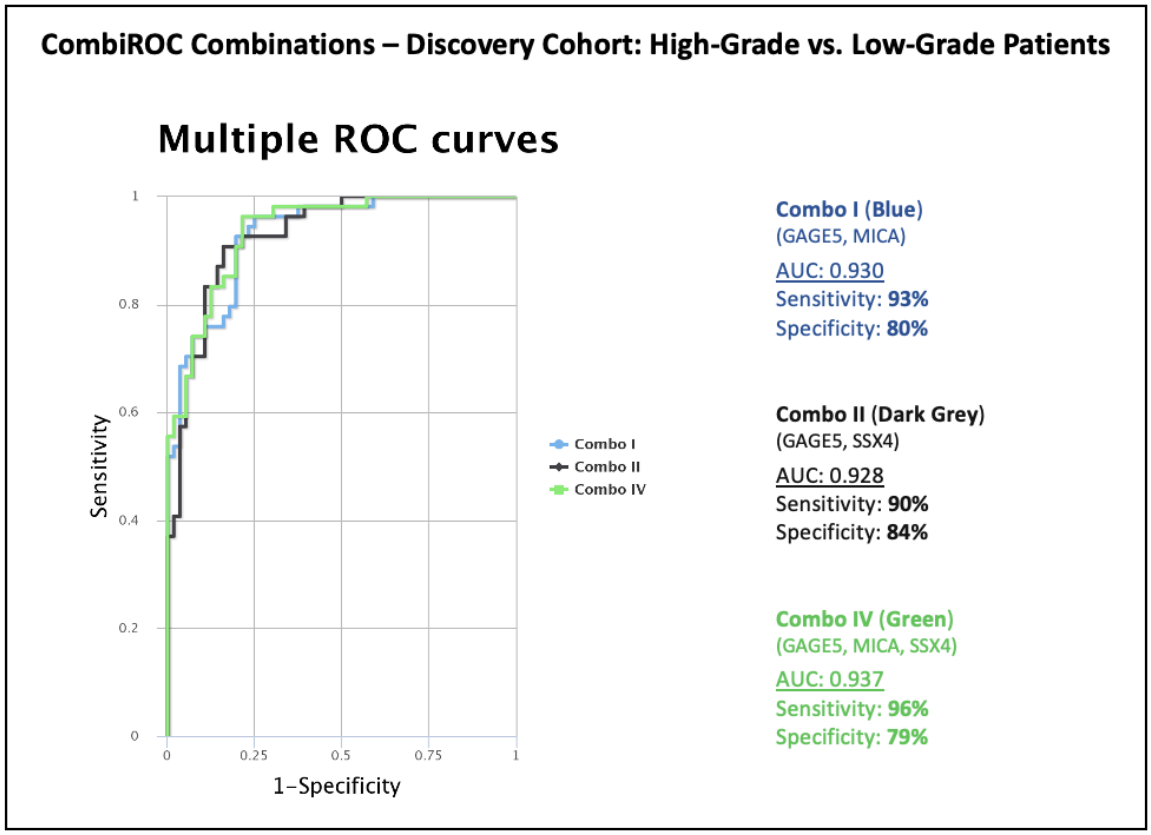


***Figure 36. Top multivariate antigen ROC curves discriminating low- and high-grade prostate cancer patients (discovery cohort).*** *Top AUC combination – Combo IV (green) consisting of GAGE5, MICA and SSX4 generating an AUC of 0.937, sensitivity of 96%, and specificity of 79%. Highest sensitivity combination – Combo I (blue) consisting of GAGE5 and MICA generating an AUC of 0.930, sensitivity of 93%, and specificity of 80%. Highest specificity combination – Combo II (dark grey) consisting of GAGE5 and SSX4 generating an AUC of 0.928, sensitivity of 90%, and specificity of 84%.*

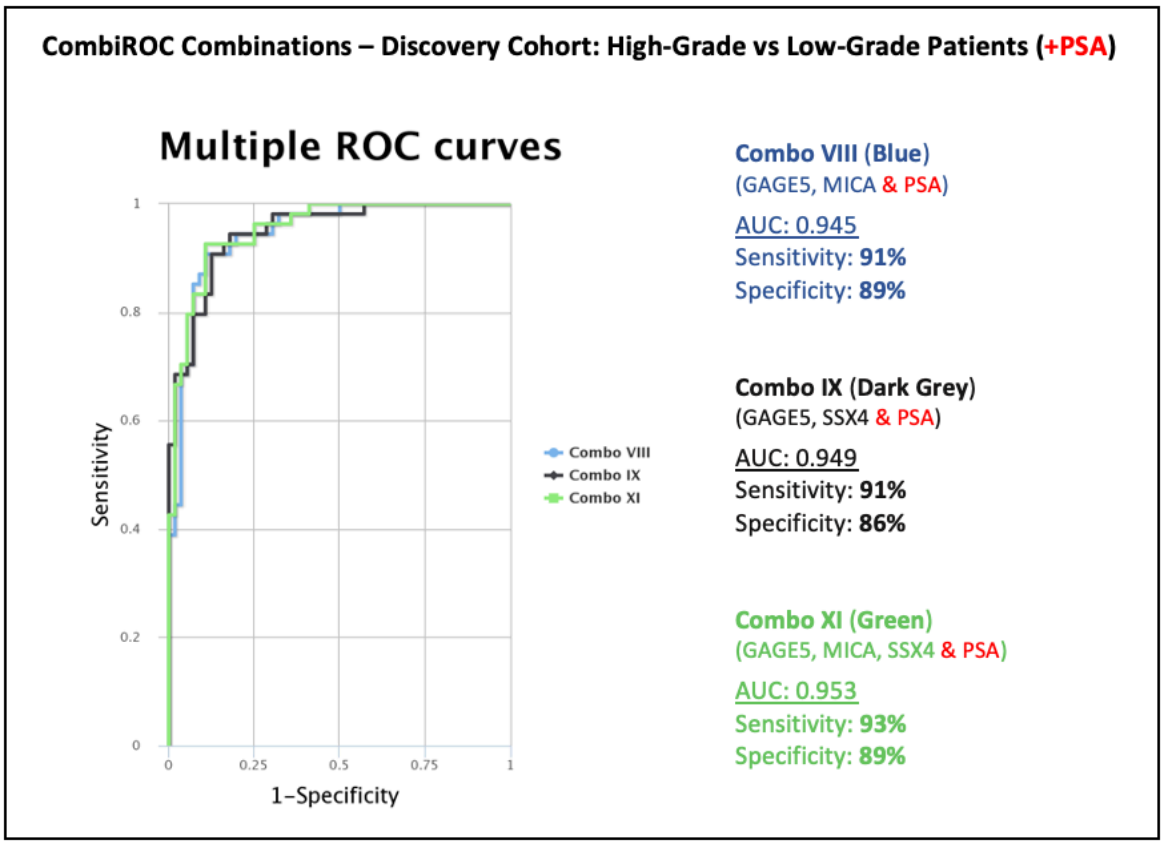


***Figure 37. Top multivariate antigen/PSA ROC curves discriminating low- and high-grade prostate cancer patients (discovery cohort).*** *Top AUC combination – Combo XI (green) consisting of GAGE5, MICA, SSX4 and PSA generating an AUC of 0.953, sensitivity of 93%, and specificity of 89%. Highest sensitivity combination – Combo IX (dark grey) consisting of GAGE5, SSX4 and PSA generating an AUC of 0.949, sensitivity of 91%, and specificity of 86%. Highest specificity combination – Combo VIII (blue) consisting of GAGE5, MICA and PSA generating an AUC of 0.945, sensitivity of 91%, and specificity of 89%.*

Following multivariate ROC analysis to distinguish low- and high-grade prostate cancer patients (discovery cohort), mRNA expression of genes associated with the antigens involved was assessed using the PanCancer Atlas cohort. Of these genes displayed in the heat map below (see **Figure 38**), MICA (100%) and KLK3 (PSA; 100%) displayed relatively high levels of mRNA transcripts in the majority of the cohort, with conversely low transcript levels seen in patients for SSX4 (6%).

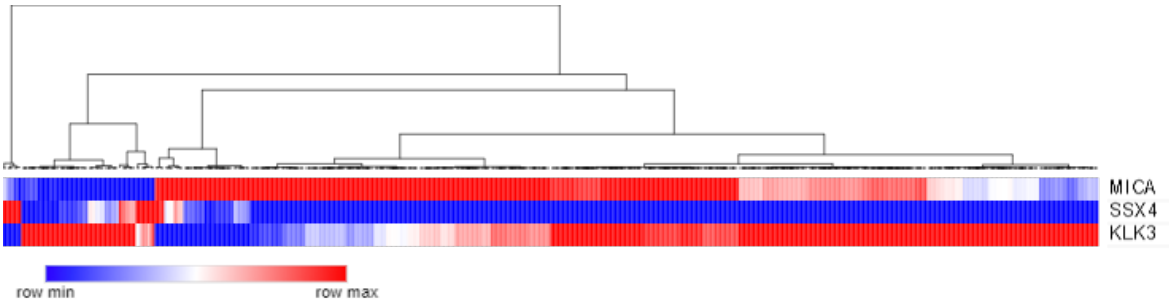


***Figure 38. mRNA expression heat map of available antigens from CBIO included in the top multivariate combinations that discriminate low- and high-grade prostate cancer patients (discovery cohort).*** *The heat map represents the hierarchical clustering by Pearson correlation of MICA, SSX4 and KLK3 (PSA) mRNA expression in 460 prostate adenocarcinoma cancer patients (PanCancer Atlas– TCGA Database). mRNA expression is displayed as z-scores (RNA Seq V2 RSEM).*

#### *3.2.3.3 Validation Cohort*

##### *3.2.3.3.1 Validation of Prevalence of Autoantibodies in Prostate Cancer (Validation Cohort)*

The following Section details the prevalence of autoantibodies in all validation cohort prostate cancer patients (n=99).

The prevalence of autoantibodies towards specific tumour antigens was determined by quantifying autoantibody signals above the determined threshold for all 99 patients. Throughout the entire cohort, autoantibody signals were detected in 59 of 99 patients (60%).

Prevalent autoantibodies were detected against 16 leading antigens, displayed below in **Figure 39**. These included MAGEB1 (n=37/99; 37%), CTNNB1 (n=34/99, 34%), GAGE1 (n=33/99, 33%), MAGEB6 (n=33/99, 33%), MAGEA1 (n=32/99, 32%), MAGEA5 (n=30/99, 30%), MAGEA2 (n=29/99, 29%), CT47.11 (n=28/99, 28%), GRWD1 (n=28/99, 28%), MAGEA4v4 (n=25/99, 25%), MAPK3 (n=25/99, 25%), SPANXC (n=24/99, 24%), GAGE4 (n=23/99, 23%), NY-ESO-1 (n=22/99, 22%), GAGE5 (n=22/99, 22%) and OIP5 (n=22/99, 22%). The number of patients exhibiting autoantibody titres towards the top 16

antigens varied from 22 – 37, with the top antigen MAGEB1, detected in 37 out of 99 patients (37% of the cohort).

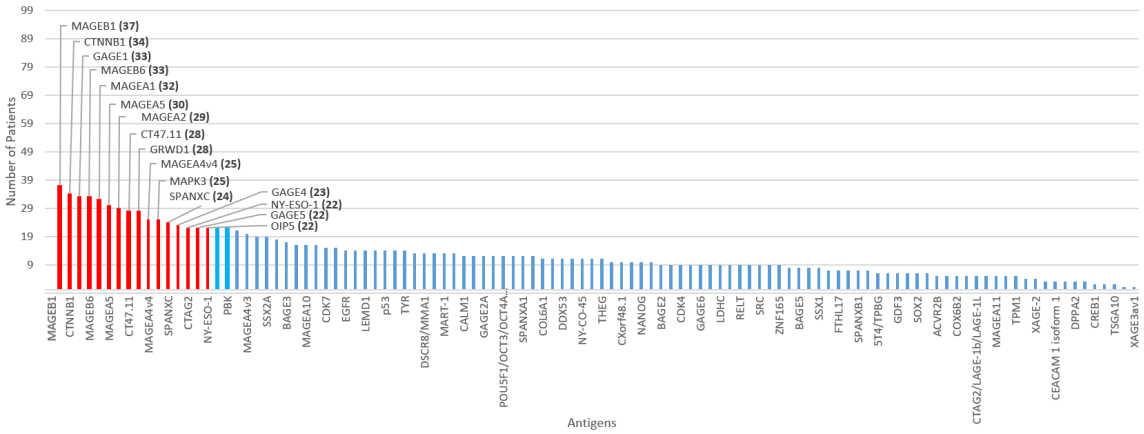


***Figure 39. Top antigens detected among the prostate cancer validation patient cohort.*** *A graphical breakdown of all antigens detected among the patient cohort determined by prevalence, with the top 16 highlighted in red. Antigens (in red) from left to right: MAGEB1 CTNNB1, GAGE1, MAGEB6, MAGEA1, MAGEA5, MAGEA2, CT47.11, GRWD1, MAGEA4v4, MAPK3, SPANXC, GAGE4, NY-ESO-1, GAGE5 and OIP5.*

When compared with the discovery cohort, 14 of the top 16 antigens previously determined as most prevalent were once again identified as predominant antigens in the validation cohort (Figure 40). Significantly larger numbers of MAGE family antigens were seen for patients in the discovery cohort as opposed to the validation cohort. Furthermore, two top antigens were unique to either the discovery cohort (MAGEB5, LEMD1), or the validation cohort (MAGEA5, NY-ESO-1).

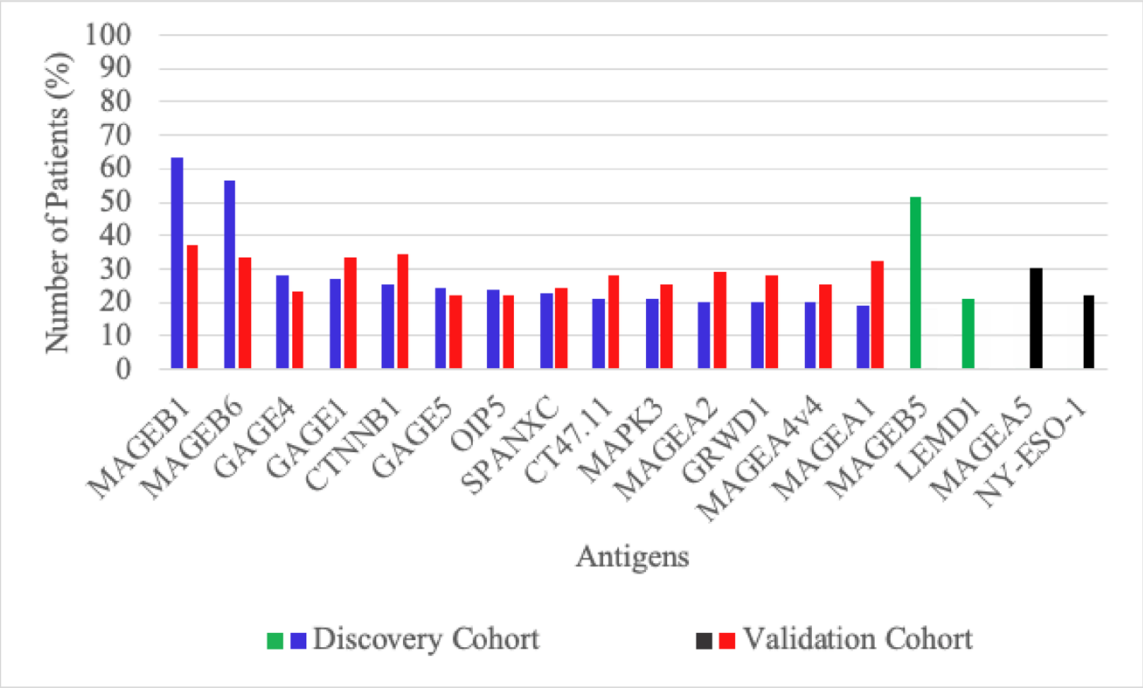


***Figure 40. Breakdown and comparison of the top prevalent antigens determined among the discovery and validation prostate cancer patient cohorts.*** *Shared top antigens and their corresponding prevalence's (as a percentage of the total number of patients in each respective cohort) can be seen highlighted in blue (discovery cohort) and red (validation cohort). Unique top antigens and their corresponding prevalence's can be seen highlighted in green (MAGEB5, LEMD1) discovery cohort, and black (MAGEA5, NY-ESO-1) validation cohort.*

STRING analysis was also performed, and the resulting network derived from our top antigens shown below (**Figure 41**) had a PPI enrichment p-value of $2.22e^{-16}$ (discovery cohort PPI enrichment p-value: $<1.0e^{-16}$), indicating that the identified top proteins were not co-occurring randomly and hence, are at least in part biologically connected as a group. The STRING analysis again revealed a high association between 8 of our identified proteins (CTAG1B unique to the validation cohort and MAGEB5 unique to the discovery cohort) with those identified in the Adeola *et al.* study with a false discovery rate of $3.56e^{-12}$ (red nodes in **Figure 41**), and the 7 proteins identified in the Heninger *et al.* study with a false discovery rate of $1.47e^{-10}$ (blue nodes in **Figure 41**).

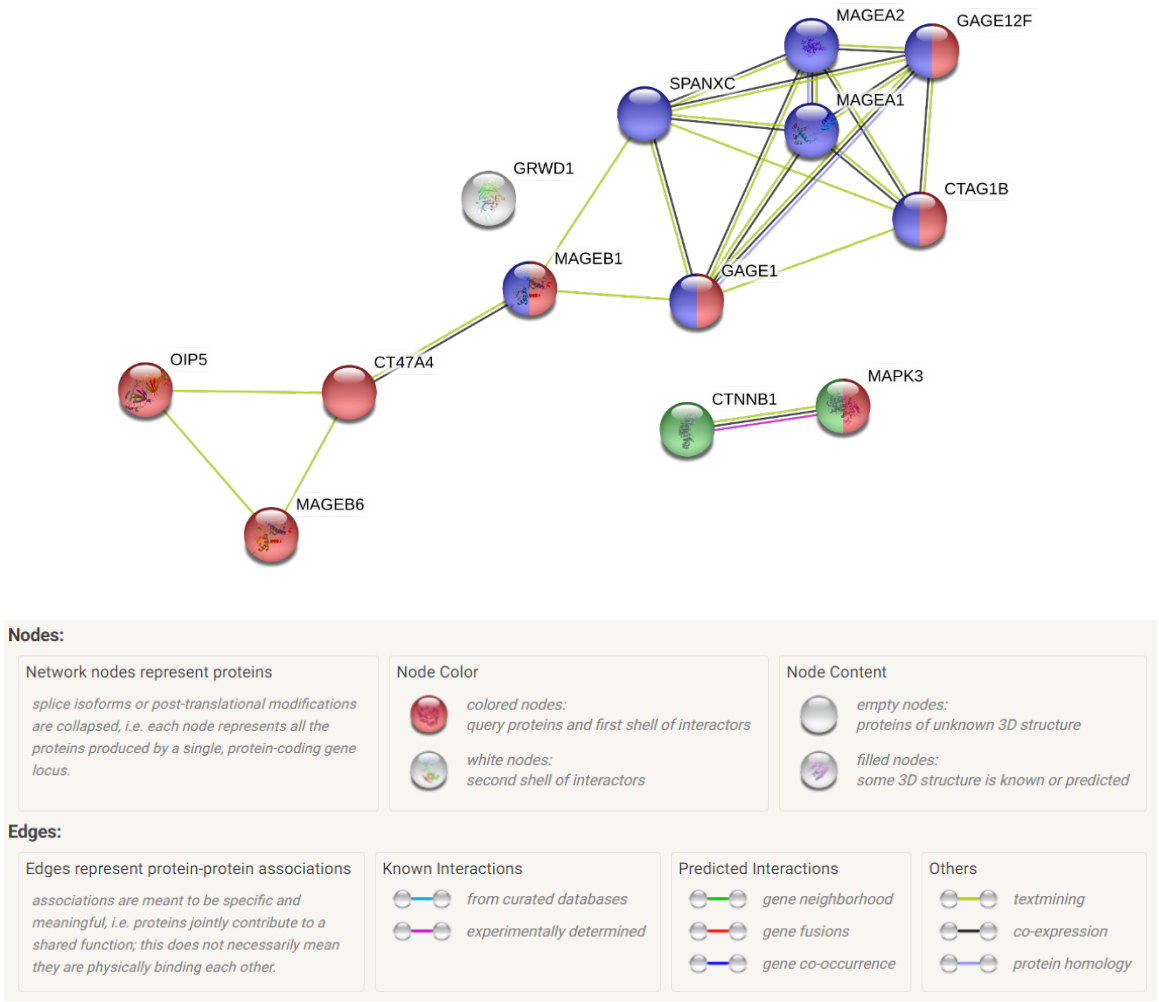


***Figure 41. STRING network of the top antigens detected among the validation patient cohort.*** *Coloured nodes are indicative of proteins found to be significant among prostate cancer patients in alternate prostate cancer related studies conducted by Adeola et al. (red nodes) and Heninger et al. (blue nodes). Protein aliases include GAGE5 = GAGE12F. Legend corresponding to the network features is displayed below the network.*

As seen in **Figure 42** below, mRNA expression was observed in relatively high levels among the majority of patients for MAPK3 (100%), GRWD1 (100%), CTNNB1 (100%), and OIP5 (100%). Varying levels of mRNA expression were seen across negligible to several prostate adenocarcinoma patients including MAGEB1 (2%), MAGEB6 (1%), GAGE4 (2%), GAGE1 (1%), MAGEA2 (15%), MAGEA4 (6%), MAGEA5 (22%), MAGEA1 (20%), CTAG1B (30%) and SPANXC (1%). Noteworthy inconsistencies

between prevalence of validation cohort antigens and external mRNA expression of related genes include MAGEB1, MAGEB6, GAGE4, GAGE1 and SPANXC.

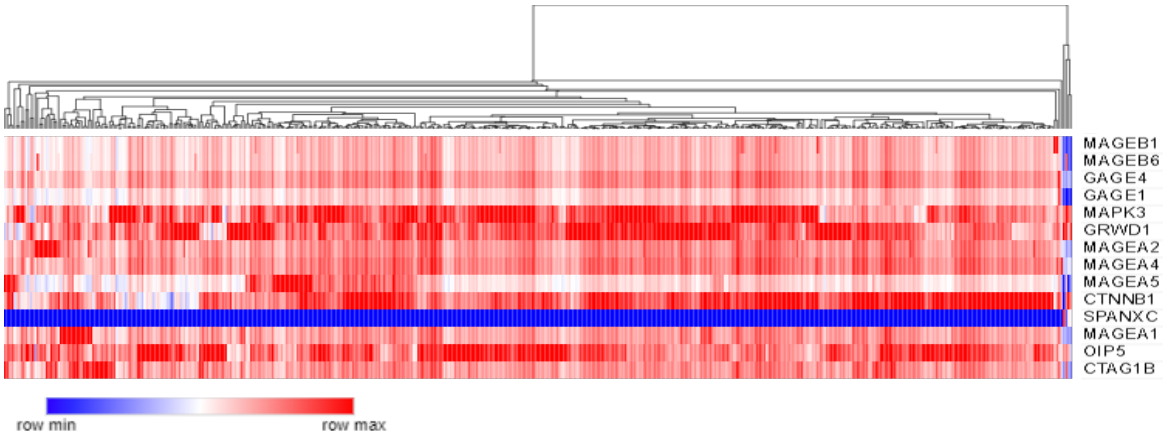


***Figure 42. mRNA expression heat map of available antigens from CBIO for the most prominent antigens in the validation cohort.*** *The heat map represents the hierarchical clustering by Pearson correlation of MAGEB1, MAGEB6, GAGE4, GAGE1, MAPK3, GRWD1, MAGEA2, MAGEA4, MAGEA5, CTNNB1, SPANXC, MAGEA1, OIP5 and CTAG1B mRNA expression in 460 prostate adenocarcinoma cancer patients (PanCancer Atlas– TCGA Database). mRNA expression is displayed as z-scores (RNA Seq V2 RSEM).*

#### *3.2.3.3.2 Validation of Diagnostic Autoantibodies in Prostate Cancer (Validation Cohort)*

The following Section details the validation of results pertaining to the assessment of cancer-associated autoantibodies as diagnostic biomarkers. This data was generated by assessing the robustness of discovery cohort findings (i.e., same univariate and multivariate antigens) on a validation cohort.

In order to validate the diagnostic potential of the multivariate antigen signatures generated during the discovery phase (APCB), the same univariate antigens were assessed on a validation cohort (VCB). Univariate antigen ROC curves and violin plots are outlined below for the 4 highly prominent antigens (CTNNB1, MAGEA1, OIP5 and SPANXC, see **Figure 43**), and 3 of the best univariate antigens (CAMEL, LAGE1b/CTAG2 and ROPN1A, see **Figure 44**). Validation of the prominent univariate antigens (MAGEA1,

SPANXC, OIP5, CTNNB1) revealed a presence of at least 22% per antigen from the discovery cohort (MAGEA1 32.3%, SPANXC 24.2%, OIP5 22.2% and CTNNB1 34.3%). The best univariate antigens (CAMEL, LAGE1b, ROPN1A) using the validation cohort revealed ROC curves with corresponding AUC values >0.5500. Mann-Whitney U tests for all univariate antigens ranged from 0.62 – 0.04.

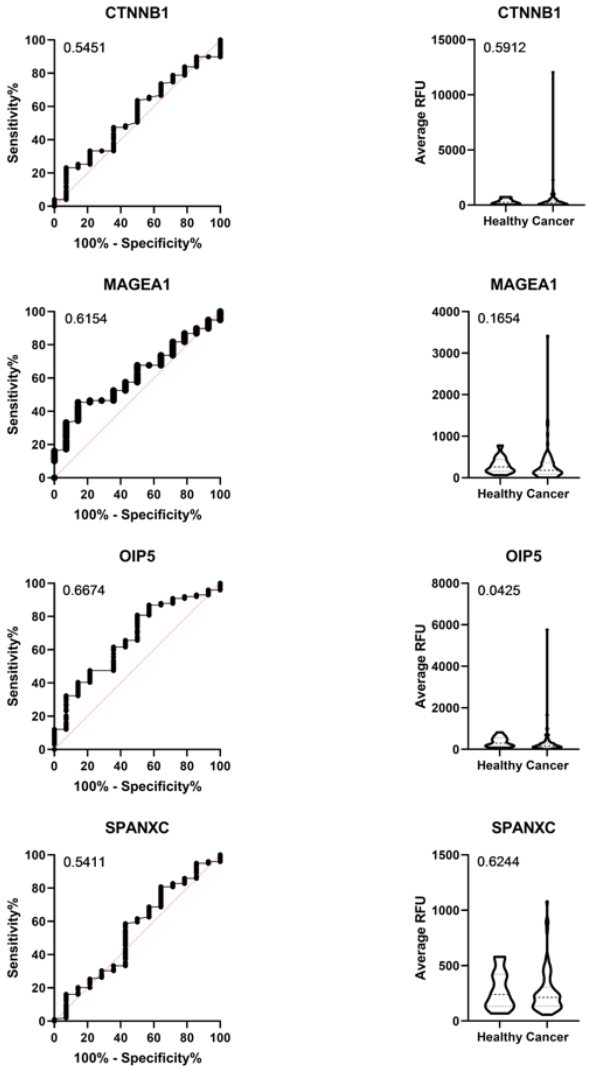


***Figure 43. Top univariate ROC curves for 4 prevalent antigens found in the discovery cohort tested on the validation cohort.*** *ROC curves for the top 4 most prevalent antigens determined by counts above threshold (≥307 RFU), generated by comparing all prostate cancer patient (discovery cohort) and healthy individual (healthy cohort) array data for each antigen (on left), on the validation cohort, with AUC values of 0.5451 (CTNNB1), 0.6154 (MAGEA1), 0.6674 (OIP5), and 0.5411 (SPANXC). Corresponding antigen violin plots are shown (on right), with included Mann-*

*Whitney U test (CI of 95%) p-values of 0.5912 (CTNNB1), 0.1654 (MAGEA1), 0.0425 (OIP5), and 0.6244 (SPANXC).*

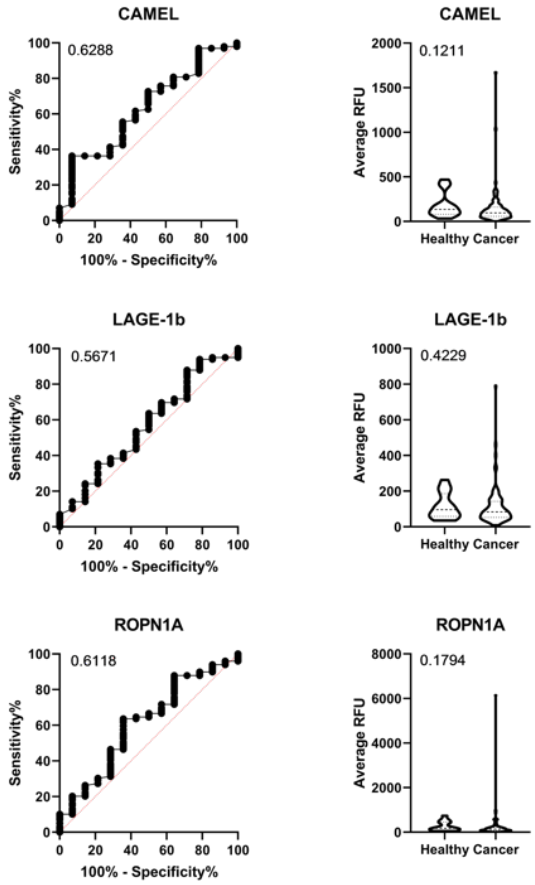


***Figure 44. Top univariate antigen ROC curves capable of distinguishing prostate cancer patients (discovery cohort) from healthy individuals (healthy cohort) tested on the validation cohort (validation cohort).*** *ROC curves for the top univariate antigens observed when comparing validation cohort prostate cancer patients from healthy individuals by validating initial top univariate antigens from the discovery cohort (on left) with AUC values of 0.6288 (CAMEL), 0.5671 (LAGE-1b), and 0.6118 (ROPN1A). Corresponding antigen violin plots are shown (on right), with included Mann-Whitney U test (CI of 95%) p-values of 0.1211 (CAMEL), 0.4229 (LAGE-1b), and 0.1794 (ROPN1A).*

In order to validate the diagnostic signature obtained in the discovery cohort, a CombiROC analysis was conducted with the same markers using the validation cohort. Of the top prior combinations of markers, Combo LXXI, had an AUC of 0.752 (original AUC for comparability: 0.847), with a 50% sensitivity a 100% specificity; Combo XCVI had an

AUC of 0.753 (original AUC: 0.847), a 49% sensitivity and a 100% specificity; and Combo C had an AUC of 0.784 (original AUC: 0.802), a 69% sensitivity and a 93% specificity. These 3 combinations were plotted below in **Figure 45**.

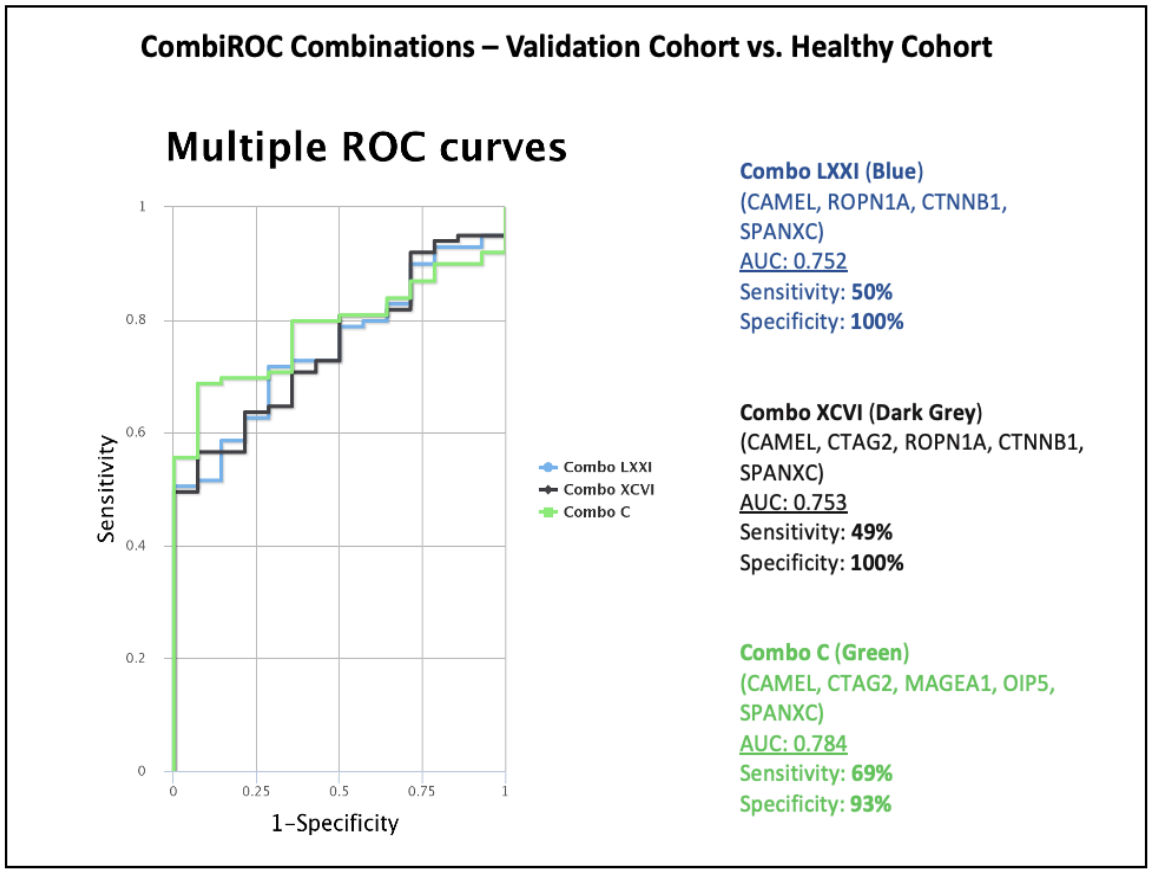


***Figure 45. Validation of multivariate antigen ROC curves and their ability to discriminate prostate cancer patients (validation cohort) from healthy individuals (healthy cohort).*** *Combo LXXI (blue) consisting of CAMEL, ROPN1A, CTNNB1 and SPANXC generating an AUC of 0.752, sensitivity of 50%, and specificity of 100%. Combo XCVI (dark grey) consisting of CAMEL, CTAG2, ROPN1A, CTNNB1 and SPANXC generating an AUC of 0.753, sensitivity of 49%, and specificity of 100%. Combo C (green) consisting of CAMEL, CTAG2, MAGEA1, OIP5 and SPANXC generating an AUC of 0.784, sensitivity of 69%, and specificity of 93%.*

To test whether the addition of patient PSA levels (univariate AUC 0.9408) also bolstered the 3 best marker combinations in the validation cohort, a second CombiROC analysis was performed. Combo CLXXXIII (above Combo LXXI +PSA) generated an AUC of 0.968, with 97% sensitivity and 88% specificity; Combo CCXIX (above Combo XCVI +PSA)

generated an AUC of 0.969, with 97% sensitivity and 88% specificity; Combo CCXXIV (above Combo C +PSA) generated an AUC of 0.963, with 96% sensitivity and 85% specificity. These 3 combinations were plotted below in **Figure 46**.

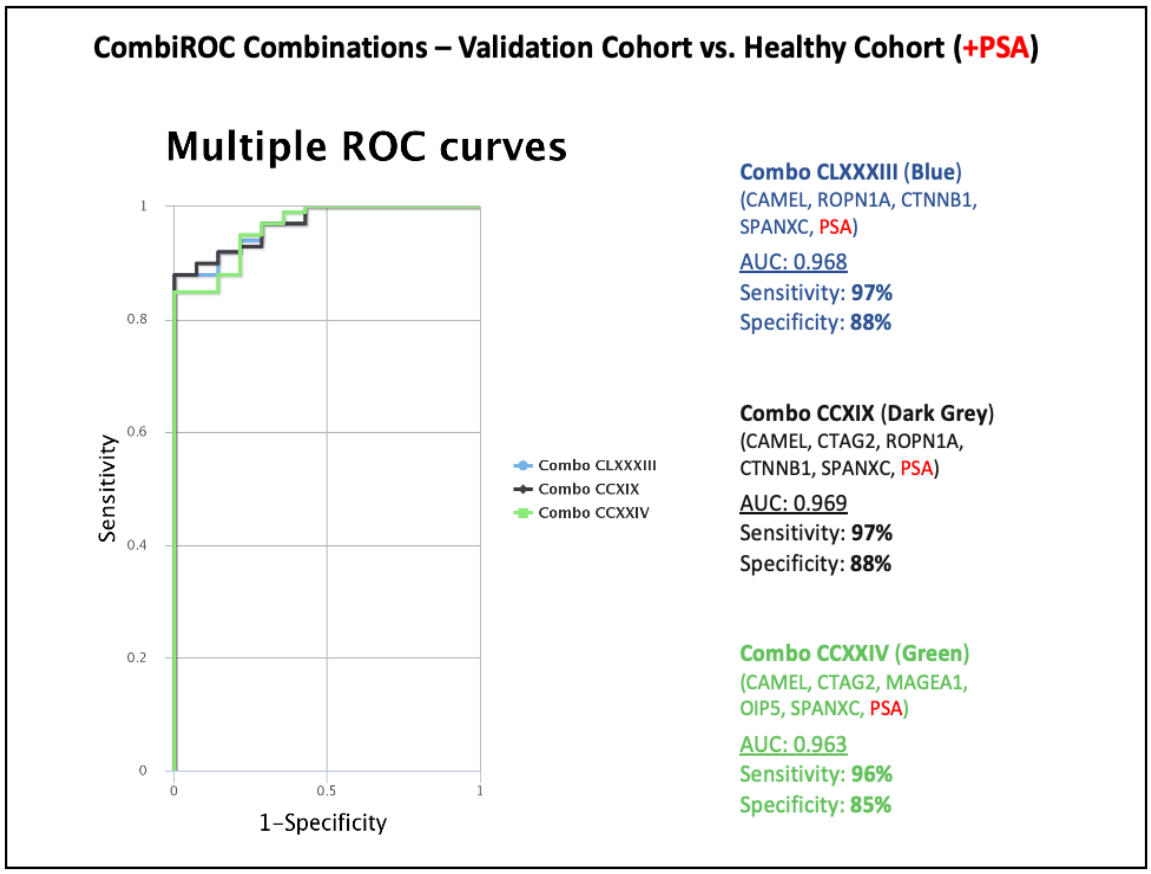


***Figure 46. Validation of multivariate antigen/PSA ROC curves and their ability to discriminate prostate cancer patients (validation cohort) from healthy individuals (healthy cohort).*** *Combo CLXXXIII (blue) consisting of CAMEL, ROPN1A, CTNNB1, SPANXC, and PSA generating an AUC of 0.968, sensitivity of 97%, and specificity of 88%. Combo CCXIX (dark grey) consisting of CAMEL, CTAG2, ROPN1A, CTNNB1, SPANXC and PSA, generating an AUC of 0.969, sensitivity of 97%, and specificity of 88%. Combo CCXXIV (green) consisting of CAMEL, CTAG2, MAGEA1, OIP5, SPANXC, and PSA generating an AUC of 0.963, sensitivity of 96%, and specificity of 85%.*

In order to validate the diagnostic potential of the multivariate antigen signatures able to distinguish prostate cancer patients from healthy and benign individuals that were generated during the discovery phase, the same univariate antigens were assessed on the validation cohort. The univariate antigen ROC curves with AUC values (ACVR2B; 0.5857,

CAMEL; 0.6105, CT47.11v; 0.6467, NY-ESO-1; 0.6416, ROPN1A; 0.6126, CALM1; 0.5507, CEP290; 0.5475, MART-1; 0.5120, PRKCZ; 0.6564) and associated violin plots with Mann-Whitney U test results (*ACVR2B; 0.1747, CAMEL; 0.0791, CT47.11v; 0.0192, NY-ESO-1; 0.0239, ROPN1A; 0.0731, CALM1; 0.4234, CEP290; 0.4533, MART-1; 0.8511, PRKCZ; 0.0124)* are displayed in **Figure 47** below.

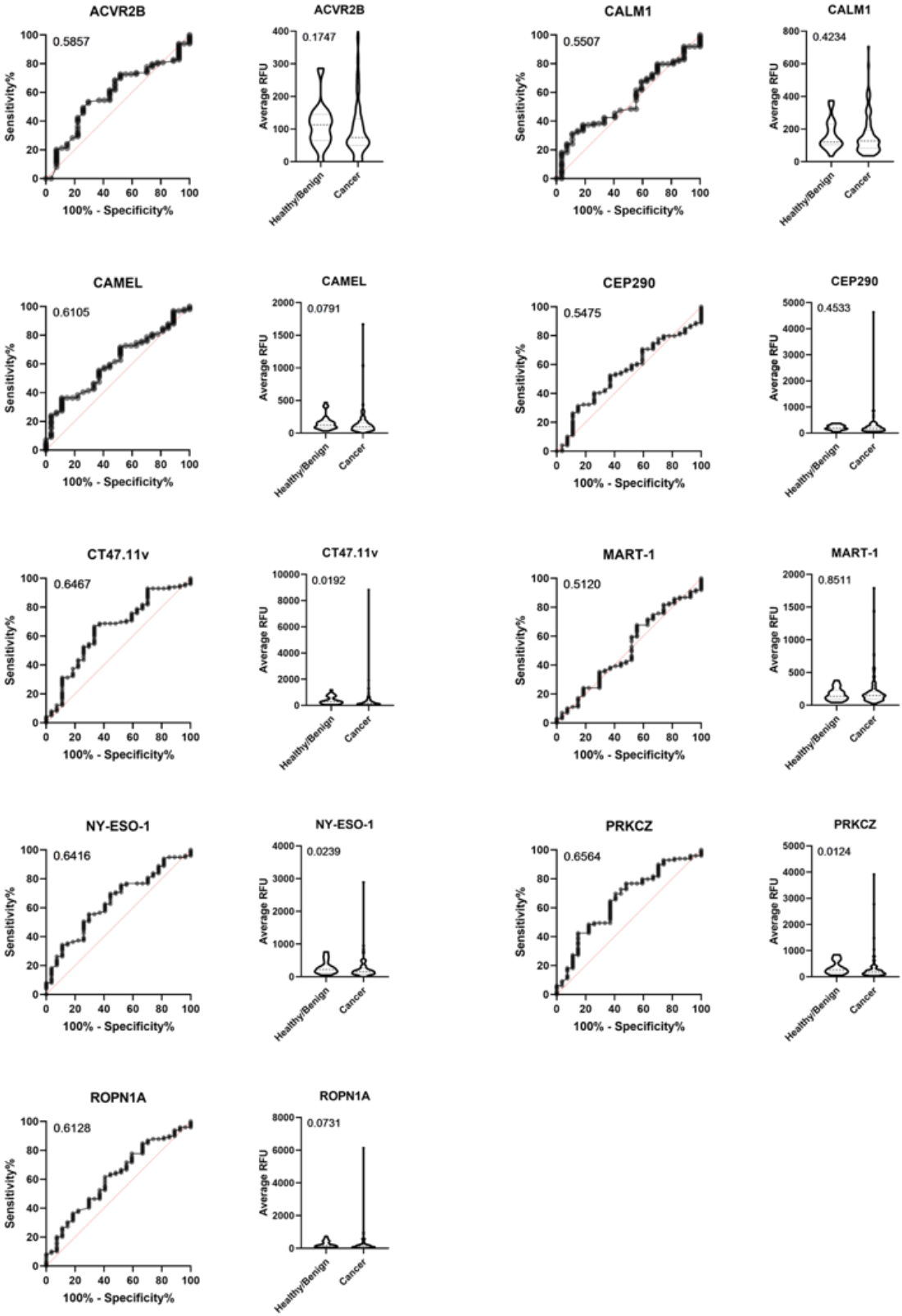


***Figure 47. Validation of top univariate antigen ROC curves capable of distinguishing prostate cancer patients (validation cohort) from healthy and benign individuals (healthy and benign cohorts).*** *ROC curves for the top univariate antigens observed when comparing prostate cancer patients from healthy individuals using array data (on left) with AUC values of 0.5857 (ACVR2B),*

*0.6105 (CAMEL), 0.6467 (CT47.11v), 0.6416 (NY-ESO-1), 0.6128 (ROPN1A), 0.5507 (CALM1), 0.5475 (CEP290), 0.5120 (MART-1), and 0.6564 (PRKCZ). Corresponding antigen violin plots are shown (on right), with included Mann-Whitney U test (CI of 95%) p-values of 0.1747 (ACVR2B), 0.0791 (CAMEL), 0.0192 (CT47.11v), 0.0239 (NY-ESO-1), 0.0731 (ROPN1A), 0.4234 (CALM1), 0.4533 (CEP290), 0.8511 (MART-1), and 0.0124 (PRKCZ).*

Validation of the top univariate antigens able to distinguish prostate cancer patients from healthy and benign individuals were plotted as multivariate antigen ROC curves without PSA (**Figure 48**). In reiteration, this signature could not be tested with PSA as we were unable to obtain PSA values for benign individuals. Combo CDLVIII generated the highest AUC of 0.788, with a sensitivity and specificity of 67% and 79%, respectively. Combo CCLXXXII (AUC 0.736) and Combo CCCXL (AUC 0.777) were also plotted as they displayed the highest sensitivity and specificity, following that Combo CDLVIII. Original AUC (discovery cohort) values for these combinations were as follows: Combo CDLVIII (0.769), CCLXXXII (0.742), and Combo CCCXL (0.754).

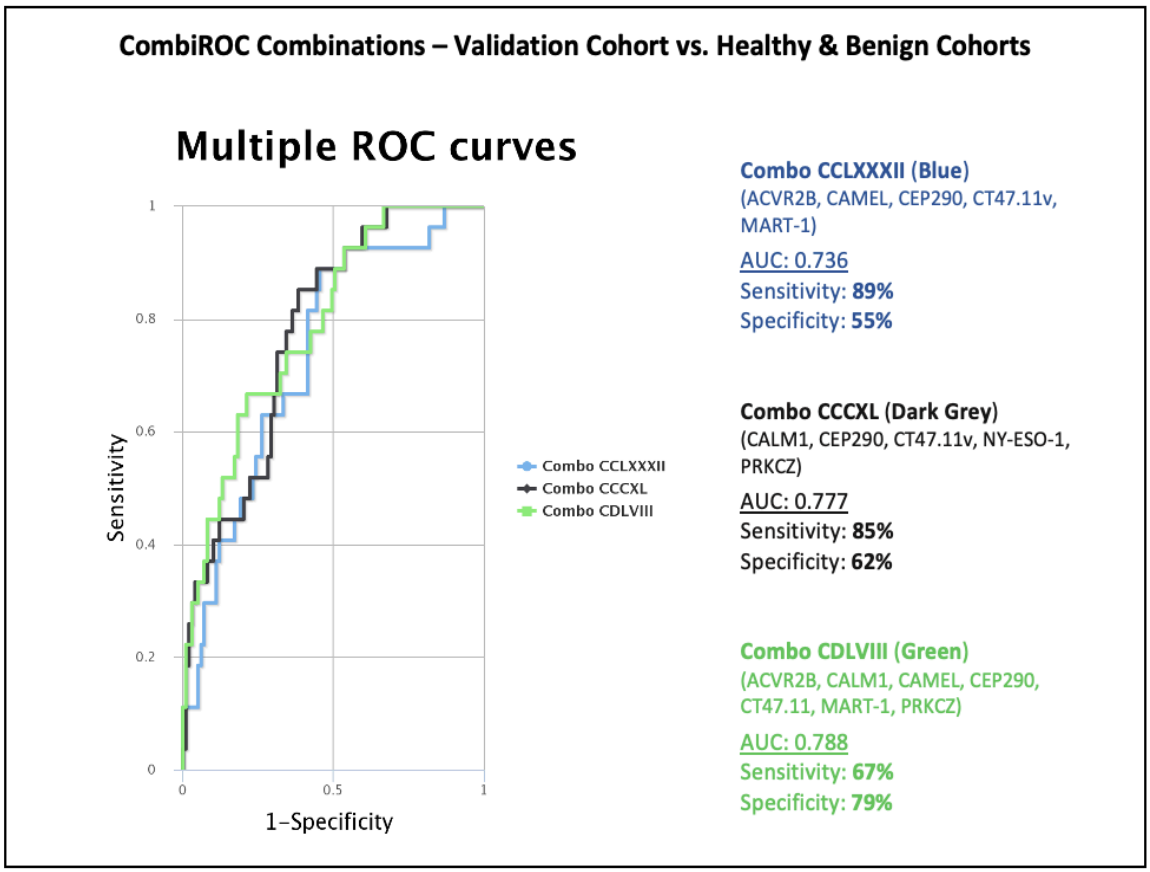

***Figure 48. Validation of multivariate antigen ROC curves discriminating prostate cancer patients (validation cohort) from healthy and benign individuals (healthy and benign cohorts).*** *Combo CCLXXXII (blue) consisting of ACVR2B, CAMEL, CEP290, CT47.11, and MART-1 generating an AUC of 0.736, sensitivity of 89%, and specificity of 55%. Combo CCCXL (dark grey) consisting of CALM1, CEP290, CT47.11, NY-ESO-1 and PRKCZ generating an AUC of 0.777, sensitivity of 85%, and specificity of 62%. Combo CDLVIII (green) consisting of ACVR2B, CALM1, CAMEL, CEP290, CT47.11, MART-1 and PRKCZ generating an AUC of 0.788, sensitivity of 67%, and specificity of 79%.*

#### *3.2.3.3.3 Validation of Disease Stratifying Autoantibodies in Prostate Cancer (Discovery Cohort)*

The following Section details the validation of results pertaining to the assessment of cancer-associated autoantibodies as disease stratifying biomarkers. This data was generated by assessing the robustness of discovery cohort findings (i.e., same univariate and multivariate antigens) on a validation cohort.

In order to validate the multivariate antigen signatures capable of distinguishing low- and high-grade disease generated during the discovery phase, the same univariate antigens were assessed using the validation cohort. The univariate antigen ROC curves with AUC values (GAGE5; 0.6841, MICA; 0.7080, SSX4; 0.7355) and associated violin plots with Mann-Whitney U test results (p-values: GAGE5; 0.0014, MICA; 0.0003, SSX4; >0.0001) are displayed in **Figure 49** below.

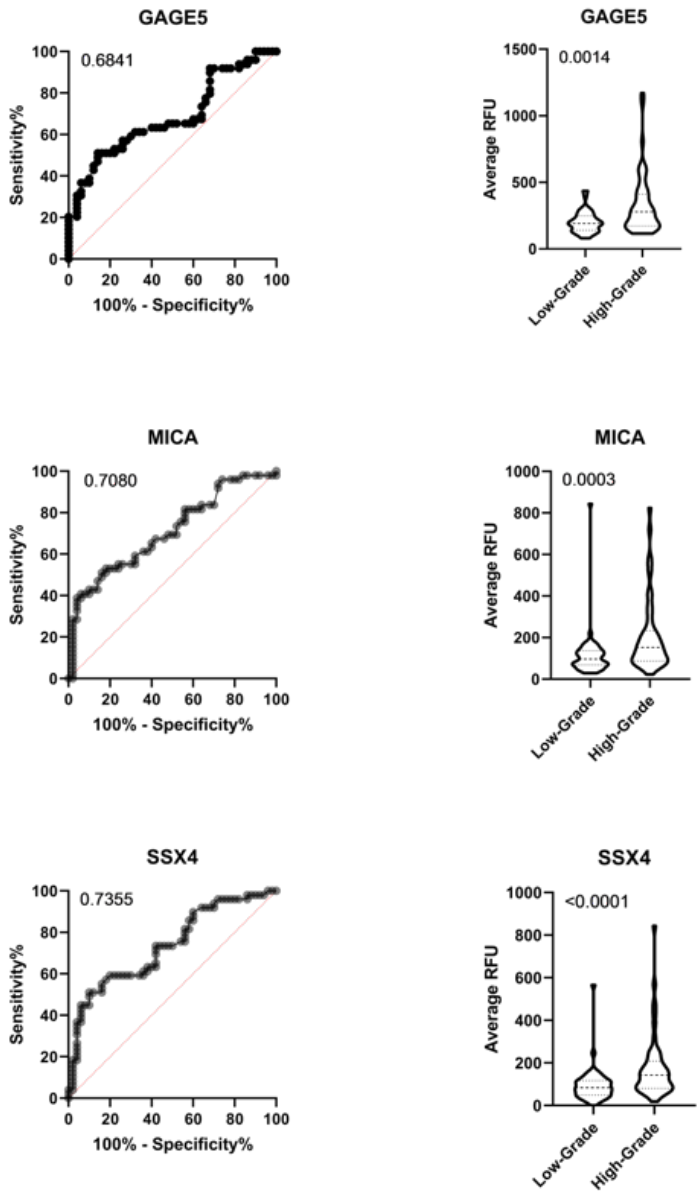


***Figure 49. Validation of top univariate antigen ROC curves capable of distinguishing low- and high-grade prostate cancer patients (validation cohort).*** *ROC curves for the univariate antigens discovered using the discovery cohort when comparing high- and low-grade prostate cancer patients within the validation cohort using array data (on left) with AUC values of 0.6841 (GAGE5), 0.7080 (MICA), and 0.7355 (SSX4). Corresponding antigen violin plots are shown (on right), with included Mann-Whitney U test (CI of 95%) p-values of 0.0014 (GAGE5), 0.0003 (MICA), and >0.0001 (SSX4).*

Top univariate antigens able to distinguish low- from high-grade prostate cancer patients were plotted as multivariate antigen ROC curves without PSA and with PSA. Without PSA (see **Figure 50**), Combo IV generated an AUC of 0.731, with a sensitivity and specificity

of 80% and 53%, respectively. Combo I generated an AUC of 0.723, with a sensitivity and specificity of 92% and 44%, respectively. Combo II generated an AUC of 0.736, with a sensitivity and specificity of 82% and 55%, respectively. With PSA (see **Figure 51**), of the 14 possible combinations, Combo XI generated an AUC of 0.871, with a sensitivity and specificity of 72% and 88%, respectively. Combo IX generated an AUC of 0.869, with a sensitivity and specificity of 72% and 86%, respectively. Combo VIII generated an AUC of 0.865, with a sensitivity and specificity of 68% and 88%, respectively.

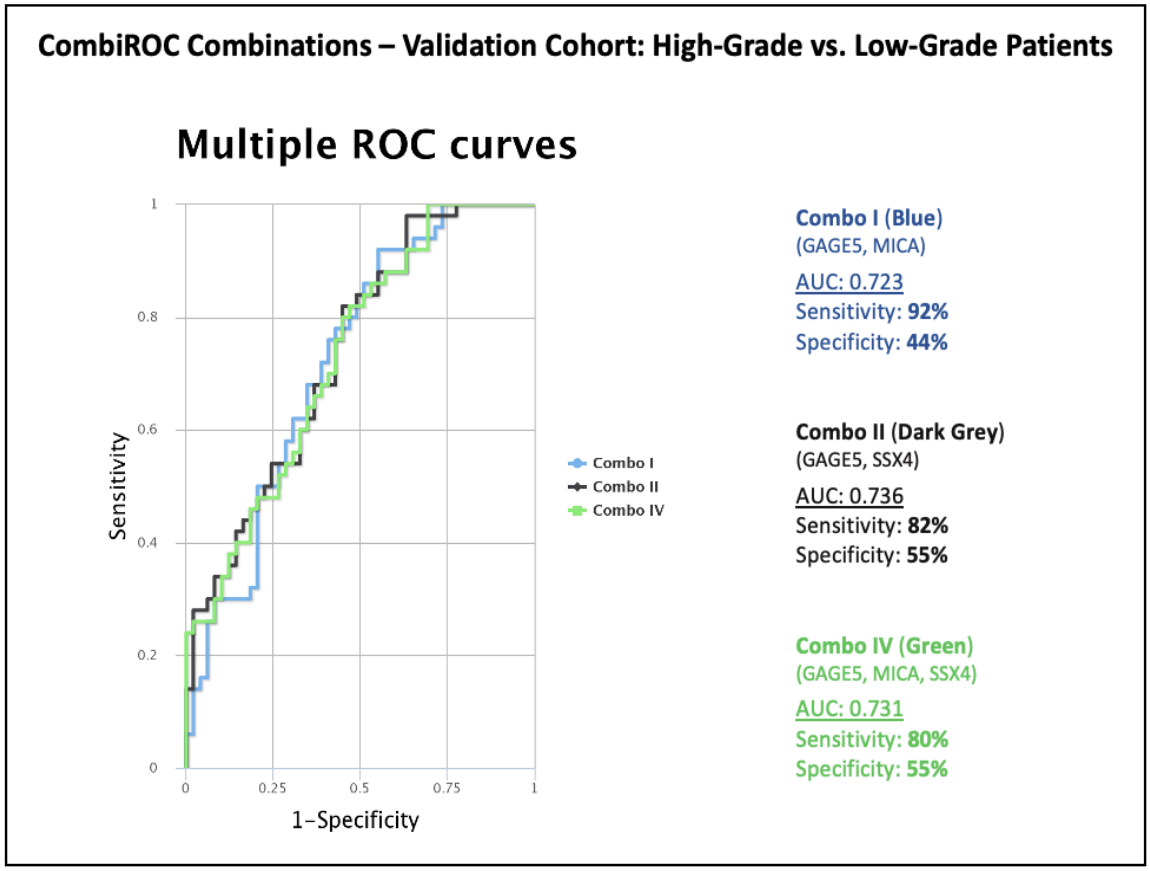


***Figure 50. Validation of top multivariate antigen ROC curves discriminating low- and high-grade prostate cancer patients (validation cohort).*** *Combo I (blue) consisting of GAGE5 and MICA generating an AUC of 0.723, sensitivity of 92%, and specificity of 44%. Combo II (dark grey) consisting of GAGE5 and SSX generating an AUC of 0.736, sensitivity of 82%, and specificity of 55%. Combo IV (green) consisting of GAGE5, MICA and SSX4 generating an AUC of 0.731, sensitivity of 80%, and specificity of 55%.*

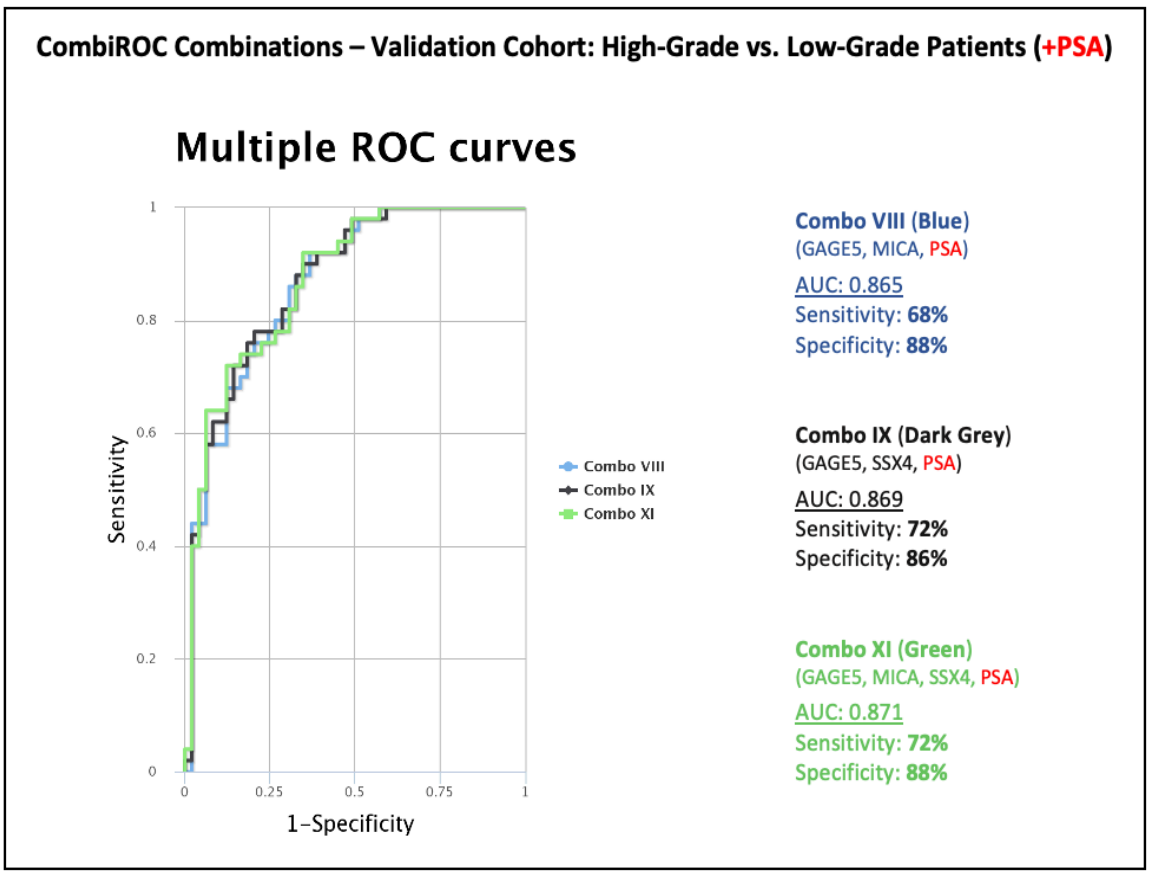


***Figure 51. Validation of top multivariate antigen/PSA ROC curves discriminating low- and high-grade prostate cancer patients (validation cohort).*** *Combo VIII (blue) consisting of GAGE5, MICA and PSA generating an AUC of 0.865, sensitivity of 68%, and specificity of 88%. Combo IX (dark grey) consisting of GAGE5, SSX4 and PSA generating an AUC of 0.869, sensitivity of 72%, and specificity of 86%. Combo XI (green) consisting of GAGE5, MICA, SSX4 and PSA generating an AUC of 0.871, sensitivity of 72%, and specificity of 88%.*

In addition to the above comparisons made between mRNA expression data generated using an external prostate cancer cohort (TCGA) with all of our available identified diagnostic, prognostic and disease stratification biomarkers, we further investigated their protein expression in prostate cancer tissues using the Human Protein Atlas database. **Table 6** details protein expression (ProteinAtlas) and/or known prognostic implications in cancer (TCGA) 6

reported for all potential biomarkers. Notably, protein expression observed for non-CT antigens in prostate cancer was as follows: ACVR2B (1/11), CEP290 (11/12), CTNNB1

(9/9), GRWD1 (2/10), KLK3 (PSA, 10/10), MAPK3 (40/47), and RAF1 (RAF, 12/12). Protein expression observed for CT antigens was as follows: CTAG1B (1/10), CTAG2 (CAMEL/LAGE1b, 3/11), MAGEA4 (MAGEA4v4, 10/11), MAGEB5, and XAGE2 (XAGE-2, 2/10). Of these proteins, twelve were of prognostic value (favourable / unfavourable) in one or more cancer types, although none were found to be prognostic in prostate cancer.

***Table 6. Protein expression summary.***

| Protein | Protein Expression (no. of tissues) | Known Prognostic Implications in Cancer |
|---|---|---|
| ACVR2B | 1 of 11 | None |
| BAGE5 | N/a | N/a |
| CALM1 | 0 of 11 | Urothelial cancer (unfavourable)<br>Pancreatic cancer (favourable)<br>Renal cancer (favourable) |
| CEP290 | 11 of 12 | Renal cancer (unfavourable) |
| COL6A1 | N/a | Renal cancer (unfavourable)<br>Urothelial cancer (unfavourable) |
| COX6B2 | 0 of 11 | None |
| CT47A11 | 0 of 11 | None |
| CTAG1B (NY-ESO-1) | 1 of 10 | None |
| CTAG2 (CAMEL, LAGE1b) | 3 of 11 | Liver cancer (unfavourable) |
| CTNNB1 | 9 of 9 | Colorectal cancer (favourable) |
| GAGE1 | 0 of 12 | None |
| GAGE4 | N/a | N/a |
| GAGE5 | N/a | N/a |
| GRWD1 | 2 of 10 | Liver cancer (unfavourable) |
| KLK3 (PSA) | 10 of 10 | None |
| LEMD1 | N/a | Ovarian cancer (favourable)<br>Pancreatic cancer (unfavourable) |
| MAGEA1 | 0 of 12 | None |
| MAGEA2 | N/a | None |
| MAGEA4 | 10 of 11 | None |
| MAGEA5 | N/a | N/a |
| MAGEB1 | 0 of 23 | None |
| MAGEB5 | 6 of 11 | None |
| MAGEB6 | 0 of 21 | None |
| MAP9 | N/a | None |
| MAPK3 | 40 of 47 | Liver cancer (unfavourable) |
| MICA | N/a | Cervical cancer (unfavourable) |
| MLANA (MART-1) | 0 of 11 | None |
| OIP5 | 0 of 11 | Pancreatic cancer (unfavourable) Liver cancer (unfavourable)<br>Lung cancer (unfavourable) |
| PRKCZ | 8 of 12 | Renal cancer (favourable) |
| RAF1 (RAF) | 12 of 12 | None |
| ROPN1 | 0 of 12 | None |
| SPANXC | 0 of 12 | None |
| SSX4 | 0 of 11 | None |
| XAGE-2 | 2 of 10 | None |

*'N/a' protein expression – staining yet to be performed or reported. 'N/a' known prognostic implication – data yet to be acquired or reported.*

### *3.2.4 Array Data vs. Clinical Cohort Characteristics*

To assess whether the detected autoantibody profiles correlated with clinical features, a summary table was generated outlining the correspondence between relevant sets of cohort characteristics and autoantibody signals (**Table 7**). The defined threshold of ≥307 average RFU was used to define true autoantibody signals. The average number of detectable antigen specificities and average RFU intensities did not vary significantly across age brackets (Kruskal-Wallis p-value=0.9919, p-value=0.8834, respectively), disease grade (Mann-Whitney p-value=0.2696, p-value=0.3688, respectively), PSA levels (Kruskal-Wallis p-value=0.3991, p-value=0.1740, respectively), or biochemical PSA recurrence (Mann-Whitney p-value=0.8424, p-value=0.9261, respectively).

Of note, true autoantibody signals were commonly seen amongst patients with a PSA below 4ng/mL indicating ability to detect cancer in patients with PSA levels below the 'level of clinical concern'.

***Table 7. Correlation of antigen specificities with relevant patient cohort characteristics (discovery cohort).***

| Characteristic | Average Antigen counts | Average RFU | Percentage of patients with autoantibody signals (%) |
|---|---|---|---|
| Age Category* | | | |
| <60 yr (n=38) | 10 | 164 | 76.32 |
| ≥60 to <70 yr (n=57) | 10 | 170 | 77.19 |
| ≥70 yr (n=15) | 10 | 151 | 86.67 |
| Gleason Score | | | |
| 6-7 (n=54) | 13 | 174 | 83.33 |
| 8-10 (n=56) | 7 | 157 | 73.21 |
| PSA Range† | | | |
| <4 ng/mL (n=16) | 10 | 178 | 81.25 |
| ≥4 to ≤12 ng/mL (n=80) | 11 | 162 | 75.00 |
| >12 ng/mL (n=14) | 9 | 171 | 92.86 |
| Biochemical Recurrence‡ | | | |
| Yes (n=16) | 8 | 160 | 81.25 |
| No (n=82) | 11 | 169 | 79.27 |

** Patient ages used for calculations were at diagnosis of disease. † PSA samples used for calculations were those provided at informed patient consent. ‡ Biochemical recurrence was determined as an observed PSA increase of more than 0.4ng/mL at any available follow-up time point after radical prostatectomy. Patients that did not receive a radical prostatectomy or lacked adequate follow-up information (more than 2 follow-up time points), were excluded from biochemical recurrence data. Average antigen specificity counts were rounded to the nearest whole number. Abbreviations: PSA, prostate-specific antigen.*

To assess whether the detected autoantibody profiles of patients from the validation cohort correlated with clinical features, a summary table was generated outlining the correspondence between relevant sets of cohort characteristics and autoantibody signals (**Table 8**). The defined threshold of ≥307 average RFU was used to define true autoantibody signals. The average number of detectable antigen specificities and average RFU intensities did not vary significantly across age brackets (Kruskal-Wallis p-value=0.3939, p-value=0.9217, respectively), or PSA levels (Kruskal-Wallis p-value=0.0764, p-value=0.2758, respectively). In regard to Gleason score, significantly higher average antigen specificities (Mann-Whitney p-value=0.0111) and RFU (Mann-Whitney p-value=0.0533) were seen in high-grade vs low-grade patients.

**Table 8. Correlation of antigen specificities with relevant patient cohort characteristics (validation cohort).**

| Characteristic | Average Antigen counts | Average RFU | Percentage of patients with autoantibody signals (%) |
|---|---|---|---|
| Age Category* | | | |
| <60 yr (n=39) | 10 | 188 | 74.4 |
| ≥60 to <70 yr (n=48) | 15 | 184 | 75.0 |
| ≥70 yr (n=12) | 19 | 275 | 83.3 |
| Gleason Score | | | |
| 6-7 (n=49) | 7 | 184 | 72.0 |
| 8-10 (n=50) | 20 | 209 | 79.6 |
| PSA Range† | | | |
| <4 ng/mL (n=14) | 12 | 165 | 83.3 |
| ≥4 to ≤12 ng/mL (n=64) | 11 | 194 | 71.2 |
| >12 ng/mL (n=21) | 22 | 225 | 90.5 |

** Patient ages used for calculations were at diagnosis of disease. † PSA samples used for calculations were those provided at informed patient consent. Average antigen specificity counts were rounded to the nearest whole number. Abbreviations: PSA, prostate-specific antigen.*

To assess whether the detected autoantibody profiles of patients from both the discovery and the validation cohort correlated with clinical features, a summary table was generated outlining the correspondence between relevant sets of cohort characteristics and autoantibody signals (**Table 9**). The defined threshold of ≥307 average RFU was used to define true autoantibody signals. The average number of detectable antigen specificities and average RFU intensities did not vary significantly across age brackets (Kruskal-Wallis p-value=0.5718, p-value=0.9935, respectively), disease grade (Mann-Whitney p-value=0.3161, p-value=0.5078, respectively). Of note, statistically significant differences in average antigen specificities (Kruskal-Wallis p-value=0.0340) and average RFU intensities (Kruskal-Wallis p-value=0.0526) were apparent across PSA ranges.

**Table 9. Correlation of antigen specificities with relevant patient cohort characteristics (combined discovery and validation cohorts).**

| Characteristic | Average Antigen counts | Average RFU | Percentage of patients with autoantibody signals (%) |
|---|---|---|---|
| Age Category* | | | |
| <60 yr (n=77) | 10 | 179 | 74.0 |
| ≥60 to <70 yr (n=105) | 12 | 179 | 76.2 |
| ≥70 yr (n=27) | 14 | 211 | 85.2 |
| Gleason Score | | | |
| 6-7 (n=104) | 7 | 182 | 72.0 |
| 8-10 (n=105) | 20 | 184 | 79.6 |
| PSA Range† | | | |
| <4 ng/mL (n=30) | 11 | 175 | 76.7 |
| ≥4 to ≤12 ng/mL (n=144) | 11 | 179 | 72.9 |
| >12 ng/mL (n=35) | 17 | 206 | 91.4 |

** Patient ages used for calculations were at diagnosis of disease. † PSA samples used for calculations were those provided at informed patient consent. ‡ Biochemical recurrence was determined as an observed PSA increase of more than 0.4ng/mL at any available follow-up time point after radical prostatectomy. Patients that did not receive a radical prostatectomy or lacked adequate follow-up information (more than 2 follow-up time points), were excluded from biochemical recurrence data. Average antigen specificity counts were rounded to the nearest whole number. Abbreviations: PSA, prostate-specific antigen.*

The observed differences in the above correlations between the array data and clinical features of the discovery, validation and combined cohorts may be explained by differences in the spread of PSA levels and/or the presence of comorbidities between disease grades.

### *3.3 Multispectral IHC Staining, Vectra Imaging and Cell Analysis*

This Section includes results obtained from optimisation, staining, imaging and analysis of mIHC-based assays. All staining was undertaken using the Bond® RX fully automated research stainer. Multispectral imaging, cell phenotyping and quantitation was completed using the Vectra® 3.0 automated quantitative pathology imaging system, together with the complimentary inForm® cell analysis software.

### *3.3.1 Spectral Library*

Prior to accurate interpretation of any staining performed, a spectral library was required and hence built containing the distinct emission wavelength of each fluorophore (see **Figure 52**) using the inForm® v2.4 software. As each OPAL™ fluorophore contains a distinct spectral wavelength, these wavelengths must be saved (as a library) and used to effectively unmix any multiplex images that contain these fluorophores. It is vital that these are defined prior to the unmixing of any stains performed using Opal™ fluorophores to achieve maximum signal resolution while mitigating any potential spectral bleed-through or cross- talk between fluorophores. The following spectral library seen below (**Figure 52**) was used to accurately unmix signals for all stains conducted throughout this study.

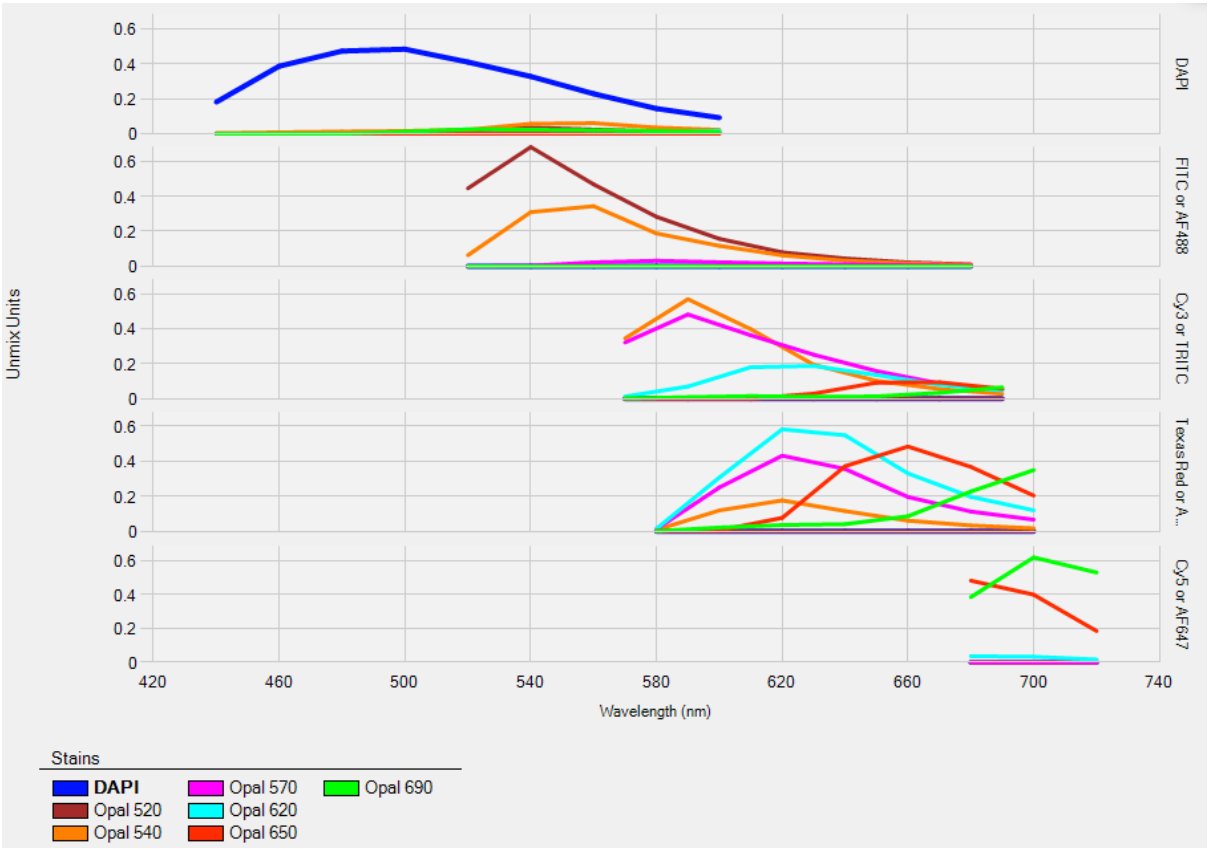


***Figure 52. Spectral library depicting emission spectra for 6 Opal fluorophores (Opal 520, Opal, 540, Opal 570, Opal 620, Opal 650, Opal 690) and DAPI built using inForm®.*** *Each fluorophore displays its unique spectral curve defined as a function of unmix units and wavelength (nm). Filter cubes encompassing all Opal fluorophores are shown on the right (DAPI, FITC, Cy3, Texas Red and Cy5).*

### *3.3.2 Primary Antibody Optimisation*

#### *3.3.2.1 ASC Panel*

Following optimisation of primary ASC panel antibodies using the aforementioned method in **Section 2.5.2**, six individual control slides (three for each concentration at epitope retrieval pH 6 - ER 6, and three for each concentration at pH 9 - ER 9) were spectrally unmixed using inForm v2.4 and visually assessed for signal intensity and background. Those that displayed the clearest signals concomitantly with the least background were selected for use in multiplex stain order optimisation. Optimal primary antibody conditions are detailed in **Table 10**.

***Table 10. Optimal concentrations and conditions of primary antibodies for the ASC panel.***

| Primary Antibody | Optimal Dilution | Epitope Retrieval (pH) |
|---|---|---|
| CD19 | 1:100 | ER 9 |
| CD38 | 1:300 | ER 9 |
| CD45 | 1:300 | ER 9 |
| CD138 | 1:100 | ER 9 |

*Refer to A**ppendix Table A1** for more details on reagents used for staining.*

Single positive control staining was performed for each ASC panel primary (positivity of cells found within tissue confirmed via the Human Protein Atlas). **Figure 53** displays positive and morphologically-sound staining of all four antibodies used for downstream ASC multiplex staining. Specifically, **a1 – a3** show clear, cytoplasmic/membranous staining of CD19+ B cells located within a germinal centre (B cell zone) in tonsil tissue; **b1 – b3** show clear, cytoplasmic/membranous staining of epithelial gland cells in prostate tissue; **c1 – c3** show clear, cytoplasmic/membranous staining of lymphocytes in tonsil tissue; and **d1 – d3** show clear, cytoplasmic/membranous staining of trophoblastic cells in placental tissue.

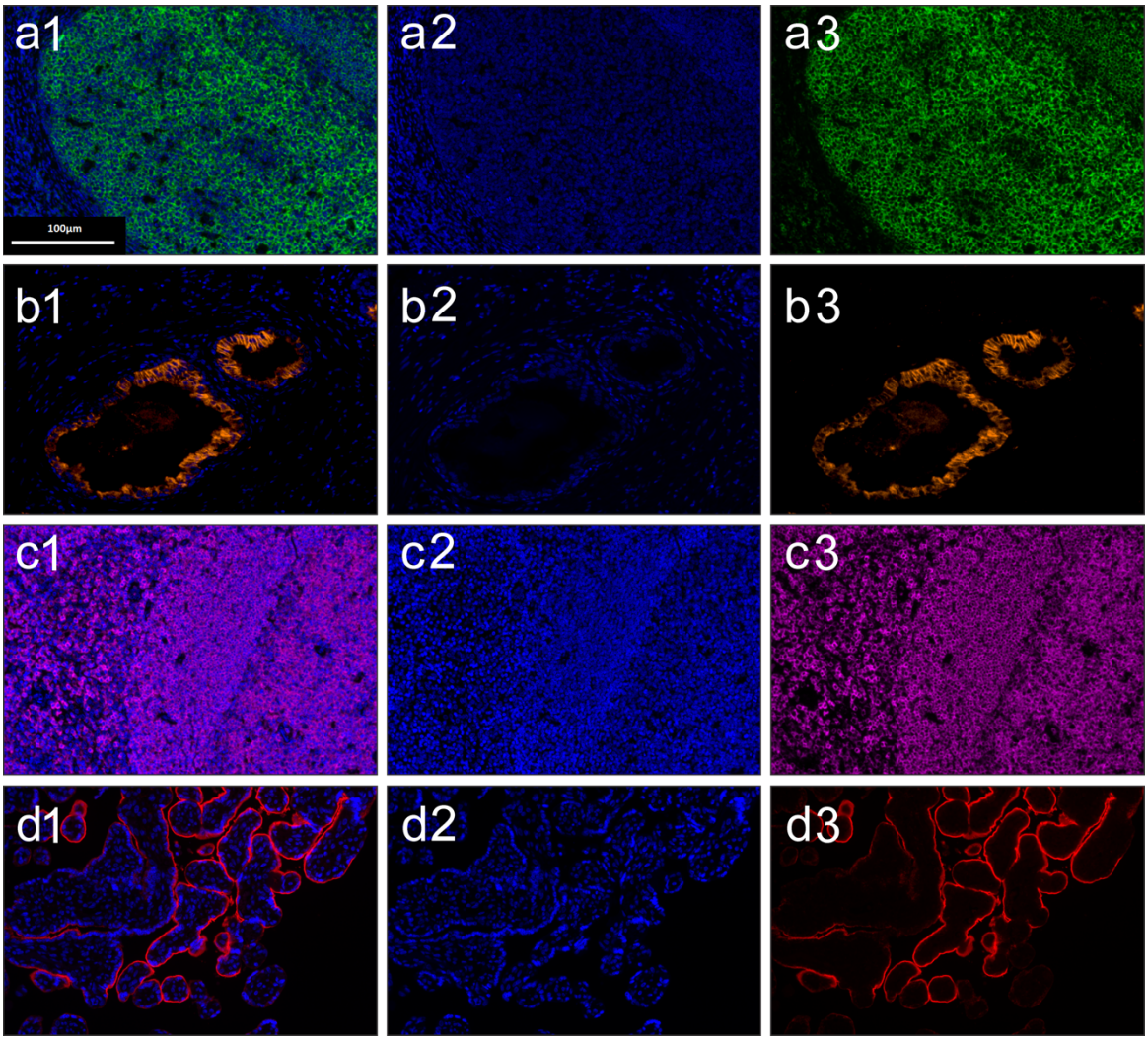


***Figure 53. Fluorescence IHC positive controls – ASC panel. a1)*** *Unmixed MSI of tonsil tissue displaying CD19+ B cells stained with anti-CD19 antibody (CD19 – green, DAPI - blue).* ***a2)*** *Unmixed MSI of tonsil tissue displaying DAPI nuclear counterstain.* ***a3)*** *Unmixed MSI of tonsil tissue displaying CD19+ B cells stained with anti-CD19 antibody (CD19 – green).* **b1)** *Unmixed MSI of prostate tissue displaying CD38+ glandular epithelial cells stained with anti-CD38 antibody (CD38 – orange, DAPI - blue).* ***b2)*** *Unmixed MSI of prostate tissue displaying DAPI nuclear counterstain.* ***b3)*** *Unmixed MSI of prostate tissue displaying CD38+ glandular epithelial cells stained with anti-CD38 antibody (CD38 – orange).* ***c1)*** *Unmixed MSI of tonsil tissue displaying CD45+ lymphocytes stained with anti-CD45 antibody (CD45 – magenta, DAPI - blue).* ***c2)*** *Unmixed MSI of tonsil tissue displaying DAPI nuclear counterstain.* ***c3)*** *Unmixed MSI of tonsil tissue displaying CD45+ lymphocytes stained with anti-CD45 antibody (CD45 – magenta).* **d1)** *Unmixed MSI of placental tissue displaying CD138+ syncytiotrophoblast cells stained with anti-*

*CD138 antibody (CD138 – red, DAPI - blue).* ***d2)*** *Unmixed MSI of tonsil tissue displaying DAPI nuclear counterstain.* ***d3)*** *Unmixed MSI of placental tissue displaying CD138+ syncytiotrophoblast cells stained with anti-CD138 antibody (CD138 – red).*

Single negative control stains were performed for each ASC panel primary antibody (see **Figure 54**) using tissue or cell lines that lacked each corresponding protein (confirmed using the Human Protein Atlas, https://www.proteinatlas.org). Specifically, **a1 – a3** show no cytoplasmic/membranous staining of anti-CD19 antibody in placental tissue; **b1 – b3** show no cytoplasmic/membranous staining of anti-CD38 antibody in a purified melanoma cell line; **c1 – c3** show no cytoplasmic/membranous staining of anti-CD45 antibody in a purified melanoma cell line; and **d1 – d3** show no cytoplasmic/membranous staining of anti-CD138 antibody in a purified gamma-delta T cell line.

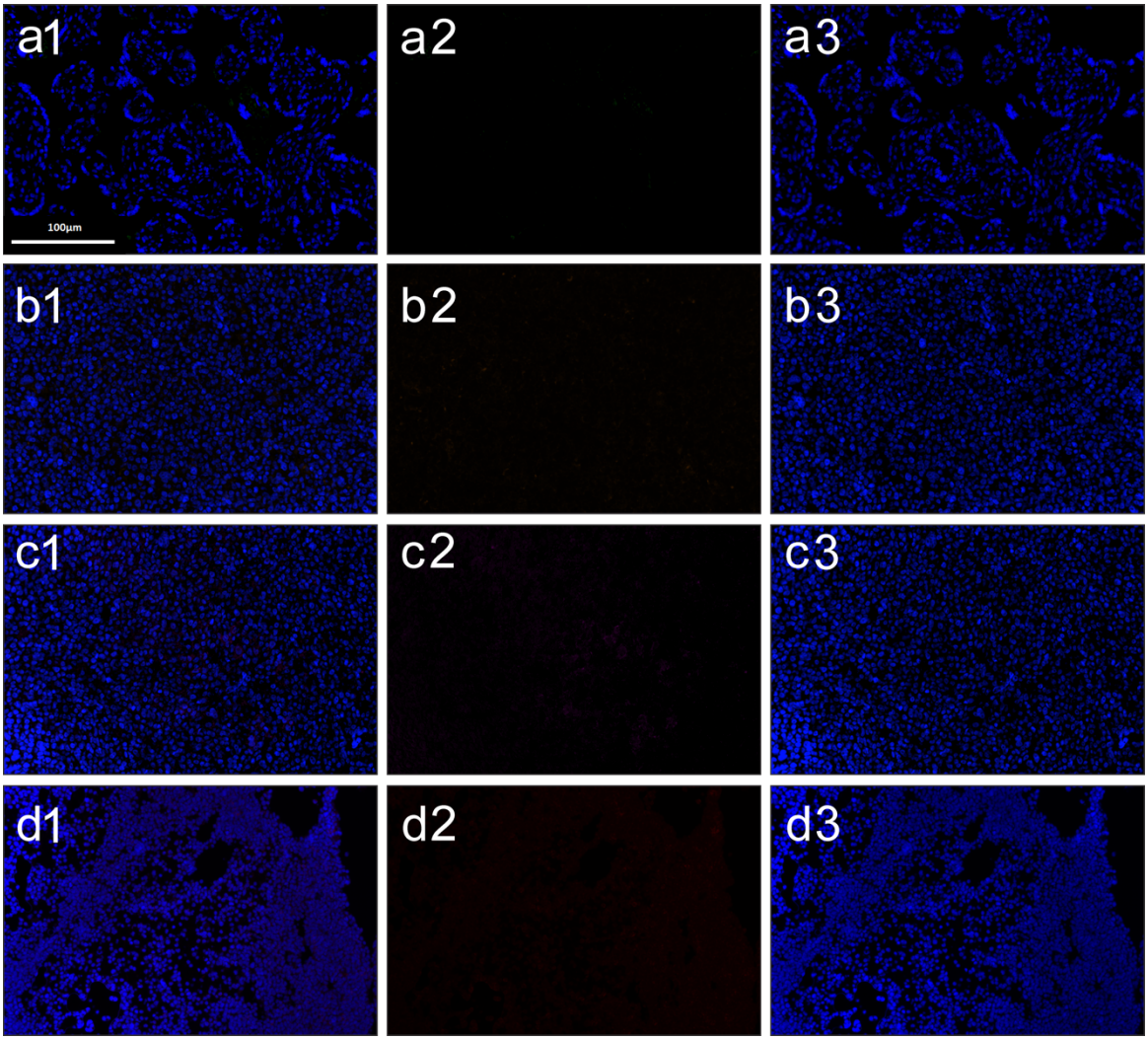


***Figure 54. Fluorescence IHC negative controls – ASC panel. a1)*** *Unmixed MSI of CD19 and DAPI in placental tissue.* ***a2)*** *Unmixed MSI of CD19 (Opal 570) in placental tissue.* ***a3)*** *Unmixed MSI of DAPI in placental tissue.* ***b1)*** Unmixed *MSI of CD38 and DAPI in a melanoma cell line (LM-MEL64)* ***b2)*** *Unmixed MSI of CD38 (Opal 620) in a melanoma cell line (LM-MEL64).* ***b3)*** *Unmixed MSI of DAPI in a melanoma cell line (LM-MEL64).* ***c1)*** *Unmixed MSI of CD45 and DAPI in a melanoma cell line (LM-MEL64).* ***c2)*** *Unmixed MSI of CD45 (Opal 690) in a melanoma cell line (LM-MEL64).* ***c3)*** *Unmixed MSI of DAPI in a melanoma cell line (LM-MEL64).* ***d1)*** *Unmixed MSI of CD138 and DAPI in a Gamma-Delta T cell line.* ***d2)*** *Unmixed MSI of CD138 (Opal 520) in a Gamma-Delta T cell line.* ***d3)*** *Unmixed MSI of DAPI in a Gamma-Delta T cell line.*

#### *3.3.2.2 TLS Panel*

Following optimisation of primary TLS panel antibodies using the aforementioned method in **Section 2.5.2**, six individual control slides (three for each concentration at epitope

retrieval pH 6 - ER 6, and three for each concentration at pH 9 - ER 9) were spectrally unmixed using inForm v2.4 and visually assessed for signal intensity and background. Those that displayed the clearest signals concomitantly with the least background were selected for use in multiplex stain order optimisation. Optimal primary antibody conditions for the TLS multiplex panel are detailed in **Table 11**.

***Table 11. Optimal concentrations and conditions of primary antibodies for ASC panel***

| **Primary Antibody** | **Optimal Dilution** | **Epitope Retrieval (pH)** |
|---|---|---|
| CD4 | 1:1000 | 9 |
| CD8 | 1:50 | 9 |
| CD19 | 1:300 | 9 |
| CD21 | 1:50 | 9 |
| DC-LAMP | 1:100 | 6 |
| PNAd | 1:100 | 9 |

*Refer to **Appendix Table A1** for more details on reagents used for staining.*

Single positive control staining was performed for each TLS panel primary antibody (positivity of cells found within tissue confirmed via the Human Protein Atlas). **Figure 55** displays positive and morphologically-sound staining of all six antibodies used for downstream TLS multiplex staining. Specifically, **a1 – a3** show clear, cytoplasmic/membranous staining of CD4+ T cells within a germinal centre (T cell zone) in tonsil tissue; **b1 – b3** show clear, cytoplasmic/membranous staining of CD8+ T cells within and surrounding a germinal centre in tonsil tissue; **c1 – c3** show clear, cytoplasmic/membranous staining of CD19+ B cells within two germinal centres (B cell zone) in tonsil tissue; **d1 – d3** show clear, cytoplasmic/membranous staining of CD21+ follicular dendritic cells (network) within two germinal centres in tonsil tissue; **e1 – e3** show clear, cytoplasmic/membranous staining of DC-LAMP+ mature dendritic cells in

tonsil tissue; and, **f1 – f3** show clear, staining of PNAd+ high endothelial venules in tonsil tissue.

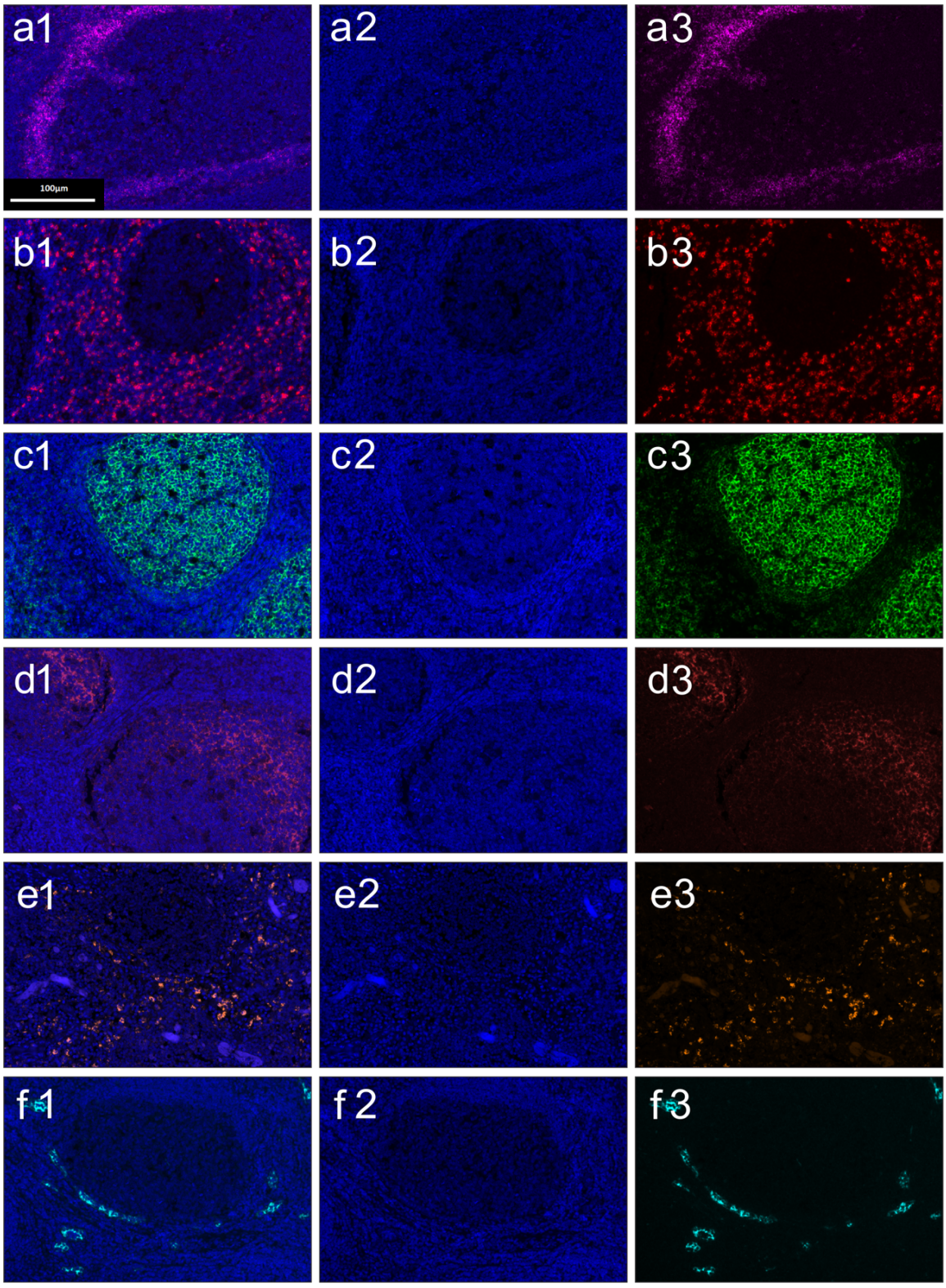


***Figure 55. Fluorescence IHC positive controls – TLS panel. a1)*** *Unmixed MSI of tonsil tissue displaying CD4+ T cells stained with anti-CD4 antibody (CD4 – magenta, DAPI - blue).* ***a2)*** *Unmixed MSI of tonsil tissue with DAPI counterstain.* ***a3)*** *Unmixed MSI of tonsil tissue displaying*

*CD4+ T cells stained with anti-CD4 antibody (CD4 – magenta).* **b1)** *Unmixed MSI of tonsil tissue displaying CD8+ T cells stained with anti-CD8 antibody (CD8 – red, DAPI - blue).* ***b2)*** *Unmixed MSI of tonsil tissue with DAPI counterstain.* ***b3)*** *Unmixed MSI of tonsil tissue displaying CD8+ T cells stained with anti-CD8 antibody (CD8 – red).* ***c1)*** *Unmixed MSI of tonsil tissue displaying CD19+ B cells stained with anti-CD19 antibody (CD19 – green, DAPI - blue).* ***c2)*** *Unmixed MSI of tonsil tissue with DAPI counterstain.* ***c3)*** *Unmixed MSI of tonsil tissue displaying CD19+ B cells stained with anti-CD19 antibody (CD19 – green).* **d1)** *Unmixed MSI of tonsil tissue displaying CD21+ follicular dendritic cells stained with anti-CD21 antibody (CD21 – brown, DAPI - blue).* ***d2)*** *Unmixed MSI of tonsil tissue with DAPI counterstain.* ***d3)*** *Unmixed MSI of tonsil tissue displaying CD21+ follicular dendritic cells stained with anti-CD21 antibody (CD21 – brown).* ***e1)*** *Unmixed MSI of lymph node tissue displaying DC-LAMP+ mature dendritic cells stained with anti-LAMP3 antibody (LAMP3 – orange, DAPI - blue).* ***e2)*** *Unmixed MSI of lymph node tissue with DAPI counterstain.* ***e3)*** *Unmixed MSI of lymph node tissue displaying DC-LAMP+ mature dendritic cells stained with anti-LAMP3 antibody (LAMP3 – orange).* **f1)** *Unmixed MSI of tonsil tissue displaying PNAd+ endothelial venules stained with anti-PNAd antibody (PNAd – cyan, DAPI - blue).* ***f2)*** *Unmixed MSI of tonsil tissue with DAPI counterstain.* ***f3)*** *Unmixed MSI of tonsil tissue displaying PNAd+ endothelial venules stained with anti-PNAd antibody (DAPI omitted). Scale bar = 100µm. Taken at 20x magnification.*

Single negative control stains were performed for each ASC panel primary antibody (see **Figure 56**) using tissue or cell lines that lacked each corresponding protein (confirmed via the Human Protein Atlas). Specifically, **a1 – a3** show no cytoplasmic/membranous staining of anti-CD4 antibody in a purified melanoma cell line; **b1 – b3** show no cytoplasmic/membranous staining of anti-CD8 antibody in a purified melanoma cell line; **c1 – c3** show no cytoplasmic/membranous staining of anti-CD19 antibody in a purified melanoma cell line; **d1 – d3** show no cytoplasmic/membranous staining of anti-CD21 antibody in a purified melanoma cell line; **e1 – e3** show no cytoplasmic/membranous staining of anti-DC-LAMP antibody in a purified melanoma cell line; and, **f1 – f3** show no

cytoplasmic/membranous staining of anti-PNAd antibody in a purified gamma-delta T cell line.

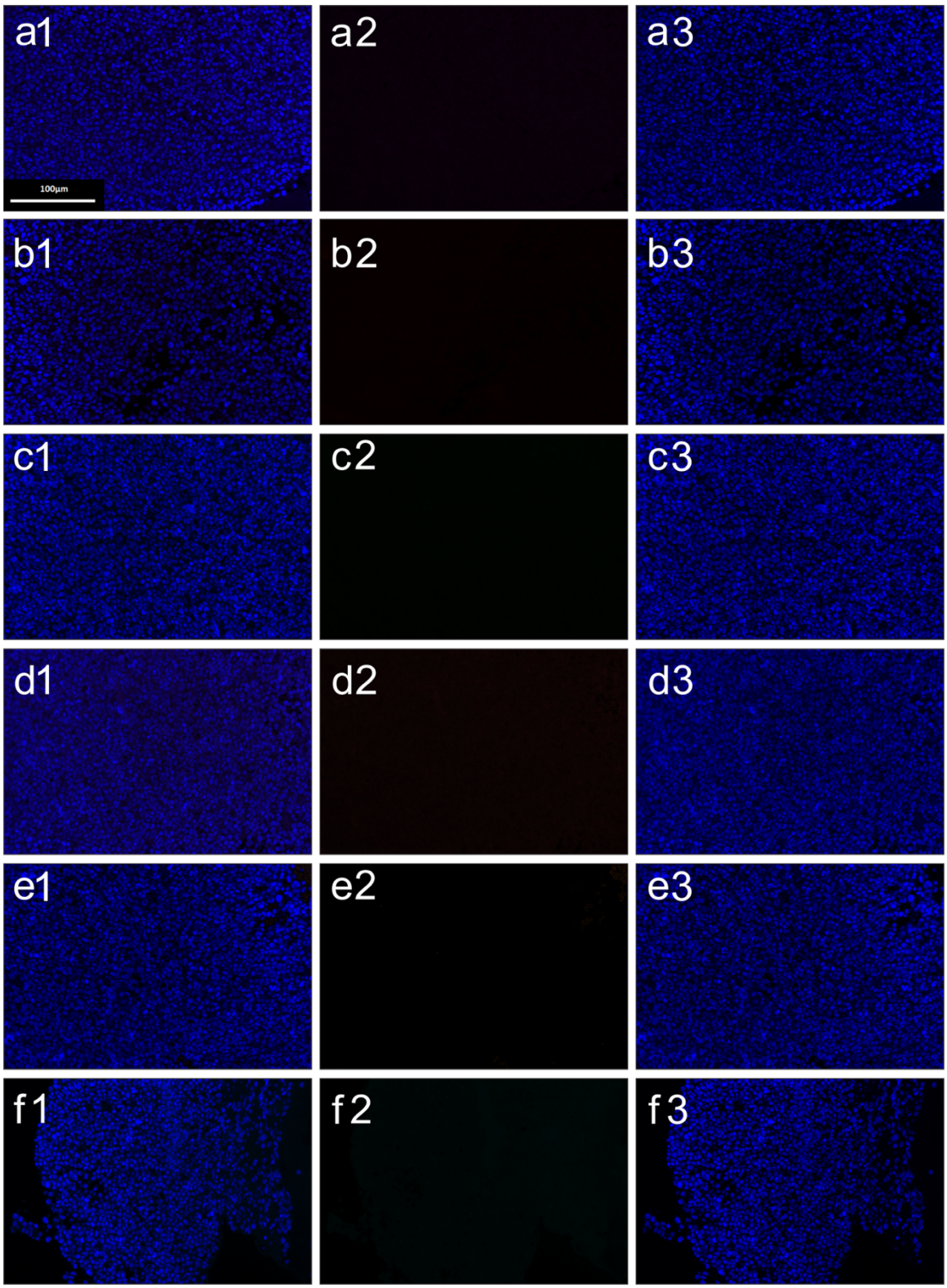


***Figure 56. Fluorescence IHC negative controls – TLS panel. a1)*** *Unmixed MSI of CD4 and DAPI in a melanoma cell line (LM-MEL64).* ***a2)*** *Unmixed MSI of CD4 (Opal 570) in a melanoma cell line (LM-MEL64).* ***a3)*** *Unmixed MSI of DAPI in a melanoma cell line (LM-MEL64).* ***b1)*** Unmixed

*MSI of CD8 and DAPI in a melanoma cell line (LM-MEL64)* ***b2)*** *Unmixed MSI of CD8 (Opal 650) in a melanoma cell line (LM-MEL64).* ***b3)*** *Unmixed MSI of DAPI in a melanoma cell line (LM-MEL64).* ***c1)*** *Unmixed MSI of CD19 and DAPI in a melanoma cell line (LM-MEL64).* ***c2)*** *Unmixed MSI of CD19 (Opal 690) in a melanoma cell line (LM-MEL64).* ***c3)*** *Unmixed MSI of DAPI in a melanoma cell line (LM-MEL64).* ***d1)*** *Unmixed MSI of CD21 and DAPI in a melanoma cell line (LM-MEL64).* ***d2)*** *Unmixed MSI of CD21 (Opal 520) in a melanoma cell line (LM-MEL64).* ***d3)*** *Unmixed MSI of DAPI in a melanoma cell line (LM-MEL64).* ***e1)*** *Unmixed MSI of DC-LAMP and DAPI in a melanoma cell line (LM-MEL64).* ***e2)*** *Unmixed MSI of DC-LAMP (Opal 540) in a melanoma cell line (LM-MEL64).* ***e3)*** *MSI of DAPI in a melanoma cell line (LM-MEL64).* ***f1)*** *Unmixed MSI of PNAd and DAPI in a Gamma-Delta T cell line.* ***f2)*** *Unmixed MSI of PNAd (Opal 620) in a Gamma-Delta T cell line.* ***f3)*** *Unmixed MSI of DAPI in a Gamma-Delta T cell line.*

### *3.3.3 Multiplex Optimisation*

#### *3.3.3.1 ASC Panel*

Effective multiplex staining is not only dependent on antibody concentration, epitope retrieval pH, and incubation times for each primary antibody, but also requires optimisation of the order in which each primary antibody is added, as well as the order of each corresponding Opal fluorophore. Though optimising primary antibodies and unmixing them at defined spectral wavelengths can provide a strong, clear signal while removing crosstalk between varying spectral wavelengths, introducing multiple different antibodies with corresponding fluorophores onto a single specimen will, in many cases, affect staining quality and downstream unmixing capabilities. Ineffective stain orders may lead to absent or excessive signal intensities or higher background intensities that may ultimately affect the accurateness of cell-based analyses. To circumvent these issues, three multiplex stain orders (**see Appendix Table A2**) were conducted (see **Section 2.5.3**), where the variability in corresponding fluorophores, their order, and the order of primary antibodies for each stain order was determined based on factors such as antigen prevalence (i.e. more antigens present on cell surface, the more cross-talk that can be removed if placed at end of the stain

order), cell prevalence (i.e. more cells stained with antibody/fluorophore, more likelihood that using an Opal fluorophore near that wavelength for the next antibody can result in bleed through of signal through channels), number of epitope retrievals for a given antigen (e.g. some antigens require multiple successive retrievals for better binding of antibody-antigen) and the most effective variant was selected as shown in **Table 12** below.

***Table 12. Multiplex stain order variant used for optimisation of ASC panel.***

| **Primary Antibody** | **Epitope Retrieval (pH)** | **Optimised Dilution** | **Opal Fluorophore** |
|---|---|---|---|
| **Multiplex Stain Order 1:** | | | |
| CD138 | ER 9 | 1:100 | Opal 520 |
| CD38 | ER 9 | 1:300 | Opal 620 |
| CD19 | ER 9 | 1:300 | Opal 570 |
| CD45 | ER 9 | 1:100 | Opal 690 |
| DAPI | - | 2 drops / mL | - |

*Refer to the **Appendix Table A1** for more details on reagents used for staining.*

Multiplex stain order 1 was selected, as it was determined to be most effective based on a visual comparison of MSIs obtained from tissues specimens that underwent each stain order. The representative image below (**Figure 57**) indicates how an effective stain order can be visually determined based on the presence of clear, morphologically-sound staining and effective unmixing of spectral wavelengths for corresponding Opal fluorophores from composite images. When unmixed, a clear fluorophore signal for CD45 (**c1 – c2**), CD19 (**d1 – d2**), CD38 (**e1 – e2**), and CD138 (**f1 – f2**) can be seen for distinct and similar cells in prostate cancer tissue. Note the distinct overlap in staining between **e1 – e2** (CD38) and **f1 – f2** (CD138), here we see how multiplex staining can be used to co-stain cells to define cell phenotypes, in this case, plasma cells.

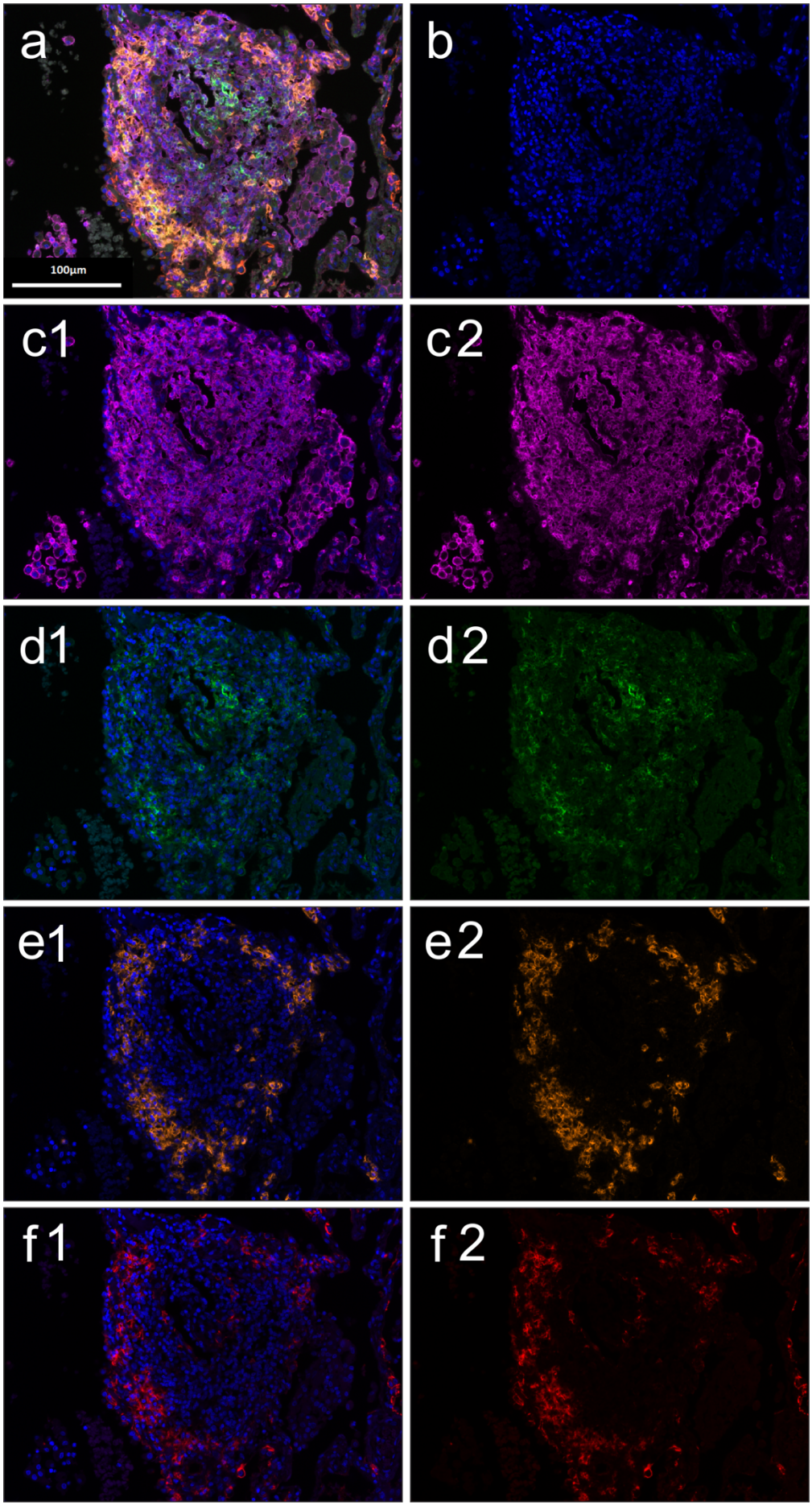
a
b
100µm
c1
c2
d1
d2
e1
e2
f1
f2

***Figure 57. An unmixed multispectral image from a specimen that underwent ASC panel stain order 1.*** *This MSI was taken from a prostate cancer specimen and depicts an aggregate of immune cells that was unmixed, showing effective staining of all markers.* ***a)*** *Merged MSI containing signals of all markers.* ***b)*** *Unmixed MSI displaying DAPI (blue).* ***c1)*** *Unmixed MSI displaying DAPI and CD45 (magenta).* ***c2)*** *Unmixed MSI displaying CD45.* ***d1)*** *Unmixed MSI displaying CD19 (green) and DAPI.* ***d2)*** *Unmixed MSI displaying CD19.* ***e1)*** *Unmixed MSI displaying CD38 (orange) and DAPI.* ***e2)*** *CD38.* ***f1)*** *Unmixed MSI displaying CD138 (red) and DAPI.* ***f2)*** *Unmixed MSI displaying CD138. Scale bar = 100µm. Taken at 20x magnification.*

#### *3.3.3.2 TLS Panel*

**Table 13** below outlines the most effective variant of stain orders (see **Appendix Table A2**) used for all TLS-based downstream patient staining following multiplex stain order optimisation (see **Section 2.5.3** for method of optimisation).

***Table 13. Multiplex stain order variant used for optimisation of TLS panel.***

| Primary Antibody | Epitope Retrieval (pH) | Optimised Dilution | Opal Fluorophore |
|---|---|---|---|
| **Multiplex Stain Order 2:** | | | |
| CD21 | ER 9 | 1:50 | Opal 520 |
| DC-LAMP | ER 6 | 1:100 | Opal 540 |
| CD4 | ER 9 | 1:1000 | Opal 570 |
| PNAd | ER 9 | 1:100 | Opal 620 |
| CD8 | ER 9 | 1:50 | Opal 650 |
| CD19 | ER 9 | 1:300 | Opal 690 |
| DAPI | - | 2 drops / mL $dH_2O$ | - |

*Refer to the* ***Appendix Table A1*** *for more details on reagents used for staining.*

Multiplex stain order 2 was selected, as it was determined to be most effective based on a visual comparison of MSIs obtained from tissues specimens that underwent each stain order. The representative image below (**Figure 58**) displays the clear, morphologically-sound staining and effective unmixing of spectral wavelengths from composite images with

minimal background for each TLS panel primary antibody in lymph node tissue. Following the merge image (**a)** and DAPI image (**b**), effective spectral unmixing of cell types can be seen for CD4 (**c1 – c2**), CD8 (**d1 – d2**), CD19 (**e1 – e2**), CD21 (**f1 – f2**), DC-LAMP (**g1 – g2**) positive cell types, and PNAd (**h1 – h2**) positive endothelial venules.

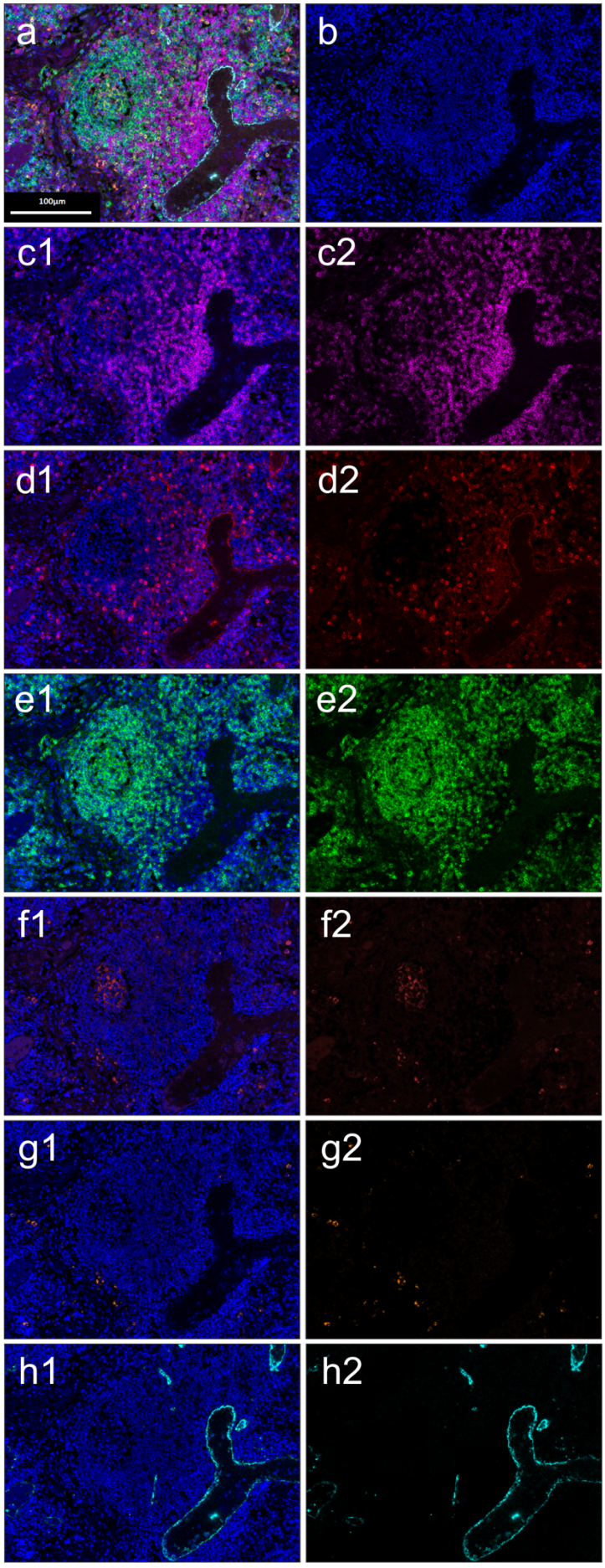
a
b
100µm
c1
c2
d1
d2
e1
e2
f1
f2
g1
g2
h1
h2

***Figure 58. An unmixed multispectral image from a specimen that underwent TLS panel stain order 2.*** *This MSI was taken from a lymph node specimen and depicts a TLS that was unmixed, showing effective staining of all markers.* ***a)*** *Merged MSI containing signals of all markers.* ***b)*** *Unmixed MSI displaying DAPI (blue).* ***c1)*** *Unmixed MSI displaying DAPI and CD4 (magenta).* ***c2)*** *Unmixed MSI displaying CD4.* ***d1)*** *Unmixed MSI displaying CD8 (red) and DAPI.* ***d2)*** *Unmixed MSI displaying CD8.* ***e1)*** *Unmixed MSI displaying CD19 (green) and DAPI.* ***e2)*** *Unmixed MSI displaying CD19.* ***f1)*** *Unmixed MSI displaying CD21 (brown) and DAPI.* ***f2)*** *Unmixed MSI displaying CD21.* ***g1)*** *Unmixed MSI displaying DC-LAMP (orange) and DAPI.* ***g2)*** *Unmixed MSI displaying DC-LAMP.* ***h1)*** *Unmixed MSI displaying PNAd (cyan) and DAPI.* ***h2)*** *Unmixed MSI displaying PNAd. Scale bar = 100µm. Taken at 20x magnification.*

### *3.3.4 Multiplex Staining, Vectra Imaging and inForm Analysis of Patient Tissue*

Using the aforementioned optimal stain orders, primary antibody concentrations and conditions for the ASC and TLS panels, all 64 Prostate cancer patient FFPE tissues were stained.

#### *3.3.4.1 ASC Panel*

Abundance of IT and PT ASCs and BCAs was determined based on a minimum of ten MSIs covering both the IT and PT areas of each specimen. **Figure 59** below displays the percentage of patient prostatectomy FFPE specimens that contained absent (n=20), scarce (n=23) or abundant (n=21) IT ASCs and absent (n=6), scarce (n=22) or abundant (n=35) PT ASCs; as well as specimens containing absent (n=24), scarce (n=28) or abundant (n=12) IT BCAs and absent (n=13), scarce (n=27) or abundant (n=23) PT BCAs (refer to **Appendix Table A3** for more details). A single patient was removed from the PT portion of the analysis as the corresponding prostatectomy section did not contain PT tissue.

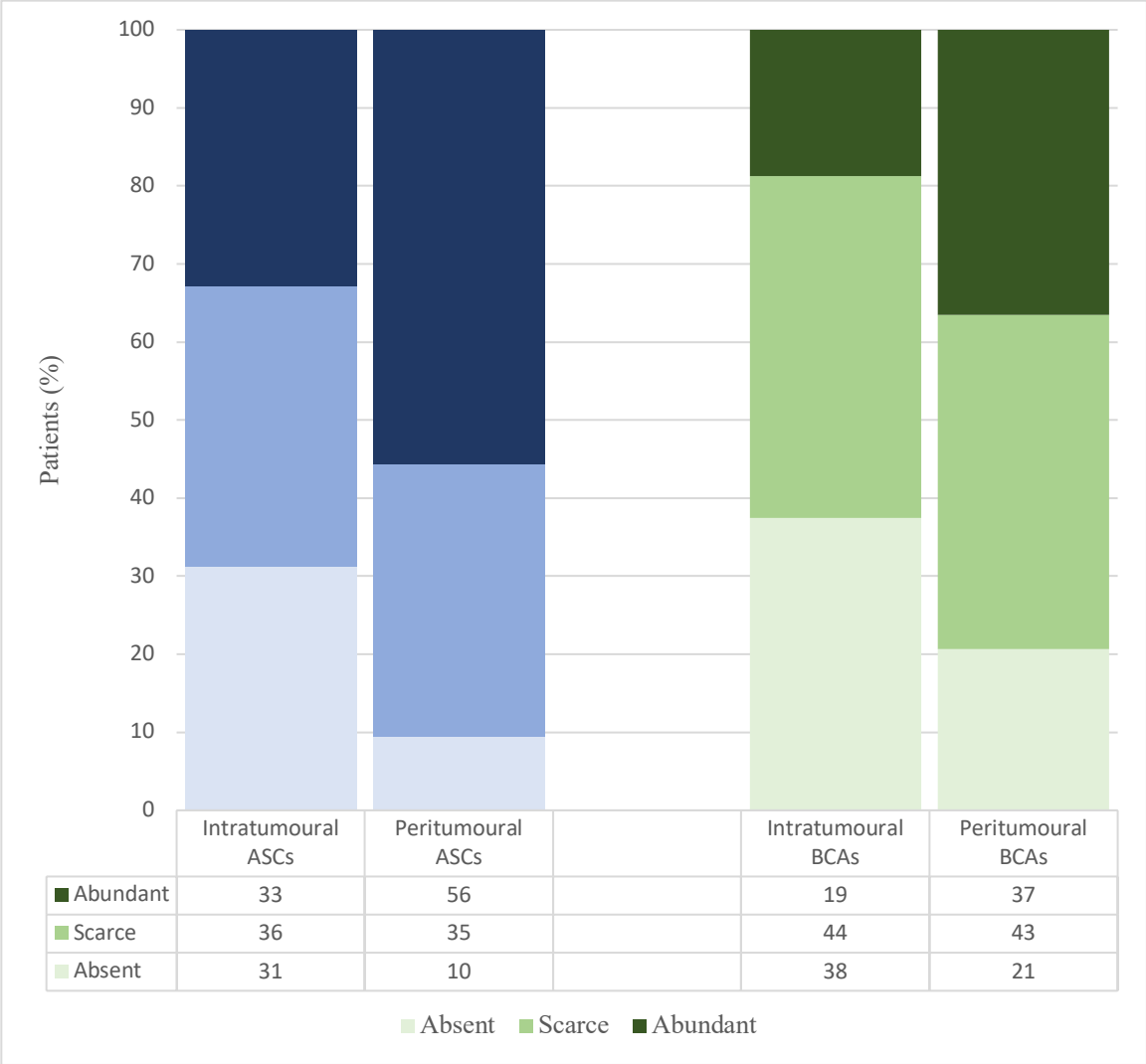


***Figure 59. Abundance of IT and PT ASCs and BCAs in patient prostatectomy tissue.*** Each category (i.e., absent, scarce, and abundant) are shown as a percentage of the total prostatectomy specimens stained. IT ASCs: *Absent, 31%; Scarce, 36%; Abundant, 33%. PT ASCs: Absent, 10%; Scarce, 35%; Abundant, 56%; N/a, 2%.* IT BCAs: *Absent, 38%; Scarce, 44%; Abundant, 19%. PT BCAs: Absent, 21%; Scarce, 43%; Abundant, 37%. Abbreviations. IT, intratumoural; PT, peritumoural; ASC, antibody-secreting cell; BCA, B cell aggregate.*

ASCs were often scarcely or abundantly detected in the assessed prostate cancer tumours and were more commonly seen surrounding tumour areas (n=57/64 detected in the PT regions vs. n=44/63 detected in the IT regions, chi-square p-value=0.0024). The presence of BCAs was also common, with a similar distribution (n=50/63 detected in the PT regions vs. n=40/64 detected in the IT regions, chi-square p-value=0365). Selected MSIs displaying

abundant and absent ASCs, and the presence of BCAs in IT and PT areas are of prostatectomy tissue are shown in **Figure 60**, below.

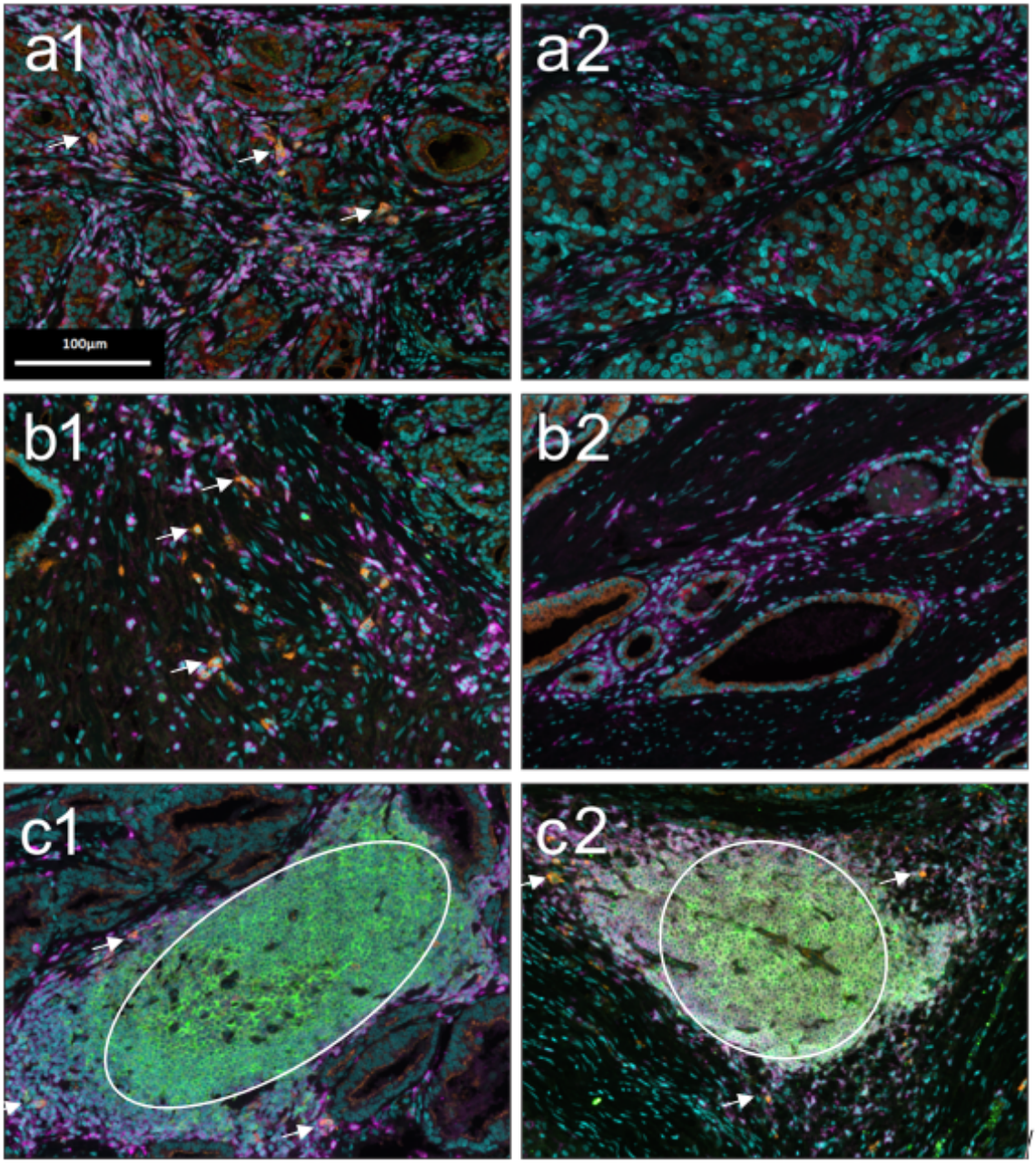


***Figure 60. Representative multispectral images of abundant and absent ASCs and presence of BCA in prostate cancer tissue. a1)*** *Abundant IT ASCs.* ***a2)*** *Absent ACSs.* ***b1)*** *Abundant PT ASCs. B2) Absent PT ASCs. C1) IT BCA among cancerous prostate glands. C2) PT BCA situated in stromal tissue. ASCs are indicated using white arrows, BCAs indicated using white circles. Scale bar = 100µm. Taken at 20x magnification. Abbreviations. IT, intratumoural; PT, peritumoural; ASC, antibody-secreting cell; BCA, B cell aggregate.*

To investigate if disease grade was correlated with the abundance of IT and PT ASCs, a brief analysis was performed comparing each factor (**Figure 61**). ASCs were more scarcely or abundantly detected in patients with high-grade disease when located in both IT (64% low-grade vs. 79% high-grade, chi-square p-value=0.0188) and PT (87% low-grade vs. 100% high-grade, chi-square p-value=0.0001) regions.

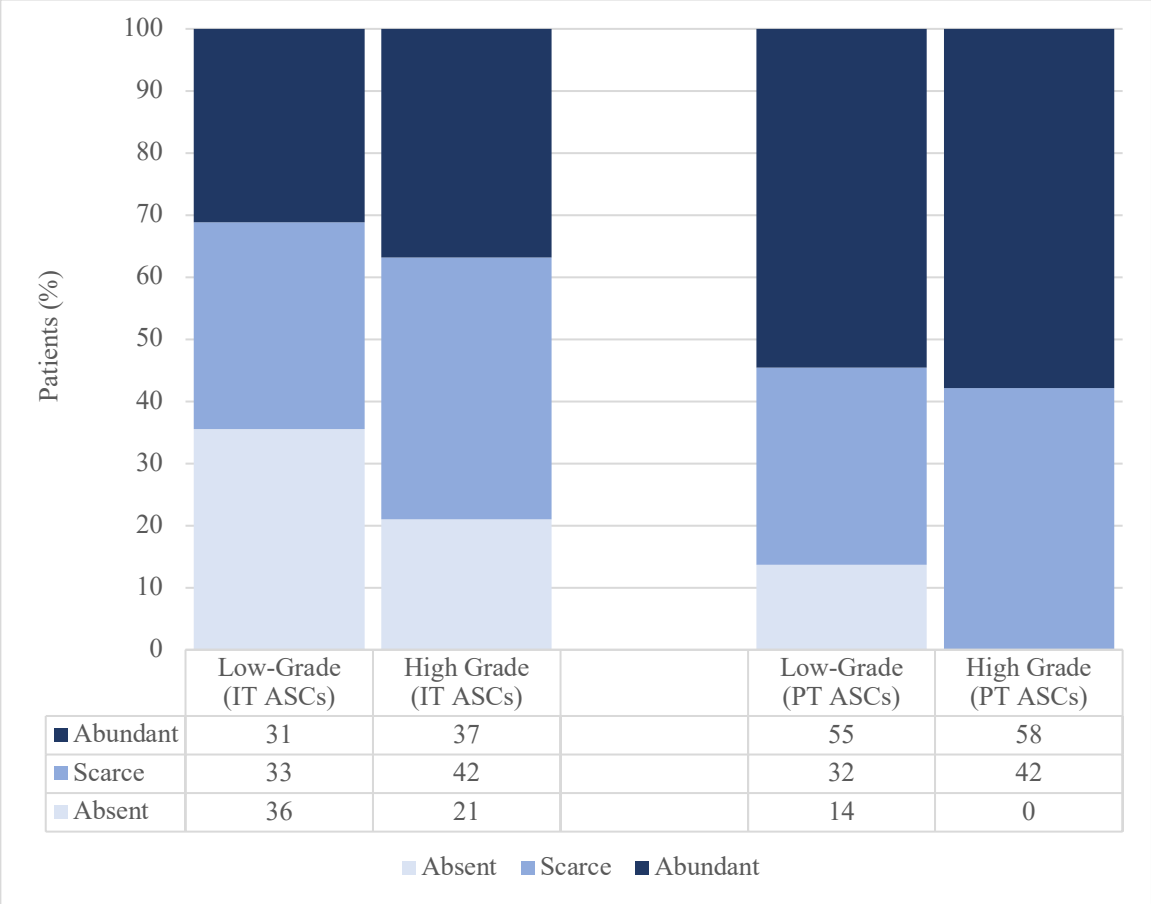


***Figure 61. Abundance of IT and PT ASCs among low- and high-grade patients.*** Each category (i.e., absent, scarce, and abundant) are shown as a percentage of the total prostatectomy specimens stained. *Low-grade patients: IT ASCs (Absent, 36%; Scarce, 33%; Abundant 31%) and high-grade patients: IT ASCs (Absent, 21%; Scarce, 42%; Abundant, 37%) shown on left. Low-grade patients: PT ASCs (Absent, 14%; Scarce, 32%; Abundant 55%) and high-grade patients: PT ASCs (Absent, 0%; Scarce, 42%; Abundant, 48%) shown on right. Abbreviations. IT, intratumoural; PT peritumoural; ASC, antibody-secreting cell.*

Similarly, to investigate if disease grade was correlated with the abundance of IT and PT BCAs, a brief analysis was performed comparing each factor (**Figure 62**). BCAs were also more scarcely or abundantly detected in patients with high-grade disease when located in both IT (55% low-grade vs. 79% high-grade, chi-square p-value=0.0004) and PT (71% low-grade vs. 100% high-grade, chi-square p-value<0.0001) regions.

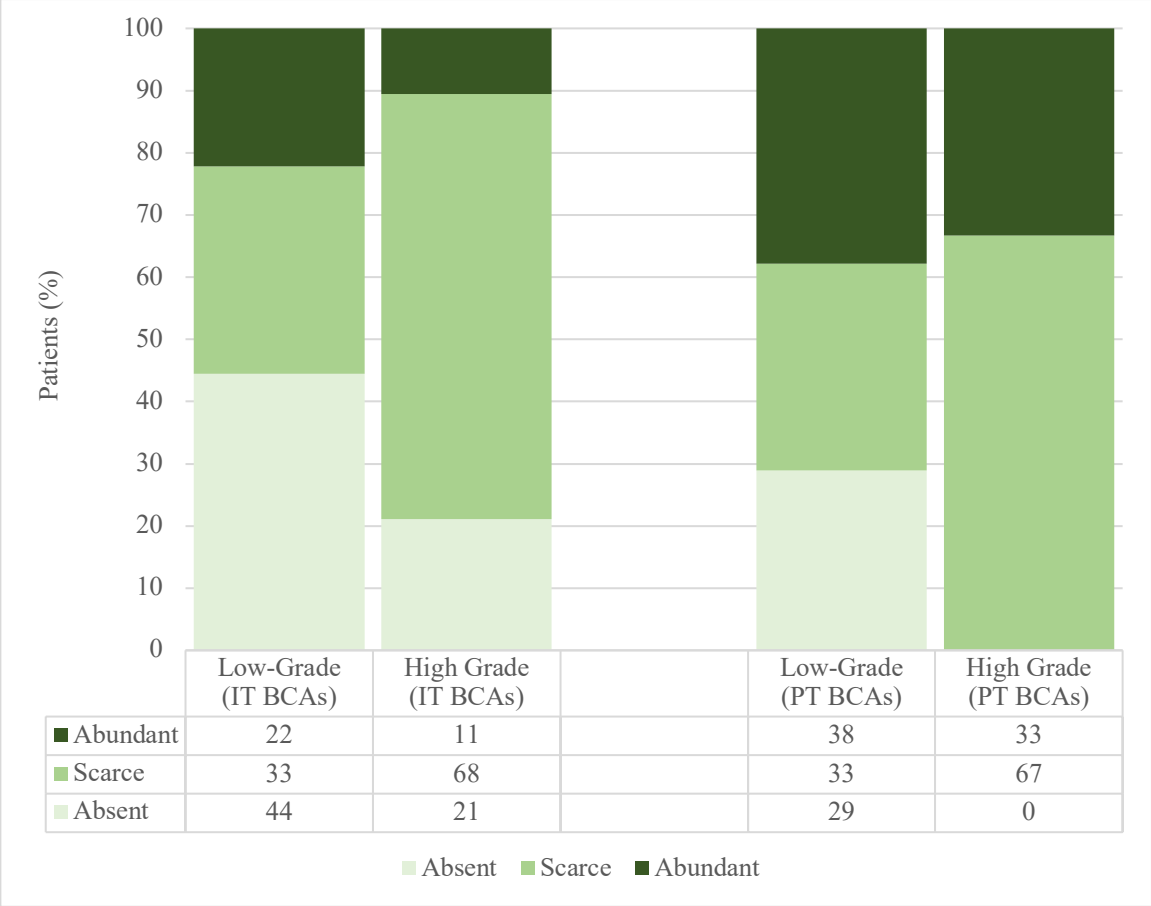


| | Low-Grade (IT BCAs) | High Grade (IT BCAs) | | Low-Grade (PT BCAs) | High Grade (PT BCAs) |
|---|---|---|---|---|---|
| Abundant | 22 | 11 | | 38 | 33 |
| Scarce | 33 | 68 | | 33 | 67 |
| Absent | 44 | 21 | | 29 | 0 |

***Figure 62. Abundance of IT and PT BCAs among low- and high-grade patients.*** Each category (i.e., absent, scarce, abundant, and N/a) are shown as a percentage of the total prostatectomy specimens stained. *Low-grade patients: IT BCAs (Absent, 44%; Scarce, 33%; Abundant 22%) and high-grade patients: IT BCAs (Absent, 21%; Scarce, 68%; Abundant, 11%) shown on left. Low-grade patients: PT BCAs (Absent, 29%; Scarce, 33%; Abundant 38%) and high-grade patients: PT BCAs (Absent, 0%; Scarce, 67%; Abundant, 33%) shown on right. Abbreviations. IT, intratumoural; PT peritumoural; BCA, B cell aggregate.*

To see whether biochemical relapse (PSA) was in any way correlated with the abundance of IT ASCs or BCAs, a brief analysis was performed comparing each factor (see **Table 14** below and refer to **Appendix Table A4** for more details).

***Table 14. Correlation between abundance of IT/PT ASCs and BCAs with biochemical relapse.***

| | **Absent** | **Scarce** | **Abundant** |
|---|---|---|---|
| **Intratumoural Antibody-Secreting Cells** | | | |
| Total (N=60) | 19 | 21 | 20 |
| Relapse (n=10) | 1 | 2 | 7 |
| Non-Relapse (n=50) | 18 | 19 | 13 |
| **Peritumoural Antibody-Secreting Cells** | | | |
| Total (N=59*) | 6 | 21 | 32 |
| Relapse (n=9) | 1 | 3 | 5 |
| Non-Relapse (n=50) | 5 | 18 | 27 |
| **Intratumoural B Cell Aggregates** | | | |
| Total (N=60) | 21 | 27 | 12 |
| Relapse (n=10) | 1 | 4 | 5 |
| Non-Relapse (n=50) | 20 | 23 | 7 |
| **Peritumoural B Cell Aggregates** | | | |
| Total (N=59*) | 13 | 24 | 22 |
| Relapse (n=9) | 3 | 2 | 4 |
| Non-Relapse (n=50) | 10 | 22 | 18 |

***** *Patient with FFPE sample containing only tumour tissue excluded from peritumoural-related analyses. Four patients were removed due to lack of biochemical relapse data. Abbreviations: IT, intratumoural; PT, peritumoural.*

It was evident that the majority of relapse patients contained abundant IT ASCs (70% of relapse vs. 26% of non-relapse patients, chi-square p-value=0.0248) and BCAs (50% of relapse vs. 14% of non-relapse patients, chi-square p-value=0.0239). However, no significant difference was observed for relapse in ASCs (56% of relapse vs. 54% of non-relapse patients, chi-square p-value=0.9861) or BCAs (44% of relapse vs. 36% of non-

relapse patients, chi-square p-value=0.4381) located in PT regions. These statistics can be further visualised in **Figure 63** and **Figure 64** below.

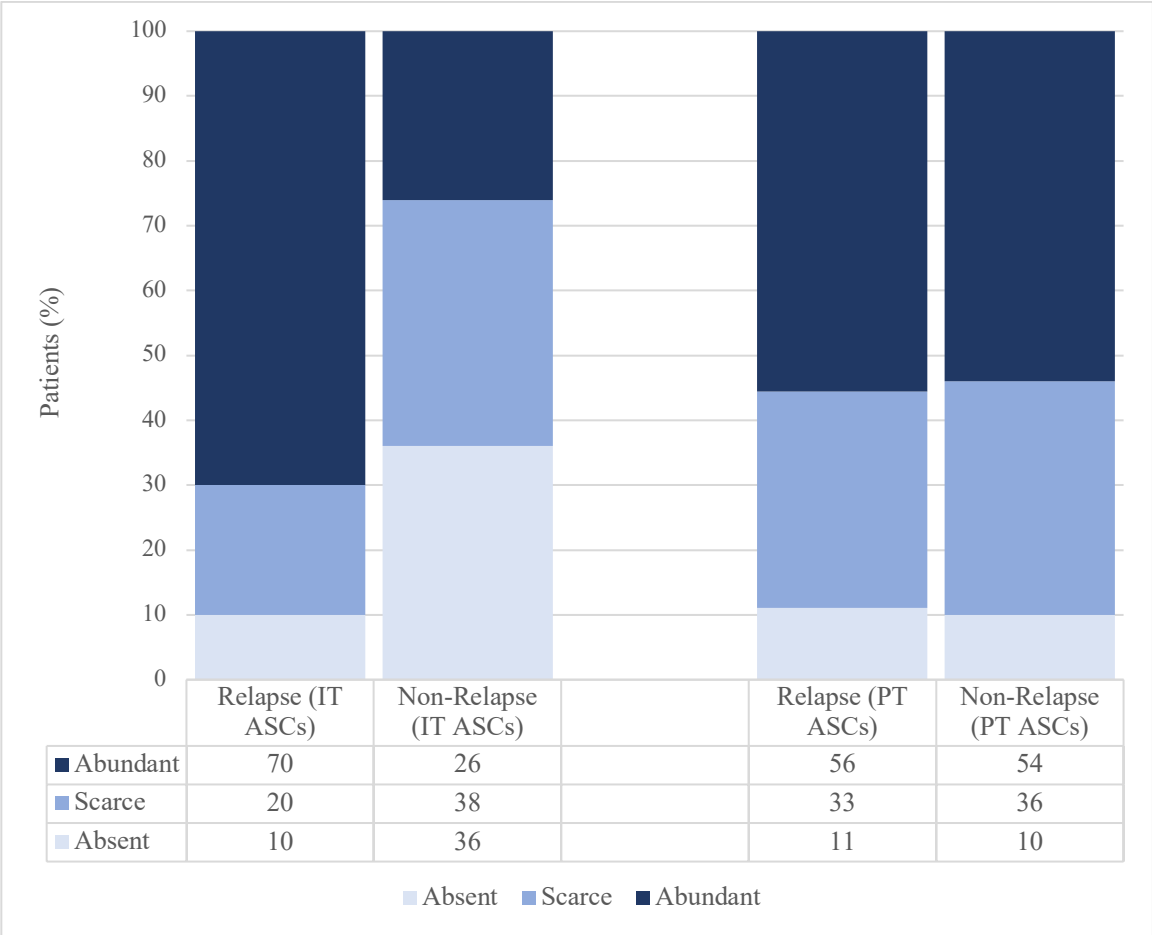


| | Relapse (IT ASCs) | Non-Relapse (IT ASCs) | | Relapse (PT ASCs) | Non-Relapse (PT ASCs) |
|---|---|---|---|---|---|
| Abundant | 70 | 26 | | 56 | 54 |
| Scarce | 20 | 38 | | 33 | 36 |
| Absent | 10 | 36 | | 11 | 10 |

***Figure 63. Abundance of IT and PT ASCs among relapse and non-relapse patients.*** *Relapse patients: IT ASCs (Absent, 10%; Scarce, 20%; Abundant 70%) and non-relapse patients: IT ASCs (Absent, 36%; Scarce, 38%; Abundant, 26%) shown on left. Relapse patients: PT ASCs (Absent, 11%; Scarce, 33%; Abundant 56%) and non-relapse patients: PT ASCs (Absent, 10%; Scarce, 36%; Abundant, 54%) shown on right. Abbreviations: IT, intratumoural; PT peritumoural; ASC, antibody-secreting cell.*

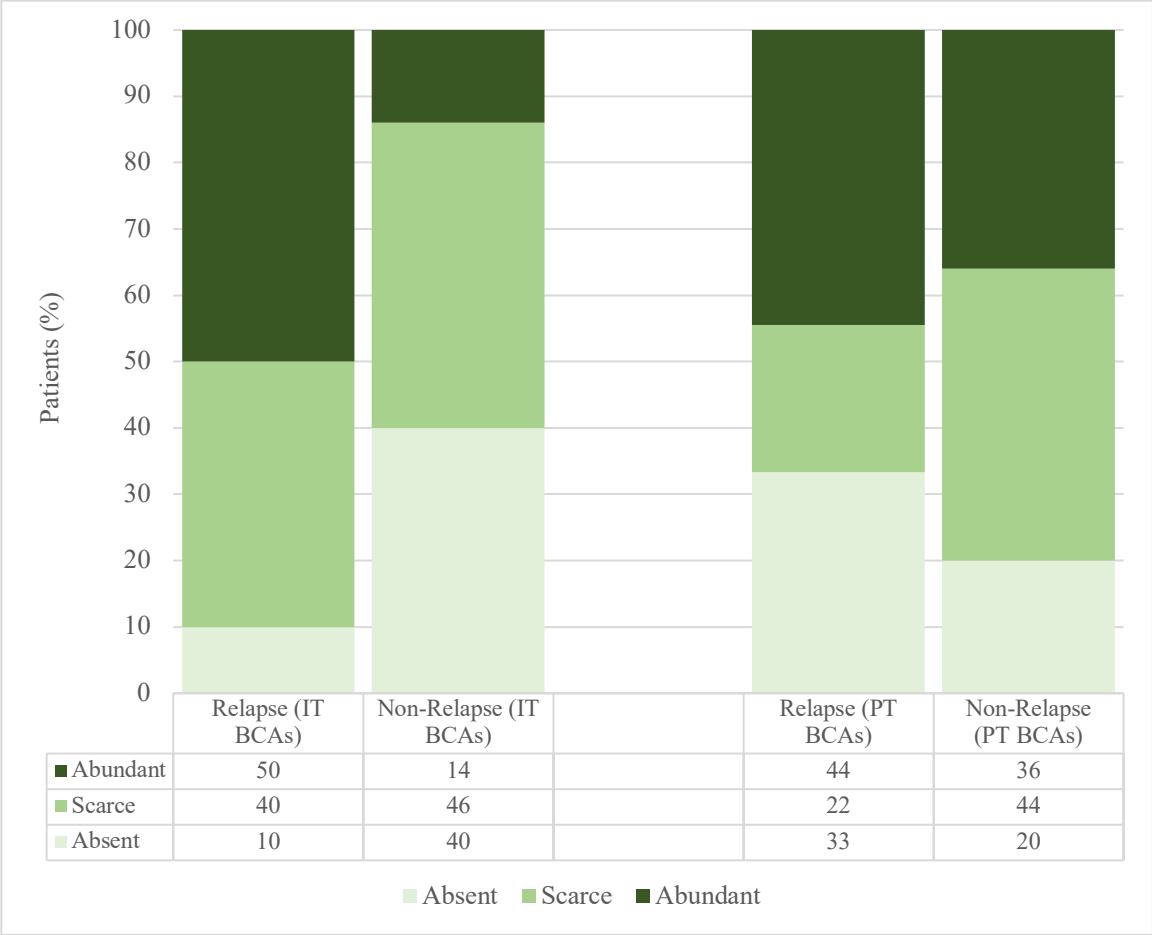


***Figure 64. Abundance of IT and PT BCAs among relapse and non-relapse patients.*** *Relapse patients: IT BCAs (Absent, 10%; Scarce, 40%; Abundant 50%) and non-relapse patients: IT BCAs (Absent, 40%; Scarce, 46%; Abundant, 14%) shown on left. Relapse patients: PT BCAs (Absent, 33%; Scarce, 22%; Abundant 44%) and non-relapse patients: PT BCAs (Absent, 20%; Scarce, 44%; Abundant, 36%) shown on right. Abbreviations: IT, intratumoural; PT peritumoural; BCA, B cell aggregate.*

Once discovered, BCAs were of particular interest due to their often-concurrent appearance with high quantities of bordering ASCs. **Figure 65** below highlights this phenomenon and displays the process of taking whole-slide scan images and unmixing multispectral regions of interest. ASCs can be seen exiting the aggregate in either the merge image (**a**; orange and red cells), or in the two unmixed images displayed at the bottom (**b5**; CD38+, orange; and **b6**; CD138+, red).

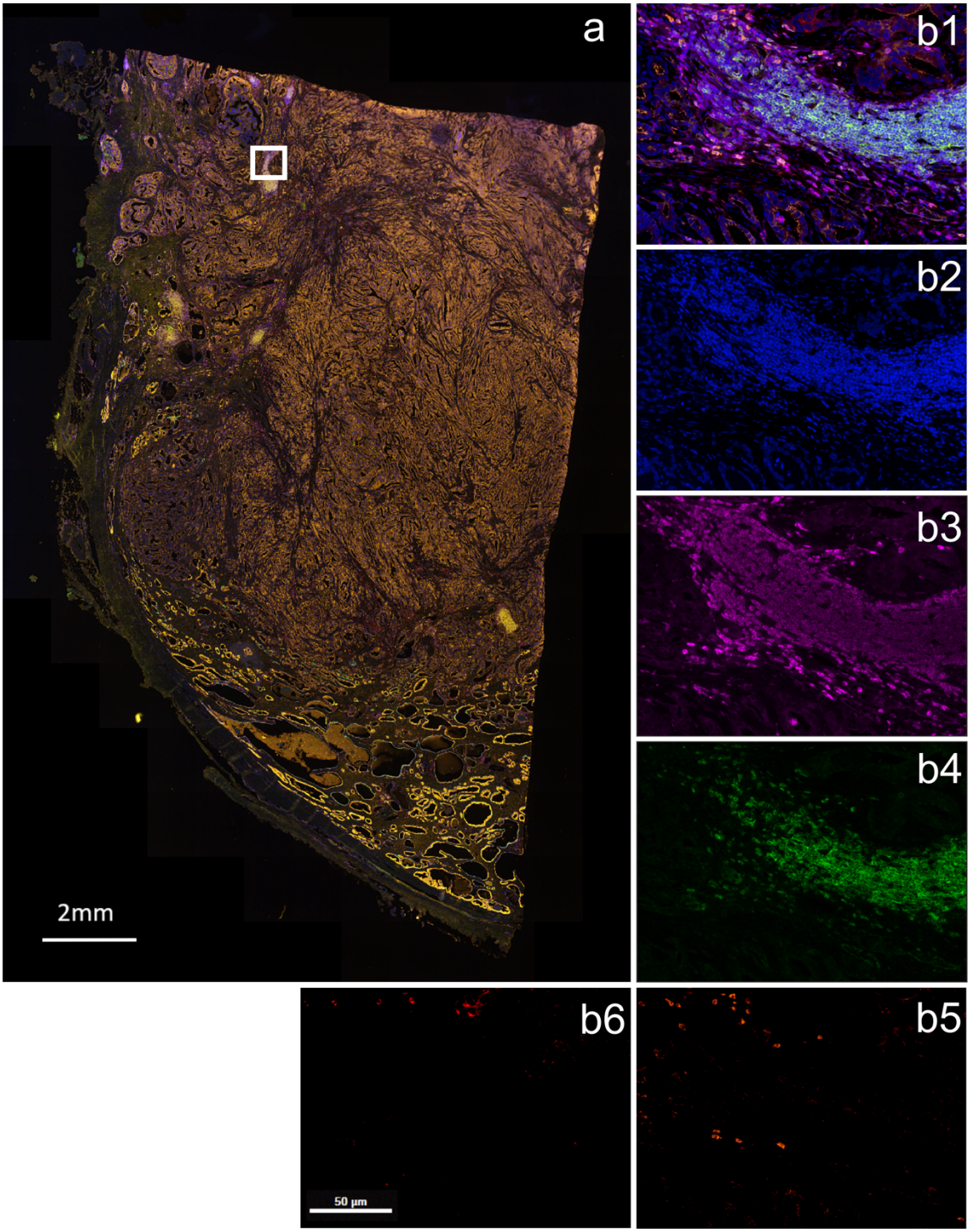


***Figure 65. Prostatectomy specimen whole slide scan and corresponding unmixed multispectral image of a portion of a BCA in prostate cancer. a)*** *Stained whole slide scan of a quarter section of patient prostatectomy tissue (taken at 10x magnification). Unmixed multispectral image of one region of interest (white box) from the whole slide scan can be seen on the right.* ***b1)*** *Merged image;* ***b2)*** *DAPI (blue);* ***b3)*** *CD45 (magenta);* ***b4)*** *CD19 (green);* ***b5)*** *CD38 (orange);* ***b6)*** *CD138 (red).*

*Both CD38 and CD138 single colour images are indicative of ASC presence surrounding the aggregate (taken at 20x magnification). Scale bar = 2mm (right), 100µm.*

Due to the abundance of BCAs seen in prostate cancer specimens, it was important to determine whether these were restricted to prostate cancer, or also present in benign and healthy prostate tissue. Investigation of 16 benign and 5 healthy H&E specimens revealed negligible number of immune cell aggregates, though many of these specimens were limited in size (core biopsies) compared with the quarter-size prostatectomy sections obtained for cancer patients. Additionally, lymphoid aggregation is a common phenomenon observed in benign conditions of the prostate.

### *3.3.4.2 TLS Panel*

TLSs were detected in 73.4% of the assessed prostate cancer tumours (n=47/64), in both proximal and distal tumour areas (**Figure 66** above). These were often mature (91.5%, n=43/47, contained scarce or abundant ASCs) (**Figure 66** below), and commonly contained abundant CD8+ T cells (93.6%, n=44/47) (**Figure 66** middle).

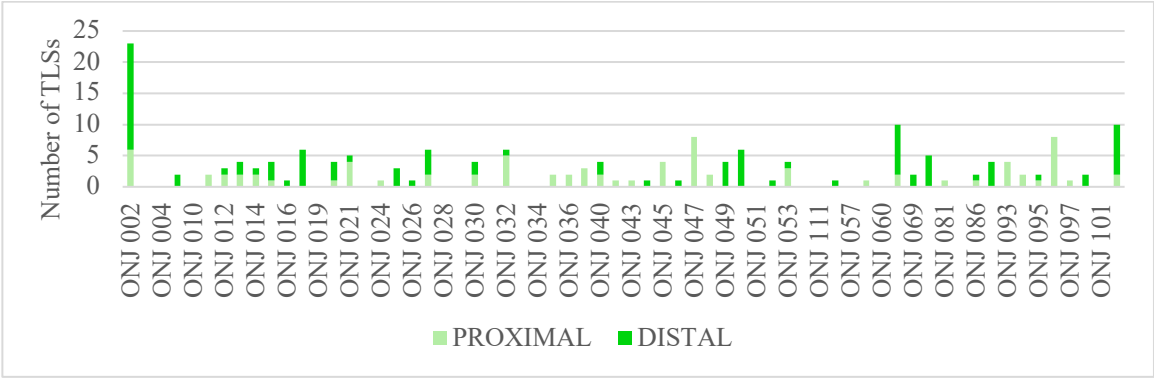


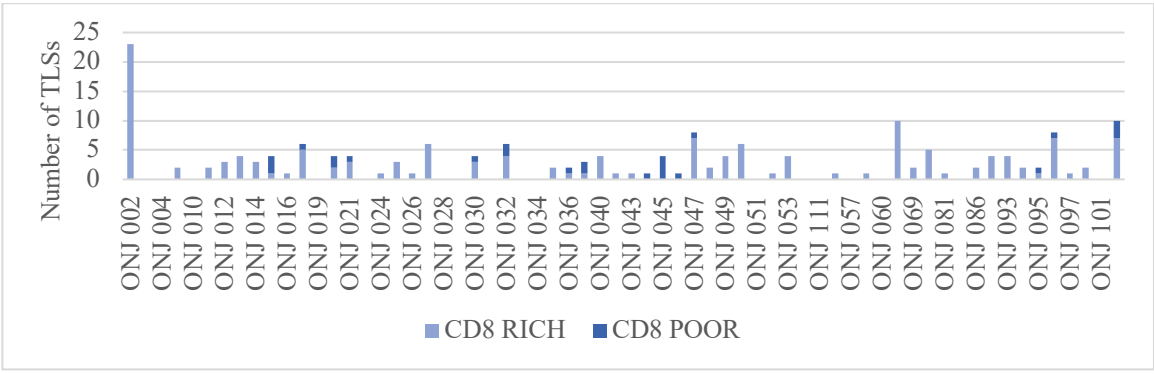

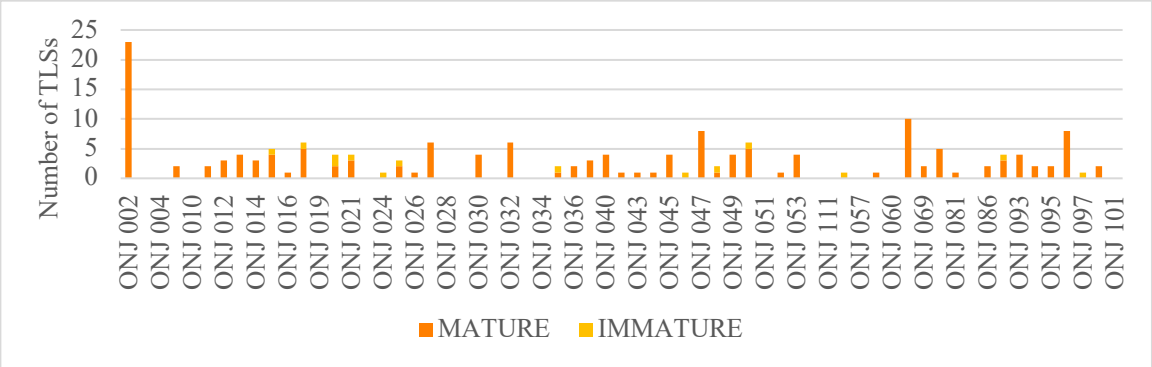


***Figure 66. Graphical representations of the abundance, location and content of TLSs identified in Prostate cancer patients.*** ***(Above)*** *The graph depicts the total TLS numbers per patient, separated by proximal and distal location.* ***(Middle)*** *The graph depicts the total TLS numbers per patient, separated by CD8 rich and CD8 poor.* ***(Below)*** *The graph depicts the total TLS numbers per patient, separated by TLS mature and TLS immature.*

Tertiary lymphoid structures were similarly distributed in patients with high- and low-grade disease (71% low-grade vs. 79% high-grade, chi-square p-value=0.1914), and in relapse and non-relapse patients (67% relapse vs. 75% non-relapse; chi-square p-value=0.2125), 2 patients lacked relapse data). In addition, mature TLSs were more abundantly seen in relapse patients (100% relapse vs. 90% non-relapse; chi-square p-value=0.0012, 2 patients lacked relapse data), while no significant differences were seen between disease grade (92% low-grade vs. 93% high-grade, chi-square p-value=0.7883) (**Figure 67**).

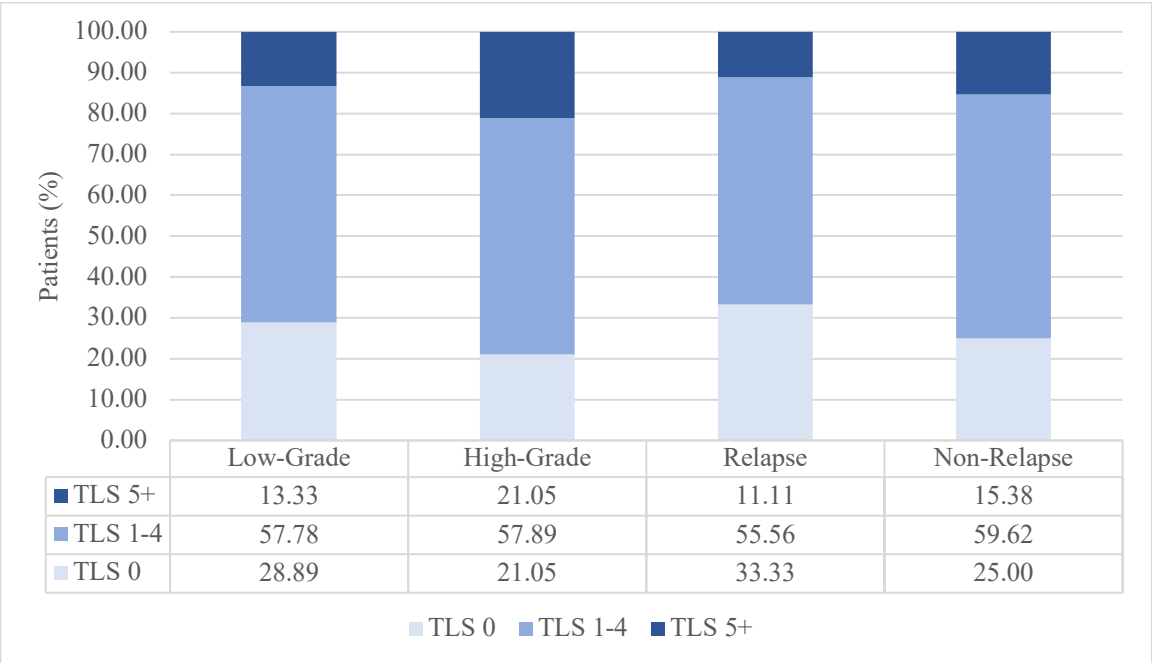


| | Low-Grade | High-Grade | Relapse | Non-Relapse |
|---|---|---|---|---|
| TLS 5+ | 13.33 | 21.05 | 11.11 | 15.38 |
| TLS 1-4 | 57.78 | 57.89 | 55.56 | 59.62 |
| TLS 0 | 28.89 | 21.05 | 33.33 | 25.00 |

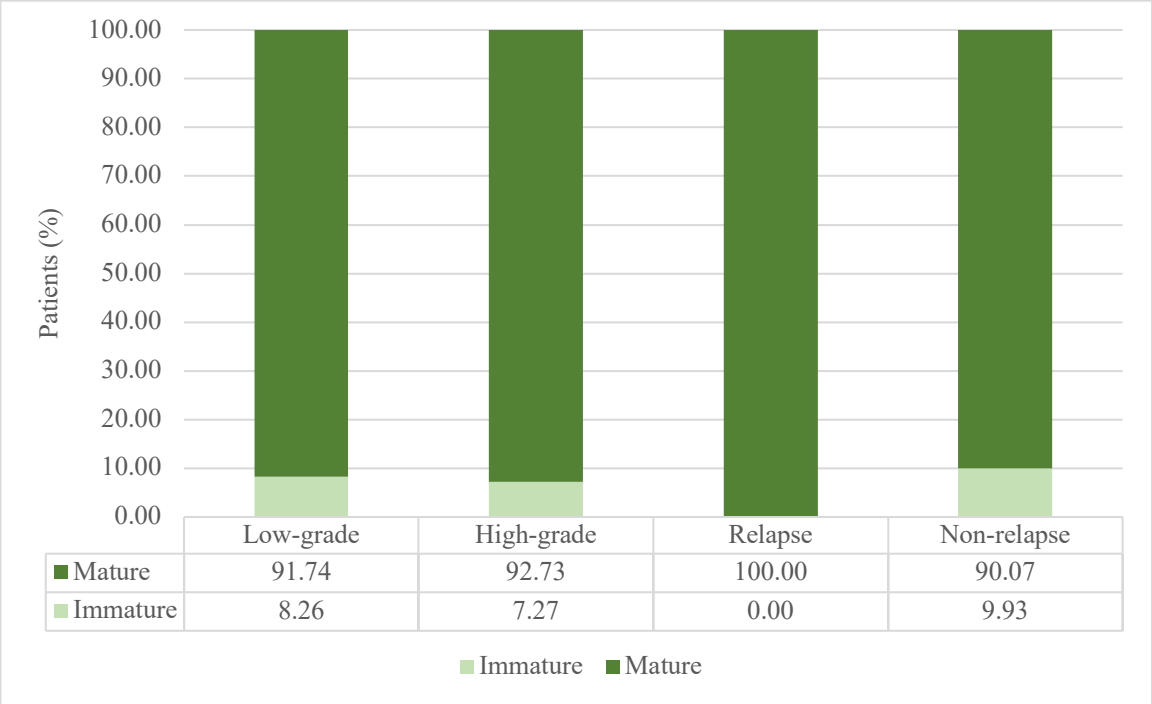


***Figure 67. Graphical representations of TLS distribution by disease grade and recurrence in prostate cancer patients. (Above)*** *The graph depicts the TLS abundance distribution in low- and high-grade patients, and in relapse and non-relapse patients. (**Below)** The graph depicts the TLS maturity distribution in low- and high-grade patients, and in relapse and non-relapse patients.*

Upon multiplexed immunohistochemical investigation of TLSs, it became apparent that unlike the typical germinal centers seen in the tonsil and lymph nodes (**Figure 58** above), differences in shape, organization, size and location were commonly seen among patients. **Figure 68** below depicts several of the various tertiary lymphoid structures that were observed in patients. Note that although differences in shape and size are observed, distinct B (outer side) and T (inner side) cell zones, follicular dendritic networks and high endothelial venules can be easily identified.

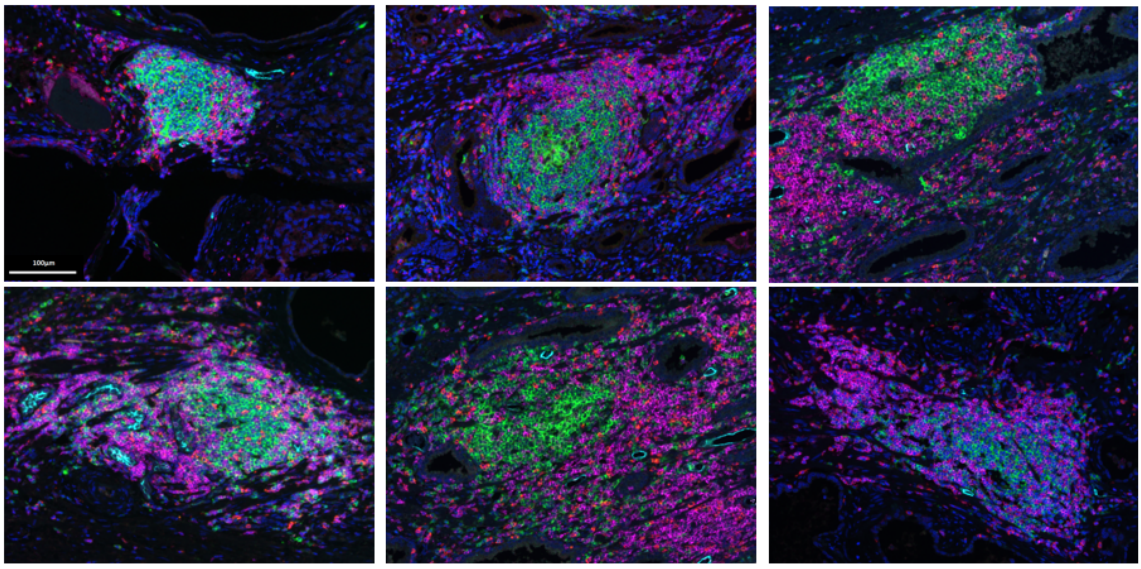

***Figure 68. Representative multispectral images of the variety of tertiary lymphoid structures seen in prostate cancer tissue.*** *TLS panel (7-plex): CD4 (CD4+ T cells, magenta), CD8 (CD8+ T cells, red), CD19 (CD19+ B cells, green), CD21 (follicular dendritic cells, brown), DC-LAMP (mature dendritic cells, orange), PNAd (high endothelial venules, cyan), DAPI (nucleus, blue). Scale bar = 100µm. Taken at 20x magnification.*

An example of how a patient specimen was stained using the multiple TLS panel of antibodies and detection fluorophores, scanned, regions of interest captured and unmixed using inform software can be seen below in **Figure 69**. The whole slide scan image can be seen on the left (**a**), with a white box surrounding the captured region of interest. The captured region of interest depicts a functional TLS and unmixing of individual fluorophores and markers can be seen on the right (**b1** – **b8**). In this particular case, no mature dendritic cells were observed (**b7**).

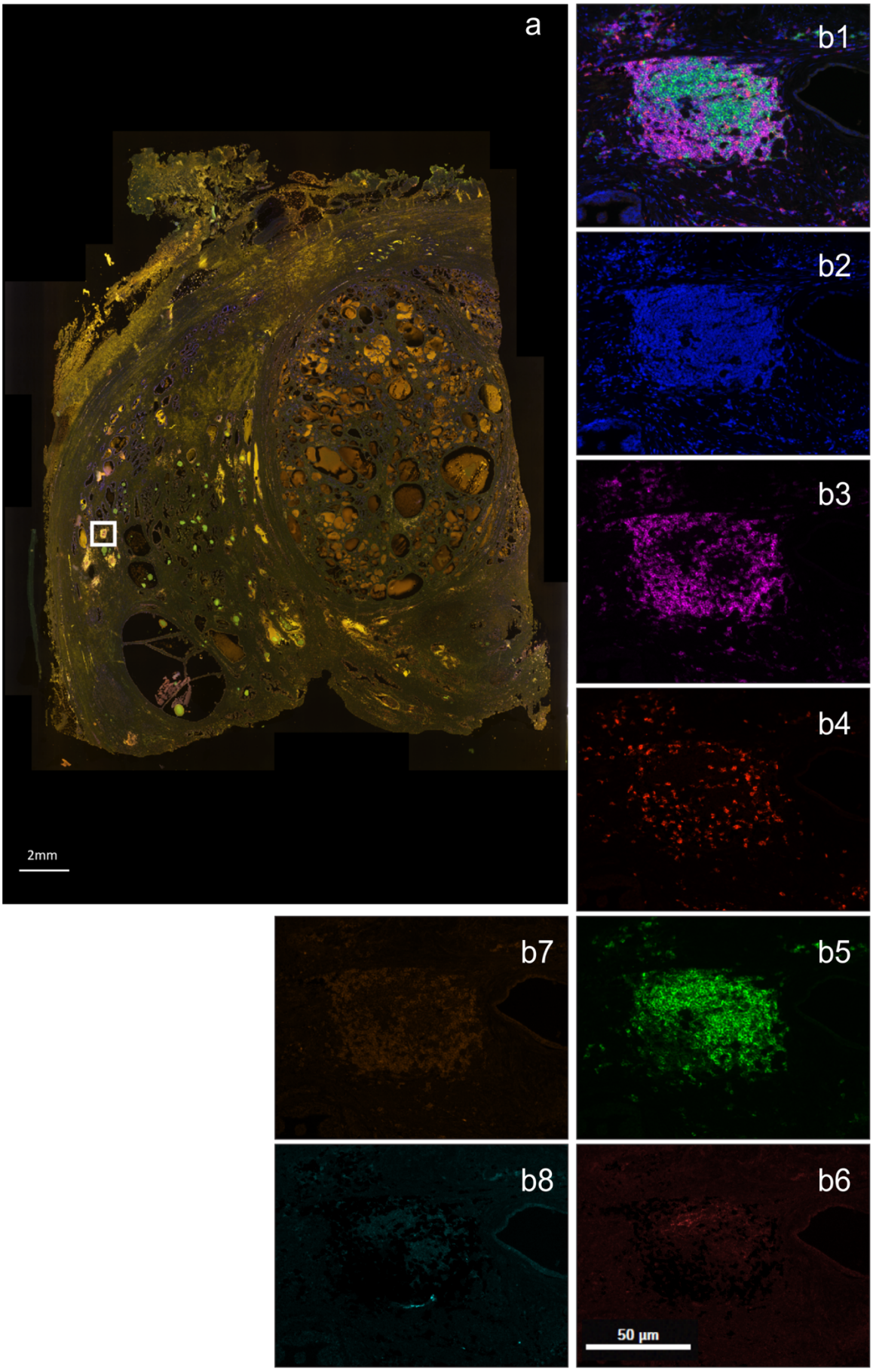


***Figure 69. Prostatectomy specimen whole slide scan and corresponding unmixed multispectral images of a functional TLS in prostate cancer. a)*** *Stained whole slide scan of a quarter section of*

*a selected patient's prostatectomy tissue taken at 10x magnification. Unmixed multispectral images of one region of interest from the whole slide scan can be seen on the right.* ***b1)*** *Merged image;* ***b2)*** *DAPI (blue); CD4 (CD4+ T cells, magenta);* ***b4)*** *CD8 (CD8+ T cells, red);* ***b5)*** *CD19 (CD19+ B cells, green);* ***b6)*** *CD21 (follicular dendritic cells, brown);* ***b7)*** *DC-LAMP (mature dendritic cells, orange);* ***b8)*** *PNAd (high endothelial venules, cyan). Taken at 20x magnification. Scale bar = 2mm (right), 100µm.*

**Figure 70** below depicts how our assumptions were correct regarding the cell phenotypes and functionality of these structures. The first stain (**above**) was the initial ASC panel, where we saw a large aggregation of b cells (green) surrounded by unknown lymphocytes (magenta). ASCs can also be seen (orange and red) exiting the structure around the periphery of the BCA. Moreover, morphologically resemblant venous-like structures could be seen inside the aggregate. The second stain (**below**) highlights that these other lymphocytes were in fact CD4+ (magenta) and CD8+ (red) T cells, and that high endothelial venules (cyan) were situated inside and surrounding the lymphoid structure as anticipated.

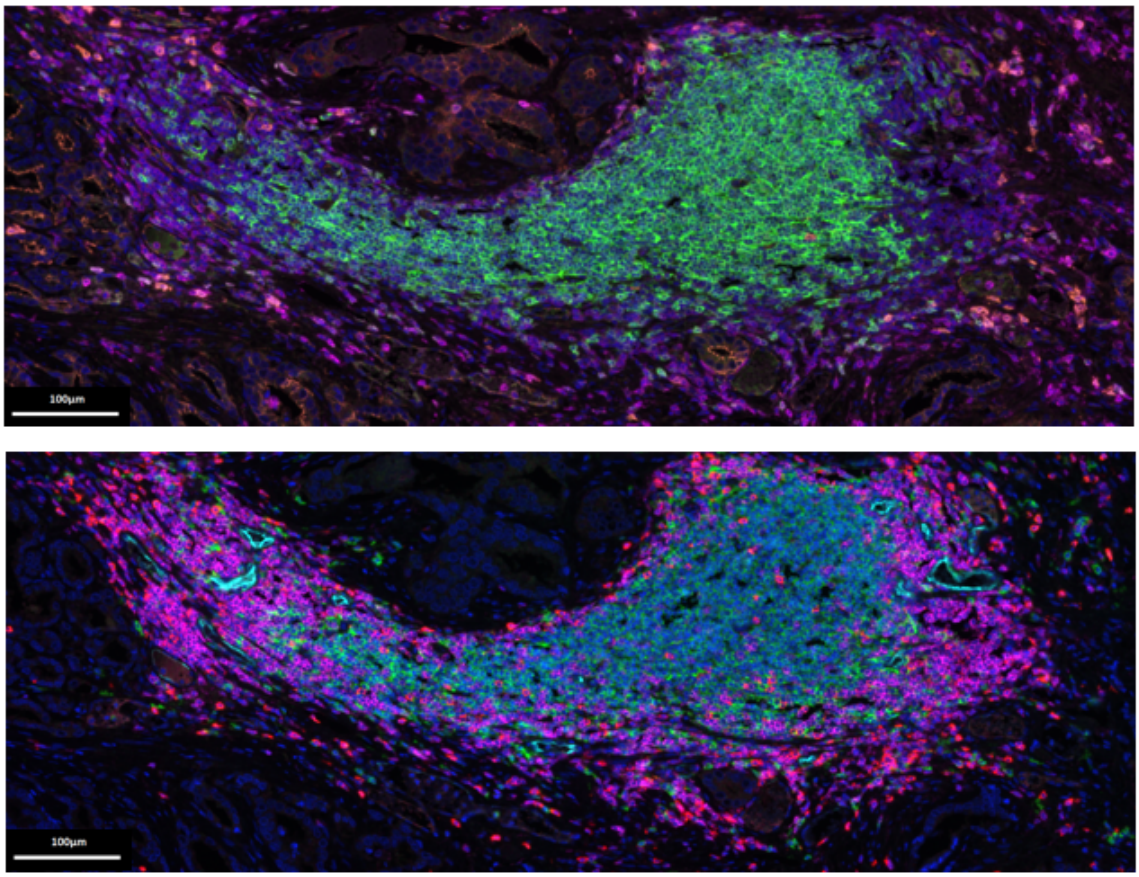


***Figure 70. Representative multispectral images of a mature tertiary lymphoid structure in prostate cancer tissue.*** **(Above)** *ASC panel (5-plex): CD45 (lymphocytes, magenta), CD19 (CD19+ B cells, green), CD38 (plasmablasts, orange), CD138 (plasma cells, red), DAPI (nucleus, blue).* ***(Below)*** *TLS panel (7-plex): CD4 (CD4+ T cells, magenta), CD8 (CD8+ T cells, red), CD19 (CD19+ B cells, green), CD21 (follicular dendritic cells, brown), DC-LAMP (mature dendritic cells, orange), PNAd (high endothelial venules, cyan), DAPI (nucleus, blue). Scale bar = 100µm. Taken at 20x magnification.*

### *3.4 Correlations between CT100+ Array and mIHC Data*

To test whether detectable autoantibodies found in patient serum correlated to the abundance of IT and PT ASCs in matched patient FFPE tissue, array and mIHC data were compared (see **Table 15** and refer to **Appendix Table A5** for more details).

***Table 15. Correlation between abundance of patient IT/PT ASCs with corresponding autoantibody profiles (patient serum).***

| | Absent | Scarce | Abundant |
|---|---|---|---|
| **Intratumoural Antibody-Secreting Cells** | | | |
| Total (n=62) | 20 | 21 | 21 |
| Avg. Antigen Specificities | 10 | 11 | 17 |
| Avg. RFU | 171 | 163 | 181 |
| **Peritumoural Antibody-Secreting Cells** | | | |
| Total (n=61) | 6 | 21 | 34 |
| Avg. Antigen Specificities | 2 | 15 | 14 |
| Avg. RFU | 112 | 197 | 171 |

*Two patients were excluded from analysis due to lack of array data (ONJ 211 / 212), and one due to lack of a PT region (ONJ 096). Abbreviations: IT, intratumoural; PT, peritumoural; ASC, antibody-secreting cell; Avg., average; RFU, relative fluorescent units.*

Average antigen specificities and intensity of detected autoantibodies was similar in patients with absent IT ASCs (average antigen specificities: 10; average RFU 171) and abundant IT ASCs (average antigen specificities: 11; average RFU 181) (Kruskal-Wallis adjusted p-value=0.9100; p-value>0.9999, respectively). Similarly, when considering the PT ASCs, no significant difference in average antigen specificities and intensities was seen between patients with absent PT ASCs (average antigen specificities: 2; average RFU 112) and those with abundant PT ASCs (average antigen specificities: 14; average RFU 171) (Kruskal-Wallis adjusted p-value=0.2199; p-value=0.4177, respectively).

To test whether detectable autoantibodies found in patient serum correlated to the abundance of IT and PT BCAs in matched patient FFPE tissue, array and mIHC data were also compared (see **Table 16** and refer to **Appendix Table A6** for more details).

***Table 16. Correlation between abundance of patient IT/PT BCAs with corresponding autoantibody profiles (patient serum).***

| | Absent | Scarce | Abundant |
|---|---|---|---|
| **Intratumoural B Cell Aggregates** | | | |
| Total (n=62) | 22 | 28 | 12 |
| Avg. Antigen Specificities | 10 | 14 | 16 |
| Avg. RFU | 164 | 181 | 167 |
| **Peritumoural B Cell Aggregates** | | | |
| Total (n=61) | 13 | 26 | 22 |
| Avg. Antigen Specificities | 10 | 12 | 17 |
| Avg. RFU | 145 | 185 | 179 |

*Two patients were excluded from analysis due to lack of array data (ONJ 211 / 212), and one due to lack of a PT region (ONJ 096). Abbreviations:*
*IT, intratumoural; PT, peritumoural; BCA, B cell aggregate; Avg., average; RFU, relative fluorescent units.*

Average antigen specificities and intensity of detected autoantibodies was not significantly different in patients with absent IT BCAs (average antigen specificities: 10; average RFU 164) and abundant IT BCAs (average antigen specificities: 16; average RFU 167) (Kruskal-Wallis adjusted p-value>0.9999; p-value>0.9999, respectively). Similarly, when considering the PT BCAs, no significant difference in average antigen specificities and intensities was seen between patients with absent PT BCAs (average antigen specificities: 10; average RFU 145) and those with abundant PT BCAs (average antigen specificities: 17; average RFU 179) (Kruskal-Wallis adjusted p-value=0.4079; p-value=0.5761, respectively).

# CHAPTER 4

# DISCUSSION

## *4.1 Tumour Antigens, B Cells and Autoantibodies*

Prostate cancer screening relies heavily on the routine measurement of PSA levels in the blood, which lack the desired sensitivity and specificity of a reliable diagnostic biomarker. This is attributed to the PSA being expressed in a healthy prostate and overexpressed in a cancerous prostate Hoffman (2011). As a result, circulating PSA levels can increase abnormally with both benign prostate conditions (e.g., benign prostatic hyperplasia) and tumourigenesis. In addition, prostate cancer patients may also present with normal PSA levels below the threshold of concern (4ng/mL) Hoffman (2011).

CT antigens have been proposed as promising tumour antigens for the detection of cancer, due to their restricted normal expression and tumour-specific overexpression across different cancer types Scanlan et al. (2002). Furthermore, several of these antigens have been reported to be expressed in prostate cancer Zaenker & Ziman (2013). These immunogenic tumour antigens can trigger an adaptive immune response, including the production of cognate autoantibodies by ASCs. Autoantibodies are detectable in the blood and have been proposed as ideal cancer biomarkers due to their ease of detection and stability Zaenker & Ziman (2013). Hence, we hypothesised that circulating autoantibodies against CT antigens could accurately detect the presence of prostate cancer and distinguish these from healthy individuals and those with benign conditions of the prostate.

## *4.2 Efficacy of Autoantibodies as Diagnostic Biomarkers*

Autoantibodies can be detected in the blood using standard ELISAs or protein microarrays depending on the required level of sensitivity and multiplexing, with protein microarrays

being highly recommended for high-throughput, sensitive and reproducible screening Duarte & Blackburn (2017). A wide range of protein microarray platforms are commercially available, but these include both self and tumour antigens, proving problematic in the search for diagnostic cancer biomarkers Chandra et al (2011). In this study, we used a novel cancer-specific protein microarray platform (CT100+ array) containing over 100 CT antigens and other tumour-associated antigens that was developed in-house Beeton-Kempen et al. (2014). The unique antigen cloning method and streptavidin-biotin surface chemistry of the array ensures that only full-length correctly folded antigens devoid of post-translational modifications or unfolding are bound to the array. This provides a platform that not only eliminates non-specific binding of other proteins present in the blood, but also ensures that circulating autoantibodies are binding to mainly discontinuous epitopes normally accessible *in vivo* with high sensitivity (pg/mL range) Beeton-Kempen et al. (2014).

Patient sera from 110 prostate cancer patients (discovery cohort) were retrospectively screened using the CT100+ array. Autoantibody signals were detected above threshold in 78.2% of patients. Of note, detectable autoantibodies were seen in patients with normal PSA levels, overcoming one of the current issues with prostate cancer diagnostics. When considering disease grade, patients with low-grade disease had on average a higher number of antigen specificities (n=13), when compared to high-grade of disease (n=7). The most prevalent antigen specificities included mainly CT antigens: MAGEB1 (63.6%), MAGEB6 (56.4%), MAGEB5 (51.8%), GAGE4 (28.2%), GAGE1 (27.3%), GAGE5 (24.5%), OIP5 (23.6%), SPANXC (22.7%), CT47.11 (2.10%), LEMD1 (20.1%), MAGEA2 (20.0%), MAGEA4v4 (20.0%) and MAGEA1 (19.1%); as well as other tumour associated antigens: CTNNB1 (25.5%), MAPK3 (20.1%) and GRWD1 (20.0%). Further validation was conducted by screening patient sera from an additional 99 prostate cancer patients (validation cohort) using the CT100+ array. Autoantibody signals were detected above threshold in 59.6% of patients, where a noticeable decrease could be explained by

differences in ethnic distributions among cohorts (cannot be more specifically alluded to due to lack of ethnic clinical data for the validation cohort). The most prevalent antigen specificities included mainly CT antigens: MAGEB1 (37.4%), GAGE1 (33.3%), MAGEB6 (33.3%), MAGEA1 (32.3%), MAGEA5 (30.3%), MAGEA2 (29.3%), CT47.11 (28.3%), MAGEA4v4 (25.3%), SPANXC (24.2%), GAGE4 (23.2%), NY-ESO-1 (22.2%), GAGE5 (22.2%), and OIP5 (22.2%); as well as other tumour associated antigens: CTNNB1 (34.3%), MAPK3 (25.3%) and GRWD1 (28.3%). Significant overlap was observed between prevalent antigens from both cohorts (14/16 of antigens), strengthening the initial data produced during discovery.

The preliminary study conducted by Adeola *et al.* using an earlier version of the CT100+ array determined a total of 41 potential antigen biomarkers for prostate cancer. In particular, four antigens, GAGE1, ROPN1, SPANXA1 and PRKCZ displayed higher autoantibody titres in prostate cancer patient serum when compared to benign prostate hyperplasia and healthy controls Adeola et al. (2016). When comparing these two studies, although unique antigens were identified, GAGE and SPANX CT antigen families were consistently detected in both cohorts. Observed differences in results may speculatively relate to differences in ethnicity and the corresponding associated genomic drivers of prostate cancer. Adeola *et al.*'s cohort consisted largely of patients with black ancestry (Indigenous African/Mixed-Ancestry, 70.0%), in contrast to our discovery cohort comprising largely of patients of European decent (82.7%), where the remaining patients (17.3%) were either unknown or undefined.

A study performed by Xie *et al*. used ELISA and novel seroMAP-based microspheres to detect autoantibodies in prostate cancer serum against specific CT antigens (NY-ESO-1, XAGE-1b, SSX-2, 4), as well as other tumour-associated (TA) antigens (AMACR, p90 autoantigen, and LEDGF), while simultaneously quantifying total PSA ('A+PSA assay') Xie et al. (2011). This assay led to a significant increase in diagnostic sensitivity and

specificity, with AUC values increasing from 0.66 with PSA alone to 0.91 (sensitivity 79%, specificity 84%) for the 'A+PSA assay' Xie et al. (2011).

Similarly, we investigated the diagnostic capability of combinations of our most prevalent or best discriminatory CT and TA antigen specificities identified in the discovery cohort when compared to healthy individuals (MAGEA1, OIP5, CTNNB1, SPANXC, CAMEL, LAGE1b and ROPN1A). We were able to confirm that combining CT antigens with matching patient PSA levels does increase the sensitivity and specificity of prostate cancer detection. An antigen signature including CAMEL, ROPN1A, CTNNB1, and SPANXC resulted in an AUC of 0.847 (sensitivity 90%, specificity 64%). When combining these antigens with PSA levels, the AUC value was improved to 0.959 (sensitivity 89%, specificity 93%). Evaluation of this antigen signature in the validation cohort yielded comparable results, with an AUC of 0.752 (sensitivity 50%, specificity 100%) without PSA, and 0.968 (sensitivity 97%, specificity 88%) with PSA. Although we see an inversion in sensitivity and specificity between the discovery and validation cohorts without PSA inclusion, this is overcome with the addition of PSA. Furthermore, in both instances, our data outperforms the maximum 'A+PSA' AUC achieved in the Xie et al. study.

Following acquisition of benign samples during the validation phase, we further investigated the diagnostic capability of combinations of our most prevalent or best discriminatory CT and TA antigen specificities identified in the discovery cohort when compared to healthy individuals and benign controls. An antigen signature including ACVR2B, CALM1, CAMEL, CEP290, CT47.11, MART-1 and PRKCZ yielded an AUC of 0.769 (sensitivity 78%, specificity 73%). Evaluation of this antigen signature in the validation cohort yielded similar results, with AUC of 0.788 (sensitivity 67%, specificity 79%), verifying its robustness at distinguishing these patient groups. Unfortunately, we were unable to complement this combination with PSA levels, as these were not accessible for benign samples.

Our findings for PSA levels at a cut-off of 4ng/mL resulted in a sensitivity and specificity of 85% and 79%, respectively, for the discovery cohort and 85% and 79%, respectively, for the validation cohort. It is necessary to disclose that PSA levels for all prostate cancer patients were determined at or near time of prostate resection, after the presence of prostate cancer had been histologically confirmed. This factor, in conjunction with our small-sized healthy donor cohort, abnormally bolsters the diagnostic capability of PSA levels alone in our cohorts in such a way that would not reflect the clinical reality. Unfortunately, age- and gender-matched healthy donor samples were difficult to obtain, but it would be critical for any subsequent external validation study based upon this research to include more of these samples. The clinical reality of PSA levels as a diagnostic biomarker at a cut-off of 4ng/ml has been detailed in a well-known meta-study conducted by Wolf *et al.* where its sensitivity and specificity were reported as 21% and 91%, respectively. In addition, its sensitivity was purported to be 51% for high-grade cancer (i.e., GS ≥8) Wolf et al (2010). Though our corresponding patient PSA values were inadvertently biased in nature, the clinical reality of PSA as a diagnostic marker (ROC AUC ~0.7000) still suggests that unbiased PSA results would, in theory, improve upon any antigen combinations determined in this study.

Although it is known that gene or mRNA expression does not necessarily always translate to protein expression, our most promising diagnostic antigen specificities able to distinguish prostate cancer from healthy individuals or healthy and benign individuals were investigated for mRNA expression using an external prostate cancer patient cohort accessible via the TCGA (n=460). In all instances, mRNA expression of the identified CT antigens (MAGEA1 (20%), OIP5 (100%), CAMEL/LAGE1b (i.e., CTAG2, 30%), ROPN1A (i.e., ROPN1, 99%), MART-1 (i.e., MLANA 82%) and non-CT (CTNNB1 (100%), ACVR2B (100%), CALM1 (100%), CEP290 (100%) and PRKCZ (100%)) was confirmed in an independent prostate cancer cohort, and fairly consistent with the autoantibody predominance seen. Heninger *et al.* further reported MAGEA1(n=3/4)) and

CAMEL/LAGE1b (n=1/4) inducible mRNA expression in prostate cancer cell lines Heninger et al. (2016).

Protein expression of our identified, potentially diagnostic antigens was investigated in a further external prostate cancer cohort accessible via the Human Protein Atlas database and confirmed for ACVR2B (n=1/11), CAMEL/LAGE1b (CTAG2, n=3/11), CEP290 (n=11/12), CTNNB1 (n=9/9), and PRKCZ (n=8/12).

To assess whether clinical cohort characteristics may impact patient autoantibody profiles, categories such as age, PSA levels, Gleason scores, and PSA relapse were correlated with antigen specificities. Similar average antigen counts were observed for all age groups in the discovery, validation and combined cohort data. Similar average antigen counts were observed when evaluating Gleason score categories in the discovery and combined cohort data. However, significantly higher average antigen counts were seen in high-grade patients in the validation cohort. Moreover, although no differences were observed when correlating PSA ranges with average antigen counts in the discovery or validation cohort data, a significant increase in average antigen counts was seen for patients exhibiting PSA levels >12ng/mL for the combined cohort. No significant differences in average antigen counts were observed between relapse and non-relapse patients in the discovery, validation and combined cohort data.

### *4.3 Efficacy of Autoantibodies as Prognostic Biomarkers*

Acquisition of comprehensive clinical cohort characteristics and follow-up for all patients screened from the discovery cohort allowed us to assess the prognostic potential of CT100+ array antigens. In particular, we assessed the presence or absence of autoantibodies towards cognate antigens in relation to biochemical relapse and survival data. We investigated the prognostic capability of combinations of our most prevalent or best discriminatory antigen

specificities identified in the discovery cohort when comparing relapse and non-relapse patients. An antigen signature including BAGE5, CAMEL (CTAG2), MART-1 and RAF yielded an AUC of 0.682 (sensitivity 50%, specificity 82%) without PSA, and an AUC of 0.704 (sensitivity 94%, specificity 45%) with PSA.

When considering overall survival with long-term follow-up, an antigen signature containing ACVR2B, BAGE5, and MAP9 generated an AUC of 0.848 (sensitivity 86%, specificity 76%) without PSA, and an AUC of 0.827 (sensitivity 88%, specificity 75%) with PSA. Interestingly, BAGE5 was identified as a prognostic biomarker with regards to both disease relapse and overall survival.

Although the addition of PSA provided incremental increases to most of the above AUC values and antigen combinations, this is not the case for the survivability panel. Although PSA levels are known to correlate with more aggressive disease and poorer outcomes Lojanapiwat et al (2014), the majority of patients in our cohort have undergone therapeutic intervention(s), including radical prostatectomy and/or systemic therapy at diagnosis or relapse which may alter the natural course of the disease and thereby affect these data.

Publicly available (TCGA) mRNA data from 460 prostate cancer patients showed common expression of the identified prognostic genes, where non-CT antigens; RAF (RAF1, 100%), ACVR2B (100%), and MAP9 (100%), and CT antigens; CAMEL/LAGE1b (CTAG2, 17%), and MART-1 (MLANA, 82%) exhibited low to high mRNA expression across the majority of the cohort. Heninger *et al*. consistently reported high mRNA expression of LAGE1 (CAMEL/LAGE1b) in 1 of 4 prostate cancer cell lines Heninger et al. (2016).

Protein expression data was collated from the Human Protein Atlas database, where immunohistochemical staining revealed positive expression of CAMEL (CTAG2, n=3/11), RAF (RAF1, n=12/12), and ACVR2B (n=1/11) in prostate cancer tissue specimens. Conversely, no protein expression was seen for MART-1 (MLANA, n=0/12). Notably, of

our prognostic biomarkers determined, CAMEL (i.e., CTAG2) was found to be an unfavourable prognostic biomarker in renal cancer. Moreover, it may hold potential value as a novel unfavourable prognostic biomarker in prostate cancer, as expression of CTAG2 was more commonly detected in prostate cancer patients that relapsed in contrast to those that didn't. Furthermore, studies have suggested that protein expression of RAF was associated with biochemical relapse in prostate cancers Mukherjee et al (2005); Mukherjee et al (2011). Similarly, elevated serum levels of Activin A (related to ACVR2B) have been implicated in the pathogenesis of bone metastasis in prostate cancer, and may serve as a marker of relapse Leto et al (2006).

### *4.4 Efficacy of Autoantibodies as Biomarkers for Disease Stratification*

Biomarkers of disease stratification enable the ability to determine at diagnosis if patients have low-grade (Gleason Score 6-7) or high-grade (Gleason Score 8-10) disease. This may enable informed patient management and therapeutic planning for patients with aggressive disease. We investigated the disease stratification capability of the antigen specificities identified in the discovery cohort when comparing low- and high-grade prostate cancer patients. An antigen signature including GAGE5, MICA, SSX4 generated an AUC of 0.937 (sensitivity 96%, specificity 79%) without PSA, and an AUC of 0.953 (sensitivity 93%, specificity 89%) with PSA. These findings were verified using the validation cohort, with the antigen signature resulting in an AUC of 0.731 (sensitivity 80%, specificity 55%) without PSA, and an AUC of 0.871 (sensitivity 72%, specificity 88%) with PSA.

Publicly available mRNA data from 460 prostate cancer patients (TCGA) confirmed expression of MICA (100%) and SSX4 (6%) in prostate cancer. In regard to protein expression (The Human Protein Atlas), no protein expression was seen for SSX4 (n=0/11) in prostate cancer tissue, while MICA was reported as an unfavourable prognostic marker

in cervical cancer. Similarly, soluble levels of MICA have been previously reported as prognostic in prostate cancer Liu et al (2018).

### *4.5 B Cell Infiltrate, ASCs and TLSs in Prostate Cancer*

We investigated the immune landscape of prostate cancer using prostatectomy tissue from 64 of the above patients (discovery cohort), with a specific focus on the abundance of IT and PT ASCs ($CD19^{+}CD38^{+}CD138^{-}$ plasmablasts and $CD19^{low/-}CD38^{high}CD138^{+}$ plasma cells). A novel customised mIHC ASC panel was specifically optimised and utilised to achieve this. A lymphocyte marker ($CD45^{+}$) was also included to determine the presence of other immune cells that may be present. Although B cell infiltrates using the pan-B cell CD20 marker have been identified in the TME of prostate cancer Flammiger et al. (2012); Fujii et al. (2013); Woo et al. (2014), to date studies are yet to adequately characterise ASCs in these tumours. The use of pan-B cell markers (CD19 or CD20) do not enable the distinction between B cell subsets, and fail to identify ASCs that lose CD19/CD20 upon terminal differentiation Da Gama Duarte et al. (2018a). As such, this study is one of the first of its kind investigating ASC infiltrates in prostate cancer.

ASCs and other immune cells were commonly detected in the investigated prostate cancer tumours. Notably, $CD19^{+}$ BCAs were also commonly seen, and therefore included in subsequent analyses.

ASCs and BCAs were more commonly detected in PT regions, when compared to IT regions. With regards to disease grade, IT and PT ASCs and BCAs were more abundant in high-grade disease, when compared to low-grade disease. Moreover, the majority of relapse patients contained abundant IT ASCs and BCAs, when compared to those that did not relapse, while no difference was seen in PT regions.

Following investigation of ASCs in prostate cancer specimens, abundantly detected BCAs with surrounding ASCs and adjacent zones of unspecified lymphocytes that resembled TLSs led us to explore these tissue specimens further. A novel customised mIHC TLS panel was specifically optimised and utilised to achieve this. The panel consisted of core (CD4, CD8, CD19, and PNAd) and additional antibody markers (CD21 and DC-LAMP) defined in the literature to define 'functional / mature' TLSs (i.e., able to produce plasmablasts and plasma cells). By staining serial sections (i.e., cuts/slices that are sequential to those previously stained with the ASC panel) of each patient prostatectomy section, we were able to compare both panels to identify functional TLSs.

Regarding TLS abundance, the majority of patient samples had at least one TLS, with no significant difference observed between proximal and distal tumour locations. Nearly all TLSs were mature and contained abundant CD8+ T cells. Additionally, mature TLSs were more abundantly seen in relapse patients, while no significant differences were seen between disease grades.

Together, these findings argue for a pro-tumoural B cell role in prostate cancer. The anti- or -pro-tumoural role of ASCs depends on the antibodies being produced, with IgG1 and IgG3 being anti-tumoural, and IgG2 and IgG4 being pro-tumoural Saul et al (2016). These IgG ratios are heavily influenced by the TME, with regulatory immune cells promoting pro-tumoural ASC functions Da Gama Duarte et al. (2018b). Functional characterisation of the IgG repertoire and the regulatory immune cell subsets in the TME is required to further determine what roles the B cell subsets may have in prostate cancer.

### *4.6 Autoantibodies in Circulation and B cells in the TME*

We further hypothesised that the non-invasive autoantibody profiling of cognate tumour antigens using blood may reflect the immune landscape of the prostate cancer TME. Hence,

the presence of detectable autoantibodies towards tumour antigens was correlated with IT ASCs, where applicable. However, we found no significant differences when comparing IT or PT ASCs or BCAs with corresponding autoantibody profiles. However, less antigen specificities were observed in patients without PT ASCs, when compared to those with PT ASCs, albeit not statistically significant.

The absence of expected IT ASCs in the TME despite the presence of detectable antigen specificities in circulation may be explained by 1) ASCs actively producing autoantibodies in circulation, without the need to be physically located in the TME; or 2) sectioned tissue slides not being representative of the complete prostate specimens which may have detectable ASCs. On the other hand, the absence of expected abundant autoantibodies against tumour antigens in circulation despite the presence of abundant IT ASCs in the TME may be explained by 1) abundant non-tumoural ASCs located in the TME associated with inflammatory disease, such as BPH; or 2) missing tumour antigens on the CT100+ array that are of relevance to prostate cancer.

In summary, trends deduced from the preliminary findings suggest that detectable autoantibody profiles may be indicative of PT ASCs in the TME of prostate cancer patients, warranting further studies. A more comprehensive characterisation of the TME is necessary to fully investigate this hypothesis, including other stimulatory and regulatory immune cells which may be of correlative value.

## APPENDIX

***Table A1. List of primary antibodies and reagents used for mIHC.***

| **Primary Antibodies (ASC Panel)** | | |
|---|---|---|
| **Target** | **Company** | **Cat#** |
| CD19 | Abcam | ab134114 |
| CD38 | Abcam | ab108403 |
| CD45 | Dako | M0701 |
| CD138 | Novus | NB100-64980 |
| **Primary Antibodies (TLS Panel)** | | |
| CD4 | Abcam | ab133616 |
| CD8 | Invitrogen | MA5-13473 |
| CD19 | Abcam | ab134114 |
| CD21 | Agilent | M0784 |
| DC-LAMP | Dako | ab111090 |
| PNAd | Novus | NB100-77673 |
| **Secondary Antibodies** | | |
| **Fluorophore** | **Company** | **Cat#** |
| Opal 520 | Perkin Elmer | FP1487A |
| Opal 570 | Perkin Elmer | FP1488A |
| Opal 620 | Perkin Elmer | FP1495A |
| Opal 690 | Perkin Elmer | FP1497A |
| Spectral DAPI | Perkin Elmer | FP1490 |
| **Other Reagents** | | |
| Antibody Diluent / Block | Perkin Elmer | ARD1001EA |
| Opal Polymer HRP Ms +Rb | Perkin Elmer | ARH1001EA |
| 1xPlus Automation Amplification Diluent | Perkin Elmer | FP1609 |

| | | |
|---|---|---|
| Dimethyl Sulfoxide | Perkin Elmer | DMSO0500UL |
| **IHC Kits** | | |
| Opal 7-Colour Automation IHC Kit 50 Slides | Perkin Elmer | NEL821001KT |

***Table A2. Table of all multiplex stain orders that were trialled during optimisation***

| **Primary Antibody** | **Epitope Retrieval (pH)** | **Optimised Concentration** | **Opal Fluorophore** |
|---|---|---|---|
| **ASC Multiplex Stain Order 1:** | | | |
| CD138 | ER 9 | 1:100 | 520 |
| CD38 | ER 9 | 1:300 | 620 |
| CD19 | ER 9 | 1:300 | 570 |
| CD45 | ER 9 | 1:100 | 690 |
| DAPI | - | 2 drops per mL | - |
| **ASC Multiplex Stain Order 2:** | | | |
| CD19 | ER 9 | 1:300 | 570 |
| CD138 | ER 9 | 1:100 | 520 |
| CD38 | ER 9 | 1:300 | 620 |
| CD45 | ER 9 | 1:100 | 690 |
| DAPI | - | 2 drops per mL | - |
| **ASC Multiplex Stain Order 3:** | | | |
| CD45 | ER 9 | 1:100 | 690 |
| CD138 | ER 9 | 1:100 | 520 |
| CD38 | ER 9 | 1:300 | 620 |
| CD19 | ER 9 | 1:300 | 570 |
| DAPI | - | 2 drops per mL | - |

| | | | |
|---|---|---|---|
| **TLS Multiplex Stain Order 1:** | | | |
| CD4 | ER 9 | 1:1000 | 520 |
| CD21 | ER 9 | 1:20 | 540 |
| CD8 | ER 9 | 1:50 | 570 |
| DC-LAMP | ER 6 | 1:100 | 620 |
| PNAd | ER 9 | 1:100 | 650 |
| CD19 | ER 9 | 1:300 | 690 |
| DAPI | - | 2 drops per mL | - |
| **ASC Multiplex Stain Order 2:** | | | |
| CD21 | ER 9 | 1:20 | 520 |
| DC-LAMP | ER 6 | 1:100 | 540 |
| CD4 | ER 9 | 1:1000 | 570 |
| PNAd | ER 9 | 1:100 | 620 |
| CD8 | ER 9 | 1:50 | 650 |
| CD19 | ER 9 | 1:300 | 690 |
| DAPI | - | 2 drops per mL | - |

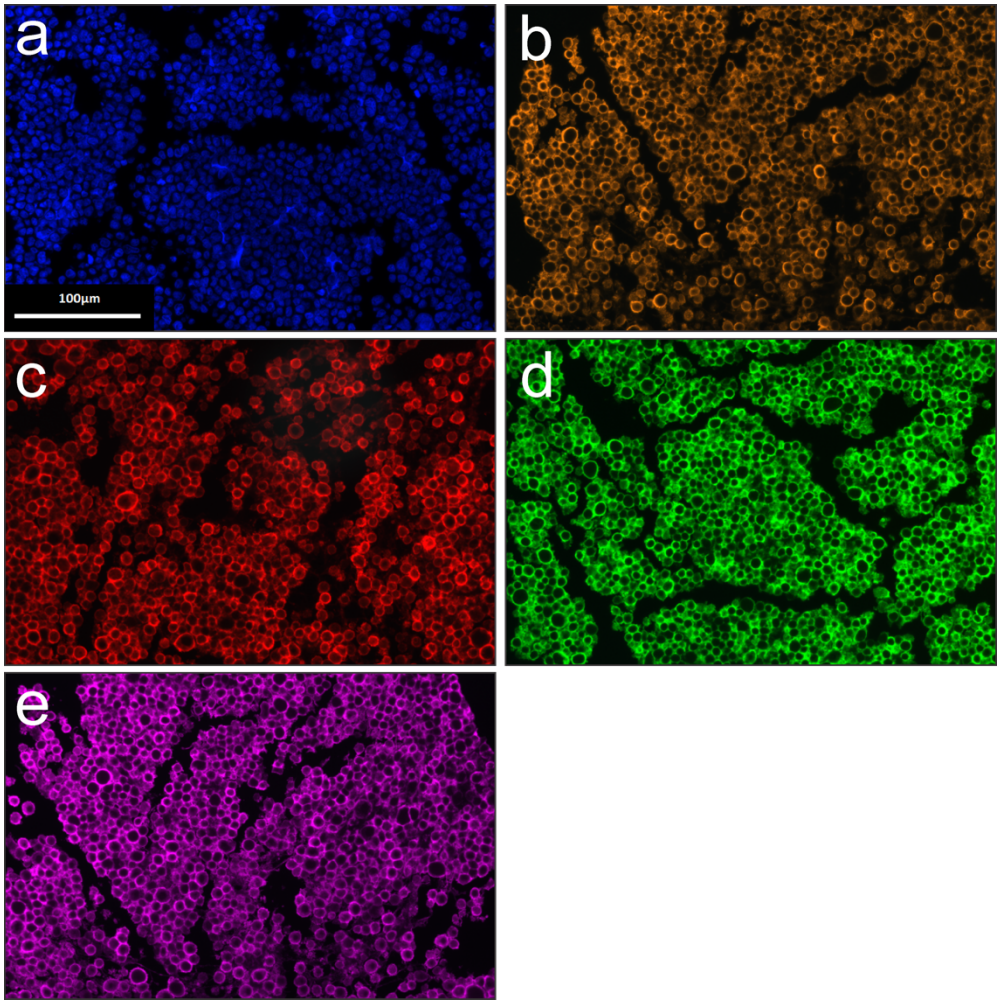


***Figure A1. ASC spectral library (Unmixed MSIs). a)*** *DAPI – HLA1+ HeLa cell line (blue).* ***b)*** *Opal 620 – HLA1+ HeLa cell line (orange).* ***c)*** *Opal 520 – HLA1+ HeLa cell line (red).* ***d)*** *Opal 570 – HLA1+ HeLa cell line (green).* ***e)*** *Opal 690 – HLA1+ HeLa cell line (magenta). Scale bar = 100µm. Taken at 20x magnification.*

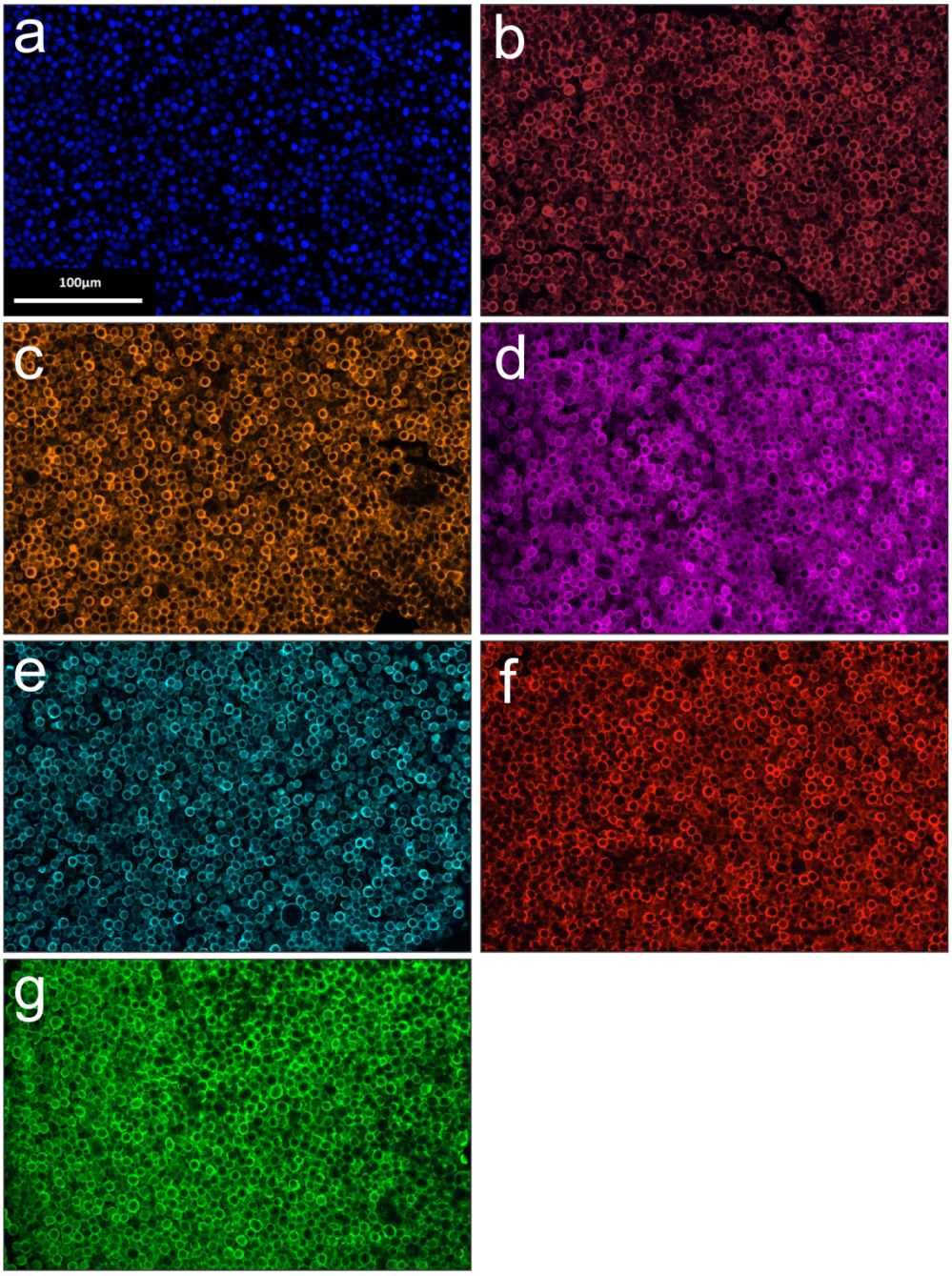


***Figure A2. TLS spectral library (unmixed MSIs). a)*** *DAPI – HLA+ HeLa cell line (blue).* ***b)*** *Opal 520 – HLA1+ HeLa cell line (brown).* ***c)*** *Opal 540 – HLA1+ HeLa cell line (orange).* ***d)*** *Opal 570 – HLA1+ HeLa cell line (magenta).* ***e)*** *Opal 620 – HLA1+ HeLa cell line (cyan).* ***f)*** *Opal 650 – HLA1+ HeLa cell line (red).* ***g)*** *Opal 690 – HLA1+ HeLa cell line (green). Scale bar = 100µm. Taken at 20x magnification.*

***Table A3. Abundance of ASCs and BCAs detected in prostate cancer tissue using mIHC.***

| Patient ID | Abundance of IT ASCs | Abundance of PT ASCs | Abundance of IT BCAs | Abundance of PT BCAs |
|---|---|---|---|---|
| ONJ 002 | Scarce | Abundant | Scarce | Abundant |
| ONJ 003 | Scarce | Abundant | Absent | Scarce |
| ONJ 004 | Absent | Absent | Scarce | Absent |
| ONJ 009 | Absent | Abundant | Absent | Abundant |
| ONJ 010 | Absent | Abundant | Absent | Scarce |
| ONJ 011 | Scarce | Abundant | Absent | Scarce |
| ONJ 012 | Abundant | Abundant | Scarce | Scarce |
| ONJ 013 | Scarce | Scarce | Absent | Scarce |
| ONJ 014 | Abundant | Abundant | Absent | Abundant |
| ONJ 015 | Absent | Scarce | Scarce | Scarce |
| ONJ 016 | Abundant | Abundant | Absent | Abundant |
| ONJ 018 | Absent | Abundant | Absent | Abundant |
| ONJ 019 | Abundant | Absent | Scarce | Absent |
| ONJ 020 | Absent | Abundant | Scarce | Scarce |
| ONJ 021 | Abundant | Abundant | Scarce | Scarce |
| ONJ 022 | Scarce | Scarce | Absent | Absent |
| ONJ 024 | Abundant | Scarce | Scarce | Absent |
| ONJ 025 | Scarce | Abundant | Scarce | Abundant |
| ONJ 026 | Scarce | Scarce | Scarce | Scarce |
| ONJ 027 | Abundant | Abundant | Scarce | Abundant |
| ONJ 028 | Absent | Scarce | Scarce | Scarce |
| ONJ 029 | Absent | Scarce | Absent | Scarce |
| ONJ 030 | Abundant | Abundant | Scarce | Scarce |
| ONJ 031 | Absent | Absent | Absent | Absent |
| ONJ 032 | Scarce | Abundant | Absent | Abundant |
| ONJ 033 | Absent | Absent | Scarce | Scarce |
| ONJ 034 | Abundant | Scarce | Scarce | Absent |
| ONJ 035 | Abundant | Abundant | Abundant | Scarce |
| ONJ 036 | Abundant | Scarce | Scarce | Absent |
| ONJ 037 | Scarce | Absent | Abundant | Scarce |
| ONJ 040 | Scarce | Abundant | Scarce | Abundant |
| ONJ 041 | Absent | Scarce | Absent | Scarce |
| ONJ 043 | Absent | Abundant | Absent | Abundant |
| ONJ 044 | Scarce | Scarce | Scarce | Scarce |
| ONJ 045 | Abundant | Scarce | Abundant | Absent |
| ONJ 046 | Scarce | Scarce | Absent | Scarce |
| ONJ 047 | Abundant | Abundant | Abundant | Scarce |
| ONJ 048 | Absent | Scarce | Scarce | Scarce |
| ONJ 049 | Absent | Scarce | Absent | Abundant |
| ONJ 050 | Absent | Abundant | Absent | Abundant |
| ONJ 051 | Scarce | Abundant | Absent | Absent |
| ONJ 052 | Scarce | Abundant | Scarce | Abundant |
| ONJ 053 | Abundant | Abundant | Scarce | Scarce |
| ONJ 054 | Absent | Abundant | Absent | Scarce |
| ONJ 055 | Absent | Scarce | Scarce | Scarce |
| ONJ 057 | Absent | Abundant | Absent | Absent |

| | | | | |
|---|---|---|---|---|
| ONJ 058 | Abundant | Scarce | Abundant | Absent |
| ONJ 060 | Abundant | Scarce | Scarce | Abundant |
| ONJ 067 | Scarce | Abundant | Scarce | Abundant |
| ONJ 069 | Absent | Abundant | Absent | Abundant |
| ONJ 080 | Scarce | Abundant | Scarce | Abundant |
| ONJ 081 | Abundant | Abundant | Abundant | Abundant |
| ONJ 084 | Abundant | Absent | Scarce | Absent |
| ONJ 086 | Abundant | Abundant | Scarce | Abundant |
| ONJ 091 | Scarce | Abundant | Scarce | Abundant |
| ONJ 093 | Scarce | Abundant | Abundant | Scarce |
| ONJ 094 | Abundant | Abundant | Abundant | Absent |
| ONJ 095 | Absent | Scarce | Absent | Abundant |
| ONJ 096* | Abundant | n/a | Abundant | Absent |
| ONJ 097 | Scarce | Scarce | Abundant | Scarce |
| ONJ 099 | Scarce | Abundant | Abundant | Abundant |
| ONJ 101 | Scarce | Scarce | Abundant | Scarce |
| ONJ 211 | Scarce | Scarce | Absent | Scarce |
| ONJ 212 | Scarce | Abundant | Absent | Abundant |

** Patient with FFPE tissue sample containing only tumour tissue. Abbreviations: IT, intratumoural; PT, peritumoural; ASCs, antigen-secreting cells; BCA, B cell aggregate.*

***Table A4. Correlation between abundance of IT/PT ASCs and BCAs with biochemical relapse.***

| Patient ID | Abundance of IT ASCs | Abundance of PT ASCs | Abundance of IT BCAs | Abundance of PT BCAs | Biochemical Relapse |
|---|---|---|---|---|---|
| ONJ 002 | Scarce | Abundant | Scarce | Abundant | N |
| ONJ 003 | Scarce | Abundant | Absent | Scarce | N |
| ONJ 004 | Absent | Absent | Scarce | Absent | N |
| ONJ 009 | Absent | Abundant | Absent | Abundant | N |
| ONJ 010 | Absent | Abundant | Absent | Scarce | n/a |
| ONJ 011 | Scarce | Abundant | Absent | Scarce | N |
| ONJ 012 | Abundant | Abundant | Scarce | Scarce | N |
| ONJ 013 | Scarce | Scarce | Absent | Scarce | N |
| ONJ 014 | Abundant | Abundant | Absent | Abundant | N |
| ONJ 015 | Absent | Scarce | Scarce | Scarce | N |
| ONJ 016 | Abundant | Abundant | Absent | Abundant | N |
| ONJ 018 | Absent | Abundant | Absent | Abundant | N |
| ONJ 019 | Abundant | Absent | Scarce | Absent | N |
| ONJ 020 | Absent | Abundant | Scarce | Scarce | N |
| ONJ 021 | Abundant | Abundant | Scarce | Scarce | N |
| ONJ 022 | Scarce | Scarce | Absent | Absent | N |
| ONJ 024 | Abundant | Scarce | Scarce | Absent | N |

| | | | | | |
|---|---|---|---|---|---|
| ONJ 025 | Scarce | Abundant | Scarce | Abundant | N |
| ONJ 026 | Scarce | Scarce | Scarce | Scarce | N |
| ONJ 027 | Abundant | Abundant | Scarce | Abundant | N |
| ONJ 028 | Absent | Scarce | Scarce | Scarce | N |
| ONJ 029 | Absent | Scarce | Absent | Scarce | N |
| ONJ 030 | Abundant | Abundant | Scarce | Scarce | n/a |
| ONJ 031 | Absent | Absent | Absent | Absent | N |
| ONJ 032 | Scarce | Abundant | Absent | Abundant | N |
| ONJ 033 | Absent | Absent | Scarce | Scarce | N |
| ONJ 034 | Abundant | Scarce | Scarce | Absent | Y |
| ONJ 035 | Abundant | Abundant | Abundant | Scarce | N |
| ONJ 036 | Abundant | Scarce | Scarce | Absent | N |
| ONJ 037 | Scarce | Absent | Abundant | Scarce | N |
| ONJ 040 | Scarce | Abundant | Scarce | Abundant | N |
| ONJ 041 | Absent | Scarce | Absent | Scarce | N |
| ONJ 043 | Absent | Abundant | Absent | Abundant | N |
| ONJ 044 | Scarce | Scarce | Scarce | Scarce | N |
| ONJ 045 | Abundant | Scarce | Abundant | Absent | Y |
| ONJ 046 | Scarce | Scarce | Absent | Scarce | N |
| ONJ 047 | Abundant | Abundant | Abundant | Scarce | N |
| ONJ 048 | Absent | Scarce | Scarce | Scarce | N |
| ONJ 049 | Absent | Scarce | Absent | Abundant | N |
| ONJ 050 | Absent | Abundant | Absent | Abundant | N |
| ONJ 051 | Scarce | Abundant | Absent | Absent | N |
| ONJ 052 | Scarce | Abundant | Scarce | Abundant | N |
| ONJ 053 | Abundant | Abundant | Scarce | Scarce | N |
| ONJ 054 | Absent | Abundant | Absent | Scarce | Y |
| ONJ 055 | Absent | Scarce | Scarce | Scarce | N |
| ONJ 057 | Absent | Abundant | Absent | Absent | N |
| ONJ 058 | Abundant | Scarce | Abundant | Absent | N |
| ONJ 060 | Abundant | Scarce | Scarce | Abundant | Y |
| ONJ 067 | Scarce | Abundant | Scarce | Abundant | N |
| ONJ 069 | Absent | Abundant | Absent | Abundant | N |
| ONJ 080 | Scarce | Abundant | Scarce | Abundant | N |
| ONJ 081 | Abundant | Abundant | Abundant | Abundant | Y |
| ONJ 084 | Abundant | Absent | Scarce | Absent | Y |
| ONJ 086 | Abundant | Abundant | Scarce | Abundant | Y |
| ONJ 091 | Scarce | Abundant | Scarce | Abundant | N |
| ONJ 093 | Scarce | Abundant | Abundant | Scarce | Y |
| ONJ 094 | Abundant | Abundant | Abundant | Absent | N |
| ONJ 095 | Absent | Scarce | Absent | Abundant | N |
| ONJ 096* | Abundant | n/a | Abundant | n/a | Y |
| ONJ 097 | Scarce | Scarce | Abundant | Scarce | N |

| | | | | | |
|---|---|---|---|---|---|
| ONJ 099 | Scarce | Abundant | Abundant | Abundant | Y |
| ONJ 101 | Scarce | Scarce | Abundant | Scarce | N |
| ONJ 211 | Scarce | Scarce | Absent | Scarce | n/a |
| ONJ 212 | Scarce | Abundant | Absent | Abundant | n/a |

** Patient with FFPE sample containing only tumour tissue. Four patients were removed due to lack of biochemical relapse data (ONJ 010, ONJ 030, ONJ 211 and ONJ 212). Abbreviations: IT, intratumoural; PT, peritumoural; ASCs, antigen-secreting cells; BCA, B cell aggregate; Y, yes; N, no.*

***Table A5. Correlation between abundance of patient IT/PT ASCs with corresponding autoantibody profiles (blood).***

| Patient ID | Abundance of IT ASCs | Abundance of PT ASCs | Antigen Counts | Average RFU |
|---|---|---|---|---|
| ONJ 002 | Scarce | Abundant | 2 | 80 |
| ONJ 003 | Scarce | Abundant | 37 | 298 |
| ONJ 004 | Absent | Absent | 3 | 128 |
| ONJ 009 | Absent | Abundant | 3 | 166 |
| ONJ 010 | Absent | Abundant | 12 | 159 |
| ONJ 011 | Scarce | Abundant | 7 | 208 |
| ONJ 012 | Abundant | Abundant | 20 | 219 |
| ONJ 013 | Scarce | Scarce | 5 | 168 |
| ONJ 014 | Abundant | Abundant | 43 | 313 |
| ONJ 015 | Absent | Scarce | 0 | 84 |
| ONJ 016 | Abundant | Abundant | 0 | 70 |
| ONJ 018 | Absent | Abundant | 1 | 96 |
| ONJ 019 | Abundant | Absent | 2 | 101 |
| ONJ 020 | Absent | Abundant | 4 | 87 |
| ONJ 021 | Abundant | Abundant | 3 | 145 |
| ONJ 022 | Scarce | Scarce | 0 | 104 |
| ONJ 024 | Abundant | Scarce | 9 | 166 |
| ONJ 025 | Scarce | Abundant | 17 | 159 |
| ONJ 026 | Scarce | Scarce | 3 | 143 |
| ONJ 027 | Abundant | Abundant | 34 | 279 |
| ONJ 028 | Absent | Scarce | 9 | 182 |
| ONJ 029 | Absent | Scarce | 1 | 131 |
| ONJ 030 | Abundant | Abundant | 33 | 342 |
| ONJ 031 | Absent | Absent | 0 | 134 |
| ONJ 032 | Scarce | Abundant | 7 | 142 |
| ONJ 033 | Absent | Absent | 3 | 141 |
| ONJ 034 | Abundant | Scarce | 6 | 141 |
| ONJ 035 | Abundant | Abundant | 0 | 74 |

| | | | | |
|---|---|---|---|---|
| ONJ 036 | Abundant | Scarce | 0 | 68 |
| ONJ 037 | Scarce | Absent | 2 | 101 |
| ONJ 040 | Scarce | Abundant | 6 | 181 |
| ONJ 041 | Absent | Scarce | 26 | 311 |
| ONJ 043 | Absent | Abundant | 0 | 55 |
| ONJ 044 | Scarce | Scarce | 7 | 156 |
| ONJ 045 | Abundant | Scarce | 5 | 141 |
| ONJ 046 | Scarce | Scarce | 0 | 132 |
| ONJ 047 | Abundant | Abundant | 11 | 192 |
| ONJ 048 | Absent | Scarce | 60 | 595 |
| ONJ 049 | Absent | Scarce | 26 | 247 |
| ONJ 050 | Absent | Abundant | 1 | 87 |
| ONJ 051 | Scarce | Abundant | 31 | 267 |
| ONJ 052 | Scarce | Abundant | 3 | 99 |
| ONJ 053 | Abundant | Abundant | 3 | 103 |
| ONJ 054 | Absent | Abundant | 0 | 99 |
| ONJ 055 | Absent | Scarce | 37 | 298 |
| ONJ 057 | Absent | Abundant | 3 | 124 |
| ONJ 058 | Abundant | Scarce | 69 | 351 |
| ONJ 060 | Abundant | Scarce | 26 | 268 |
| ONJ 067 | Scarce | Abundant | 7 | 160 |
| ONJ 069 | Absent | Abundant | 13 | 199 |
| ONJ 080 | Scarce | Abundant | 77 | 400 |
| ONJ 081 | Abundant | Abundant | 85 | 453 |
| ONJ 084 | Abundant | Absent | 1 | 67 |
| ONJ 086 | Abundant | Abundant | 10 | 154 |
| ONJ 091 | Scarce | Abundant | 4 | 112 |
| ONJ 093 | Scarce | Abundant | 0 | 86 |
| ONJ 094 | Abundant | Abundant | 1 | 92 |
| ONJ 095 | Absent | Scarce | 0 | 106 |
| ONJ 096* | Abundant | n/a | 0 | 71 |
| ONJ 097 | Scarce | Scarce | 2 | 102 |
| ONJ 099 | Scarce | Abundant | 1 | 104 |
| ONJ 101 | Scarce | Scarce | 21 | 241 |

***** *Patient with FFPE sample containing only tumour tissue. Two patients were removed from analysis due to lack of array data (ONJ 211 / 212). Abbreviations: IT, intratumoural; PT, peritumoural; ASCs, antigen-secreting cells; RFU, relative fluorescent units.*

***Table A6. Correlation between abundance of patient IT/PT BCAs with corresponding antigen specificities and average RFU.***

| Patient ID | Abundance of IT BCAs | Abundance of PT BCAs | Antigen Specificities | Average RFU |
|---|---|---|---|---|
| ONJ 002 | Scarce | Abundant | 2 | 80 |
| ONJ 003 | Absent | Scarce | 37 | 298 |
| ONJ 004 | Scarce | Absent | 3 | 128 |
| ONJ 009 | Absent | Abundant | 3 | 166 |
| ONJ 010 | Absent | Scarce | 12 | 159 |
| ONJ 011 | Absent | Scarce | 7 | 208 |
| ONJ 012 | Scarce | Scarce | 20 | 219 |
| ONJ 013 | Absent | Scarce | 5 | 168 |
| ONJ 014 | Absent | Abundant | 43 | 313 |
| ONJ 015 | Scarce | Scarce | 0 | 84 |
| ONJ 016 | Absent | Abundant | 0 | 70 |
| ONJ 018 | Absent | Abundant | 1 | 96 |
| ONJ 019 | Scarce | Absent | 2 | 101 |
| ONJ 020 | Scarce | Scarce | 4 | 87 |
| ONJ 021 | Scarce | Scarce | 3 | 145 |
| ONJ 022 | Absent | Absent | 0 | 104 |
| ONJ 024 | Scarce | Absent | 9 | 166 |
| ONJ 025 | Scarce | Abundant | 17 | 159 |
| ONJ 026 | Scarce | Scarce | 3 | 143 |
| ONJ 027 | Scarce | Abundant | 34 | 279 |
| ONJ 028 | Scarce | Scarce | 9 | 182 |
| ONJ 029 | Absent | Scarce | 1 | 131 |
| ONJ 030 | Scarce | Scarce | 33 | 342 |
| ONJ 031 | Absent | Absent | 0 | 134 |
| ONJ 032 | Absent | Abundant | 7 | 142 |
| ONJ 033 | Scarce | Scarce | 3 | 141 |
| ONJ 034 | Scarce | Absent | 6 | 141 |
| ONJ 035 | Abundant | Scarce | 0 | 74 |
| ONJ 036 | Scarce | Absent | 0 | 68 |
| ONJ 037 | Abundant | Scarce | 2 | 101 |
| ONJ 040 | Scarce | Abundant | 6 | 181 |
| ONJ 041 | Absent | Scarce | 26 | 311 |
| ONJ 043 | Absent | Abundant | 0 | 55 |
| ONJ 044 | Scarce | Scarce | 7 | 156 |
| ONJ 045 | Abundant | Absent | 5 | 141 |
| ONJ 046 | Absent | Scarce | 0 | 132 |

| | | | | |
|---|---|---|---|---|
| ONJ 047 | Abundant | Scarce | 11 | 192 |
| ONJ 048 | Scarce | Scarce | 60 | 595 |
| ONJ 049 | Absent | Abundant | 26 | 247 |
| ONJ 050 | Absent | Abundant | 1 | 87 |
| ONJ 051 | Absent | Absent | 31 | 267 |
| ONJ 052 | Scarce | Abundant | 3 | 99 |
| ONJ 053 | Scarce | Scarce | 3 | 103 |
| ONJ 054 | Absent | Scarce | 0 | 99 |
| ONJ 055 | Scarce | Scarce | 37 | 298 |
| ONJ 057 | Absent | Absent | 3 | 124 |
| ONJ 058 | Abundant | Absent | 69 | 351 |
| ONJ 060 | Scarce | Abundant | 26 | 268 |
| ONJ 067 | Scarce | Abundant | 7 | 160 |
| ONJ 069 | Absent | Abundant | 13 | 199 |
| ONJ 080 | Scarce | Abundant | 77 | 400 |
| ONJ 081 | Abundant | Abundant | 85 | 453 |
| ONJ 084 | Scarce | Absent | 1 | 67 |
| ONJ 086 | Scarce | Abundant | 10 | 154 |
| ONJ 091 | Scarce | Abundant | 4 | 112 |
| ONJ 093 | Abundant | Scarce | 0 | 86 |
| ONJ 094 | Abundant | Absent | 1 | 92 |
| ONJ 095 | Absent | Abundant | 0 | 106 |
| ONJ 096* | Abundant | n/a | 0 | 71 |
| ONJ 097 | Abundant | Scarce | 2 | 102 |
| ONJ 099 | Abundant | Abundant | 1 | 104 |
| ONJ 101 | Abundant | Scarce | 21 | 241 |

***** *Patient with FFPE sample containing only tumour tissue. Two patients were removed from analysis due to lack of array data (ONJ 211 / 212). Abbreviations: IT, intratumoural; PT, peritumoural; BCA, B cell aggregate; RFU, relative fluorescent units.*

## References


Adeola HA, Smith M, Kaestner L, Blackburn JM, Zerbini LF (2016) Novel potential serological prostate cancer biomarkers using CT100+ cancer antigen microarray platform in a multi-cultural South African cohort. *Oncotarget* 7: 13945-13964

Artibani W (2012) Landmarks in prostate cancer diagnosis: the biomarkers. *BJU international* 110 Suppl: 8-13

Attard G, Parker C, Eeles RA, Schröder F, Tomlins SA, Tannock I, Drake CG, de Bono JS (2016) Prostate cancer. *Lancet (London, England)* 387: 70-82

Beeton-Kempen N, Duarte J, Shoko A, Serufuri JM, John T, Cebon J, Blackburn J (2014) Development of a novel, quantitative protein microarray platform for the multiplexed serological analysis of autoantibodies to cancer-testis antigens. *International Journal of Cancer* 135: 1842-1851

Boström PJ, Bjartell AS, Catto JWF, Eggener SE, Lilja H, Loeb S, Schalken J, Schlomm T, Cooperberg MR (2015) Genomic Predictors of Outcome in Prostate Cancer. *European Urology* 68: 1033-1044

Bray F, Ferlay J, Soerjomataram I, Siegel RL, Torre LA, Jemal A (2018) Global cancer statistics 2018: GLOBOCAN estimates of incidence and mortality worldwide for 36 cancers in 185 countries. *CA: A Cancer Journal for Clinicians* 68: 394-424

Bruno TC (2020) New predictors for immunotherapy responses sharpen our view of the tumour microenvironment. *Nature* 577: 474-476

Cabrita R, Lauss M, Sanna A, Donia M, Skaarup Larsen M, Mitra S, Johansson I, Phung B, Harbst K, Vallon-Christersson J *et al* (2020) Tertiary lymphoid structures improve immunotherapy and survival in melanoma. *Nature* 577: 561-565

Carl PL, Temple BRS, Cohen PL (2005) Most nuclear systemic autoantigens are extremely disordered proteins: implications for the etiology of systemic autoimmunity. *Arthritis research & therapy* 7

Cerami E, Gao J, Dogrusoz U, Gross BE, Sumer SO, Aksoy BA, Jacobsen A, Byrne CJ, Heuer ML, Larsson E *et al* (2012) The cBio cancer genomics portal: an open platform for exploring multidimensional cancer genomics data. *Cancer Discov* 2: 401-404

Chandra H, Reddy PJ, Srivastava S (2011) Protein microarrays and novel detection platforms. *Expert Review of Proteomics* 8: 61-79

Cuzick J, Thorat MA, Andriole G, Brawley OW, Brown PH, Culig Z, Eeles RA, Ford LG, Hamdy FC, Holmberg L *et al* (2014) Prevention and early detection of prostate cancer. *The Lancet Oncology* 15: e484-e492

Cyster JC (1999) Chemokines and cell migration in secondary lymphoid organs. *Science* 286: 2098-2102

Da Gama Duarte J, Peyper JM, Blackburn JM (2018a) B cells and antibody production in melanoma. *Mammalian Genome* 29: 790-805

Da Gama Duarte J, Woods K, Andrews MC, Behren A (2018b) The good, the (not so) bad and the ugly of immune homeostasis in melanoma. *Immunology and Cell Biology* 96: 497-506

De Visser KE, Eichten A, Coussens LM (2006) Paradoxical roles of the immune system during cancer development. *Nature Reviews Cancer* 6: 24-37

Dieu-Nosjean M-C, Giraldo NA, Kaplon H, Germain C, Fridman WH, Sautès-Fridman C (2016) Tertiary lymphoid structures, drivers of the anti-tumor responses in human cancers. *Immunological Reviews* 271: 260-275

Dieu-Nosjean MC, Goc J, Giraldo NA, Sautès-Fridman C, Fridman WH (2014) Tertiary lymphoid structures in cancer and beyond. *Trends in Immunology* 35: 571-580

Disis ML (2010) Immune regulation of cancer. *Journal of Clinical Oncology* 28: 4531-4538

Duarte JG, Blackburn JM (2017) Advances in the development of human protein microarrays. *Expert Review of Proteomics* 14: 627-641

Dunn GP, Bruce AT, Ikeda H, Old LJ, Schreiber RD (2002) Cancer immunoediting: From immunosurveillance to tumor escape. *Nature Immunology* 3: 991-998

Dunn GP, Old LJ, Schreiber RD (2004) The immunobiology of cancer immunosurveillance and immunoediting. *Immunity* 21: 137-148

Esserman LJ, Thompson IM, Reid B, Nelson P, Ransohoff DF, Welch HG, Hwang S, Berry DA, Kinzler KW, Black WC *et al* (2014) Addressing overdiagnosis and overtreatment in cancer: a prescription for change. *The Lancet Oncology* 15: e234-e242

Filella X, Foj L (2015) Emerging biomarkers in the detection and prognosis of prostate cancer. *Clinical Chemistry and Laboratory Medicine* 53: 963-973

Flammiger A, Bayer F, Cirugeda-Kühnert A, Huland H, Tennstedt P, Simon R, Minner S, Bokemeyer C, Sauter G, Schlomm T *et al* (2012) Intratumoral T but not B lymphocytes are related to clinical outcome in prostate cancer. *Apmis* 120: 901-908

Fujii T, Shimada K, Asai O, Tanaka N, Fujimoto K, Hirao K, Konishi N (2013) Immunohistochemical analysis of inflammatory cells in benign and precancerous lesions and carcinoma of the prostate. *Pathobiology* 80: 119-126

Gao J, Aksoy BA, Dogrusoz U, Dresdner G, Gross B, Sumer SO, Sun Y, Jacobsen A, Sinha R, Larsson E *et al* (2013) Integrative analysis of complex cancer genomics and clinical profiles using the cBioPortal. *Sci Signal* 6: pl1

Garside P, Ingulli E, Merica RR, Johnson JG, Noelle RJ, Jenkins MK (1998) Visualization of specific B and T lymphocyte interactions in the lymph node. *Science* 281: 96-99

Gorosito Serrán M, Fiocca Vernengo F, Beccaria CG, Acosta Rodriguez EV, Montes CL, Gruppi A (2015) The regulatory role of B cells in autoimmunity, infections and cancer: Perspectives beyond IL10 production. *FEBS Letters* 589: 3362-3369

Grönberg H (2003) Prostate cancer epidemiology. *Lancet* 361: 859-864

Gundem G, Van Loo P, Kremeyer B, Alexandrov LB, Tubio JMC, Papaemmanuil E, Brewer DS, Kallio HML, Högnäs G, Annala M *et al* (2015) The evolutionary history of lethal metastatic prostate cancer. *Nature* 520: 353-357

Guo L-H, Wu R, Xu H-X, Xu J-M, Wu J, Wang S, Bo X-W, Liu B-J (2015) Comparison between Ultrasound Guided Transperineal and Transrectal Prostate Biopsy: A Prospective, Randomized and Controlled Trial. *Scientific Reports* 5: 16089-16089

Hanahan D, Weinberg RA (2000) The hallmarks of cancer. *Cell* 100: 57-70

Hanahan D, Weinberg RA (2011) Hallmarks of cancer: The next generation. *Cell* 144: 646-674

He Y, Qian H, Liu Y, Duan L, Li Y, Shi G (2014) The roles of regulatory B cells in cancer. *Journal of immunology research* 2014: 215471-215471

Helmink BA, Reddy SM, Gao J, Zhang S, Basar R, Thakur R, Yizhak K, Sade-Feldman M, Blando J, Han G *et al* (2020) B cells and tertiary lymphoid structures promote immunotherapy response. *Nature* 577: 549-555

Heninger E, Krueger TEG, Thiede SM, Sperger JM, Byers BL, Kircher MR, Kosoff D, Yang B, Jarrard DF, McNeel DG *et al* (2016) Inducible expression of cancer-testis antigens in human prostate cancer. *Oncotarget* 7: 84359-84374

Hoffman RM (2011) Clinical practice. Screening for prostate cancer. *N Engl J Med* 365: 2013-2019

Ilic D, Neuberger MM, Djulbegovic M, Dahm P (2013) Screening for prostate cancer. *Cochrane Database of Systematic Reviews*

Kim HJ, Verbinnen B, Tang X, Lu L, Cantor H (2010) Inhibition of follicular T-helper cells by CD8+regulatory T cells is essential for self tolerance. *Nature* 467: 328-332

Krahn MD, Zagorski B, Laporte A, Alibhai SMH, Bremner KE, Tomlinson G, Warde P, Naglie G (2010) Healthcare costs associated with prostate cancer: Estimates from a population-based study. *BJU International* 105: 338-346

Leto G, Incorvaia L, Badalamenti G, Tumminello FM, Gebbia N, Flandina C, Crescimanno M, Rini G (2006) Activin A circulating levels in patients with bone metastasis from breast or prostate cancer. *Clin Exp Metastasis* 23: 117-122

Li B, Dewey CN (2011) RSEM: accurate transcript quantification from RNA-Seq data with or without a reference genome. *BMC Bioinformatics* 12: 323-323

Liu T, Wang X, Karsdal MA, Leeming DJ, Genovese F (2012) Molecular serum markers of liver fibrosis. *Biomarker Insights* 7: 105-117

Liu Y, Guo X, Xing M, Zhao K, Luo L, Du J (2018) Prognostic value of serum levels of soluble MICA (sMICA) in patients with prostate cancer. *Br J Biomed Sci* 75: 98-100

Loeb S, Bjurlin MA, Nicholson J, Tammela TL, Penson DF, Carter HB, Carroll P, Etzioni R (2014) Overdiagnosis and overtreatment of prostate cancer. *European Urology* 65: 1046-1055

Lojanapiwat B, Anutrakulchai W, Chongruksut W, Udomphot C (2014) Correlation and diagnostic performance of the prostate-specific antigen level with the diagnosis, aggressiveness, and bone metastasis of prostate cancer in clinical practice. *Prostate Int* 2: 133-139

Marks L, Young S, Natarajan S (2013) MRI-ultrasound fusion for guidance of targeted prostate biopsy. *Current Opinion in Urology* 23: 43-50

Mazzara S, Rossi RL, Grifantini R, Donizetti S, Abrignani S, Bombaci M (2017) CombiROC: An interactive web tool for selecting accurate marker combinations of omics data. *Scientific Reports* 7: 1-11

Menegoz F, Lutz JM, Mousseau M, Orfeuvre H, Schaerer R (1994) Descriptive Epidemiology of Prostate Cancer. 10: 1-6

Mukherjee R, Bartlett JM, Krishna NS, Underwood MA, Edwards J (2005) Raf-1 expression may influence progression to androgen insensitive prostate cancer. *Prostate* 64: 101-107

Mukherjee R, McGuinness DH, McCall P, Underwood MA, Seywright M, Orange C, Edwards J (2011) Upregulation of MAPK pathway is associated with survival in castrate-resistant prostate cancer. *Br J Cancer* 104: 1920-1928

O'Rourke DJ, DiJohnson DA, Caiazzo RJ, Nelson JC, Ure D, O'Leary MP, Richie JP, Liu BCS (2012) Autoantibody signatures as biomarkers to distinguish prostate cancer from benign prostatic hyperplasia in patients with increased serum prostate specific antigen. *Clinica Chimica Acta* 413: 561-567

Peter C, Wesselborg S, Herrmann M, Lauber K (2010) Dangerous attraction: phagocyte recruitment and danger signals of apoptotic and necrotic cells. *Apoptosis* 15: 1007-1028

Petitprez F, de Reyniès A, Keung EZ, Chen TW, Sun CM, Calderaro J, Jeng YM, Hsiao LP, Lacroix L, Bougoüin A *et al* (2020) B cells are associated with survival and immunotherapy response in sarcoma. *Nature* 577: 556-560

Pienta KJ (1993) Risk Factors for Prostate Cancer. *Annals of Internal Medicine* 118: 793-793

Pishgar F, Ebrahimi H, Saeedi Moghaddam S, Fitzmaurice C, Amini E (2018) Global, Regional and National Burden of Prostate Cancer, 1990 to 2015: Results from the Global Burden of Disease Study 2015. *Journal of Urology* 199: 1224-1232

Rao AR, Motiwala HG, Karim OMA (2008) The discovery of prostate-specific antigen. *BJU International* 101: 5-10

Roca H, Keller ET, Lu Y, Keller JM, McCauley LK, Dai J, Zhang J (2017) Immune mediators in the tumor microenvironment of prostate cancer. *Chinese Journal of Cancer* 36: 1-8

Sadi MV (2017) PSA screening for prostate cancer. *Revista da Associacao Medica Brasileira* 63: 722-725

Sakr WA, Haas GP, Cassin BF, Pontes JE, Crissman JD (1993) The frequency of carcinoma and intraepithelial neoplasia of the prostate in young male patients. *Journal of Urology* 150: 379-385

Saul L, Ilieva KM, Bax HJ, Karagiannis P, Correa I, Rodriguez-Hernandez I, Josephs DH, Tosi I, Egbuniwe IU, Lombardi S *et al* (2016) IgG subclass switching and clonal expansion in cutaneous melanoma and normal skin. *Scientific Reports* 6: 1-12

Scanlan MJ, Gure AO, Jungbluth AA, Old LJ, Chen Y-T (2002) Cancer/testis antigens: an expanding family of targets for cancer immunotherapy. *Immunological reviews* 188: 22-32

Shalapour S, Font-Burgada J, Di Caro G, Zhong Z, Sanchez-Lopez E, Dhar D, Willimsky G, Ammirante M, Strasner A, Hansel DE *et al* Immunosuppressive plasma cells impede T-cell-dependent immunogenic chemotherapy.

Simpson AJG, Caballero OL, Jungbluth A, Chen YT, Old LJ (2005) Cancer/testis antigens, gametogenesis and cancer. *Nature Reviews Cancer* 5: 615-625

Stephenson AJ, Kattan MW, Eastham JA, Dotan ZA, Bianco FJ, Lilja H, Scardino PT (2006) Defining biochemical recurrence of prostate cancer after radical prostatectomy: A proposal for a standardized definition. *Journal of Clinical Oncology* 24: 3973-3978

Swann JB, Smyth MJ (2007) Review series Immune surveillance of tumors. *The Journal of Clinical Investigation* 117: 1137-1146

Tan EM, Zhang J (2008) Autoantibodies to tumor-associated antigens: reporters from the immune system. *Immunological Reviews* 222: 328-340

Vigneron N (2015) Human Tumor Antigens and Cancer Immunotherapy. *BioMed Research International* 2015: 1-17

Wang X, Yu J, Sreekumar A, Varambally S, Shen R, Giacherio D, Mehra R, Montie JE, Pienta KJ, Sanda MG *et al* (2005) Autoantibody signatures in prostate cancer. *New England Journal of Medicine* 353: 1224-1235

Watanabe N, Arase H, Onodera M, Ohashi PS, Saito T (2000) The Quantity of TCR Signal Determines Positive Selection and Lineage Commitment of T Cells. *The Journal of Immunology* 165: 6252-6261

Whitehurst AW (2014) Cause and Consequence of Cancer/Testis Antigen Activation in Cancer. *Annual Review of Pharmacology and Toxicology* 54: 251-272

Wolf AM, Wender RC, Etzioni RB, Thompson IM, D'Amico AV, Volk RJ, Brooks DD, Dash C, Guessous I, Andrews K *et al* (2010) American Cancer Society guideline for the early detection of prostate cancer: update 2010. *CA Cancer J Clin* 60: 70-98

Woo JR, Liss MA, Muldong MT, Palazzi K, Strasner A, Ammirante M, Varki N, Shabaik A, Howell S, Kane CJ *et al* (2014) Tumor infiltrating B-cells are increased in prostate cancer tissue. *Journal of Translational Medicine* 12: 30-30

Xie C, Kim HJ, Haw JG, Kalbasi A, Gardner BK, Li G, Rao J, Chia D, Liong M, Punzalan RR *et al* (2011) A novel multiplex assay combining autoantibodies plus PSA has potential implications for classification of prostate cancer from non-malignant cases. *Journal of translational medicine* 9: 43-43

Zaenker P, Gray ES, Ziman MR (2016) Autoantibody Production in Cancer-The Humoral Immune Response toward Autologous Antigens in Cancer Patients. *Autoimmunity Reviews* 15: 477-483

Zaenker P, Ziman MR (2013) Serologic autoantibodies as diagnostic cancer biomarkers - A review. *Cancer Epidemiology Biomarkers and Prevention* 22: 2161-2181